PhD-FSTC-2019-39
The Faculty of Sciences, Technology and Communication

École Doctoral IAEM Lorraine
Département Contrôle Identification Diagnostic (CID), CRAN

DISSERTATION

Defence held on 07/06/2019 in Luxembourg
to obtain the degree of

DOCTEUR DE L'UNIVERSITÉ DU LUXEMBOURG EN SCIENCES DE L'INGENIEUR

AND

DOCTOR DE L'UNIVERSEITÉ DE LORRAINE EN AUTOMATIQUE, TRAITEMENT DU SIGNAL ET DES IMAGES, GÉNIE INFORMATIQUE

by

Serket QUINTANAR GUZMÁN
Born on 16 June 1988 in Jojutla, Morelos (México)

NONLINEAR OBSERVATION AND CONTROL OF A LIGHTWEIGHT ROBOTIC MANIPULATOR ACTUATED BY SHAPE MEMORY ALLOY (SMA) WIRES

Dissertation defence committee

Dr-Ing Holger VOOS, dissertation supervisor
Professor, Université du Luxembourg

Dr-Ing Mohamed DAROUACH, dissertation supervisor
Professor, Université de Lorraine

Dr-Ing Jean-Regis HADJI-MINAGLOU, Chairman
Professor, Université du Luxembourg

Dr Marouane ALMA, dissertation co-supervisor
Associate Professor, Université de Lorraine

Dr-Ing Antoine FERREIRA, dissertation reviewer
Professor, INSA Centre Val de Loire

Dr Carlos Manuel ASTORGA ZARAGOZA, Deputy Chairman
Professor, Centro Nacional de Investigación y Desarrollo Tecnológico (CENIDET)

Declaration of Authorship

I, Serket Quintanar Guzmán, declare that this thesis titled, 'Nonlinear Observation and Control of a Lightweight Robotic Manipulator Actuated by Shape Memory Alloy (SMA) Wires' and the work presented in it are my own. I confirm that:

- This work was done wholly or mainly while in candidature for a research degree at this University.
- Where any part of this thesis has previously been submitted for a degree or any other qualification at this University or any other institution, this has been clearly stated.
- Where I have consulted the published work of others, this is always clearly attributed.
- Where I have quoted from the work of others, the source is always given. With the exception of such quotations, this thesis is entirely my own work.
- I have acknowledged all main sources of help.
- Where the thesis is based on work done by myself jointly with others, I have made clear exactly what was done by others and what I have contributed myself.

Signed: 

Date: 01 / May / 2019

"Why fit in when you were born to stand out?."

Dr. Seuss

Acknowledgements

First of all, I would like to express my sincere gratitude to my supervisors, Prof. Dr-Ing Holger VOOS, Prof. Dr-Ing Mohamed DAROUACH and A-Prof. Dr Marouane ALMA for their guidance, support and the knowledge shared with me throughout the years of my PhD.

I would like to thank Prof. Dr-Ing Jean-Régis HADJI-MINAGLOU, who was a part of my committee and my reviewers Prof. Dr. Carlos Manuel ASTORGA ZARAGOZA and Prof. Dr-Ing Antoine FERREIRA for their insightful reviews and valuable feedback which helped me improve my work.

A especial thanks to Dr. Somasundar KANNAN for all the hours dedicated to guide my work and all those long hours of fruitful discussions to set me on the right path to achieve my objective. I would like to thank Dr. Seyed Amin SAJADI ALAMDARI for always having his door open to discuss any new ideas or thoughts. Also my sincere gratitude to all the team members of the SnT Automation & Robotic Research Group, for every helpful discussion and the amazing working atmosphere.

I am extremely grateful to all my friends in Luxembourg, Mexico and any other part of the world where they might be. Anush, Amin Sajadi, Manuel, Jorge, Amin Sleimi, Kerstin, Sandra, Mauri, Jey, Nancy, Jashiel, Amy, Eric Tillous, Bárbara, Hugo, Félix, Arun, thank you for the immense support and for making this journey fun and memorable. A hearty thanks to Waleed, for being there for me during the hardest times as well as bringing some of the best. A special thanks to Adriana, for her constant guidance and advice, both academic and personal, and for never letting me feel that I was far from my home or family.

Finally, I deeply thank my family. My parents, Aida and Sergio, whose support and teachings throughout my life made me the person I am today; to my sister, Alitzel, for bringing that much needed spark of craziness into my life and whose love drives me to be a better person every day and then to my grandma Marina, whom I know is always proud, I still don't know what I did so good to deserve you.

I am truly blessed to be surrounded by such great people in my life.

Serket QUINTANAR GUZMÁN

Grand Duchy of Luxembourg, 2019

Contents

List of Figures

List of Tables

Abbreviations

UAV	**U**nmanned **A**erial **V**ehicle
SMA	**S**hape **M**emory **A**lloy
SDRE	**S**tate-**D**ependet **R**iccati **E**quation
DSDRE	**D**iscrete-time **S**tate-**D**ependet **R**iccati **E**quation
EKF	**E**xtended **K**alman **F**ilter
LWRA	**L**ight **W**eight **R**obotic **A**rm
SME	**S**hape **M**emory **E**ffect
EKF-UI	**E**xtended **K**alman **F**ilter with **U**nknown **I**nput
VToL	**V**ertical **T**ake-**o**ff and **L**anding
DoF	**D**egrees **o**f **F**reedom
PDF	**P**robability **D**ensity **F**unction
KP	**K**rasnosel'skii-**P**okovskii
PI	**P**randtl-**I**shlinskii
CAD	**C**omputer **A**ided **D**esign
ROS	**R**obot **O**perating **S**ystem
CDSA	**C**ompliant **D**ifferential **S**MA **A**ctuator
PWM	**P**ulse **W**idth **M**odulation
PID	**P**roportional-**I**ntegral-**D**erivative
PWPF	**P**ulse **W**idth **P**ulse **F**requency
MINIR	**M**inimally **I**nvasive **N**eurosurgical **I**ntracranial **R**obot
VSC	**V**ariable **S**tructure **C**ontrol
SMC	**S**liding **M**ode **C**ontrol
TDE	**T**ime **D**elay **E**stimation
MRC	**M**odel **R**eference **C**ontrol
AC	**A**daptive **C**ontrol

DNN	**D**ynamic **N**eural **N**etwork
ANN	**A**rtifical **N**eural **N**etwork
LPV	**L**inear **P**arameter **V**arying
SDC	**S**tate-**D**ependent **C**oefficients
DARE	**D**iscrete **A**lgebraic **R**iccati **E**quation
ADC	**A**nalog **D**igital **C**onverter

*To **my parents**, for letting me have big dreams and teaching me how to make them come true.*

*To **my sister**, for your unconditional love and the spark of craziness you bring to my life everyday.*

*To **Adriana**, for becoming my family when I was so far from home.*

Résumé Étendu

Observation et Commande non Linéaire d'un Manipulateur Robotique Léger Actionné Par Des Fils En Alliage À Mémoire De Forme (SMA)

par Serket Quintanar Guzmán

Chapitre 1. Introduction

Depuis leur introduction en tant que ressource militaire, les véhicules aériens sans pilote (UAV) ont pris une importance croissante dans différents secteurs de l'industrie. Jusqu'à présent, la plupart des applications d'UAV impliquent uniquement des tâches de surveillance et/ou de télédétection. Actuellement, une variété d'applications mettant en œuvre une manipulation aérienne peut être trouvée dans la littérature. Par exemple, un actionneur simple et léger pour les tâches d'ouverture de porte est présenté dans [6]. Les auteurs de [16] proposent un système d'inspection des contacts de pont utilisant la manipulation aérienne et [17] étudient la conception et le contrôle d'un bras double conforme pour la capture d'objets.

La proposition présentée dans cette thèse vise à fournir une solution alternative à la capacité de charge utile limitée des UAV. Pour résoudre ce problème, il est nécessaire d'envisager la mise en œuvre d'actionneurs non conventionnels, tels que des matériaux intelligents, tels que: des alliages à mémoire de forme.

Problème et motivation

Les câbles SMA constituent une excellente alternative aux actionneurs classiques en raison de leur rapport résistance-poids élevé. Cependant, leur dynamique hautement non linéaire les rend difficiles à contrôler. Un ensemble de techniques capables de gérer des systèmes hautement non linéaires sont celles de la commande par retour d'état. Dans le cas des fils SMA, peu de recherches ont été rapportées dans cette domaine [18, 19].

La principale raison à cela est le manque d'accès à certains états du fil SMA lors de la mise en œuvre. La meilleure solution à ce problème est la mise en place d'un observateur d'état. Néanmoins, l'estimation des états fils SMA présente son propre ensemble de défis, en raison de la nature hystérétique des fils SMA.

Le but de cette étude est la mise en œuvre expérimentale d'une commande par retour d'état pour la régulation de la position d'un bras robotique léger actionné par des fils

SMA. La conception d'un modèle observable et l'estimation de l'état font partie de la portée de ce travail. Une étude formelle sur l'observabilité du modèle mathématique proposé et la convergence de la technique d'estimation développée est fournie.

Chapitre 2. Manipulateurs aériens légers

La manipulation aérienne est définie, d'une manière générale, comme l'action de saisie, de transport, de positionnement et/ou d'assemblage de pièces mécaniques, instruments, etc., effectuée par un véhicule aérien sans pilote à décollage et atterrissage vert (VToL) équipés d'un dispositif de préhension et/ou d'un bras robotique [20].

Dans la littérature, on peut trouver différents types de manipulateurs aériens à des fins différentes. On trouve également peu d'approches légères. Un simple manipulateur aérien est présenté dans [4], où l'UAV est capable d'interagir avec son environnement en appliquant une force à un mur. De même, les auteurs de [5] présentent un prototype de manipulateur aérien, constitué d'un hélicoptère miniature à quadrimoteurs capable d'appliquer une force à l'environnement en vol.

Le contrôle d'un bras robotique à liaisons multiples ayant un poids total de 400 g est présenté dans [8]. Dans [21], un bras robotique conforme à la réglementation 2 DoF est développé à l'aide de servos linéaires, d'un poids total d'environ 325 grammes. Dans [7], les auteurs modélisent et contrôlent un bras de robot léger imprimé en 5 DF, imprimé en 3D, d'un poids total de 250 grammes.

Les actionneurs classiques tels que les servomoteurs, les moteurs à courant continu ou les actionneurs hydrauliques présentent un faible rapport poids/puissance, comme le montre la Fig. 2.9. Ainsi, la conception d'applications robotiques légères basées sur des actionneurs conventionnels est limitée. Dans cet esprit, la présente recherche propose un bras robotique léger actionné par des fils en alliage à mémoire de forme (SMA) et des mécanismes personnalisés imprimés en 3D, d'un poids total inférieur à 100 g.

Alliages à mémoire de forme (SMA)

Les alliages à mémoire de forme (SMA) sont un type de matériaux intelligents qui peuvent "se rappeler" de leur forme d'origine après avoir subi une déformation physique. Ce type d'alliages a la capacité de retrouver sa forme prédéfinie d'origine en appliquant certains stimuli tels que des variations thermomécaniques. Ce phénomène est appelé Effet de Mémoire de Forme (SME). Le SME se produit en raison d'une transformation interne de la structure cristalline du matériau. Cette transformation se produit entre

deux phases appelées martensite et austénite. Lorsque le SMA est à une température plus basse, sa structure passe à la phase de martensite, phase relativement molle et malléable, au cours de laquelle le fil peut être facilement déformé. Lorsque chauffé à une température supérieure à sa température de transformation, le fil SMA se transforme en phase austénite, phase dure, retrouvant ainsi sa forme et ses dimensions initiales [22].

Plusieurs propriétés physiques des fils en NiTi sont étudiées et testées. Pour leur utilisation en ingénierie en tant qu'actionneurs, les principaux avantages sont les suivants: 1) Rapport poids/puissance élevé, 2) Petite taille et miniaturisation aisée, et 3) Fonctionnement sans bruit.

Malgré leurs nombreux avantages, les câbles SMA présentent également différentes limites et défis: 1) Faible efficacité énergétique. 2) Dégradation et fatigue, 3) Vitesse lente et 4) Non linéarité.

Chapitre 3. Conception mécanique et modèle mathématique

Cette section présente la conception mécanique d'un bras de robot léger actionné par SMA, destiné à servir de manipulateur aérien pour les petits UAV. Ce bras robotique consiste en un seul degré de liberté (DoF) actionné par des fils SMA. La Fig. 3.1 montre un modèle de conception assistée par ordinateur (CAO) de la conception du bras du robot. Parmi les caractéristiques prises en compte pour la conception et le développement de cet actionneur, on peut citer: 1) Légère et petite taille, 2) Compatibilité ROS (Robot Operating System), 3) Communication sans fil et 4) Construction simple.

Conception mécanique

La conception donnée propose un bras robotique avec 1 DoF activé par un ou deux (selon la configuration, voir la sous-section 3.1.2) Flexinol® fils. La pince est activée par un troisième fil Flexinol® plus fin. Des détails supplémentaires sur la configuration expérimentale sont donnés dans la sous-section 3.1.6.

Le bras robotique comporte deux liaisons imprimées en 3D sur mesure (longueur 100 mm) et une plage de mouvements le long du plan vertical X-Z entre 90 et 110 degrés avec deux coupleurs cylindriques. Son poids total est d'environ 80 g, ce qui ne représente que 40% environ du poids des designs légers trouvés dans la littérature, comme celui présenté dans [7]. Le mécanisme d'enroulement (voir la sous-section 3.1.3) permet d'utiliser des fils SMA plus longs afin d'augmenter la liberté de rotation sans augmenter la dimension du bras robotique.

La Fig. 3.10 montre un schéma fonctionnel de la configuration expérimentale et du banc de test conçus pour les résultats présentés dans cette thèse. Une image de la configuration expérimentale réelle est affichée dans la Fig. 3.11.

L'entrée de contrôle est calculée dans Matlab/Simulink. Cette valeur de tension est envoyée via l'interface série au microcontrôleur ESP-12E, puis transformée en un signal PWM et appliquée à chaque fil via une interface d'alimentation basée sur MOSFET. La position angulaire est mesurée au moyen d'un potentiomètre (Bourne 3382G) associé à un CAN ADS1115 16 bits. La mesure est traitée par le microcontrôleur et renvoyée à l'interface Matlab/Simulink via une communication série.

Modèle mathématique

D'une manière générale, le modèle mathématique peut être divisé en deux sous-systèmes: 1) fil SMA et 2) cinématique et dynamique de robot. Ces sous-systèmes sont interconnectés de manière récursive, comme le montre la Fig. 3.13.

1. Le modèle de fil SMA décrit la relation entre la tension appliquée et la force générée dans le fil. Ce modèle est divisé en 3 sous-systèmes: modèle de transfert de chaleur, modèle de transformation de phase et modèle constitutif. La Fig. 3.14 montre l'interaction entre ces 3 sous-systèmes.

    - Le modèle de transfert de chaleur décrit le chauffage électrique du fil par effet Joule et le processus de refroidissement par convection naturelle [23] (voir Eq.(3.1)).
    - La transformation de phase du fil SMA dépend directement de la direction de la dérivée temporelle de la température et de la contrainte. Par conséquent, en raison du comportement d'hystérésis, deux équations sont nécessaires pour décrire complètement ce phénomène. La dynamique du processus de transformation complet est décrite dans Eq.(3.6) [24].
    - Le modèle constitutif du fil décrit la relation entre contrainte (σ), déformation (ε), température (T) et fraction de martensite (ξ). Ce modèle a été proposé pour la première fois par [25], puis amélioré par [26]. Le modèle constitutif est écrit en Eq.(3.9).

2. Le modèle cinématique et dynamique décrit le modèle de conception mécanique et ses relations avec le reste du système.

- Le modèle cinématique associe le modèle du fil SMA à la mécanique du bras robotique lui-même. Le rapport de contrainte du fil SMA et la vitesse angulaire du bras dépendent de la géométrie du design. Cette relation cinématique est en Eq.(3.12)
- Le modèle dynamique décrit la dynamique du système mécanique. Ce modèle établit la relation entre le mécanisme de coupleur, le ressort de torsion et les couples appliqués par les fils SMA, ainsi que les effets de la charge et du préhenseur. Ce modèle est dérivé du modèle général pour un système mécanique rigide à n degrés de liberté. Le modèle est donné dans Eq.(3.14) et Eq.(3.15) pour la configuration biaisée et antagoniste, respectivement.

Enfin, Eq.(3.22) et Eq.(3.22) présentent respectivement le modèle d'espace à états pour les configurations biaisée et antagoniste, les vecteurs d'état étant définis comme suit: $x(t) = \begin{bmatrix} \theta_1 & \dot{\theta}_1 & T_1 & \sigma_1 & \xi_1 \end{bmatrix}^\top$ et $x(t) = \begin{bmatrix} \theta_1 & \dot{\theta}_1 & T_1 & \sigma_1 & \xi_1 & \theta_2 & \dot{\theta}_2 & T_2 & \sigma_2 & \xi_2 \end{bmatrix}^\top$ pour les configurations biaisée et antagoniste respectivement.

La validation du modèle est effectuée à travers une série de tests expérimentaux et de simulation. Le but de ces tests est de valider le modèle sous différents points et conditions de fonctionnement, c'est-à-dire différentes charges utiles et différentes fréquences et amplitudes d'entrée de commande. Les dix scénarios différents ont été testés en simulation et à titre expérimental. Les figures de 3.19 à 3.26 montrent les résultats de tous les tests effectués. Le tableau 3.4 condense les résultats des tests effectués pour la validation du modèle.

Chapitre 4. Commande par retour de sortie

Les performances de trois approches de contrôle différentes sont comparées pour la régulation et le suivi de la position angulaire de la configuration biaisée du bras robotique proposé. Les contrôleurs sélectionnés pour cette étude sont: le contrôle PID, le contrôle du mode de glissement (SMC) et le contrôle adaptatif (AC).

Aux fins de comparaison, nous commençons par la mise en œuvre d'un contrôle PID, qui est l'une des approches les plus simples pour le contrôle de la position angulaire de l'articulation robotique. La Fig. 4.3 montre le diagramme pour le contrôleur PID. Dans ce diagramme, la plante est décrite par le modèle présenté dans Eq.(3.21).

En matière de contrôle des systèmes non linéaires, le SMC est l'une des stratégies les plus appliquées en raison de sa robustesse et de sa conception relativement simple. Le SMC est un type spécifique de VSC, qui consiste en une loi de contrôle de commutation

à grande vitesse. Le SMC a pour objectif de piloter les états de l'usine sur une surface définie par l'utilisateur (surface glissante). La structure du contrôle appliqué dépendra du fait que la trajectoire de la plante soit au-dessus ou au-dessous de la surface de glissement [27]. Le schéma de principe de ce contrôleur est présenté dans la Fig. 4.4.

Les techniques de contrôle adaptatives comprennent un ensemble de techniques différentes permettant de régler automatiquement les paramètres de contrôle en temps réel, afin de maintenir les performances souhaitées tout en gérant les incertitudes des paramètres et des modèles [28]. Différentes techniques de contrôle adaptatif ont été appliquées pour le contrôle des fils SMA. La méthode choisie pour cette étude comparative sur le contrôle du retour de sortie est le contrôle adaptatif présenté par les auteurs dans [29].

Simulation et résultats expérimentaux

Les trois approches de contrôle présentées sont testées en simulation et des expériences sous différents scénarios. Les scénarios d'opération comprennent la régulation et le suivi des positions angulaires et des conditions de charge utile souhaitées.

Les figures 4.6 à 4.11 montrent les résultats de tous les tests en simulation. La table 4.2 résume les résultats pour la régulation de position et la table 4.3 montre les résultats du suivi de la position avec et sans charge utile.

Les résultats expérimentaux sont illustrés aux figures 4.12 à 4.17. La table 4.5 résume les résultats pour la régulation de position et la table 4.6 affiche les résultats pour le suivi de position.

Le contrôle adaptatif et le SMC se révèlent capables de gérer la dynamique non linéaire du système pour la régulation et le suivi. Le contrôle adaptatif présente des résultats légèrement meilleurs dans la plupart des tests. Le contrôle adaptatif s'est avéré être la meilleure approche pour le type de système traité dans cette thèse.

Chapitre 5. Filtre de Kalman étendu et observateur à mode glissant

Lorsqu'on parle d'estimation pour les SMA, les recherches dans la littérature sont limitées et portent principalement sur l'estimation des états mécaniques (position et vitesse) des actionneurs à base de SMA. Nous avons trouvé peu d'observateurs pour l'estimation des états de fil SMA où la dynamique de commutation du SMA est prise en compte. Cependant, le plus souvent, les travaux trouvés dans la littérature ne fournissent aucune analyse de stabilité ou de convergence. Le chapitre 5 décrit le processus

de modélisation permettant d'obtenir un modèle observable du bras robotique à fil SMA sans commutation et adapté au développement d'un observateur d'état à entrées inconnues.

Pour répondre au besoin de la loi de commutation pour l'estimation d'état, une approche de saisie inconnue est proposée. Considérer le terme de commutation ($\dot{\xi}$) comme une entrée inconnue élimine la commutation du modèle du système. Avec cette approche, il n'est pas nécessaire de déterminer la loi de commutation du système. Le système devient un système non linéaire sans commutation, permettant la mise en œuvre de techniques plus simples d'estimation et de contrôle.

En prenant le taux de fraction de martensite comme entrée inconnue, un modèle de la forme en Eq.(5.3) est proposé. Par conséquent, la théorie du modèle de perturbation singulière est appliquée au modèle avec une entrée inconnue. Cette procédure est effectuée afin de gérer la grande rigidité du système. Nous considérons la vitesse angulaire comme un état quasi statique et son équation dynamique est remplacée par un équivalent algébrique. Après la normalisation des équations d'état du bras robotique biaisé, nous obtenons le modèle présenté dans Eq.(5.14), avec un nouveau vecteur d'état $x_s = \begin{bmatrix} \theta & T & \sigma & \xi \end{bmatrix}$.

Il est clair que le modèle présenté dans Eq.(5.14) n'est pas observable conformément à la théorie proposée par [30] pour une observabilité non linéaire d'entrée inconnue. En supposant que la vitesse angulaire puisse être "mesurée", en calculant la dérivée de la position angulaire mesurée, nous définissons un nouveau vecteur de sortie ($h_s(t)$) décrit dans Eq.(5.21), étant donné que le tenseur $\mu_1^1 = \frac{A_1 r_1}{b}\Omega \neq 0 \ \forall x(t)$. Nous pouvons en conclure que l'entrée inconnue est observable depuis la sortie à tout moment et à tous les points d'opération. La codistribution complète observable est calculée à l'aide de la méthode proposée par [30]. La codistribution observable Ω_1 a le rang complet et toutes les différences d'état. En conclusion, le système présenté est faiblement localement observable.

Enfin, le modèle présenté dans Eq.(5.14) est discrétisé par une approximation d'Euler de premier ordre.

Filtre de Kalman étendu à entrées inconnues

Pour l'estimation de l'état et des entrées inconnues d'un système du type traité dans cette thèse, nous proposons un filtre de Kalman étendu avec des modes glissants pour une estimation d'entrée inconnue. Cet observateur est présenté dans les équations (5.38) à (5.45).

L'entrée inconnue est estimée avec un estimateur basé sur le mode glissant. En utilisant cette approche, l'entrée inconnue peut être estimée à l'aide d'une surface glissante définie en fonction du terme d'erreur utilisé pour estimer l'entrée inconnue donnée (e_{i_k}).

Une analyse de convergence et de stabilité est présentée pour l'observateur d'état à entrées inconnues proposé.

Validation d'observateur

Trois scénarios ont été testés en simulation (avec et sans bruit de sortie ajouté) et en expériences. Les figures de 5.2 à 5.7 montrent les résultats de ces tests. Les tables 5.4 et 5.6 condensent les résultats des tests effectués pour la validation de l'observateur.

Le filtre de Kalman étendu proposé avec estimation de l'entrée inconnue en mode glissant (EKF-UI) est capable de traiter le bruit de mesure avec une estimation moins précise de l'entrée inconnue, sans affecter la précision de l'estimation d'état. Il montre une convergence rapide et une bonne précision sous différents scénarios avec et sans charge utile.

Chapitre 6. Commande par retour d'état

La stratégie de contrôle basée sur l'équation de Riccati en fonction de l'état (SDRE) est une technique de régulation optimale non linéaire. La méthode SDRE implique la factorisation (paramétrisation) du système non linéaire en le produit d'une fonction à valeur matricielle (dépendante de l'état) et du vecteur d'état. Cette factorisation amène le système à une structure linéaire ponctuelle avec des matrices de coefficients dépendants de l'état (SDC) [31].

Peu de recherches ont été rapportées sur la mise en œuvre du contrôle SDRE pour les systèmes basés sur SMA. La difficulté de mesurer les états des fils SMA et l'exigence d'un retour d'état complet rendent cette technique difficile à mettre en œuvre expérimentalement. Sur la base de la synthèse de la littérature, nous proposons la mise en œuvre de l'approche de contrôle SDRE pour la régulation et le suivi de la position angulaire du bras robotique à fil SMA biaisé présentés au Chapitre 3. Une approche basée sur l'observateur est utilisée pour fournir le vecteur d'état complet à la boucle de contrôle SDRE.

L'implémentation des techniques de contrôle SDRE nécessite un système non linéaire contrôlable de la classe $\mathcal{C}^1$, c'est-à-dire pouvant être dérivé en permanence. Le système

non linéaire dans Eq.(6.13) est un modèle de commutation dans lequel la loi de commutation dépend de plusieurs facteurs, tels que les températures de transformation, la température et les contraintes du fil SMA et leurs dérivées temporelles respectives. Cependant, il est possible d'inférer la loi de commutation directement à partir du signe de la dérivée temporelle de la fraction de martensite $\left(\dot{\xi}\right)$. Nous rapprochons la fonction de commutation d'une fonction différenciable continue en implémentant des fonctions arc tangentes du taux de fraction de martensite. Nous pouvons reformuler Eq.(3.7) et Eq.(3.8) comme indiqué dans Eq.(6.19).

Par conséquent, le modèle obtenu par cette procédure n'est pas entièrement contrôlable en raison de la dépendance de la position angulaire (x_1) sur la température (x_3) et du stress (x_4). Nous proposons un nouveau vecteur d'état contrôlable réduit $x_c = \begin{bmatrix} \theta & \dot{\theta} & \sigma \end{bmatrix}^\top$ et le vecteur d'état non contrôlable $\eta = T$, où le vecteur d'état non contrôlable est stable d'entrée à sortie. Enfin, nous réécrivons le modèle comme indiqué dans Eq.(6.24).

Le modèle dans Eq.(6.24) convient à l'application du SDRE en temps continu. Ce modèle est ensuite discrétisé à l'aide d'une approximation d'Euler du premier ordre afin d'obtenir un modèle à temps discret pour la mise en œuvre de SDRE à temps discret. Avant la discrétisation, la théorie du modèle de perturbation singulière est à nouveau appliquée pour traiter la rigidité du système.

Après paramétrage des modèles à temps continu et discret, les contrôles SDRE et DSDRE proposés pour le bras robotique SMA biaisé sont testés en simulation et en expérimentation.

Les figures 6.1 à 6.6 montrent les résultats de tous les tests pour SDRE, DSDRE et le contrôle adaptatif en simulation. La table 6.1 résume les résultats pour la régulation de position dans la simulation, tandis que la table 6.2 montre les résultats du suivi de position avec et sans charge utile.

Les figures 6.7 à 6.12 montrent les résultats de tous les tests effectués pour les contrôles SDRE, DSDRE et adaptatif à titre expérimental. Le tableau 6.3 résume les résultats de la régulation de position dans les expériences. Le tableau 6.4 affiche les résultats du suivi de position avec et sans charge utile.

Le contrôle DSDRE s'est révélé être la meilleure approche pour la régulation et le suivi de la position angulaire du système traité dans cette thèse. Cette approche montre une réponse plus rapide et une erreur relative plus faible au total pour tous les scénarios testés.

Chapitre 7. Conclusions et perspectives d'avenir

Cette recherche a présenté la mise en œuvre expérimentale d'une approche de commande par retour d'état pour la position angulaire d'un bras robotique léger (LWRA) actionné par des fils en alliage à mémoire de forme (SMA).

La mise en œuvre expérimentale d'approches de contrôle par retour d'état a été limitée en raison du manque d'accès aux états du fil SMA. Ces techniques de contrôle permettent d'obtenir de meilleurs résultats en termes de précision et de temps de réponse en contrôle, en fonction des résultats obtenus dans cette recherche. La mise en œuvre de l'interface EKF-UI proposée ouvre la possibilité à la mise en œuvre expérimentale de ce type d'approches, permettant ainsi le développement d'approches de contrôle plus rapides et plus précises pour les systèmes basés sur SMA.

Chapter 1

Introduction

This thesis presents the design, estimation and control of a Lightweight Robotic Arm (LWRA) actuated by Shape Memory Alloy (SMA) wires . In section 1.1, the research context is discussed, followed by the motivation to conduct this study and the research challenges in section 1.2. Section 1.3 presents the aim and scope of this study. The scientific and practical contributions of this research are outlined in section 1.4. Finally, in section 1.5 the structure of the thesis is presented and section 1.6 lists the publication outputs of this research and related collaborative projects.

1.1 Context of the Study

Since their introduction as a military asset, Unmanned Aerial Vehicles (UAV) have come a long way, gaining big importance in different fields of industry and becoming an ever increasing market in the last decade. Only in 2016, the global market for commercial applications of drone technology was estimated at about $2 billion dollars with exponential growth projections to as much as $127 billion by 2020 [32]. The advances on UAV technology have led to an important commercialization and huge diversification on the use of UAVs. Nowadays, commercial applications of UAVs can be found in a wide range of industries, such as infrastructure, agriculture, transport, security, entertainment and media, insurance, telecommunications and even mining.

Up until now, most of UAV applications involve only monitoring and/or remote sensing tasks, implicating little to no physical interaction with the environment. It is only in recent years that the field of aerial manipulation has become a topic of interest for researchers and industrial development. The possibility to equip a UAV with an actuator, to give it the ability to interact with its surroundings, opens a wide range

of possibilities for new applications. Currently, a variety of applications implementing aerial manipulation can be found in the literature. For example, in [33] a valve turning task with a double arm manipulator is discussed. In [34], the authors propose a canopy sampling of the environment. Furthermore, in [6] a simple lightweight actuator for door opening tasks is presented. The authors in [16] propose a system for contact inspection on bridges using aerial manipulation, and in [17] the design and control of a compliant dual arm for object grasping is discussed.

In spite of the mentioned advances and new implementations on aerial manipulation, there still exist multiple issues that need to be addressed in the field of aerial manipulation. Some of the main issues are listed as follows [35]:

1. Due to the lack of a stable base, any movement of the manipulation mechanism and/or the payload, directly affects the position and stability of the UAV;
2. The propulsion performance of UAVs varies according to the surroundings, such as, open spaces or walls in close vicinity;
3. UAVs are highly nonlinear coupled systems, often under-actuated, which increases the complexity of their control design;
4. The payload limitation of most UAV systems renders impossible for them to accommodate industrial dexterous robotic manipulators.

The proposal in this research seeks to provide an alternative solution for the fourth point, the limited payload capability of UAVs. Although there has been progress on the development of lightweight manipulators, employing lightweight materials and different methods of manufacturing, the current conventional actuators are an important constraint to achieve lighter systems. Conventional actuators, such as servomotors or hydraulic actuators, have a low Weight/Power ratio (See Fig. 2.9) and frequently, they do not allow a further reduction in weight and/or size without an important lost on power capabilities of the manipulator. The limited availability of payload on small aerial vehicle has motivated the robotic community to further study the problem [1–3]. However, the available solutions are still not sufficient when applied to small UAVs, where the available payload is considerably reduced.

To address this issue, it is necessary to look into the implementation of unconventional actuators, such as intelligent materials, as for instance among others, the SMAs. These alloys are materials with Shape Memory Effect (SME), a phenomenon which allows them to recover their original form upon external mechanical or thermal stimuli. These characteristic allows them, under specific circumstances, to generate movement, thus

actuate systems (the full characteristics and dynamics of these materials are given in Chapter 2).

Although the implementation of SMAs as alternative actuators for lightweight manipulators promises numerous advantages, it also presents several challenges that need to be addressed. The implications and difficulties of the implementation of SMAs as alternative actuators are discussed in the next subsection.

1.2 Problem statement and Motivation

SMA wires are a great alternative to conventional actuators due to their high force to weight ratio. However, their highly nonlinear dynamics makes them difficult to be controlled, thus to develop applications based on them. A set of techniques capable of dealing with highly nonlinear systems, are those of the state feedback control. This control approach allows to take into account the behavior of all the states of the controlled system to compute the control input. In the case of SMA wires, few research works are reported in this area [18, 19]. In addition, none of them, to the best of our knowledge, has reported experimental results. The main reason for this is the lack of access to some of the states of the SMA wire during implementation. Inner states of the material, such as martensite fraction (see section 2.2), are impossible to measure in out-of-the-lab environments. Other states, such as the temperature, are difficult to measure, as the thickness of the wires represents a challenge in this aspect.

In order to implement and test any feedback control approach, it is necessary to develop a way to access these states without increasing the weight of the prototype with numerous sensors. The best solution to this issue is the implementation of a state observer, in order to estimate the states. Nevertheless, the estimation of the SMA wire states carries its own set of challenges, due to the hysteretic nature of SMA wires. Although some efforts have been made on this topic, most of the implementations reported in the literature lack formal proofs of stability for a switching system or even observability proofs of the model. This work is aimed to address these problems.

1.3 Aim and Scope

The aim of this study is the experimental implementation of a state feedback control for position regulation of a lightweight robotic arm actuated by SMA wires. This control approach will have to fulfill the following requirements:

- Real-time compatible. The selected control approach must be feasible to be applied experimentally in real-time.
- Capable of dealing with the highly nonlinear dynamics of the SMA wires.
- Show a better performance than current output feedback control approaches in terms of accuracy and response time.

The development of a state feedback control implies the implementation of a state estimation technique as discussed in the previous subsection. Consequently, the design of an observable model and state estimation are part of the scope of this work. A formal study on the observability of the proposed mathematical model and convergence of the developed estimation technique is provided.

1.4 Significance of the Study

The contributions of this research project in the fields of lightweight manipulators and SMA wires observation and control are highlighted in this section.

1. *A Lightweight Robotic Arm (LWRA) actuated by SMA wires is proposed and tested in simulation and experiments.*
   A lightweight robotic arm actuated by SMA wires with a weight of less than 100 g is tested in simulation and experiments under different scenarios, including a grasping and carrying task.
2. *A nonlinear non-switched observable model for the LWRA actuated by SMA wires is presented.*
   A nonlinear non-switched mathematical model using the singular perturbation theory and unknown inputs is proposed for a lightweight robotic arm actuated by SMA wires. This technique is based on constitutive modeling of SMA.
3. *The nonlinear observability is proven.*
   A nonlinear observability analysis for system with unknown inputs is performed for the proposed nonlinear non-switched system of the proposed LWRA.
4. *An Extended Kalman Filter with state and unknown input estimation (EKF-UI) is proposed.*
   An EKF-UI is proposed for the estimation of states and unknown input of the LWRA, based on a nonlinear non-switched observable model. The proposed observer estimates the mechanical states of the system's overall actuation (angular position and velocity) and its internal states, such as martensite fraction and stress.

5. *A stability and convergence analysis is carried out.*
   A stability and convergence analysis is performed for the proposed EKF-UI, given necessary conditions for convergence on the estimation of the states and unknown input.

6. *A controllable continuously differentiable model is proposed.*
   A controllable model is proposed based on arctangent functions to render the model continuously differentiable.

7. *A State-Dependent Riccati Equation (SDRE) control approach is developed for the proposed system.*
   The SDRE control is tested in simulation and experiments in continuous and discrete-time.

8. *A comparative study among different approaches in control theory is carried out.*
   The results of different output feedback and state feedback control techniques are quantitatively and qualitatively compared, for different scenarios.

1.5 Thesis Outline

The remaining of this thesis is formed by six further chapters, organized as detailed in the following paragraphs.

In Chapter 2, an analysis of existing lightweight aerial manipulators is given. Subsequently, the theory on SMAs and their dynamics is discussed. Finally, an overview of the state of the art on applications and mathematical models for SMAs is given.

In Chapter 3, the mechanical design of the proposed LWRA actuated by SMA wires is presented. The mathematical model is then presented and an experimental validation is discussed.

In Chapter 4, a comparative study among three different approaches of output feedback control is presented. The three proposed controllers are tested in simulation and experimentally. This study is later used for comparative analysis with a state feedback control approach.

Chapter 5 presents the modeling process to obtain a non-switched observable model of the proposed lightweight robotic arm. Subsequently, an Extended Kalman Filter with state and unknown input estimation (EKF-UI) is proposed together with a stability and convergence analysis. Finally, the proposed observer is tested in simulation and experiments.

Chapter 6 details the modeling process to obtained a controllable model suitable for SDRE control implementation, in continuous and discrete time. This model is developed based on the model presented in Chapter 3. A continuous-time SDRE control and a discrete-time SDRE are presented and tested in simulation and experiments. The results of these two control approaches are compared with the results of the Adaptive Control approach presented in Chapter 4.

Finally, Chapter 7 concludes the thesis with the summary of the findings and contributions, followed by an outlook of future projects.

1.6 Publications

Part of the scientific contributions and content of this thesis have been published in journal and conference proceedings. This publications can be accessed at the following sources:

- S. Quintanar-Guzmán, S. Kannan, H. Voos, M. Darouach, and M. Alma, "Adaptive control for a lightweight robotic arm actuated by a shape memory alloy wire," in *ACTUATOR 2018 16th International Conference on New Actuators*, 2018
- S. Quintanar-Guzmán, S. Kannan, H. Voos, M. Darouach, and M. Alma, "Experimental validation of adaptive control for a shape memory alloy actuated lightweight robotic arm," in *ASME. Smart Materials, Adaptive Structures and Intelligent Systems, Volume 1: Development and Characterization of Multifunctional Materials; Modeling, Simulation, and Control of Adaptive Systems; Integrated System Design and Implementation*, no. 51944, p. V001T03A032, 2018
- S. Quintanar-Guzmán, S. Kannan, H. Voos, M. Darouach, and M. Alma, "Observer design for lightweight robotic arm actuated by shape memory alloy (SMA) wire," in *14th International Workshop on Advanced Control and Diagnosis (ACD)*, 2017
- S. Quintanar-Guzmán, S. Kannan, A. Aguilera-González, M. A. Olivares-Mendez, and H. Voos, "Operational space control of a lightweight robotic arm actuated by shape memory alloy wires: A comparative study," *Journal of Intelligent Material Systems and Structures*, vol. 30, no. 9, pp. 1368–1384, 2019
- S. Quintanar-Guzmán, S. Kannan, M. A. Olivares-Mendez, and H. Voos, "Lightweight robotic arm actuated by shape memory alloy (SMA) wires," in *2016 8th International Conference on Electronics, Computers and Artificial Intelligence (ECAI)*, pp. 1–6, June 2016

- S. Quintanar-Guzmán, S. Kannan, M. A. Olivares-Mendez, and H. Voos, "Operational space control of a lightweight robotic arm actuated by shape memory alloy (SMA) wires," in *ASME. Smart Materials, Adaptive Structures and Intelligent Systems, Volume 2: Modeling, Simulation and Control; Bio-Inspired Smart Materials and Systems; Energy Harvesting*, no. 50497, p. V002T03A012, 2016

In cooperation with different colleagues, various conference papers were published as result of lateral projects on SMA wires not completely under the scope of this thesis.

- S. Kannan, S. Bezzaoucha, S. Quintanar-Guzmán, J. Dentler, M. A. Olivares-Mendez, and H. Voos, "Hierarchical control of aerial manipulation vehicle," in *International Conference on Mathematical Problems in Engineering, Aerospace and Sciences*, vol. 1798 of *American Institute of Physics Conference Series*, p. 020069, Jan. 2017
- L. A. van der Elst, S. Quintanar-Guzmán, and J.-R. Hadji-Minaglou, "Design of an electromechanical prosthetic finger using shape memory alloy wires," in *2017 IEEE International Symposium on Robotics and Intelligent Sensors (IRIS)*, pp. 56–61, October 2017
- S. Kannan, S. Bezzaoucha, S. Quintanar-Guzmán, M. A. Olivares-Mendez, and H. Voos, "Adaptive control of robotic arm with hysteretic joint," in *Proceedings of the 4th International Conference on Control, Mechatronics and Automation*, ICCMA '16, (New York, NY, USA), pp. 46–50, ACM, 2016
- S. Kannan, S. Quintanar-Guzmán, S. Bezzaoucha, M. A. Olivares-Mendez, and H. Voos, "Adaptive control of hysteretic robotic arm in operational space," in *Proceedings of the 5th International Conference on Mechatronics and Control Engineering*, ICMCE '16, (New York, NY, USA), pp. 92–96, ACM, 2016
- S. Kannan, S. Quintanar-Guzmán, J. Dentler, M. A. Olivares-Mendez, and H. Voos, "Control of aerial manipulation vehicle in operational space," in *2016 8th International Conference on Electronics, Computers and Artificial Intelligence (ECAI)*, pp. 1–4, June 2016

Within the framework of this research, the following research projects with student were conducted:

- K. Paul, "Development of a robotic manipulator based on Shape Memory Alloy wires," Master's thesis, University of Luxembourg, Luxembourg, 2018

- L. A. van der Elst, "Design of an electromechanical prosthetic finger using shape memory alloy wires," Master's thesis, University of Luxembourg, Luxembourg, 2017

Chapter 2

Lightweight aerial manipulators

This chapter presents a literature overview on aerial manipulation and the necessary concepts on Shape Memory Alloy (SMA) wires to fully comprehend the following chapters on observation and control of systems actuated by SMA wires. First, a review of the existing solution for lightweight aerial manipulation reported in the literature is presented in section 2.1. Following, a lightweight aerial manipulator design based on SMA wires is proposed and the theory and characteristics of SMAs are laid out in section 2.2. Finally, a literature overview on current SMA wire applications reported in literature is discussed in section 2.3 and the conclusions of the chapter presented in secition 2.5.

2.1 Aerial Manipulators

Aerial manipulation is defined, in a general fashion, as the action of grasping, transportation, positioning, and/or assembly of mechanical parts, instruments, etc., performed by a Vertical Take-off and Landing (VToL) Unmanned Aerial Vehicle (UAV) equipped with a gripper and/or robotic arm [20]. In recent years, aerial manipulation has attracted increasing interest as a relatively new field of research. The ability of interacting with the environment from an aerial base, opens the possibility to a wide range of applications, such as remote inspection in areas difficult to reach for humans [47], automated package delivery [20], construction tasks in hostile environments [48], among others.

The field of aerial manipulation includes a wide range of aspects, such as, study and design of aerial platforms, actuators, grippers and end-effectors, dynamic interaction between UAV and aerial manipulator, control and estimation development, trajectory planning, and environment interaction (sensing of the environment, camera configuration, etc.).

FIGURE 2.1: ARCAS multirotor with the attached 6-DoF manipulator [1].

In the literature, different types of aerial manipulators for different purposes can be found, for example, the authors in [16] present a one Degree of Freedom (DoF) actuator designed for an octo-rotor UAV to conduct hammering test by applying contact force. On the other hand, we find approaches with hyper-redundant manipulators with numerous DoF. The authors in [2] present a set of two seven DoF manipulators to perform a grasping task. These manipulators are designed to be mounted on a 20 kg payload helicopter (see Fig. 2.2). In [1], the authors present a novel mechanism considering a moving battery to counterweight the statics of a 6-DoF robotic arm, and a multilayer architecture to control a multirotor UAV. This approach has a total weight of 8.2 kg including the counterweight system (see Fig. 2.1). Another example is the one presented in [3, 49], where the authors design and control a hyper-redundant manipulator for mobile manipulating UAVs. Here, the objective is to use the redundancy of the manipulator to minimize the influence of the manipulator on the stability of the aerial vehicle. In this approach, at least 9 servo joints are used, which leads to a total weight of approximately 1.3 Kg (see Fig. 2.3). In [50] the authors discuss the mechanical design of a 6 DoF aerial manipulator for the purpose of assembly using UAVs. Here, commercially available servos are used for actuation, with a total weight of 1.5 Kg.

The authors in [17] proposed the first anthropomorphic, compliant dual arm system designed for aerial manipulation with multirotor platform. The proposed systems has a total weight of 1.3 kg with a lifting capability of 0.3 kg per arm.

All the above mentioned aerial manipulators require UAVs with high payloads available to be installed on. None of these proposals can be implemented in small UAVs with payloads in the order of 500 grams. The next subsection reviews the existing solutions on lightweight manipulation, designed for small UAVs.

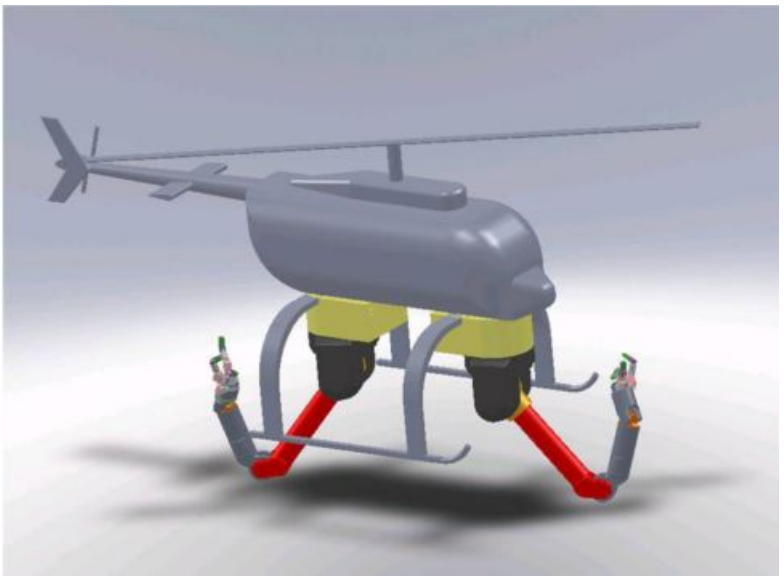

FIGURE 2.2: 7-DoF grasping manipulators for a 20 kg Payload Helicopter [2].

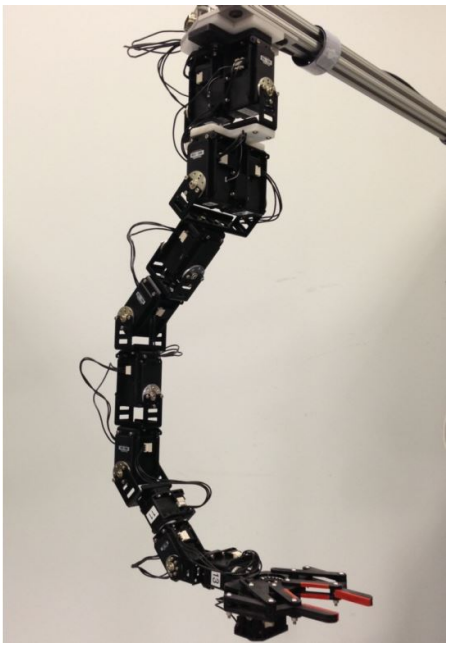

FIGURE 2.3: 6 DoF hyper-redundant manipulator for Mobile Manipulating UAVs [3]

2.1.1 Lightweight aerial manipulators

Lightweight approaches are found in the literature, where the manipulator is only capable to apply force to its surroundings. A simple aerial manipulator is presented in [4], where the UAV is capable of interacting with its environment by applying force to a wall. This manipulator is capable of forces up to 5 N and has a weight of 200 g (see Fig. 2.4). Similarly, the authors in [5] present the design, modeling and control of an

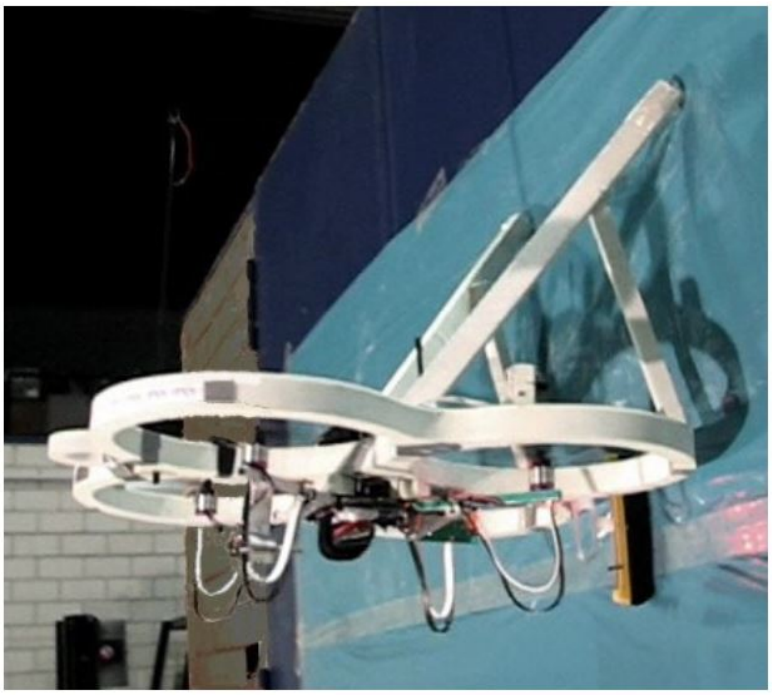

FIGURE 2.4: Flying robot applying force to a wall [4].

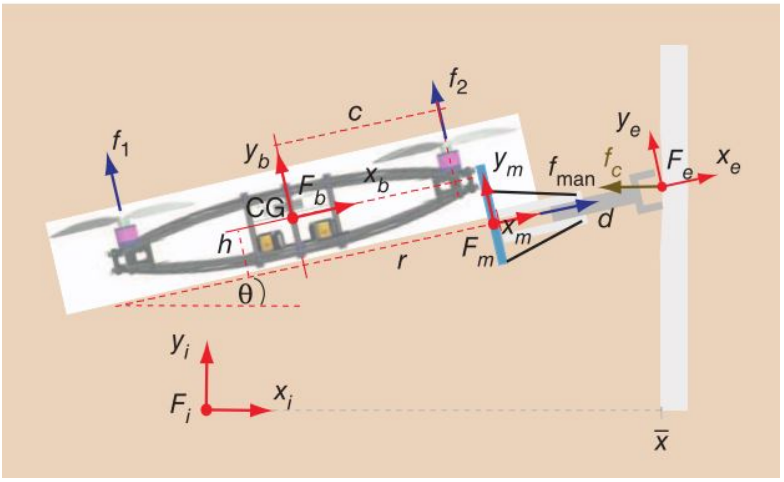

FIGURE 2.5: Schematics of the aerial manipulator proposed by the authors in [5].

aerial manipulator prototype, consisting of a miniature quadrotor helicopter capable of applying force to its surroundings while flying. The total weight of this design is around 100 g (see Fig. 2.5).

Among these non robotic arm lightweight approaches, in [6], an aerial robot with a manipulator to perform door opening missions is designed and controlled. Its weight is 160 g and it is composed of an air-bag actuator (see Fig. 2.6).

In [8], the control of a robotic multi-link arm is presented. This robotic arm is a 3-link

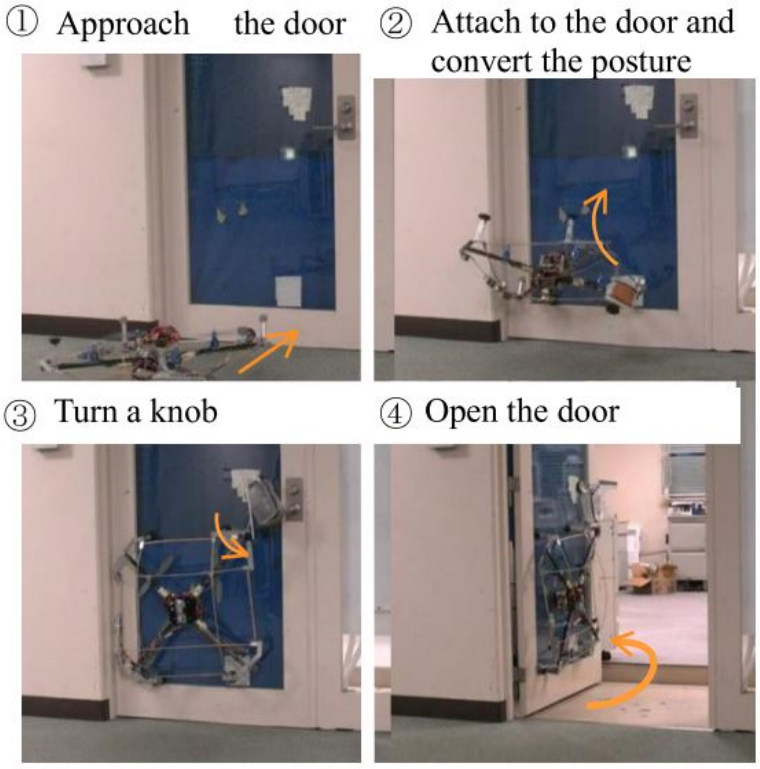

FIGURE 2.6: Implementation of the door opening mission [6]

lightweight manipulator with a total weight of 400 g, leaving a 200 g payload available (see Fig. 2.8). In [21], a lightweight compliant 2 DoF robotic arm is developed using linear servos, with a total weight of about 325 grams. In [7], the authors model and control a 3D printed 5-DoF lightweight robot arm with a total weight of 250 grams (see Fig. 2.7).

Conventional actuators such as servomotors, DC motors or hydraulic actuators present a low power to weight ratio as it can be appreciated in Fig. 2.9. Thus the design of lightweight robotic applications based on conventional actuators is limited. With this in mind, the present research proposes a lightweight robotic arm actuated by Shape Memory Alloy (SMA) wires and custom-designed 3D printed mechanisms, with a total weight of less than 100 g. This design is aimed for small UAVs with payloads up to 500 g, leaving more than 80 % of the payload available for carrying tasks. The following section details what SMAs are, their advantages and disadvantages as actuators, and applications found in the literature.

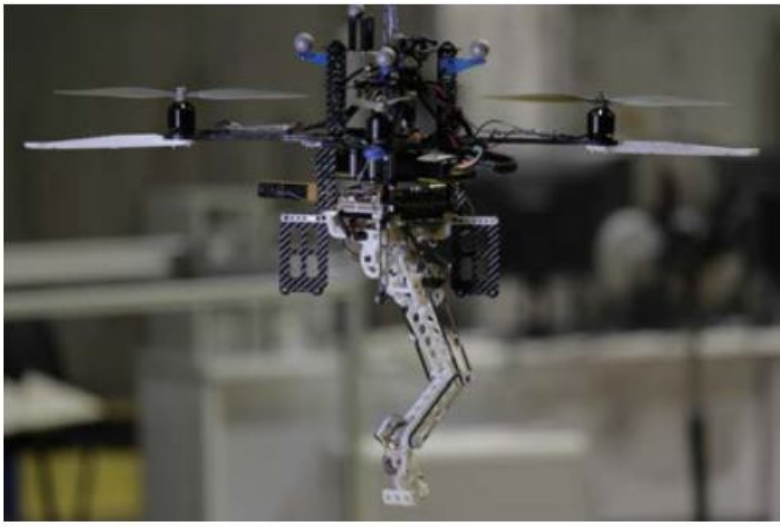

FIGURE 2.7: 3D printed 5-DoF lightweight robot arm [7].

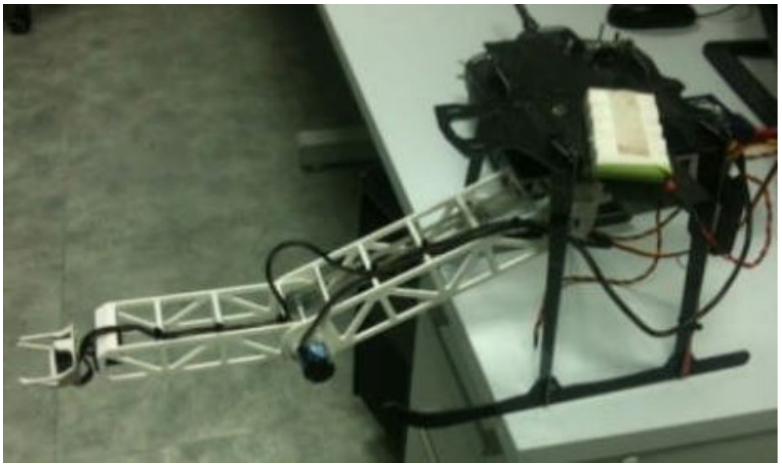

FIGURE 2.8: 3-link lightweight manipulator [8]

2.2 Shape Memory Alloys Background

Shape Memory Alloys (SMA) are a type of smart materials that can "remember" their original shapes after undergoing physical deformation. This type of alloys has the ability to recover its original pre-defined shape by applying certain stimuli such as thermo-mechanical variations. This phenomenon is known as Shape Memory Effect (SME). The SME occurs due to an inner transformation of the material's crystalline structure. This transformation happens between two phases called martensite and austenite. When the SMA is at a lower temperature its structure shifts to the martensite phase, which is a relatively soft and malleable phase, during which the wire can be easily deformed. When heated over its transformation temperature, the SMA wire transforms back into

the austenite phase, a hard phase, recovering its initial form and size [22]. This heating can be done through different techniques as it will be discussed later on.

Through the years, multiple materials have been found and developed which posses this SME. Among the most common SMAs one can find for example Nickle-Titanium, Gold-Cadmium and Copper-Zinc-Aluminum. However, the Nickel-Titanium alloy (commonly know as NiTi) has proven to be the more effective and suitable for engineering applications [51]. For this research, Flexinol (Dynalloy commercial NiTi wires) wires will be used for the develop of the model and experimentation.

2.2.1 Advantages and Limitations

There are several physical properties of NiTi wires being studied and tested, such as: shape memory, pseudo-elasticity, corrosion resistance, magnetic susceptibility, damping, mass ratio, miniaturization capability, noiseless operation, heat capacity, bio-compatibility, thermal conductivity, and other mechanical properties including hardness, impact toughness, fatigue strength and machinability. These properties make SMA wires ideal for a wide range of applications in fields like bio-medical, aerospace, engineering and sports equipment, micro-actuators, among others.

For their application in engineering as actuators, the main advantages are:

1. High power-to-weight ratio. As shown in Fig. 2.9, SMA wires have the highest weight to power ratio among all conventional actuators such as DC Motors or Hydraulic actuator. This characteristic makes them ideal for lightweight applications.

2. Small size. In addition to their lightweight, this material can be easily adapted to small environments and can be easily miniaturized. Together with mechanical simplicity, we can develop small size actuators with low production and maintenance costs.

3. Noiseless operation. Being driven by internal material transformation, SMA based actuators are virtually noiseless.

In spite of their numerous advantages, SMA wires also present different limitations and challenges.

1. Low energy efficiency. Since this material need thermal stimuli to change phases, it has a high energy consumption when compared to other classical actuators such as DC motor. During the actuation of these type of materials, most of the heat

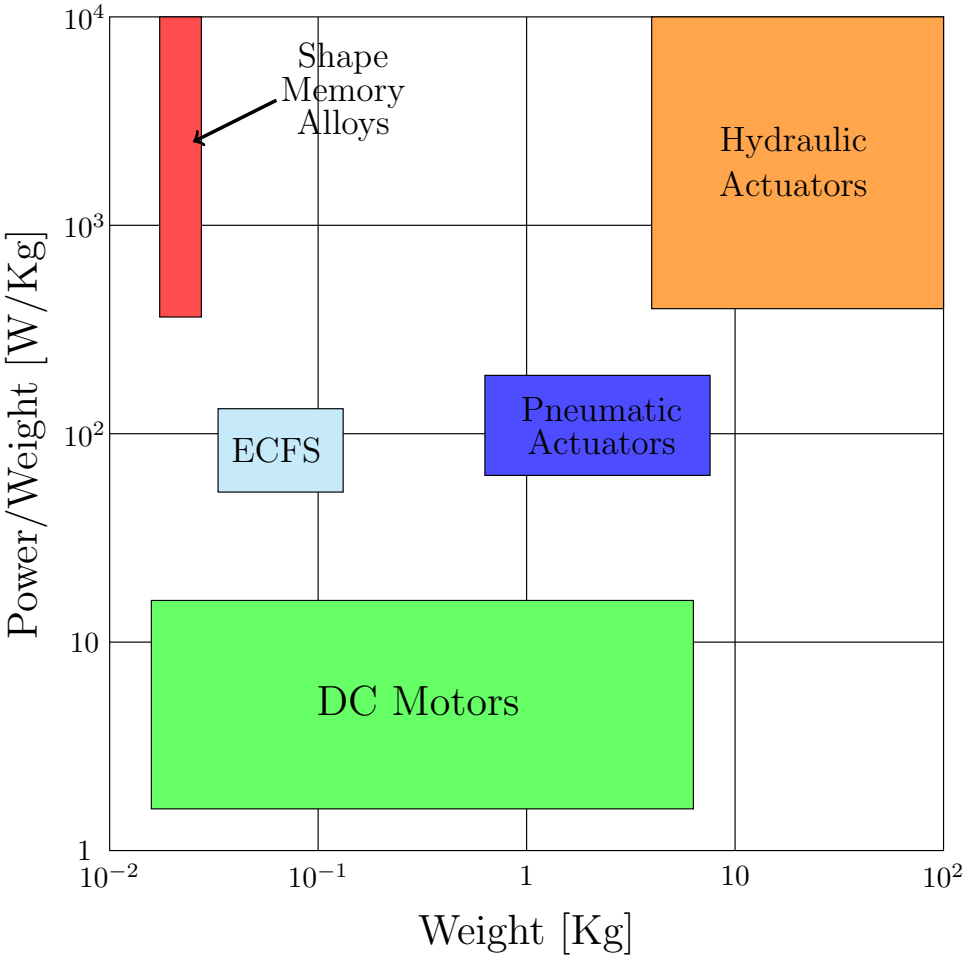

FIGURE 2.9: Comparison Weight/Power ratio for different kinds of actuators [9]

energy is lost to the environment, leading to a low efficiency, often less than 1% [52].

2. Degradation and fatigue. Exceeding the mechanical or thermal limits of SMA wires, if not damaging the memory effect, can seriously reduce their life span. However, even when working within the safe operational limits, SMA wires are susceptible of changes in parameters and dynamics due to degradation and thermal or mechanical fatigue. Good quality materials, as Flexinol, can reduce this effect.

3. Slow speed. The overall dynamic of a SMA based actuator depends on the thermal dynamics of the wire itself. The thermal dynamic is often restricted by environmental conditions (for cooling) or operational thermal limits (for heating) leading to slow response.

4. Nonlinearity. SMA wires are a great challenge in terms of control and mathematical modeling. Being a highly nonlinear system, their behavior is often difficult to model or predict, leading to inaccuracies in control performance. Among these

nonlinearities there are dead zone, strict thermal and mechanical limits, hysteresis, among other. Although all of these characteristics represent certain problem when using SMA wires, the main and most challenging one is hysteresis. Thus SMA wires have not only a big major loop of hysteresis, but also minor loops that appear when an incomplete transformation is carried out. This phenomenon will be further explained in the next subsection.

2.2.2 Hysteresis in SMA

Let us define a system $f(t, u)$ where $u(t)$ is the input signal and $y(t)$ the output. The system will be called hysteretic if its response is multivalued, depending not just on the input $u(t)$, but also on its previous values. The hysteresis loop $u - y$ defined by this behavior has dimensions of energy, and is the macroscopic manifestation of the energy dissipation and memory in the system [53]. In the specific case of SMA actuators, the most important hysteresis loop is the martensite fraction - temperature one. This loop occurs during the phase transformation of the SMA material due to the friction that the movement of the austenite-martensite interface generates [54]. Hysteresis is an important part of the dynamics of any SMA based actuator, and it is of great importance for model and control development.

Figure 2.10 shows the hysteresis loop of a single SMA wire based actuator under different amplitudes of sinusoidal voltages. In this figure, the major and minor hysteresis loops can be observed. The major loop occurs with a full cycle of the SMA wire transformation, thus a complete forward and reverse transformation martensite - austenite - martensite. The minor loops happen due to partial transformation cycles, when the SMA wire is heated or cooled without reaching its final transformation temperatures (M_f or A_f). Beside this behavior, it is reported in literature that the major and minor hysteresis loops can shift depending on conditions such as stress or pre-strain, causing the loop to extend vertically with an increase in stress or a decrease in applied pre-strain [54], as shown in Fig. 2.11.

The transformation temperature's stress dependency is approximately represented as [55]:

$$\frac{d\sigma}{dT} = \frac{1}{C_m} \tag{2.1}$$

where $\frac{1}{C_m}$ is the stress rate.

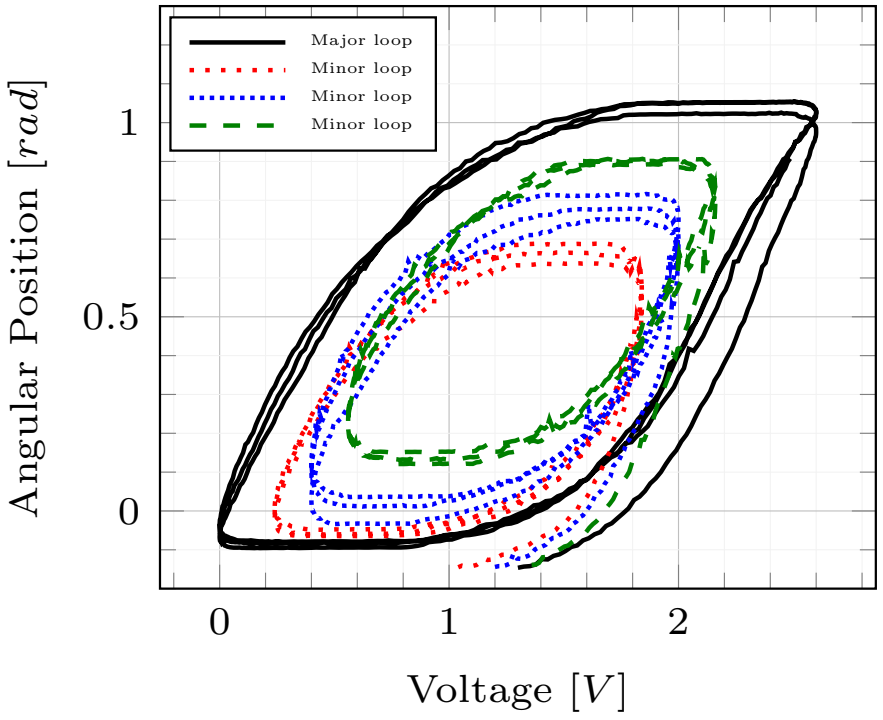

FIGURE 2.10: SMA wire major and minor $R_m - T$ hysteresis loops for a single SMA wire actuator. System response under different amplitudes of sinusoidal voltage.

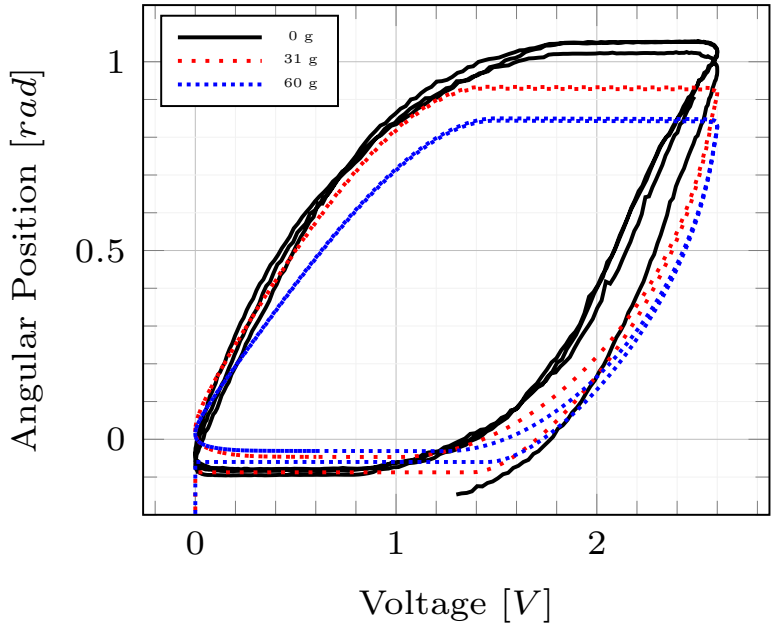

FIGURE 2.11: SMA wire hysteresis loops for different stresses for a single SMA wire actuator.

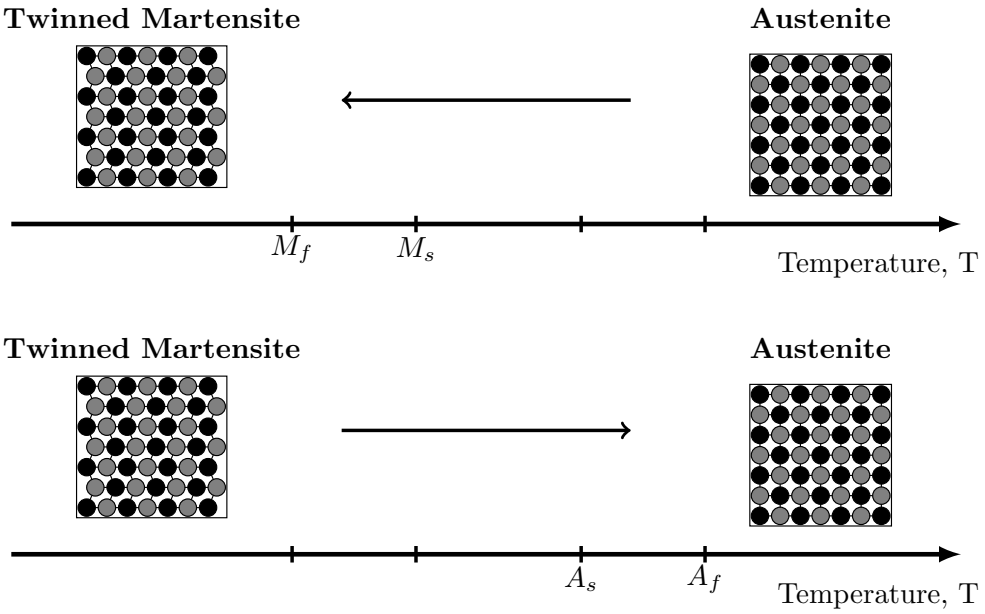

FIGURE 2.12: SMA crystalline structure transformation without mechanical loading [10].

2.2.3 Phases of SMA

SMAs consist of two different micro-structural phases, each one with different crystalline structures, thus different characteristics and behavior. The reversible transformation from one phase to another gives to SMAs their particular behavior. The first phase exists at high temperature and is called austenite (A, parent phase) while the second one called martensite (M, product phase) appears at low temperatures. This transformation, known as martensitic transformation, occurs by shear lattice distortion. In addition, the martensite phase can have two forms dependent on the different orientation of the crystalline structure: *twinned* martensite (M^t), and *detwinned* or reoriented martensite (M^d) [10].

The *forward transformation* (austenite to martensite) takes place when the system is cooled down in the absence of mechanical loading, resulting in *twinned martensite*. Upon heating, a *reverse transformation* occurs and the crystalline structure transforms back to austenite. Figure 2.12 shows the forward and reverse transformation with no applied load, together with the four characteristic SMA transformation temperatures. The forward transformation will start at the martensitic start temperature (M_s) and finish at the martensitic finish temperature (M_f) while for the reverse transformation starts at the austenitic start temperature (A_s) and finished at the austenitic (A_f), only under zero load. If the system stress is augmented by applying a mechanical load at low temperatures, there will be a transformation from *twinned martensite* to *detwinned martensite*, resulting in a shape change that will be retained even after the load is released. A further

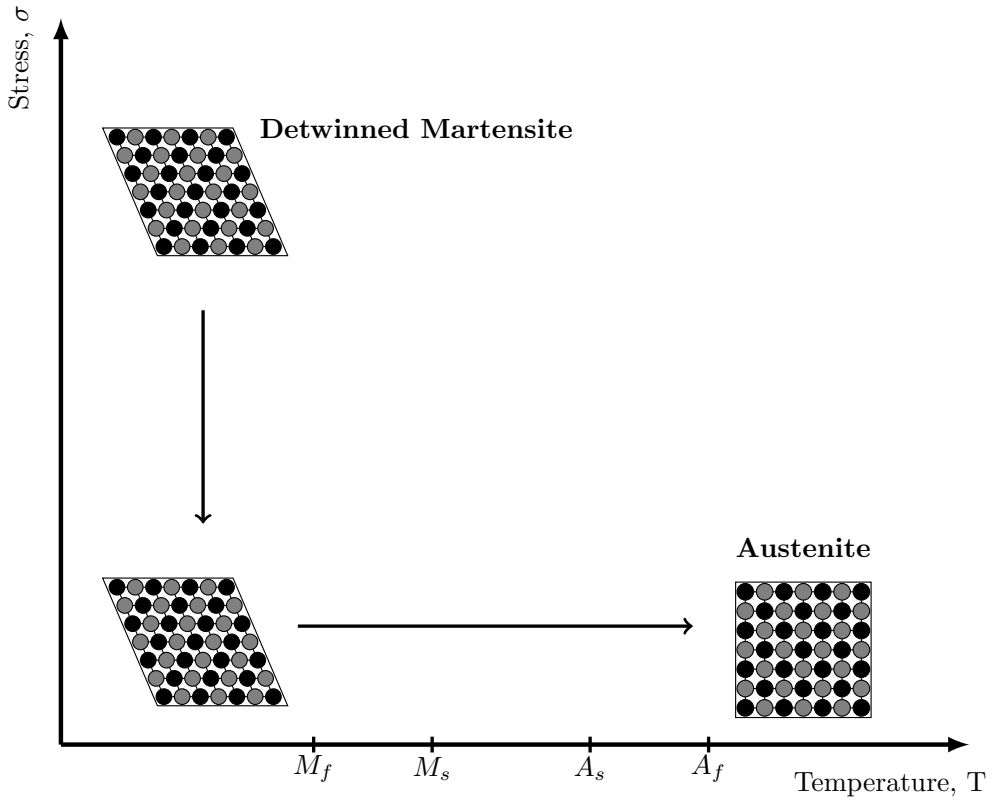

FIGURE 2.13: SMA crystal structure transformation, unloading and subsequent heating [10].

reverse transformation (heating over A_f) will lead to complete shape recovery (due to SME). When the SMA is cooled down again (below M_s), a forward transformation to twinned martensite will take place again, as shown in Fig. 2.13 [10].

Finally, when a reverse transformation takes place at a non zero load, a direct transformation from austenite to detwinned martensite occurs (See Fig. 2.14). It is important to notice that the transformation temperatures strongly depend on the magnitude of the applied stress. Higher stress will lead to higher transformation temperatures [10].

In the present dissertation it is assumed that the proposed SMA actuated robotic arm has a pre-stress always present and high enough to generate a direct transformation from austenite to detwinned martensite upon appropriate thermal stimuli.

2.2.4 Shape Memory Effect

Shape Memory Effect in the case of SMA can be categorized into 3 different types [56]

1. One-way memory effect. In this case, the material retains the deformation caused by external forces once these are removed. When heated over the transformation

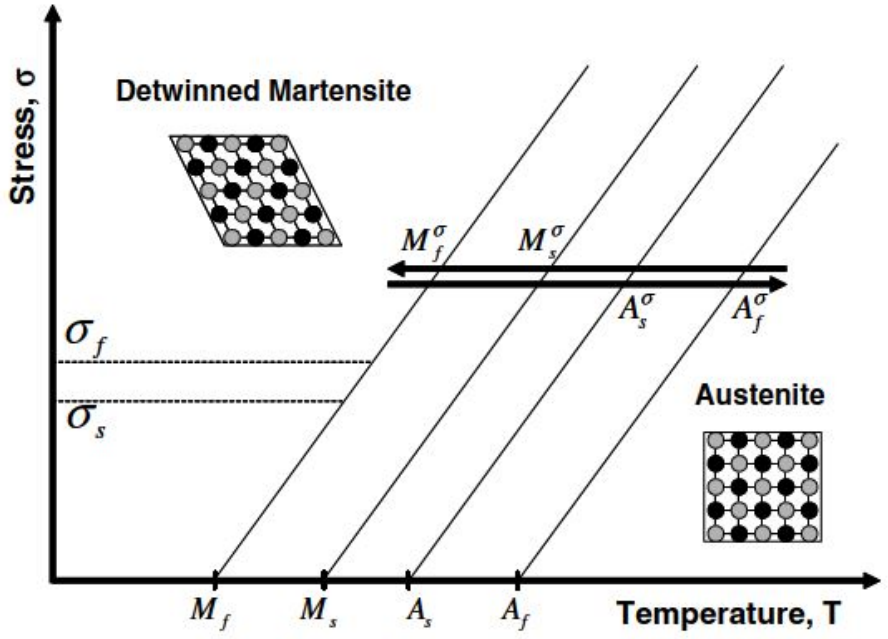

FIGURE 2.14: SMA crystal structure transformation, in presence of applied load [10].

temperature, it recovers its original shape, and subsequent cooling does not lead to any further deformation.

2. Two-way memory effect. Materials with this effect present the same behavior as the ones with one-way effect, with the exception that shape change occurs when cooling even with no external forces applied.

3. Pseudoelasticity. Phase transformation, hence shape change, occurs without thermal stimuli when mechanical loading is applied at temperatures over A_f.

The present work focuses on one-way memory effect wires for the design, control and observation of the proposed system.

2.2.5 Pseudoelasticity

The pseudoelasticity effect, also known as superelasticity, occurs when high levels of stress are applied to the SMA at temperatures above A_f. As discussed before, an increase in the stress levels results in an increase of the transformation temperatures. This increased temperature causes a stress induced reverse transformation (austenite - martensite), when the stress is released, a forward transformation takes place and the material transforms back to austenite. This transformation stress induced transformation, as the temperature induced, also presents a hysteretic behavior. The hysteresis of this phenomenon can be represented by the stress - martensite fraction ($\sigma - Rm$)

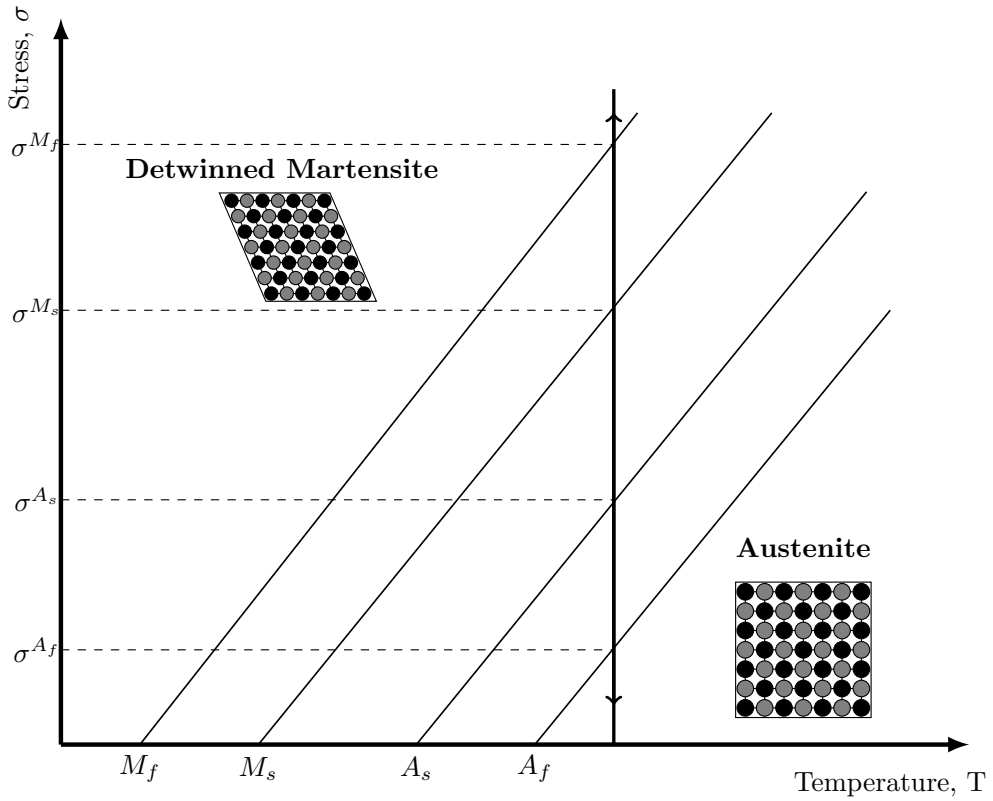

FIGURE 2.15: Pseudoelastic behavior of SMA [10].

hysteresis loop. The reverse transformation starts at σ^{M_s} and finishes at σ^{M_f}, while the forward transformation starts at σ^{A_s} finishing at σ^{A_f}, as shown in Fig. 2.15 [10].

The present work does not deal with pseudoelasticity, thus it is assumed that the transformations in the system occur due to thermal stimuli.

2.2.6 Heating and Cooling methods

As explain before, SMAs respond to thermal stimuli. To apply these stimuli, there are different methods for both heating and cooling processes. Table 2.1 summarizes the different cooling and heating techniques found in the literature. Each of these techniques are explained below.

2.2.6.1 Heating techniques

1. Resistive heating: also known as Joule effect, is the process by which a conductor produces heat when an electrical current is applied to its terminals. For SMA based micro or lightweight actuators, this is the most common technique due to

TABLE 2.1: Heating and cooling methods for shape memory alloys.

Heating	Cooling
Resistive heating	Natural convection
Capacitance-assisted resistive [57]	Forced convection
Ambient heating	Cools chips technology [58]
Peltier heating	Peltier cooling
Laser [59]	[60]
Induction [61]	

its convenience and susceptibility to miniaturization since it does not require any extra systems or moving parts.

2. Capacitance-assisted resistive: this process is also based on Joule effect, where the material is heated by applying an electric current. However, in this technique the current is applied by discharging a large capacitor, which decreases considerably the heating time [57].

3. Ambient heating: this technique consists in heating the surroundings of the SMA so thermal convection takes place. This can be done through any kind of fluid, such as air, or liquids, such as water or oil.

4. Peltier heating: Peltier effect is a temperature difference created by applying electric current across a junction between two semiconductor materials. Depending on the direction of the current and increase or decrease of temperature can be generated on every side of the device. The reduced available contact area between the SMA and the Peltier plate, is the greatest inconvenient of this approach. In addition, the high energy consumption of this method, often does not justify its implementation.

5. Laser: in this technique, laser light is used as a wireless thermal actuation energy. The SMA wire is irradiated with the laser source which produces a temperature rise. Currently, there are few studies on the effect that changing the laser parameters, such as wavelength and optical power, has on the heating effect of this method [59].

6. Induction: The inductive heat transfer is done through microwaves or electromagnetic fields, thus it does not require physical contact with the SMA [61].

2.2.6.2 Cooling techniques

1. Natural convection: this technique consists of cooling the device by contact with still fluids such as gases and liquids. Natural air convection is the most common

and easiest cooling approach but also the slowest. The immersion in different liquids, such as oil or water, has also been studied [62]. This method, although it provides a faster cooling, is inefficient and difficult to implement for small applications or lightweight approaches.

2. Forced convection: it consist in cooling the material by contact with a flow of fluid (gas or liquid). The effectiveness of this method depends on the flow rate and the type of fluid use. A study on this method is presented in [62]. In this study, it is clear that the smallest increment in the flow, even with air, results in a faster cooling dynamic. Nonetheless, it is important to mention that uncontrolled air flow introduces disturbances in the system.

3. Peltier cooling: Peltier effect, previously explained, is used for both, heating and cooling through thermal conduction.

4. Cool chips technology: this technology uses electrons to carry the heat from one side of a vacuum diode to the other. This method does not contain moving parts, thus is suitable for micro-applications [58].

2.2.7 SMA actuator layouts

As mentioned before, a one way SMA wire needs an opposite force to generate a mechanical deformation effort when cooling in order to generate movement. To generate this force there are different actuator layouts, each with different characteristics, advantages and disadvantages.

The SMA actuator layouts can be classified into different categories, most commonly by the number of SMA wires in the layout [63] or the type of movement they generate [64]. By the type of movement we can find two basic classifications: 1) Linear SMA wire actuator and 2) Rotary actuator. The linear actuator, as the name indicates, generates a linear movement, parallel to the SMA wire length (Fig. 2.16 (a)). On the other hand, the rotary actuator generates work over a revolute joint, which produces a rotary motion (Fig. 2.16 (b)).

The classification by number of SMA wires consists of three main types: 1) Single SMA wire, 2) Antagonistic SMA wires and 3) Bundle SMA wires. This classification is further subdivided according to the way the bias force is generated. Table 2.2 shows the complete classification.

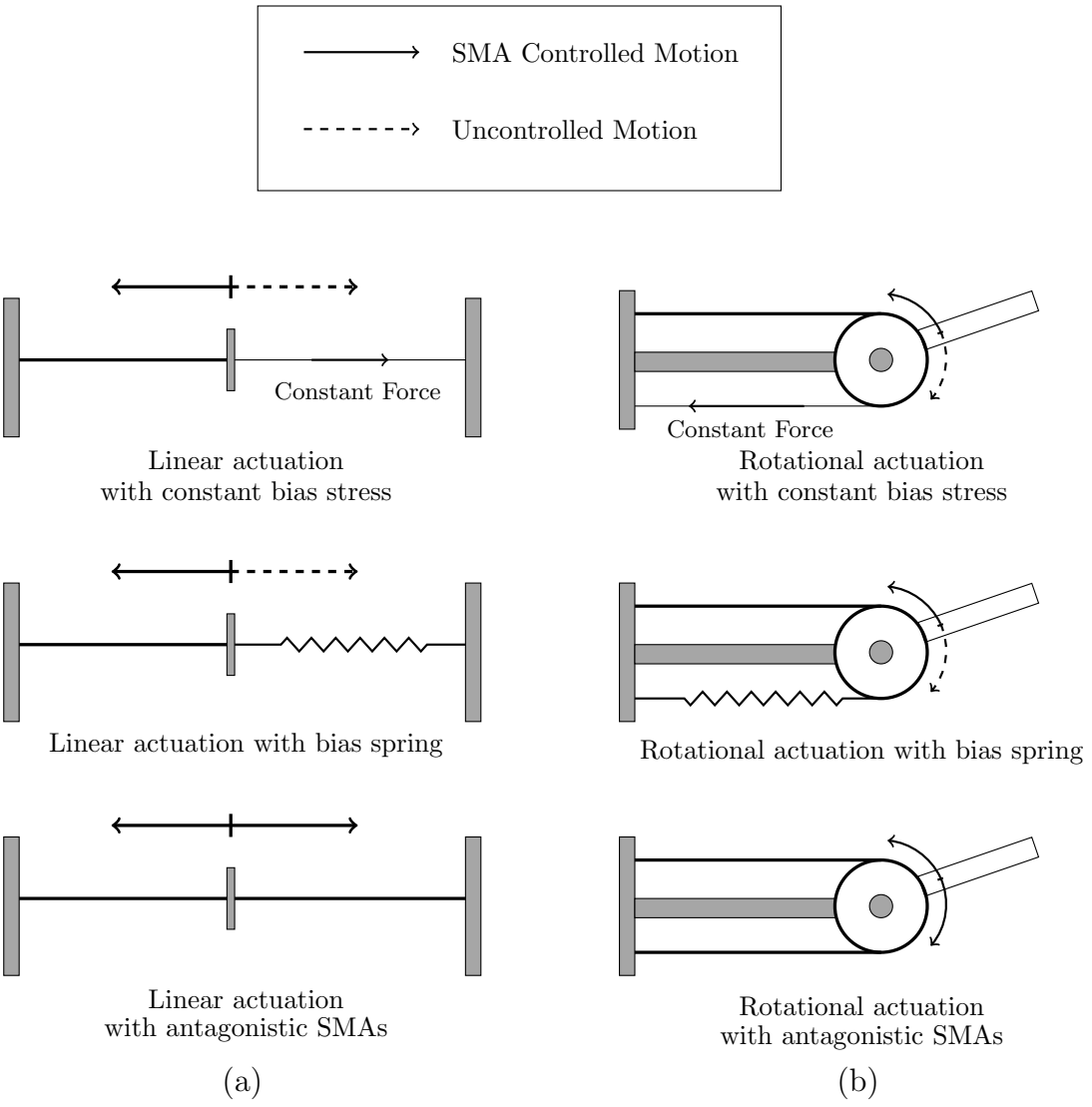

FIGURE 2.16: Motion SMA wire actuator layouts classification (a) Linear and (b) Rotary.

2.2.7.1 Single SMA Wire - Constant stress

This type of layout uses one single SMA wire and, as previously discussed, with the one-way SMA wires a bias mechanism is necessary as the one-way SMA wire can only provide force in one direction. In this class, the bias force is generated by a non-smart material. Depending on this material one can find two sub-classes. First the constant stress type, where the deformation force is generated by a constant weight attached to one end of the SMA wire (Fig. 2.17 (a)), which, as the name indicates, applies a constant force over the SMA wire. This configuration permits to consider the stress over the SMA wire as constant, which makes the transformation temperatures constant, simplifying considerably the control and modeling. This approach is rarely

Table 2.2: SMA actuator layout classifications

SMA number \motion	**Linear**	**Rotary**
Single SMA Wire	Constant stress	
	Spring biased	
Antagonistic SMA wires		
Bundle SMA wires	Constant stress	
	Spring biased	
	Equal antagonistic	
	Non-equal antagonistic	

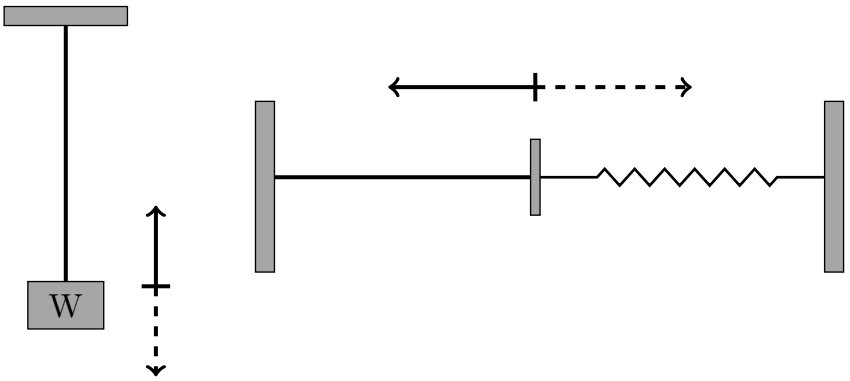

(a) Single SMA actuator

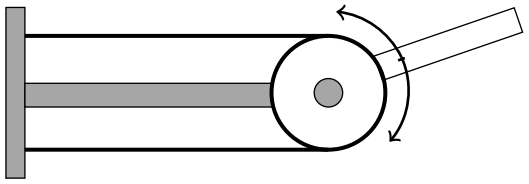

(b) Antagonistic SMA actuator

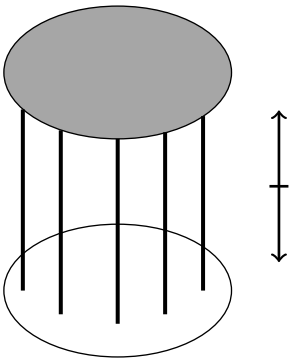

(c) Bundle SMA actuator

Figure 2.17: Classification of SMA wire actuator layouts by amount of SMA wires (a) Single wire, (b) Antagonistic and (c) Bundle Wires.

used in real applications due to the inconvenience of adding weight to the actuator and the additional space needed for this weight. In addition, this configuration has a low maximum displacement, when compared to other approaches, such as antagonistic.

2.2.7.2 Single SMA Wire - Spring biased

The second single SMA wire layout sub-class is the spring biased. In this approach a spring (linear or torsional) is used to apply the deformation force over the SMA wire (Fig. 2.17 (b)). When the length of the SMA wire changes, also does the spring's applied force. This dynamic loading also generates a dynamic stress. The changing stress has to be considered during modeling and control, due to the dependency of the transformation temperatures on the stress. Even though this approach increases the modeling and control difficulty, it also generates higher displacements.

It is important to mention that the spring selection during the design stage is critical for the good operation of this layout. The spring stiffness must allow sufficient contraction of the SMA wire to generate displacement, while providing sufficient bias force to strain the SMA wire during the cooling process.

2.2.7.3 Antagonistic SMA Wires

In this actuator layout, two SMA wires are set to apply their forces opposite to each other over the same axis (See Fig. 2.17 (b)). This antagonistic force generates the bias force needed to deform each SMA wire. The dynamic of this layout is as follows, when the first SMA wire is cooled, the second wire is heated to contract and apply force over the first one, so the first wire is strained. On the contrary, when this first wire is heated, the second one is cooled to relax and decrease the force applied, which allows a higher contraction, thus larger displacements.

Although this approach has better results in achieving larger displacements, it also has some important disadvantages. The use of a second wire implies more complicated models and control laws, due to the double loop hysteresis generated. In addition, the correct synchronization of both wires work-cycle is critical for the good operation of this design. Other disadvantages like higher energy consumption have to be taken into account as well.

2.2.7.4 SMA Bundle Actuator

This approach is used to magnify the actuator force. This happens when more than one SMA wire actuate in the same direction, parallel to each other (See 2.17 (c)). The main advantage of this layout is the increment in the available force without increasing the cooling-heating cycle time. However, the high energy consumption has to be considered.

The bias force can be applied by a dead weight (Constant stress Fig. 2.18 (a)), by a spring (linear or torsional) (Spring biased Fig. 2.18 (b)) or by other SMA wire (antagonistic Fig. 2.18 (c) and (d)). The antagonistic arrangement can be at the same time equal (Fig. 2.18 (c)) or non-equal (Fig. 2.18 (d)) depending on the number of wires, if it is symmetric or not.

2.3 SMA Applications

SMAs have drawn significant attention and interest since a few decades. However, it was not until recent years when the term shape memory technology (SMT) was introduced and a wide range of SMA wires' applications started to be developed. Their various characteristics make SMA wires suitable for a wide range of fields. An example of these applications is the bio-inspired micro-robots manufacturing, where SMAs are considered as a good alternative to traditional actuators, due to characteristics such as corrosion resistance, simple mechanical structure and bio-compatibility [65–68]. SMA wires have also been used in medical devices like intra-arterial supports [69] or wires for suturing [70], in orthopedic devices as a spinal cage implant [71], adaptive ankle–foot orthoses [72] or skeletal fixation devices (mandibular segmental) [73], as well as dental and orthodontic applications [74, 75].

In parallel, SMA wires have also proved to be a good alternative when dealing with aerodynamic problems requiring high-precision coordination, and some solutions have been applied for small prototypes and UAVs. For example in [76], a morphing segment actuated by multiple embedded SMA wires was implemented in a UAV wing, where the capability to maintain a smooth twisting concentrated on a segment of the wing was tested with a prototype. Similarly, one can include the work in [77], which presents a wing shape control using SMA wires as actuation devices. Furthermore, the authors in [78] present a blade actuator that is developed for the helicopter blade-tracking problem, which utilizes the SMA as the active actuator material to drive a rotor blade trim tab for the purpose of maintaining rotor tracking. All these articles and several others propose solutions to improve the aerodynamic properties of the flying devices.

Among the many applications of the SMA wires, several specific purpose actuators have been reported in the literature, such as: construction vibrations dampers [79], camera lens focus actuators [80], car mirror actuators [81] or SMA based motors [82]. Moreover, SMA wires have become alternative actuators of particular interest in recent years in robotic manipulators since they allow motion without using larger drives. For instance, the human-like robotic arm developed by [83], where a neural network control for artificial muscles was implemented on a robotic arm joint using a SMA wire as actuator.

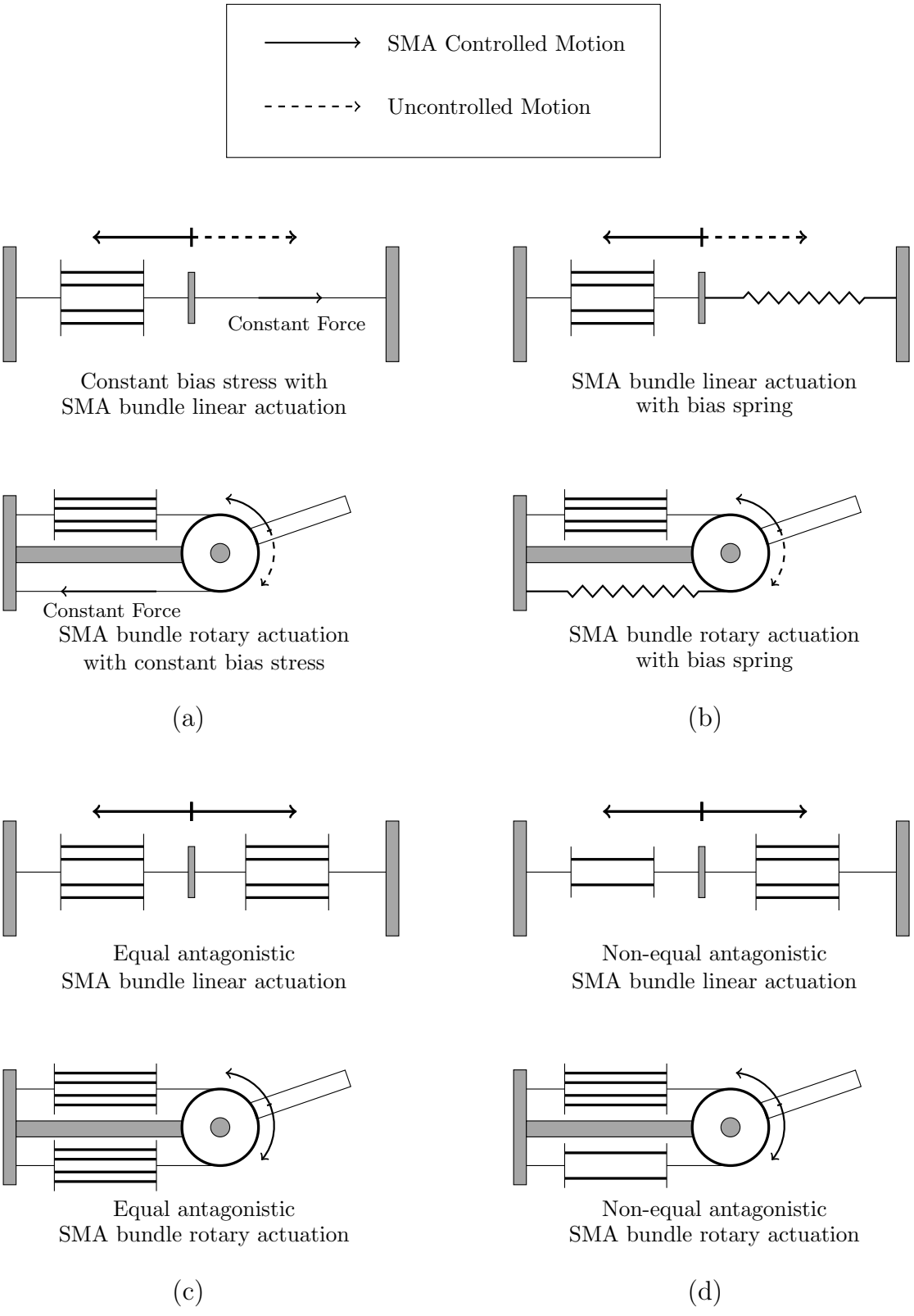

FIGURE 2.18: SMA wire bundle actuator layouts (a) Constant stress, (b) Spring biased, (c) Equal Antagonistic and (d) Non-equal Antagonistic.

Another example is given by [84], where the authors propose a fuzzy-PID control of an anthropomorphic artificial finger actuated by three antagonistic SMA muscle pairs.

Different robotic applications can be found in the literature. For example in [11], the authors propose a novel compliant SMA actuated rotary system. Also, there exist multiple designs for SMA actuated endoscopy reported in the literature [85–87]. These designs achieve compliant miniature actuators with low forces. On the other hand, one can also find robotic arms designed to lift considerable payloads, however comparatively heavy and big [26, 83]. In addition, one can find various works on robotic hands, prosthetic and grippers using SMA wires as actuators [43, 88–90]. In addition to the aforementioned, multiple general purpose actuators have been developed for micro-positioning applications using advanced control techniques [91–93].

Nonetheless, most of the mentioned applications are micro-scale or require complicated mechanical systems to be implemented. For this reason, the design presented throughout this thesis, seeks to keep the simplicity of the mechanics and therefore achieves a lightweight actuator capable of producing a relevant amount of force, leading to a suitable performance per weight ratio.

In spite of their multiple advantages, SMA wires (as previously discussed) present several challenges for accurate control due to their hysteretic behavior. A reliable model is crucial for the development of an accurate control law. Nowadays, there exist multiple models and different approaches for modeling SMA wires, as well as control strategies. The following subsection reviews the most relevant modeling strategies.

2.4 SMA Modeling

There are several models in the literature for describing the behavior of SMAs. Generally speaking, these models can be classify into two categories: microscopic and macroscopic models. The first category refers to the models from the material science perspective, where the model is concerned with the microscopical internal behavior of the SMA (crystallographic transformations). On the other hand, macroscopic models focus on the thermomechanical relations and the hysteresis effects, in order to simulate SMA's behavior in an overall mechatronic system and thereby, function as a control design aid. The literature review in this work, is concerned only with the macroscopic models, since the final goal is to develop control and estimation approaches for a SMA wire based actuator.

Macroscopic SMA models are classified into three different categories depending on the approach used to describe the material's behavior. First, one finds the phenomenological

models, where the system is described as a general linear system plus a mathematical hysteresis model. Second, the constitutive models, where the physical laws acting over the SMA and their interaction are modeled explicitly. Finally, we have the Input-Output models, where little to no previous knowledge of the system is needed, thus the parameters are identified online and then the model developed. A literature overview on SMA models is discussed in the next subsections.

2.4.1 Phenomenological models

The models in this classification consider the hysteresis phenomenon as an isolated mathematical phenomenon and not as a part of the systems dynamics itself. In these modeling methods, a transfer function is constructed to describe the observed hysteresis between a forcing function and the output variable [94].

Preisach model is the most common approach for SMA hysteresis modeling. Various authors have investigated this technique, including [95–98]. Preisach model is based on the integration of the individual response of a series of relays (hysterons) switching between two fixed states ($\gamma_{\alpha\beta}$). For every pair of threshold values (β, α), where $\alpha \geqslant \beta$, a hysterion $\hat{\gamma}_{\beta,\alpha}[\cdot,\cdot]$ is defined. Every hysterion is then weighted using the Preisach function or density function $\mu(\beta, \alpha)$, so there is a unique representation of the collection of relays integrating the half-plane $P = \{(\beta, \alpha) \,|\alpha \geqslant \beta\}$. Finally the complete Preisach model is described by the integration of each individual hysteron adjusting its output according to the current input value as follows:

$$y(t) = \int \int_P \mu(\beta, \alpha)\, \gamma_{\alpha\beta}[u(t)]\; d\alpha\, d\beta \tag{2.2}$$

where $y(t)$ is the measured output and $u(t)$ the input [52].

Other methods found in the literature for hysteresis modeling include Duhem-Madelung model [99], where the hysteresis is modeled by a series of integrated gaussian probability density functions (PDFs). We also find Krasnosel'skii-Pokovskii (KP) model [100], whose principle is similar to Preisach method, where a series of individual hysteresis operators are integrated. Likewise, we find the Prandtl-Ishlinskii (PI) model [101], also known as stop operator, where the individual hysteresis element is modeled based on the backlash operator, also known as play operator. The classical PI hysteresis is defined as the sum of several backlash operators, each one having a different threshold and slope. These models do not concern the final objective of this thesis, so they will not be further discussed.

2.4.2 Input-Output models

Input-Output models use online parameter identification to construct a model where the characteristics of the system are completely or partially unknown. For this approach, the system can be considered as a grey or black box. The system is considered a grey box if partial information of the system is known and included as a physical nonlinear model in the process. The system is considered as a black box if no physical information of the system is used to develop the model. From the grey or black box an input-output model is developed. Among these models we can find the grey box model presented in [102], which is based on the numerical knowledge of the input-output behavior of the plant. The estimated function F is defined as [102]:

$$[F(k)]_e = \left[y^{(\nu)}(k)\right]_e - \alpha u(k-1) \tag{2.3}$$

where $\left[y^{(\nu)}(k)\right]_e$ is the estimation of the ν-st derivative of the output and u is the control input. Then a cancellation of the non-linear terms F is established as [102]:

$$u(k) = \underbrace{-\frac{[F(k)]}{\alpha}}_{\text{NL Cancellation}} \underbrace{+\frac{\left[y^{*(\nu)}(k)\right]_e + \Delta(\epsilon(k))}{\alpha}}_{\text{Closed loop tracking}} \tag{2.4}$$

where $\epsilon(k) = y(k) - y^*(k)$ is the tracking error and $\Delta(\epsilon(k))$ is a closed-loop feedback controller based on the tracking error.

Black box models are also widely used for model free control. Example of this is the Laguerre filters based model presented in [93]. Among these input-output models there exist also models based on frequency response, as the one presented in [103], or models based on the estimation of a different time constant for each part of the hysteresis loop as in [88]. Here, the authors present a dynamic model of the actuator, while the SMA model is treated as a grey box and identified online.

2.4.3 Constitutive models

Finally there are the constitutive models. As mentioned before, constitutive models are physical models of the system, where the relation between the microscopic behavior of the crystalline structure of the SMA and the thermodynamic behavior is described. Within this classification one can find three different types of models, 1) microscopic, 2) micro-macro models and 3) macroscopic models.

Numerous constitutive models have been proposed to describe the SMA dynamics. The earliest SMA constitutive model reported, is the free-energy model presented by Falk in

[104], where a polynomial-free energy model with only two states variables (strain and temperature) is introduced. Several improvements and modifications to this model are reported in the literature. This is considered a microscopic model, which is out of the scope of the present work. For further details on constitutive microscopic models refer to [105].

The second type of constitutive models, are the micro-macro models. This type of models relies on micro-mechanics to describe the material behavior at microscopic scales, using then scale transitions to derive macroscopic equations [105]. Micro-macro constitutive models can be, at the same time, classified into two main modeling approaches, micro-mechanical [106] and micro-plane/micro-sphere models [107]. Micro-micro models provide an accurate description of the SMA behavior. However, they need several state variables and material parameters, which makes them challenging and computationally expensive to implement. On the other hand, the third type of constitutive models, macroscopic models, generally use a simplified approximation of micro-macro models or phenomenological considerations. This characteristic makes them easier and more efficient to implement, which in turn makes them more suitable for mechatronics applications, as the one presented in this dissertation.

There exists several macroscopic constitutive models reported in the literature. These models can be broadly classified into four different categories according to the theory used for their development. First one find the models based on the theory of plasticity. In these models, the phase transformation process and detwinning process are modeled by loading functions and flow rules analogous to classic plasticity theories. In this category one can find models like the one proposed in [108], where a 3D model to simulate the polycrystalline behavior of CuZnAlMn alloy is described. Or the model presented in [109], where, using Gibbs free energy expression, a model is derived.

Second one finds the thermodynamic potentials based models. The models of this category are developed from the construction of an energy potential from microscopic or physical considerations and constitutive relations are then derived based on thermodynamic principles. In this category one finds models as those proposed in [110–112]. The third category corresponds to the models based on finite deformation and geometric nonlinearity. These models use finite strain formulation to accurately simulate large structural rotations and distortions, as the models proposed in [113, 114]. Finally one finds the models based on statistical physics, which are based on local equilibrium considerations for single crystal SMAs. Example of this is the model proposed in [115].

All these models allow to describe the inner transformation of the SMAs in relation to

variables like temperature and stress. Based on these models, a mechatronic-application-oriented constitutive model was developed over the years. In [116], a two-phase microscopic phase transformation model of SMAs was introduced for the first time using the sub-layer model. In a following publication [55], the same authors extended their model to include a third newly discovered phase called rhombohedral phase. Sub-layer model considers the different phases coexisting inside the SMA in parallel sub-layers with their respective characteristics. Few years later, [117] extended this work to model minor hysteresis loops. This model allows to compute the martensite fraction rate of the SMA, thus opens the possibility to retake the model proposed by Tanaka in [118], where the first SMA thermomechanical model was presented. This work assumes that the thermomechanical behavior of the SMA can be fully described by strain, temperature and martensite fraction as state variables, and proposes the following constitutive relation:

$$\dot{\sigma} = E\dot{\varepsilon} + \Omega\dot{\xi} + \Theta\dot{T}, \tag{2.5}$$

where σ is the SMA wire stress, ε the strain, T the temperature and ξ the SMA martensite fraction. E, Ω and Θ are the material parameters, Young modulus, thermal expansion coefficient and phase transformation constant respectively. The martensite fraction (ξ) is an internal variable of the SMA, used to describe the phase transformation process, which is the part of the model that defines the hysteresis of the material. This stress and temperature dependent variable describes the transformation from full martensite ($\xi = 1$) to full austenite ($\xi = 0$). The authors in [25, 26, 119] present different improvements to Tanaka's model using different phase transformation kinetics and including the stress and temperature dependency of martensite fraction in the model. The authors in [26] present the most significant improvement to the constitutive SMA model for mechatronics implementations. Here, the authors propose a simple and application oriented model, which through dynamic and kinematic relations, provides a complete position model for a SMA based actuator system. This model is divided into four sub-models describing the complete dynamics of a SMA based actuator (see Fig. 2.19): 1) Heat transfer model, 2) SMA wire phase transformation model, 3) Wire constitutive model and 4) Actuator dynamics. The system proposed in this dissertation is based on the model presented in [26]. This model is detailed in Chapter 3.

2.5 Conclusions

In the first section of this chapter, an overview of the aerial manipulators found in literature is discussed. This discussion is focus on the lightweight aerial manipulator and manipulators design for small UAVs. In the following section, the theoretical background

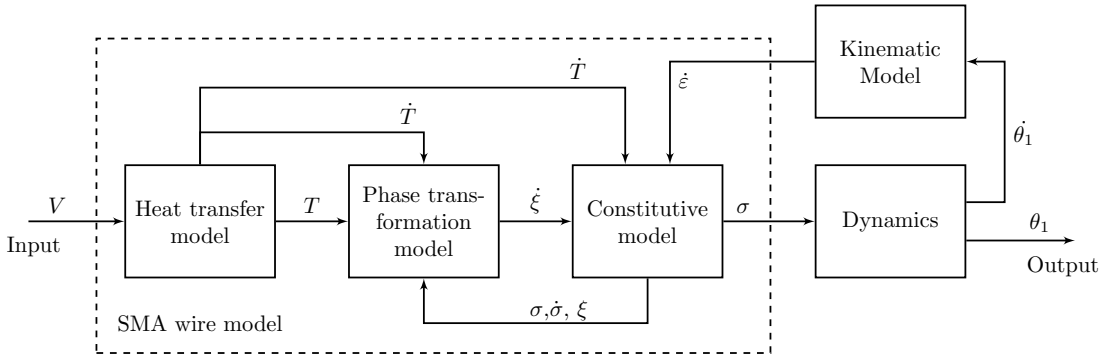

FIGURE 2.19: Elahinia's block diagram SMA actuator based model.

of Shape Memory Alloys is presented. In this section, the characteristics, advantages and disadvantages of SMAs are presented. Characteristic as phase transformation and hysteretic behavior are explained in detail. Following, some of the current applications for SMA systems are outlined. Finally, the different classification for SMA modeling are discussed.

Chapter 3

Mechanical design and Mathematical model

This chapter presents the mechanical design, mathematical model development and validation, of the SMA wire actuated robotic arm. The first section 3.1 presents the mechanical characteristics and details of the robotic arm, the different possible configurations and describes the electronics used on the control board as interface with the control software. Section 3.2 describes the mathematical model of the robotic arm. This section is mainly composed of two subsections: 1) SMA wire model and 2) Kinematic and Dynamic model. Finally, section 3.3 presents a series of tests to validate the proposed mathematical model based on experimental data. The chapter conclusions are presented in section 3.4.

3.1 Mechanical Design

This section presents the mechanical design of a lightweight SMA actuated robot arm intended as an aerial manipulator for small UAVs. The optimal use of available payload of an aerial vehicle is critical for the design of aerial manipulators in general. In the current dissertation, a small lightweight robotic arm is proposed. This robotic arm consists of a single Degree of Freedom (DoF) actuator actuated by SMA wires. Figure 3.1 shows a Computer Aided Design (CAD) model of the robot arm design. Among the characteristics taken into account for the design and development of this actuator are:

- Lightweight and small size,
- Robot Operating System (ROS) compatibility (for further implementation with UAVs),

- wireless communication,
- simple construction,

The given design proposes a robotic arm with 1 DoF activated by one or two (depending on the configuration, see subsection 3.1.2) Flexinol® wires. The gripper is activated by a third thinner Flexinol® SMA wire. Further details on the experimental setup are given in subsection 3.1.6.

The robotic arm has two custom-made 3D printed links (100 mm length) and a range of movement along the vertical plane X-Z between 90 and 110 degrees with two cylindrical couplers. It has a total weight of about 80 g, which is only about 40% of the weight of lightweight designs found in the literature, such as the one presented in [7]. The winding mechanism (see subsection 3.1.3) enables the use of longer SMA wires in order to increase the rotation span without increasing the dimension of the links. It is important to emphasize that an increase in the length of the wires will increase the energy consumption. For this reason a balance between range of motion and energy consumption should be considered, especially when considering a mobile application like aerial manipulator. The following subsection describes in detail every mechanical part of the robotic arm.

3.1.1 Joint Mechanism

The joint mechanism is the system responsible for the conversion of the SMA wire's strain into angular displacement of the arm (see Fig. 3.2). The design of this mechanism is inspired on the work presented by the authors in [11].

In [11], a Compliant Differential SMA Actuator (CDSA) inspired by the biological structure of the human elbow joint is proposed. This actuator mimics the extension/flexion motion of the human arm. The joint is composed of three main elements: 1) two SMA wires in antagonistic configuration, 2) two cylindrical couplers and 3) a torsion spring. Figure 3.3 shows a CAD assembly of the CDSA model proposed by [11].

In the system shown in Fig. 3.3, each SMA wire is attached directly to each individual coupler. The wires actuate as antagonistic artificial muscles and provide a bidirectional driving force to the couplers. The spring, embedded between the couplers, allows to transmit the force between couplers, acting as the tendon on the human elbow. The torsion spring provides a coupling between cylindrical couplers, as well as the necessary recovery force for the SMA wires. This kind of coupling allows certain control over the overall stiffness of the actuator. As mentioned before, the transformation temperatures of the wires depend, among other factors, on the wire stress. If the stress is reduced,

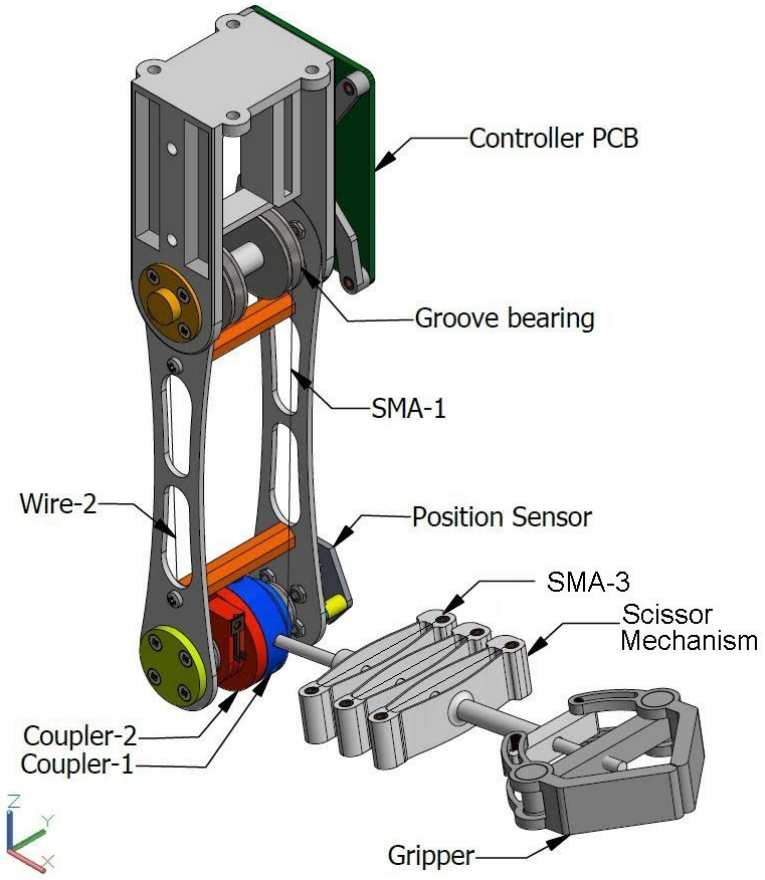

FIGURE 3.1: CAD model of the proposed SMA wire actuated robotic arm.

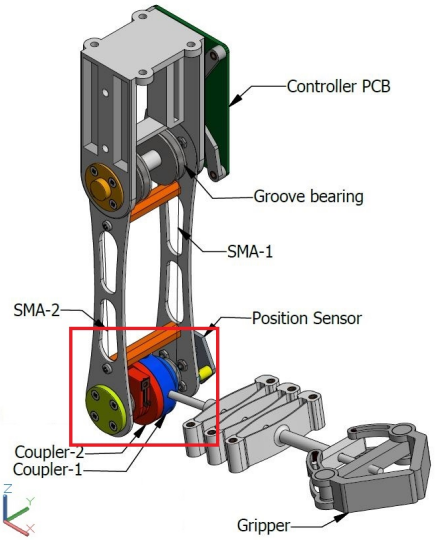

FIGURE 3.2: CAD model of the proposed SMA wire actuated robotic arm. Joint Mechanism.

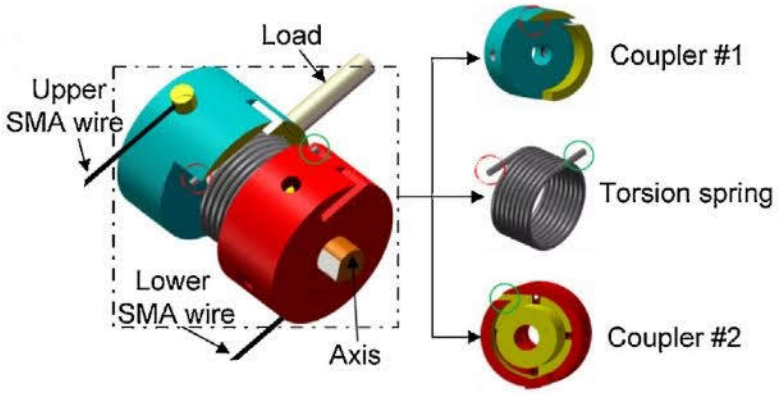

FIGURE 3.3: Compliant Differential SMA actuator (CDSA) [11].

so are the transformation temperatures. When the stiffness of the joint is controlled by cooling or heating the antagonistic SMA wires, a faster or slower response of the actuator ca be generated as needed.

The CDSA works as follows: When the Upper SMA wire is heated, it applies a pulling force over the Coupler-1 due to the contraction of the wire. This force generates an angular displacement of the coupler. The load attached to Coupler-1, follows the movement of the later one. With the rotation of Coupler-1, the torsion spring is twisted and transmits this force to Coupler-2. This generates a pulling force over the Lower SMA, so it strains. On the contrary, when the Lower SMA wire is heated, the forces are transmitted in the opposite direction, straining the Upper SMA wire.

For the design of the joint mechanism presented in Fig. 3.2, the CDSA was taken as a design reference. The couplers were adapted and optimized to reduce the weight and increase the rotation/strain ratio. The couplers have an external radius of 12.5 mm and a 7.5 mm radius to the SMA wire, maximizing the rotation/strain ratio, while allowing easy manipulation for assembly with elements as shaft, sensor and SMA attachment (See Fig. 3.4). The coupler design ensures maximizing torque transfer between SMA wire and coupler since the force of the wire is applied tangentially to the coupler at every position. The pieces are 3D printed using GreenTEC PRO material. GreenTEC PRO is made from a high-performance and heat-resistant renewable biodegradable biopolymer. The extruding material, is high temperature, impact and stress resistant. These characteristics make the GreenTEC PRO an ideal material for applications with SMA wires.

Table 3.1 shows the final weight of each coupler alone and with the respective additional pieces for assembly included. Figure 3.5 shows the assembly of the joint mechanism.

The Coupler-1 is mechanically fixed to the shaft, so the position of this coupler, and the position of the final actuator, can be measured. The angular position of Coupler-1

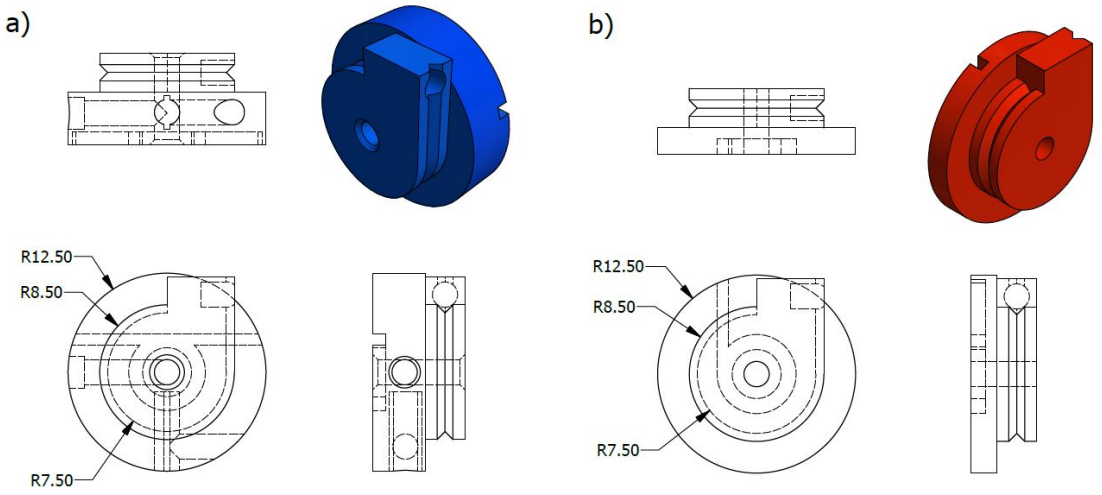

FIGURE 3.4: CAD notations of arm's couplers. a) Coupler-1, b) Coupler-2.

TABLE 3.1: Coupler weights alone and fully assembled.

Coupler	Stand alone [g]	Assembly [g]
`Coupler-1`	5.6	6
`Coupler-2`	3.8	4

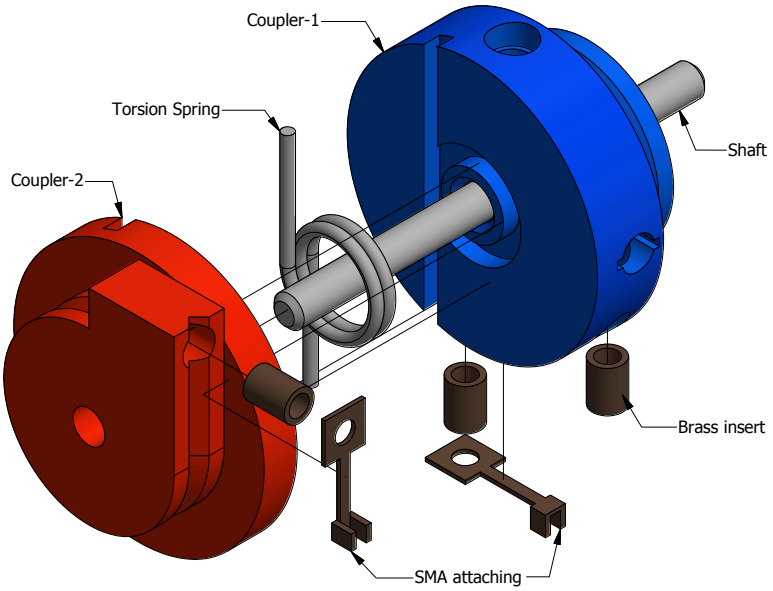

FIGURE 3.5: Joint mechanism assembly.

(θ_1) is measured with respect to the $Z - axis$. For more detailed information on the construction of the arm please refer to [12].

3.1.2 Robotic arm configurations

With the given joint mechanism presented, it is possible to have two different configurations of actuation. The first configuration is proposed by the authors in [11], referred to as antagonistic configuration. This configuration uses two SMA wires as previously discussed, where Wire-2 (see Fig. 3.1) becomes SMA-2. The second configuration consists in replacing the Wire-2 by a hard wire, restricting the movement of Coupler-2. This restriction brings the system to a single wire biased configuration, where the bias force is caused by the torsion spring.

Every configuration has different characteristics, advantages and disadvantages. As reported by the authors in [11] an antagonistic configuration can offer a higher strain to rotation ratio and faster response of the actuator. However, the use of a second wire also implies higher energy consumption and a significant increase in the complexity of the system for estimation and control tasks. Since the final goal of the robotic arm is to be implemented in mobile environments, the energy consumption is a very important factor in the design.

3.1.3 Winding mechanism

For applications in mobile and reduced environments it is important to keep the dimensions of the system restricted. A winding mechanism is designed with this purpose. This mechanism allows the implementation of longer SMA wires, to achieve higher rotational displacements, without increasing the overall dimension of the arm.

The system consists of two groove bearings per wire, where the wire is wound around. This system provides little friction and weight increase, while increasing by three the possible length of the wire with the same arm dimensions. Figure 3.6 shows the winding system assembly.

The lower shaft is mechanically fixed to the position sensor so the position of the coupler can be measured. The majority of pieces in this section are custom designed and 3D printed with a low density and temperature resistant coPolyester.

3.1.4 Gripper mechanism

This mechanism consists of 3 main parts: 1) Scissor mechanism, 2) Gripper and 3) Shaft. Figure 3.7 shows the assembly of this section of the arm. With exception of the shaft, which is a carbon fiber commercial shaft, all the pieces of the gripper are 3D printed. The gripper, printed as one piece, reduces the need of external attachments which, at

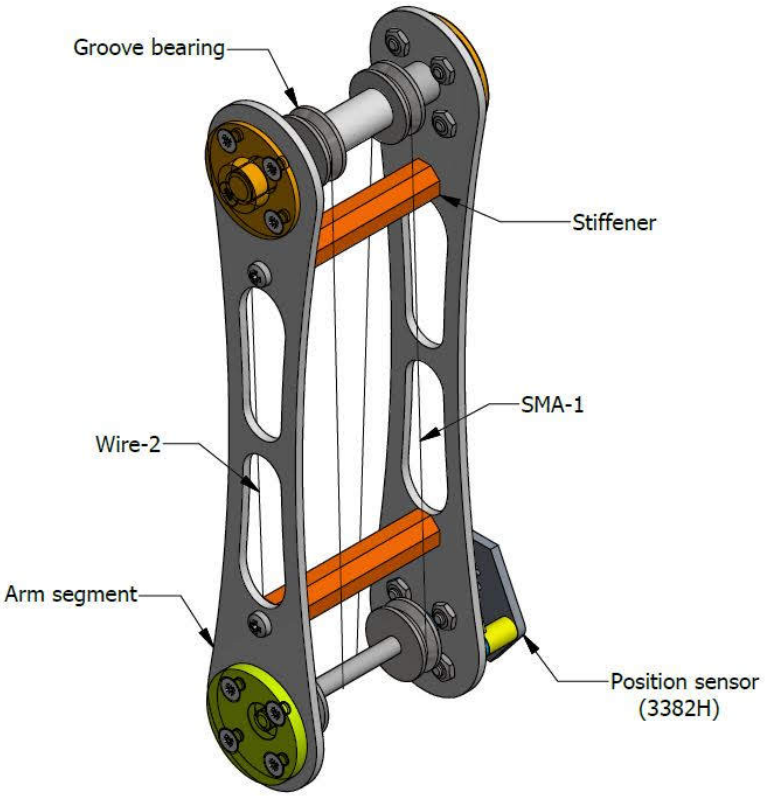

FIGURE 3.6: Joint mechanism assembly.

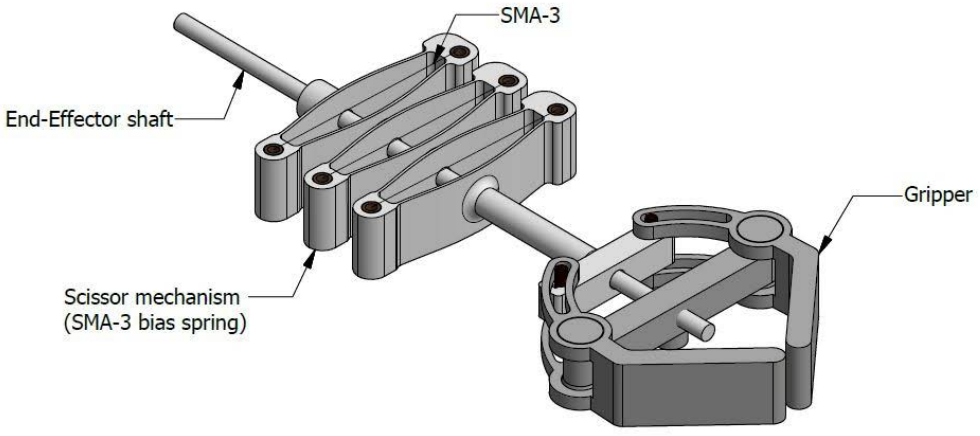

FIGURE 3.7: Gripper mechanism assembly [12].

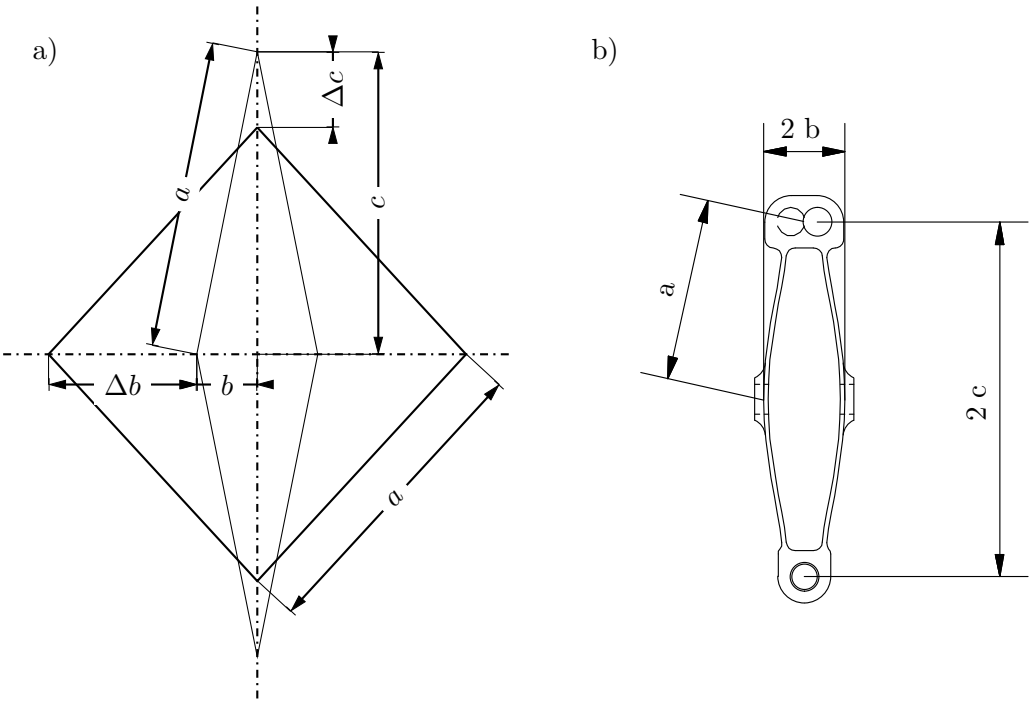

FIGURE 3.8: Scissor mechanism (gripper bias spring). a) Spring segment kinematic, undeformed (plain) and deformed (thick) b) CAD spring segment [12].

the same time, decreases the weight to be lifted. This system is activated by a SMA wire (SMA-3) wound through the scissor mechanism. This mechanism transforms the strain of the SMA wire into linear displacement along the shaft, which is later converted into rotational displacement by the gripper mechanism (see Fig. 3.8). The scissor mechanism also actuates as bias spring for the SMA wire, providing the necessary recovery force. For further details on the construction and design of the gripper refer to [12].

3.1.5 Control board

A custom made control board based on [12] is used to communicate and control the robotic arm. This board is capable of wireless communication (via Wi-Fi) and ROS interoperability. It can control up to three SMA wires with a MOSFET interface and monitor the ambient temperature.

The board also provides the angular position measurements of Coupler-1. The position is measured with the rotational sensor 3382H. This information is acquired by an ADS1115, a 16 bit ADC, and then sent to the control board. The system is powered with 7.6 V and programmed using arduino interface. The code of the control board is shown in Appendix A.

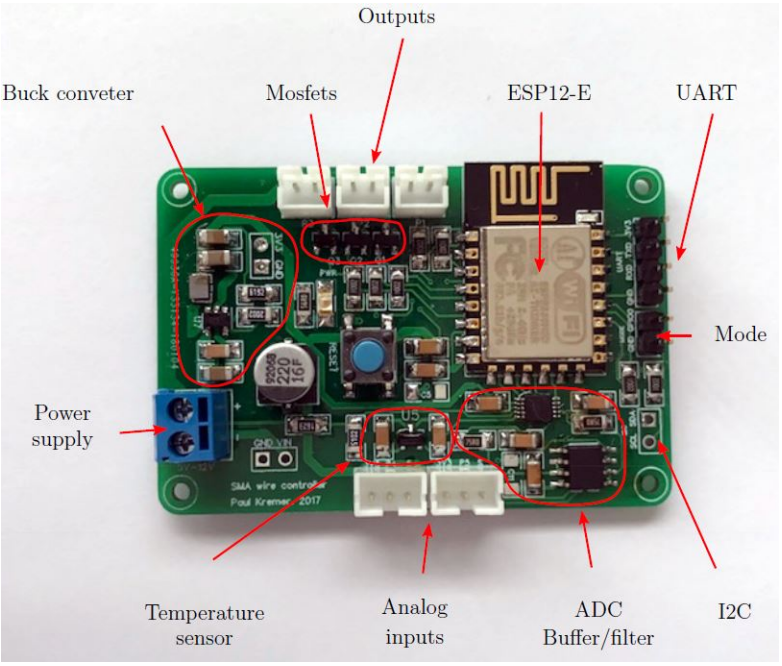

FIGURE 3.9: Robotic arm control board [12].

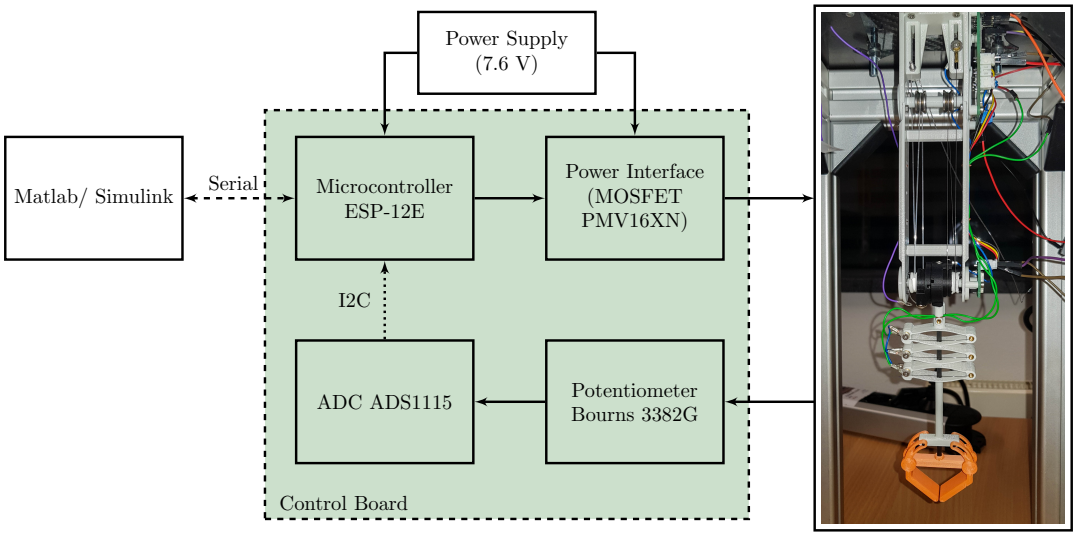

FIGURE 3.10: Experimental setup block diagram.

3.1.6 Experimental setup

Figure 3.10 shows a block diagram of the experimental setup and test bench designed for the results presented in this dissertation. An image of the actual experimental setup is displayed in Fig. 3.11.

The control input is computed in Matlab/Simulink. This voltage value is sent via serial interface to the micro-controller ESP-12E, then processed into a PWM signal and applied to each wire through a MOSFET based power interface. The angular position is

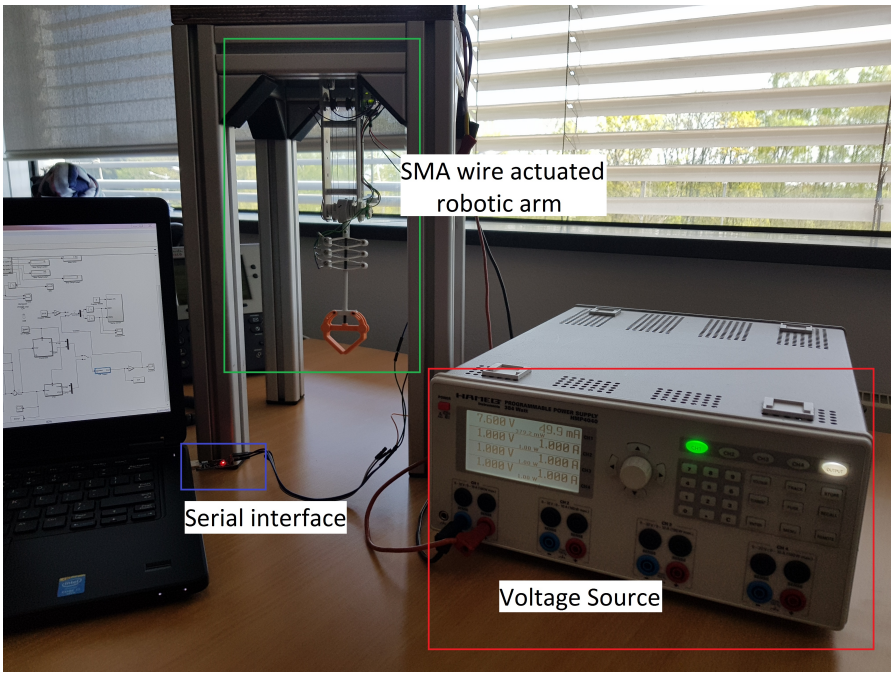

FIGURE 3.11: Experimental setup.

measured through a potentiometer (Bourne 3382G) in combination with an ADS1115 16 bits ADC. The measurement is processed by the micro-controller and sent back to the Matlab/Simulink interface via serial communication. The SMA wires used for these experiments are manufactured by Dynalloy. Flexinol® wires of 0.31 mm diameter and 40 cm length are used for SMA-1 and SMA-2, while the gripper is actuated by a third Flexinol® wire of 0.22 mm diameter and 10 cm length. The two cylindrical couplers are joined together by a torsion spring with a stiffness coefficient of 3.2 Nmm per degree. Table 3.2 shows the characteristics of the 3 SMA wires used as actuators in the proposed system.

TABLE 3.2: SMA wires characteristics.

Wire	Diameter [mm]	Length [mm]	Pull force [N]	Cooling time [s]
SMA-1	0.31	40	12.55	6.8
SMA-2	0.31	40	12.55	6.8
SMA-3	0.22	7.5	5.59	2.7

All the experimental results shown in the current work were obtained with the test bench shown in Fig. 3.12 with the robotic arm grounded.

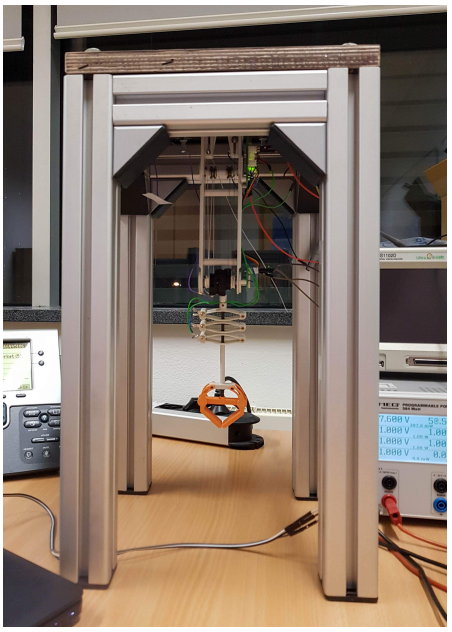

FIGURE 3.12: Test bench.

3.2 Mathematical model

This section details the mathematical model of the SMA actuated robotic arm, for both configurations (biased and antagonistic). In a general form, the mathematical model can be divided into two subsystems: 1) SMA wire and 2) Robot kinematics and dynamics. These subsystems are recursively interconnected as can be seen in Fig. 3.13

3.2.1 SMA wire model

The SMA wire model describes the relation between the applied voltage and the generated force in the wire. This model is divided into 3 subsystems: Heat transfer model, phase transformation model and constitutive model. Figure 3.14 shows the interaction among these 3 subsystems, which are detailed in the following subsections.

3.2.1.1 Heat transfer model

The heat transfer model describes the electrical heating of the wire by Joule effect and the cooling process by natural convection [23]:

$$m_w c_p \frac{dT}{dt} = \frac{V^2}{R(\xi)} - h(T) A_w (T - T_{amb}) \tag{3.1}$$

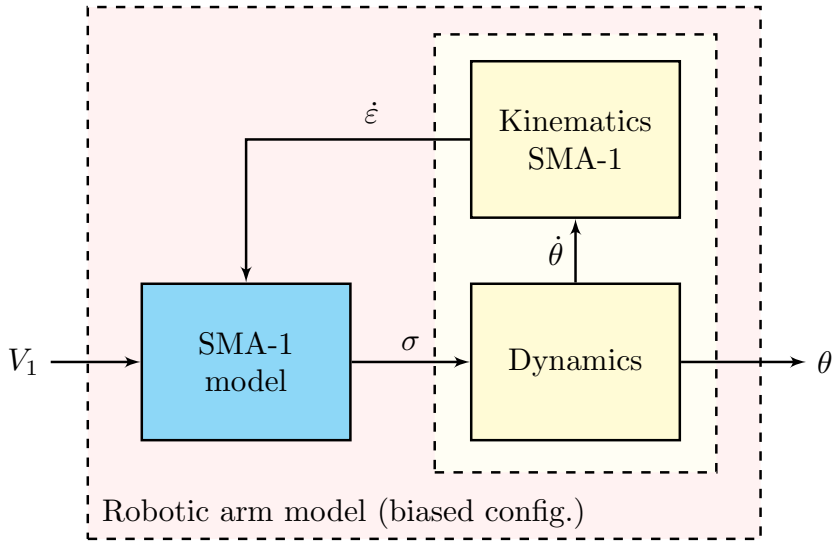

(A) Biased SMA wire configuration.

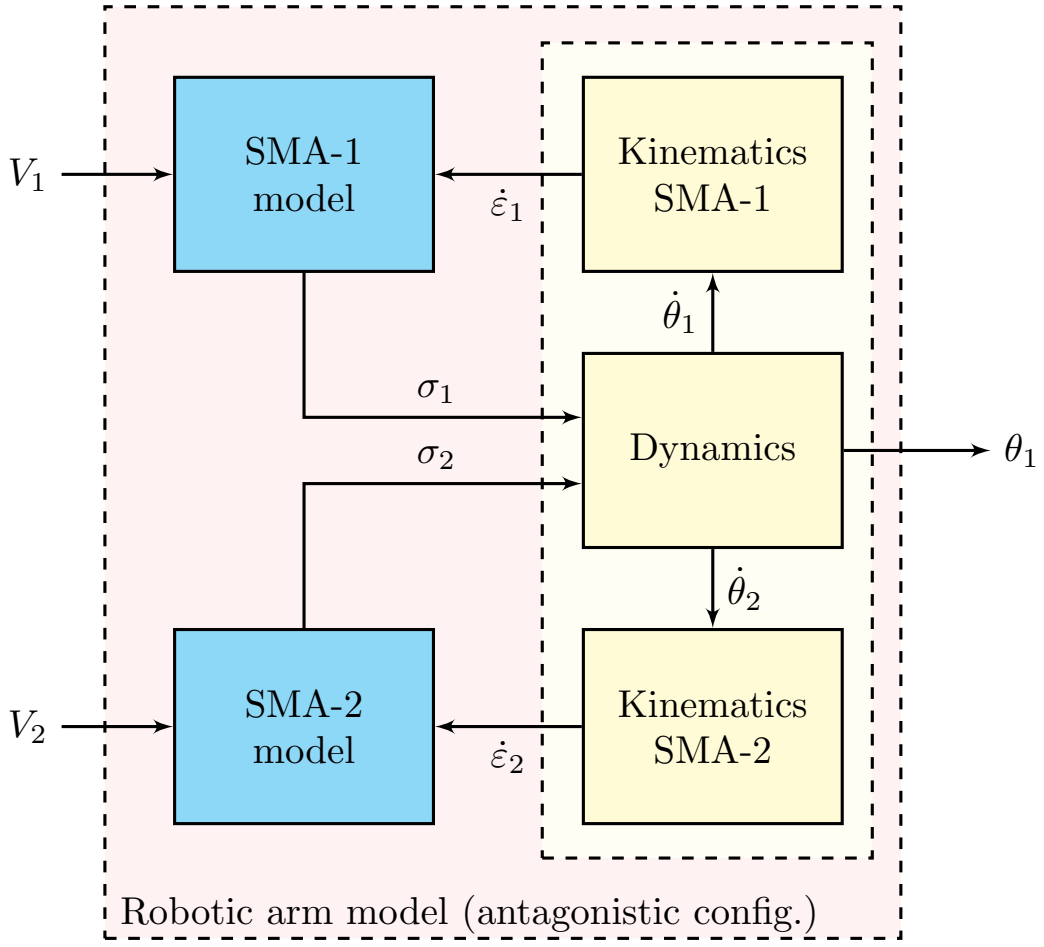

(B) Antagonistic SMA wires configuration.

FIGURE 3.13: SMA actuated robotic arm model block diagram.

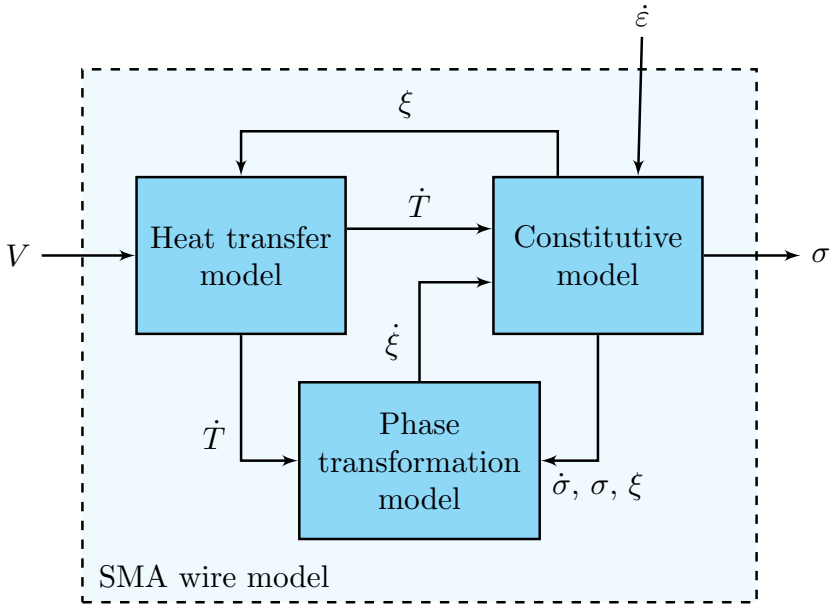

FIGURE 3.14: SMA wire model block diagram.

where V is the voltage, R is the electric resistance, c_p is the specific heat, m_w is the mass per unit length, A_w is the wire surface area, T_{amb} the ambient temperature and T is the SMA wire temperature. Here the convection coefficient h is approximated by a second order polynomial of the temperature:

$$h\left(T\right) = h_0 + h_2 T^2 \tag{3.2}$$

It has been reported in the literature that the electric resistance of the SMA wires is not a constant parameter [120]. Not only this parameter has a different value for martensitic and austenitic material, but it is a function of the temperature and stress of the wire [121]. However, the variations on the electric resistance due to temperature and stress are negligible with respect to the changes due to phase transformation. For this reason, the dependence of the electric resistance on the temperature and stress is neglected. The resistance is mathematically described as:

$$R\left(\xi\right) = R_m \xi + (1 - \xi) R_a \tag{3.3}$$

where R_m and R_a are the electric resistance in full martensite and full austenite respectively.

3.2.1.2 SMA wire phase transformation model

This model computes the martensite fraction (ξ). The phase transformation of the SMA wire depends directly on the direction of the time derivative of the temperature and stress. Therefore, due to the hysteresis behavior, two equations are needed to fully describe this phenomenon. The phase transformation while heating (forward transformation) is given by [25]:

$$\xi = \frac{\xi_M}{2}\left\{\cos\left[a_A\left(T - A_s\right) + b_A\sigma\right] + 1\right\} \tag{3.4}$$

for $A_s + \frac{\sigma}{C_A} \leq T \leq A_f + \frac{\sigma}{C_A}$.

Inversely, the transformation from austenite to martensite, during cooling, is described by the following equation [25]:

$$\xi = \frac{1 - \xi_A}{2}\cos\left[a_M\left(T - M_F\right) + b_M\sigma\right] + \frac{1 + \xi_A}{2} \tag{3.5}$$

for $M_s + \frac{\sigma}{C_M} \leq T \leq M_f + \frac{\sigma}{C_M}$, where M_s, M_f, A_s, A_f are the start and end transformation temperatures for martensite and austenite transformation respectively, ξ_M and ξ_A are the maxima of ξ at the martensite and austenite phase respectively. Here $a_A = \frac{\pi}{\left(A_f - A_s\right)}$, $a_M = \frac{\pi}{\left(M_s - M_f\right)}$, $b_A = -\frac{a_A}{C_A}$, $b_M = -\frac{a_M}{C_M}$, C_A and C_M are material parameters.

The full transformation process dynamics is described as follows [24]:

$$\dot{\xi} = \xi_T\left(T, \sigma\right)\dot{T} + \xi_\sigma\left(T, \sigma\right)\dot{\sigma} \tag{3.6}$$

where

$$\xi_T(T,\sigma) = \begin{cases} -\frac{\xi_M}{2}\sin\left(a_A\left(T - A_s - \frac{1}{c_A}\sigma\right)\right)a_A, \\ \qquad \text{if } A_s < T - \frac{\sigma}{c_A} < A_f \;\&\; \dot{T} - \frac{\dot{\sigma}}{c_A} > 0 \\ -\frac{1-\xi_A}{2}\sin\left(a_M\left(T - M_f - \frac{1}{c_M}\sigma\right)\right)a_M, \\ \qquad \text{if } M_f < T - \frac{\sigma}{c_M} < M_s \;\&\; \dot{T} - \frac{\dot{\sigma}}{c_M} < 0 \\ 0, \qquad \text{otherwise} \end{cases} \tag{3.7}$$

$$\xi_\sigma(T,\sigma) = \begin{cases} -\frac{1}{c_A}\xi_T(T,\sigma), & \text{if } A_s < T - \frac{\sigma}{c_A} < A_f \;\&\; \dot{T} - \frac{\dot{\sigma}}{c_A} > 0 \\ -\frac{1}{c_M}\xi_T(T,\sigma), & \text{if } M_f < T - \frac{\sigma}{c_M} < M_s \;\&\; \dot{T} - \frac{\dot{\sigma}}{c_M} < 0 \\ 0, & \text{otherwise} \end{cases} \tag{3.8}$$

3.2.1.3 Wire constitutive model

The wire constitutive model describes the relation between stress (σ), strain (ε), temperature (T) and martensite fraction (ξ). This model was first proposed by [25] and later improved by [26]. The constitutive model is written as follows:

$$\dot{\sigma} = E\dot{\varepsilon} + \Omega\dot{\xi} + \Theta\dot{T}, \tag{3.9}$$

where Ω and Θ represent the phase transformation constant and thermal expansion coefficient, respectively. Herein

$$\Omega = -E\varepsilon_0 \tag{3.10}$$

and ε_0 is the initial strain. The Young's modulus (E) is computed as a function of the martensite fraction and the martensite and austenite Young's modulus as follows [119]:

$$E(\xi) = E_A + \xi(E_M - E_A) \tag{3.11}$$

3.2.2 Kinematic and dynamic model

This subsection describes the model of the mechanical design (corresponding to the kinematic and dynamic model) and its relation with the rest of the system.

3.2.2.1 Kinematic model

The kinematic model relates the SMA wire model to the mechanics of the robotic arm itself. The strain ratio of the SMA wire and angular velocity of the arm depends on the

geometry of the design. This kinematic relation is given as:

$$\dot{\varepsilon} = -\frac{r\dot{\theta}}{l_0} \tag{3.12}$$

where r is the coupler radius, l_0 the initial length of each wire and $\dot{\theta}$ the angular velocity of the coupler. Equation (3.12) describes the inversely proportional relation between the angular position of each coupler (θ) and the strain of the wire (ε).

3.2.2.2 Dynamic model

The dynamic model describes the dynamics of the mechanical system (i.e. robotic arm). This model establishes the relation between the coupler mechanism, torsion spring and torques applied by the SMA wires, as well as the effects of the load and the gripper. The dynamic model of an n-degrees-of-freedom, rigid mechanical system is given by the following nonlinear equation [122]:

$$M(\theta)\ddot{\theta} + V_m\left(\theta, \dot{\theta}\right)\dot{\theta} + G(\theta) + F_d\dot{\theta} = \tau \tag{3.13}$$

where $\theta, \dot{\theta}, \ddot{\theta}$ represent the position, velocity and acceleration vectors respectively; $M(\theta) \in \mathbb{R}^{nxn}$ is the inertia matrix; $V_m\left(\theta, \dot{\theta}\right) \in \mathbb{R}^{nxn}$ is the centripetal-Coriolis matrix; $G(\theta) \in \mathbb{R}^n$ describes the effect of gravity; F_d is a constant, diagonal, positive definite, viscous coefficient matrix; and τ_ω is the input torques vector. For the particular case of the proposed SMA-actuated robotic arm there exist two possible cases. For the biased SMA wire system we have:

$$J_1\ddot{\theta} + m_L g r_{load}\sin(\theta) - b_1\dot{\theta} = \tau_{\omega_1} - \tau_s \tag{3.14}$$

while for the antagonistic configuration the dynamic model is described as:

$$\begin{cases} J_1\ddot{\theta}_1 + m_L g r_{load}\sin(\theta_1) + b_1\dot{\theta}_1 &= \tau_{\omega_1} - \tau_s \\ J_2\ddot{\theta}_2 + b_2\dot{\theta}_2 &= -\tau_{\omega_2} + \tau_s \end{cases} \tag{3.15}$$

where the subindex 1 and 2 denote the respective Coupler-1 and Coupler-2, J is the inertia of the coupler, g is the gravity constant, r_{load} is the radius from the center of the joint to the load. The term m_L is the total mass at the end-effector center of gravity:

$$m_L = m_g + m_{load} \tag{3.16}$$

where m_g and m_{load} are the gripper and payload mass respectively. In addition, τ_ω and τ_s are the torques applied by the SMA wires and torsion spring respectively. The torsion spring and SMA wires torques are obtained from basic physical laws, where the SMA wire's force (F_w) is deduced by a proportional relation to the stress (σ). The stress can be computed by integration of Eq. (2.5):

$$\tau_{wi}\left(\sigma_i\right) = F_{wi} r_i = A \sigma_i r_i \tag{3.17}$$

where $i = 1, 2$ is for SMA-1 and SMA-2, r is the coupler radius and A the cross-sectional area of the wire. The stress is considered to be completely transmitted to the coupler since the force is applied tangentially independently of the coupler's position, and the losses caused by friction on the winding mechanism are neglected. The torsion spring torque τ_s depends on the configuration of the system. For the biased SMA wire system the torque is equivalent to:

$$\tau_s\left(\theta_1, \dot{\theta}_1\right) = k_s \theta_1 + b_s \dot{\theta}_1 + \tau_{s_0} \tag{3.18}$$

For a two SMA wires system, the spring torque is calculated as:

$$\tau_s\left(\theta_1, \theta_2, \dot{\theta}_1, \dot{\theta}_2\right) = k_s\left(\theta_1 - \theta_2\right) + b_s\left(\dot{\theta}_1 - \dot{\theta}_2\right) \tag{3.19}$$

where k_s is the spring constant and b_s is the spring's friction factor, θ_i is the angular position of coupler-i with respect to Z-axis and τ_{s_0} is the initial torque of the spring.

3.2.3 Robotic arm state space model

Here, the state space models of the biased SMA wire and antagonistic systems are briefly studied.

3.2.3.1 Biased SMA wire system state space model

Consider the following non-linear system:

$$\begin{cases} \dot{x}\left(t\right) &= f\left(x\left(t\right), u\left(t\right)\right) \\ y\left(t\right) &= h\left(x\left(t\right)\right) \end{cases} \tag{3.20}$$

where $x\left(t\right) = \left[x_1, x_2, \cdots, x_n\right]^T$ is the state vector and $u\left(t\right)$ is the control input.

For the biased SMA wire system, the state vector is defined as $x\left(t\right) = \begin{bmatrix} \theta_1 & \dot{\theta}_1 & T_1 & \sigma_1 & \xi_1 \end{bmatrix}^\top$

and the system model is:

$$\begin{cases} f(x,u) &= \begin{bmatrix} x_2 \\ \frac{A_1 r_1}{J_1} x_4 - \frac{b_1}{J_1} x_2 - \frac{m_{load} g r_{load}}{J_1} \sin(x_1) - \frac{1}{J_1} \tau_s(x_1, x_2) \\ T_{e_1}(x_3, x_5) \\ -\frac{E_1(x_5) r_1}{l_{10}} x_2 + \Theta_1 T_{e_1}(x_3, x_5) + \Omega_1 \dot{x}_5 \\ \xi_T(x_3, x_4) T_{e_1}(x_3, x_5) + \xi_\sigma(x_3, x_4) \dot{x}_4 \end{bmatrix} \\ y(t) &= x_1 \end{cases} \tag{3.21}$$

where

$$T_{e_1}(x_3, x_5) = \frac{1}{R_1(x_5) m_{w_1} c_{p_1}} u_1 - \frac{h_1(x_3) A_{w_1}}{m_{w_1} c_{p_1}} (x_3 - T_{amb})$$
$$u_1 = V_1^2$$

and $R_1(x_5)$, $h_1(x_3)$ and $\tau_s(x_1, x_2)$ are described by the eq. (3.2), (3.3) and (3.18) respectively.

The switching of the system is implicit in states x_4 and x_5 with the martensite fraction rate term, which is fully described in Eq. (3.6).

3.2.3.2 Antagonistic system state space model

Consider the non-linear system of the form presented in Eq. (3.20), and a state vector defined as $x(t) = \begin{bmatrix} \theta_1 & \dot{\theta}_1 & T_1 & \sigma_1 & \xi_1 & \theta_2 & \dot{\theta}_2 & T_2 & \sigma_2 & \xi_2 \end{bmatrix}^\top$

Let us then redefine the function $f(x,u)$ as follows:

$$\begin{cases} f(x,u) &= \begin{bmatrix} x_2 \\ \frac{A_1 r_1}{J_1} x_4 - \frac{b_1}{J_1} x_2 - \frac{m_{load} g r_{load}}{J_1} \sin(x_1) - \frac{1}{J_1} \tau_s(x_1, x_2, x_5, x_6) \\ T_{e_1}(x_3, x_5) \\ -\frac{E_1(x_5) r_1}{l_{10}} x_2 + \Theta_1 T_{e_1}(x_3, x_5) + \Omega_1 \dot{x}_5 \\ \xi_T(x_3, x_4) T_{e_1}(x_3, x_5) + \xi_\sigma(x_3, x_4) \dot{x}_4 \\ x_7 \\ -\frac{A_2 r_2}{J_2} x_9 + \frac{b_2}{J_2} x_7 + \frac{1}{J_2} \tau_s(x_1, x_2, x_6, x_7) \\ T_{e_2}(x_8, x_{10}) \\ -\frac{E_2(x_{10}) r_2}{l_{20}} x_7 + \Theta_2 T_{e_2}(x_8, x_{10}) + \Omega_2 \dot{x}_{10} \\ \xi_T(x_8, x_9) T_{e_1}(x_8, x_{10}) + \xi_\sigma(x_8, x_9) \dot{x}_9 \end{bmatrix} \\ y(t) &= x_1 \end{cases} \tag{3.22}$$

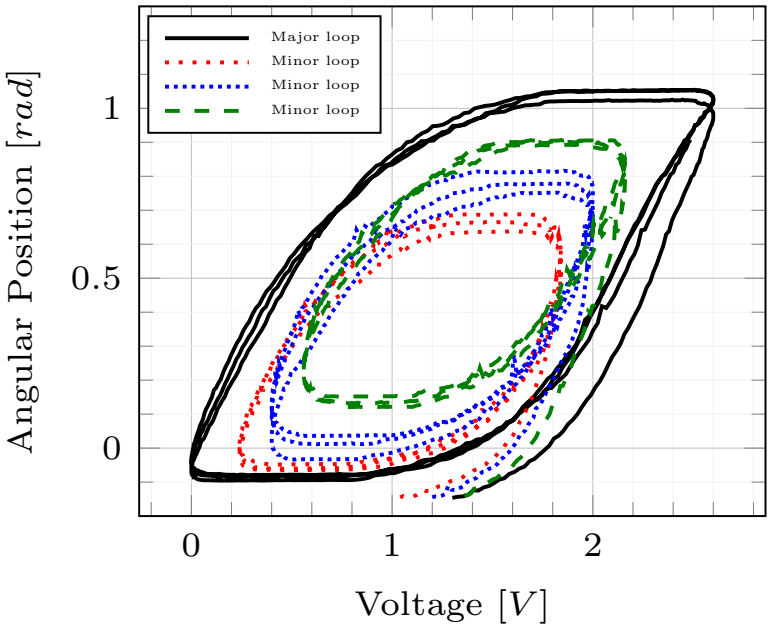

FIGURE 3.15: Hysteresis major and minor loops. Experimental results.

where

$$T_{e_1}(x_3, x_5) = \frac{1}{R_1(x_5)\, m_{w_1} c_{p_1}} u_1 - \frac{h_1(x_3)\, A_{w_1}}{m_{w_1} c_{p_1}} (x_3 - T_{amb})$$

$$T_{e_2}(x_8, x_{10}) = \frac{1}{R_2(x_{10})\, m_{w_2} c_{p_2}} u_2 - \frac{h_2(x_7)\, A_{w_2}}{m_{w_2} c_{p_2}} (x_8 - T_{amb})$$

$$u = \begin{bmatrix} u_1 \\ u_2 \end{bmatrix} = \begin{bmatrix} V_1^2 \\ V_2^2 \end{bmatrix}$$

In the case of the antagonistic configuration, the system can switch into four different modes while cooling and/or heating SMA-1 and SMA-2. The switching of the system is implicit in states x_4, x_5, x_9 and x_{10} with the martensite fraction rate term of each wire, which is fully described in Eq. (3.6).

3.2.4 Hysteresis

As discussed in Chapter 2, one of the main nonlinear dynamics of the SMAs is the hysteresis. These materials present a hysteretic behavior that depends not only on the input but on operation conditions like the pre-stress. Figure 3.15 shows the major and minor hysteresis loops of the proposed biased SMA wire robotic arm. These hysteresis loops were obtained with the series of sinusoidal waves shown in Fig. 3.16.

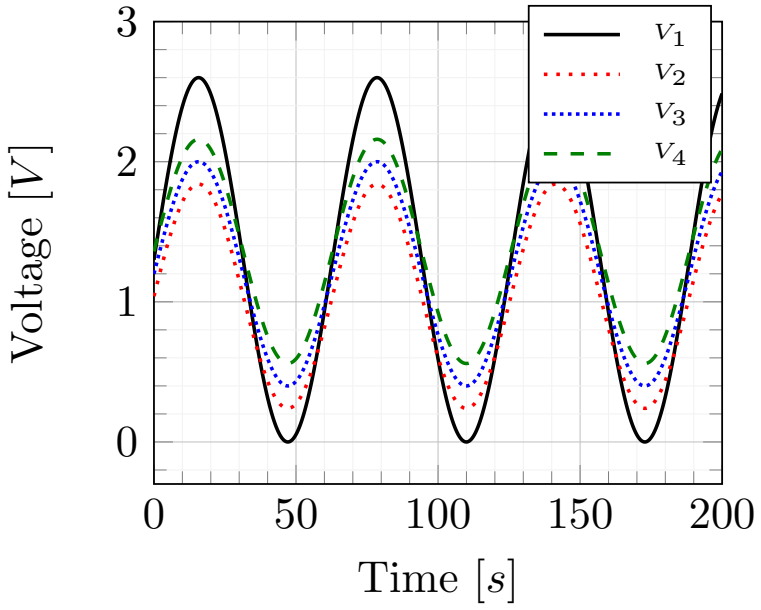

FIGURE 3.16: Sinusoidal voltages at different amplitudes.

3.3 Model validation

This section presents the validation of the state space model presented in Eq. (3.21). Table 3.3 shows the parameters used to obtain the results discussed in this section.

The validation of the model is performed through a series of experimental and simulation tests. The purpose of these tests is to validate the model under different operation points and conditions, i.e. different payloads and control input frequencies and amplitudes. The system was tested under the following conditions:

1. No Load: First the system was tested with no added payload. Two different kinds of tests were performed.
   (a) Step Signal - The system was tested at several consecutive step signals of different amplitudes. Figure 3.17 shows the voltage signal used for this test.
   (b) Sinusoidal Signal - The system was tested at three different sine waves with same amplitude (2.6 V peak-peak voltage) and different frequencies (0.1, 0.2 and 0.3 rad/s). The sine waves are shown in Fig. 3.18
2. Load test: The arm was tested under three different payloads: 14 g, 31 g and 60 g. For each added weight, the system was tested in two different scenarios:
   (a) Step Signal - In this scenario, the same methodology applied for the No Load, Step Signal test was used (See Fig. 3.17).

TABLE 3.3: Model Parameters.

Pr	**Vl**	**Pr**	**Vl**
	Thermal Model		
R_m	4.3836 Ω	R_a	5.4795 Ω
h_0	95 J/m^2Cs	h_2	0.0001 J/m^2C^3s
A	3.8956E-4 m^2	ρ	6450 kg/m^3
C_p	320 J/kg^oC	T_{amb}	26 ^oC
	Constitutive Model		
E_M	28 GPa	E_A	75 GPa
Θ	-0.055 $MPa/^oC$	A_w	0.073 mm^2
ξ_0	1	σ_0	180 MPa
	Phase Transformation		
A_s	68 ^oC	A_f	78 ^oC
M_s	62 ^oC	M_f	52 ^oC
C_A	5.6 $Mpa/^oK$	C_M	5.6 $Mpa/^oK$
	Kinematics and Dynamics		
ε_0	0.03	L_0	0.4 m
r_1	7.5E-3 m	c_1	0.3 $Nms/1^o$
k_s	0.0025 $Nm/1^o$	b_s	0.3 $Nms/1^o$
τ_{s_0}	0.5 Nm		

Pr: Parameter, Vl: Parameter Value.

(b) Sinusoidal Signal - The system was tested with a sine wave of 2.6 V peak-peak amplitude and 0.1 rad/s frequency(see Fig. 3.18, solid line).

3.3.1 Validation criteria

Five different criteria were used to validate the proposed model. These five parameters allow to determine the pertinence of the mathematical model for estimation of the real plant dynamics and control development. Let us define the estimation error as the difference between the measurements (y) and the model prediction ($\hat{y}$),

$$e_y = y - \hat{y} \tag{3.23}$$

The five parameters of the error considered as a mean to determine the performance of the model are the following:

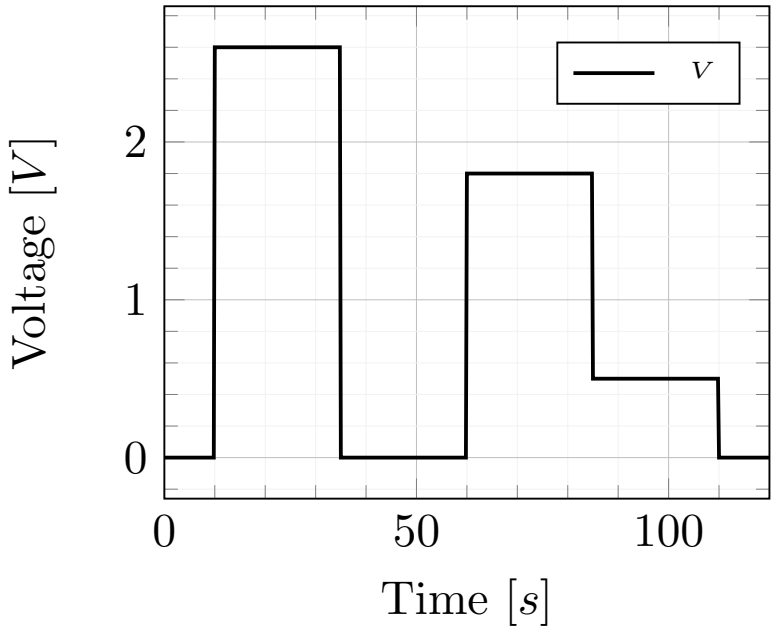

FIGURE 3.17: Series of voltage steps.

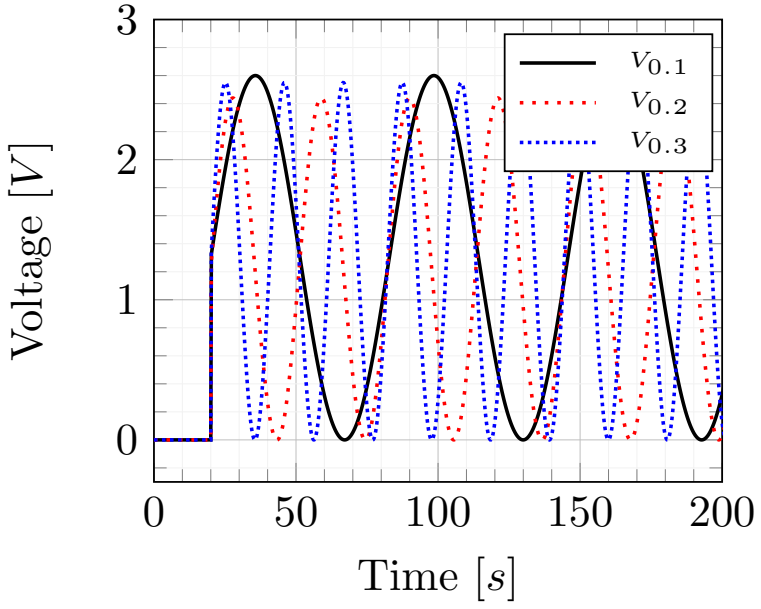

FIGURE 3.18: Different frequency sine voltages.

1. Mean (EM): Defined as the arithmetic mean of the error vector.

$$EM = \frac{1}{n}\sum_{i=1}^{n} e_y\,(i)$$

2. Relative error (E_r): Defined as the quotient between the L^2-norms of the error and measurements.

$$E_r = \frac{\|e_y\|_2}{\|y\|_2}$$

3. Maximum error (MxE): Defined as $MxE = max\,(|e_y|)$

4. Standard Deviation (SD): Used to measure the dispersion of a set of values, defined as:

$$SD = \sqrt{\frac{\sum_{i=1}^{n} (e_y\,(i) - EM)^2}{n-1}}$$

5. Best Fit Percentage (BFP): Defined as the percentage of the measurements that the output reproduces [123].

$$BFP = \left(1 - \frac{\|e_y\|_2}{\|y - \bar{y}\|_2}\right)$$

where $\bar{y}$ is the mean of y.

3.3.2 Model validation results

The ten different scenarios presented at the beginning of this section (3.3) were tested in simulation and experimentally. Figures from 3.19 to 3.26 show the results of all the performed tests. Table 3.4 condenses the results of the tests performed for the model validation.

The two first tests under no load conditions (step response and sine at 0.1 rad/s) show a good capability of the model to predict the plant's behavior under sudden and smooth changes at the control input. For both tests we have a BFP over 92% and a relative error accurate up to 2 decimals. Although the maximum error value is around 9%, this occurs only during the first cycle. This can be confirmed with the standard deviation, which is under 3%. This discrepancy in the first cycle occurs during all the tests. We attribute this phenomenon to the difference in initial conditions between the real plant and the mathematical model.

Next we analyze the response of the system under different frequencies (See Fig. 3.20 and Fig. 3.21). The performance of the model decreases when the frequency increases.

TABLE 3.4: Model validation results.

Test		EM [rad]	E_r	MxE [rad]	SD[rad]	BFP [%]
No load tests						
Steps		0.0007	0.0759	0.1125	0.0435	92.4
Sine 0.1 rad/s		-0.0156	0.0576	0.1120	0.0384	94.3
Sine 0.2 rad/s		-0.0238	0.1283	0.1984	0.0705	87.5
Sine 0.3 rad/s		-0.0437	0.1844	0.2783	0.0946	82.6
Load tests						
Steps	14 g	-0.0073	0.0742	0.1393	0.0409	92.6
	31 g	-0.0164	0.6373	0.0844	0.0279	93.7
	60 g	-0.0099	0.0893	0.1269	0.0386	91.2
Sine	14 g	-0.0138	0.0626	0.1051	0.0381	93.8
	31 g	-0.0118	0.0578	0.1028	0.0325	94.3
	60 g	-0.0113	0.0686	0.0978	0.0332	93.2

EM: Error Mean, E_r: Relative error, MxE: Maximum Error, SD: Standard Deviation, BFP: Best Fit Percentage.

After further analysis, we attribute this decrease on the performance to a change on the system underlying dynamics due to higher frequency input signals. As seen in Fig. 3.22, the shape of the hysteresis changes in response to the input frequency. Even though the model seeks to follow the inputs, it becomes clear that this model, with the given parameters it is not suited for higher frequency applications. This finding does not present a major disadvantage for the use of this model, since a tracking speed of 0.1 rad/s is a good enough speed for the current application.

Finally, the tests executed under added load show that the model can predict correctly the behavior of the system under different payloads. A good performance of the model under different payloads is critical for the current robotic application, where the final goal is to perform grab and carry tasks. The presented model shows a good prediction of the robotic arm behavior under different scenarios. We conclude the proposed model is suitable for further estimation and control development.

3.4 Conclusions

In the first section of this chapter, the mechanical design for a lightweight robotic arm actuated by SMA wires has been presented. The proposed design has an overall weight of less than 100 g and can be actuated by two or three SMA wires depending on the chosen configuration (biased or antagonistic configuration). In the following section, the mathematical model for the two different configurations is presented in state space

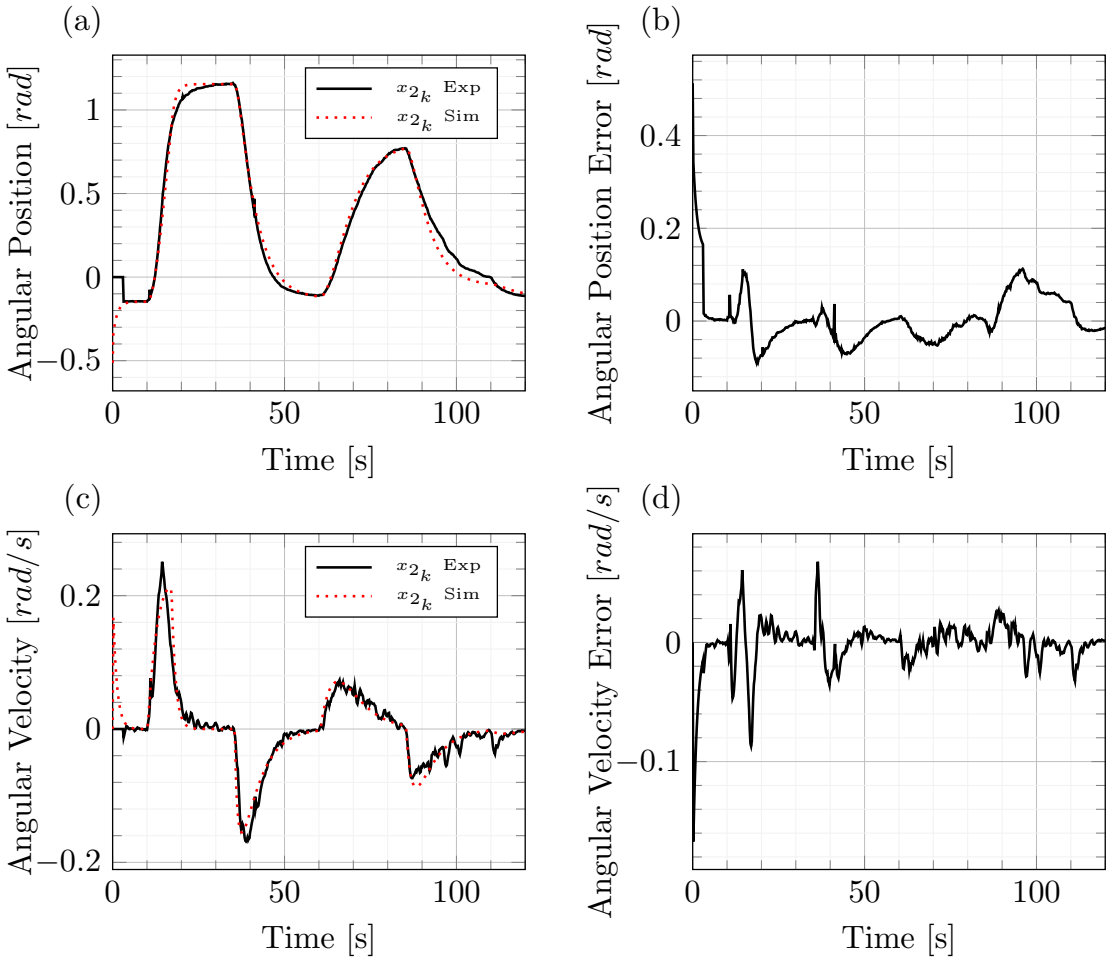

FIGURE 3.19: Model *vs* Measurements, a) Angular position, b) Angular position error, c) Angular velocity, d) Angular velocity error.

form. The presented model is a highly nonlinear switching system with 5 and 10 states for the biased and antagonistic configurations respectively. Finally, in the final section, the mathematical model for the biased configuration of the lightweight robotic arm is validated in simulations and experimentally. The model was tested under 10 different scenarios including step and sinusoidal voltage inputs, as well as changes on the lifted payload. The model shows a good behavior, with a Best Fit Percentage value over 90 % for most of the scenarios. The validated model is used in following chapters to validate the proposed observer and controller development.

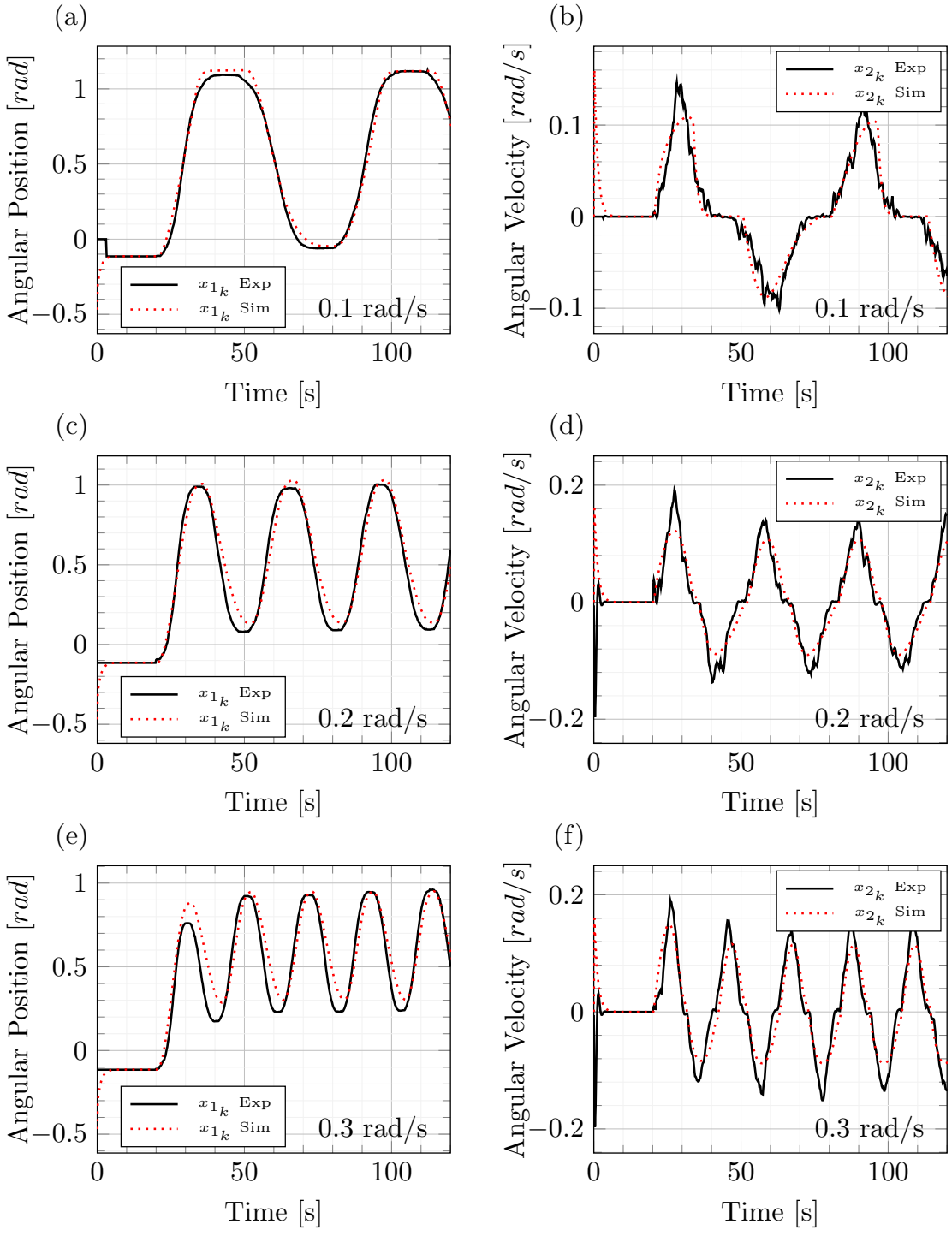

FIGURE 3.20: Model *vs* Measurements, a) Angular position for 0.1 rad/s sine voltage, b) Angular velocity for 0.1 rad/s sine voltage, c) Angular position for 0.2 rad/s sine voltage, d) Angular velocity for 0.2 rad/s sine voltage, e) Angular position for 0.3 rad/s sine voltage, f) Angular velocity for 0.3 rad/s sine voltage.

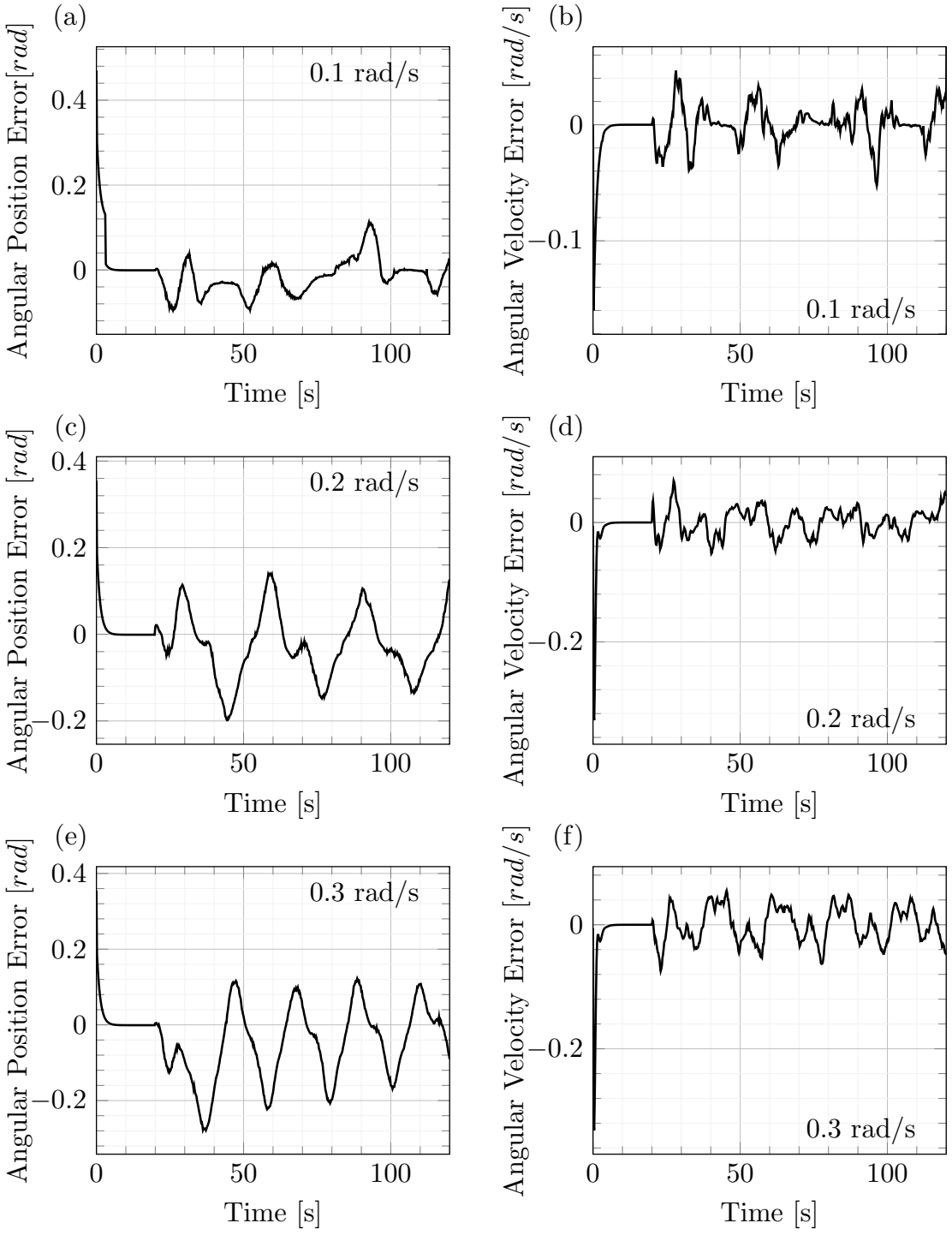

FIGURE 3.21: Model *vs* Measurements error, a) Angular position error for 0.1 rad/s sine voltage, b) Angular velocity error for 0.1 rad/s sine voltage, c) Angular position error for 0.2 rad/s sine voltage, d) Angular velocity error for 0.2 rad/s sine voltage, e) Angular position error for 0.3 rad/s sine voltage, f) Angular velocity error for 0.3 rad/s sine voltage.

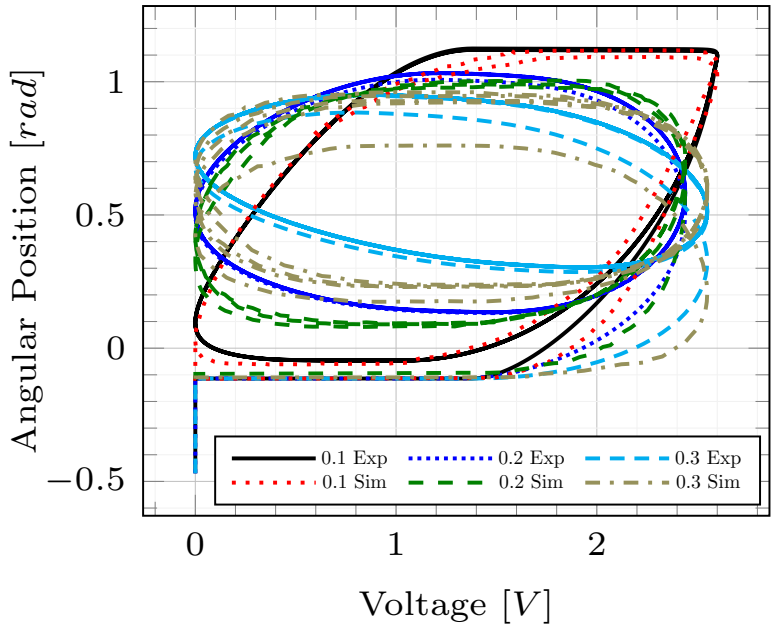

FIGURE 3.22: Experimental *vs* Simulation Hysteresis loops under sinusoidal voltage at different frequencies.

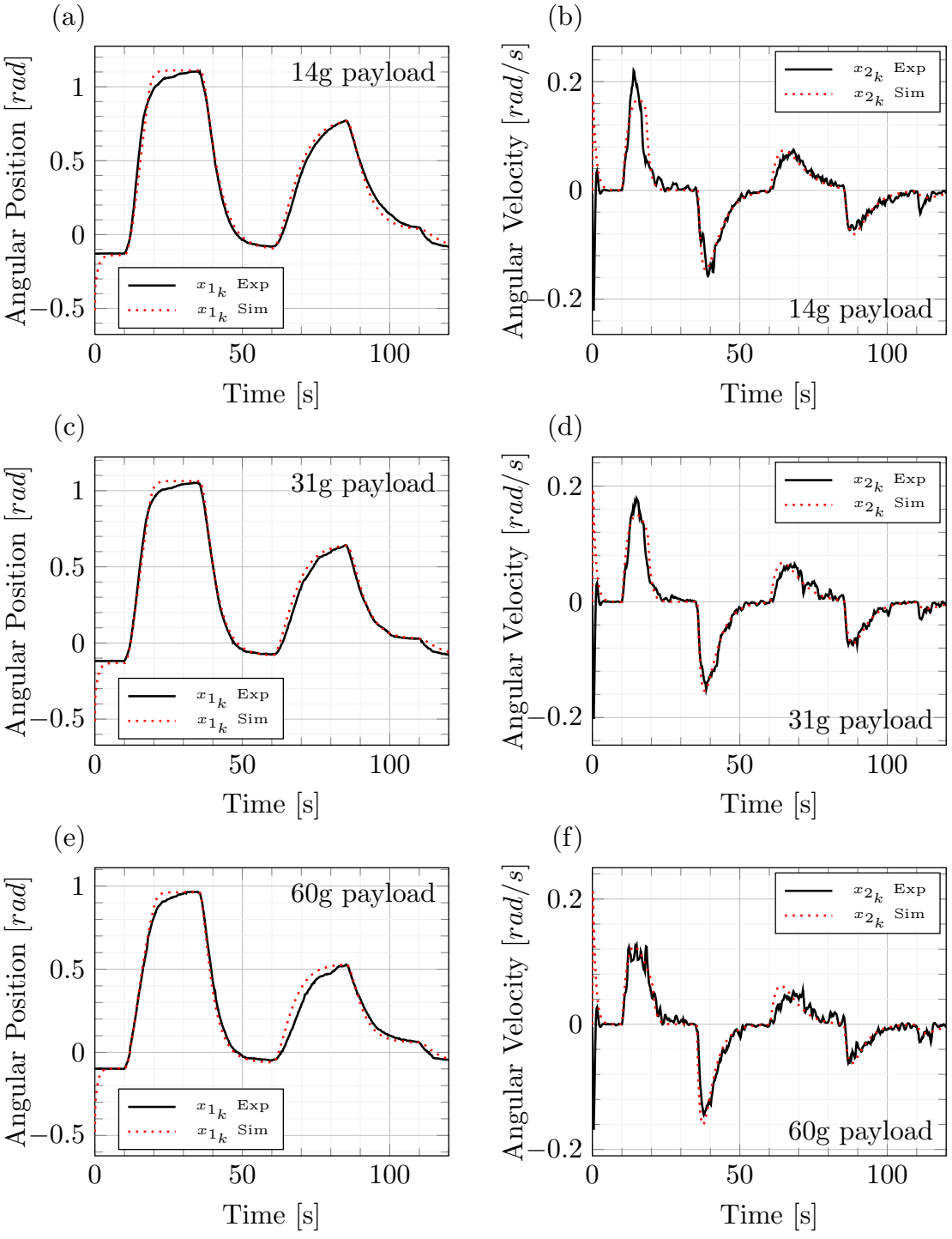

FIGURE 3.23: Model *vs* Measurements step response with different added payloads, a) Angular position with 14 g payload, b) Angular velocity with 14 g payload, c) Angular position with 31 g payload, d) Angular velocity with 31 g payload, e) Angular position with 60 g payload, f) Angular velocity with 60 g payload.

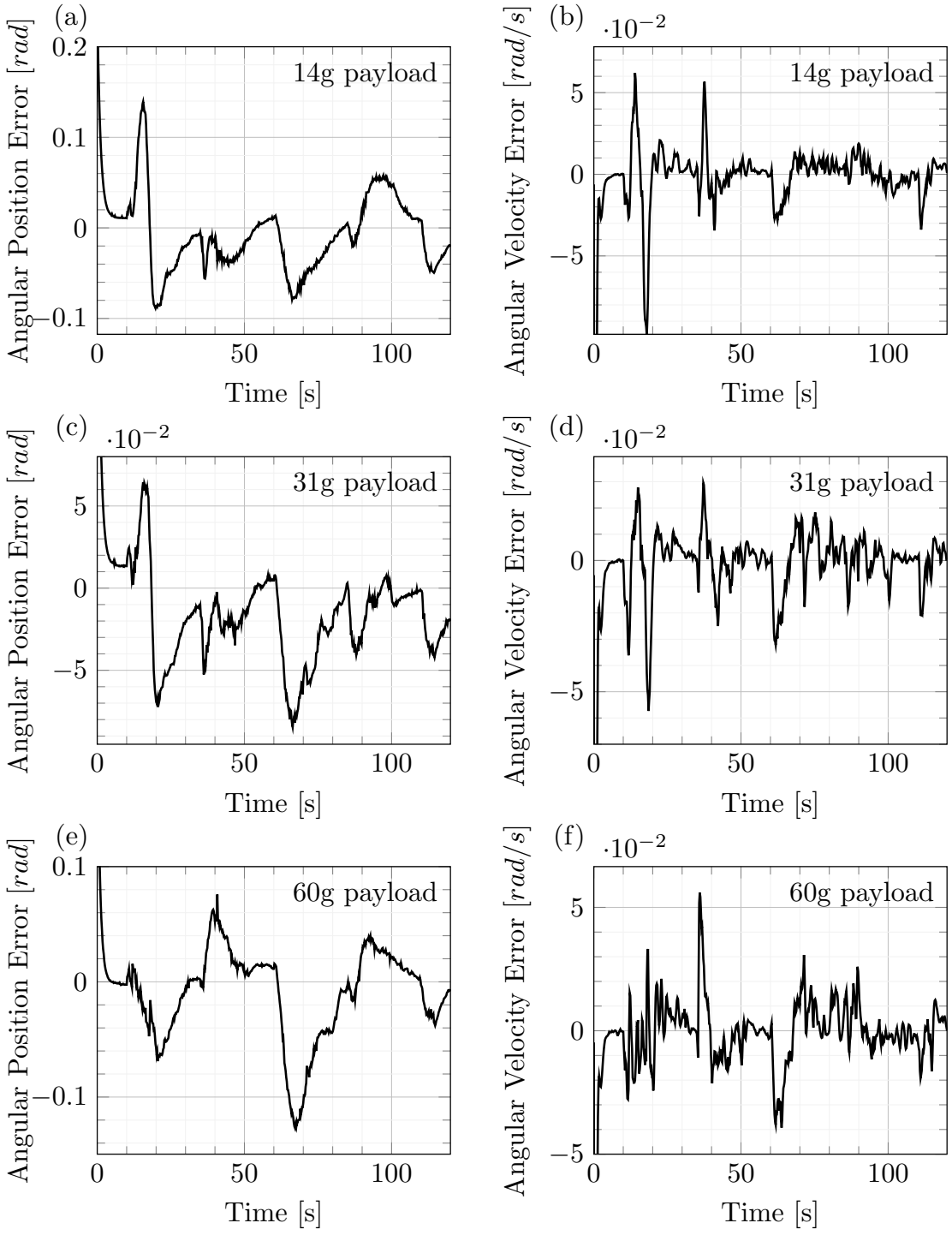

FIGURE 3.24: Model *vs* Measurements error step response with different added payloads, a) Angular position error with 14 g payload, b) Angular velocity error with 14 g payload, c) Angular position error with 31 g payload, d) Angular velocity error with 31 g payload, e) Angular position error with 60 g payload, f) Angular velocity error with 60 g payload.

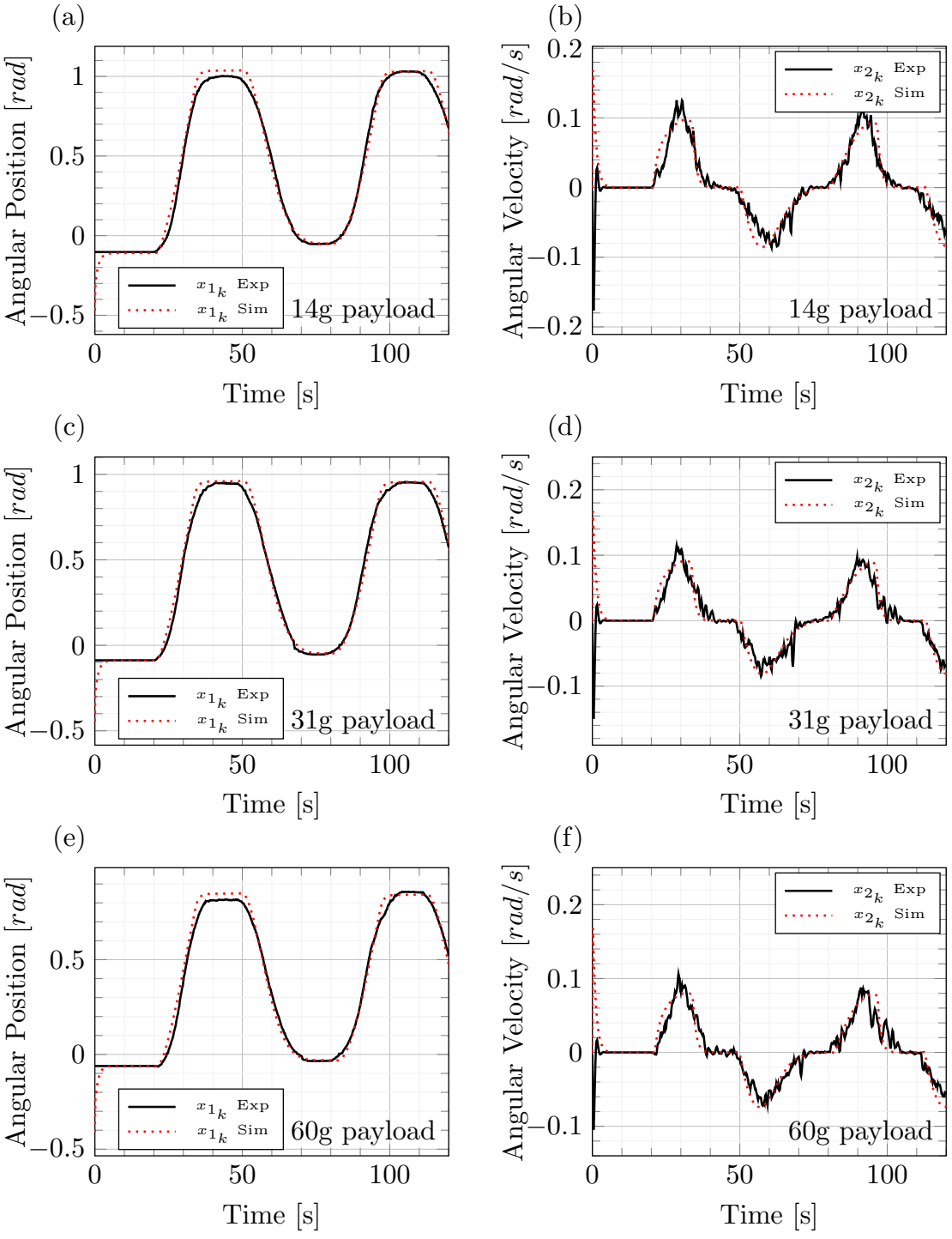

FIGURE 3.25: Model *vs* Measurements tracking response with added payload at 0.1 rad/s sine voltage, a) Angular position with 14 g payload, b) Angular velocity with 14 g payload, c) Angular position with 31 g payload, d) Angular velocity with 31 g payload, e) Angular position with 60 g payload, f) Angular velocity with 60 g payload.

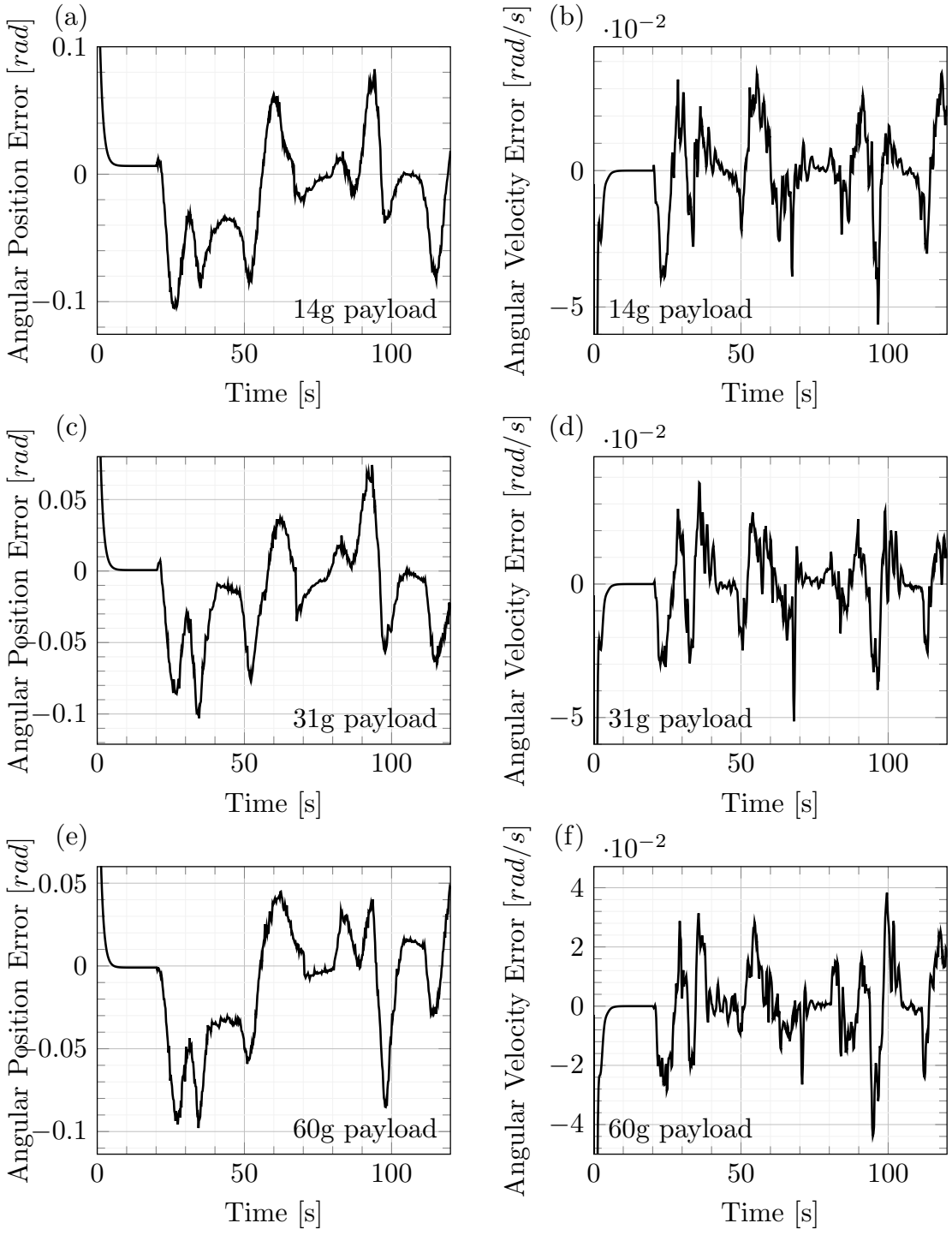

FIGURE 3.26: Model *vs* Measurements error tracking response with added payload at 0.1 rad/s sine voltage, a) Angular position error with 14 g payload, b) Angular velocity error with 14 g payload, c) Angular position error with 31 g payload, d) Angular velocity error with 31 g payload, e) Angular position error with 60 g payload, f) Angular velocity error with 60 g payload.

Chapter 4

Output Feedback Control

This chapter presents the results of a comparative analysis among three different types of output feedback controllers. These controllers are tested in simulation and experiments over different scenarios for angular position regulation and tracking of the SMA wire actuated robotic arm presented in Chapter 3. Section 4.1 presents an overview of the types of output feedback controls found in literature for SMA wire based systems. Section 4.2 describes the mathematical model of the three control strategies chosen for comparison in this chapter. Finally, section 4.3 discusses the results in simulation and experiment of the three applied control approaches. The results of this analysis will be used in Chapter 6 to validate the performance of the proposed observer based control. The chapter conclusions are presented in section 4.4.

4.1 Literature Overview

In the literature, there exist several different approaches for the control of SMA wires, varying from the controlled variable to the chosen technique. In most of the cases, the model and control technique are deeply connected. Until few years ago, the control techniques for SMAs found in literature could be classified into three categories: linear control and Pulse Width Modulation (PWM), nonlinear control, and inverse model based control. Nowadays, a new approach has emerged with the implementation of intelligent control, such as neural networks or fuzzy control. This section will give an overview of the research concerning the SMA control.

4.1.1 Linear control strategies

Many linear control strategies can allow a fairly accurate control without complicated calculations or any previous knowledge of the controlled plant. This category is constituted by the classical Proportional-Integral-Derivative (PID) control and its variations as P, PD or PI control, among others. Some of the most relevant works on linear control is for example the one presented by Ikuta in [116], where a PID control is proposed to control an antagonistic SMA based actuator with combined electric resistance and position feedback. This approach allowed Ikuta to experiment with direct stiffness control and indirect force control. Also, in [124] a PI control is implemented for a SMA based six-segment hydrofoil after a new adaptive actuation control approach failed to be implemented in real-time. In [125], the authors propose a two step PI control for position control. In this approach, when the position error is large, a high proportional gain is applied with a low pass filter, once the error has reached the boundary layer, the control switches to a PI controller to minimize the steady state error. Some further improvements have been made to PID control, as the one presented in [102], where a PID together with a model free control is applied to control a SMA spring based actuator. This combination of control techniques is called intelligent PID (i-PID). In addition to PID, in this category we also find the PWM based controls. Some studies have been conducted to analyze the effect of a PWM or Pulse Width Pulse Frequency (PWPF) control signal over the SMA systems. Among these studies we find the one presented by the authors in [126]. Here, a PWM based control for an SMA based actuator showed 30% less energy consumption than an equivalent PI control without PWM, maintaining the same level of accuracy. The authors in [127] propose the control of an SMA based Minimally Invasive Neurosurgical Intracranial Robot (MINIR), with temperature feedback, PWM control and switching circuits. The switching circuits allow to actuate multiple SMA wires simultaneously and independently using only one power supply.

Different intelligent control approaches have been reported, where the authors improve the simple PID control using intelligent control techniques such as Fuzzy control. In [128], a Fuzzy PID control is proposed for the control of a 3 link snake robot. This approach is later improved by the implementation of a Fuzzy PD+I, which allows to reduce from 125 rules for the fuzzy control to just 30.

The authors in [129], improve significantly the PID control performance by using fuzzy control technique for online tuning. This work attempts to control a compact rotational manipulator. In addition, we find the literature techniques which also apply PWM to the Fuzzy-PID, allowing less energy consumption and the advantages of an improved PID with intelligent control approach. Example of this are the results presented in [130]

where a two DOF joint actuated by three SMA wires is controlled, and the artificial finger in [84] is controlled using a fuzzy PWM-PID approach.

4.1.2 Nonlinear control strategies

In this category we can find all type of controls with nonlinear structures as for example the Variable Structure Controls (VSC). The VSCs are a type of control techniques that change their structure at different operating conditions, frequently depending on the tracking error. Elahinia in [131] presents a VSC for force control of a rotary SMA based actuator. Another type of VSC was applied in [132] to control the position of an antagonistic rotary actuator, where a set of High and Low structures were designed for large and small position errors. The authors in [133], propose a different type of VSC called Sliding Mode Control (SMC). The SMC is one of the most used controls for SMAs, due to its robustness and ability to deal with the hysteretic behavior of the SMAs. In [133], a SMC is used together with a Luenberger observer for position control of a flexible beam through temperature references. Furthermore, in [134] a simple and robust tracking control method based on a hyperbolic tangential SMC and Time Delay Estimation (TDE) is proposed. Here the TDE is used to compensate for the hysteresis of the SMA dynamics, while the hyperbolic tangential SMC drives the system to the sliding surface in an hyperbolic trajectory, without exceeding the velocity limitation for the actuator.

Nonlinear controls also include other techniques as Backstepping or feedback linearization. In [13], a backstepping control is proposed for a rotary SMA based actuator. This technique uses the nonlinear model of the plant to calculate a desired internal variable from the desired reference, until the needed control signal is obtained, as shown in Fig.4.1. In addition, the authors in [135] introduce a feedback linearization for position control of an antagonistic SMA rotary actuator based on the continuous nonlinear model of the actuator. Almost two decades later, Tabrizi et al. [24] proposed a force control scheme based on partial feedback linearization and sliding surfaces. In this work, a position controller is used to generate a desired torque which is then used as reference for the force tracking controller.

In recent years, thanks to the increased computational capacity of modern computational systems, intelligent control techniques such as Neural networks have become prominent topic of research for SMA based system control. The authors in [136] present an output-feedback adaptive neural control for position control of a compliant differential SMA actuator. Here, based on a fourth-order strict-feedback nonlinear model, an adaptive

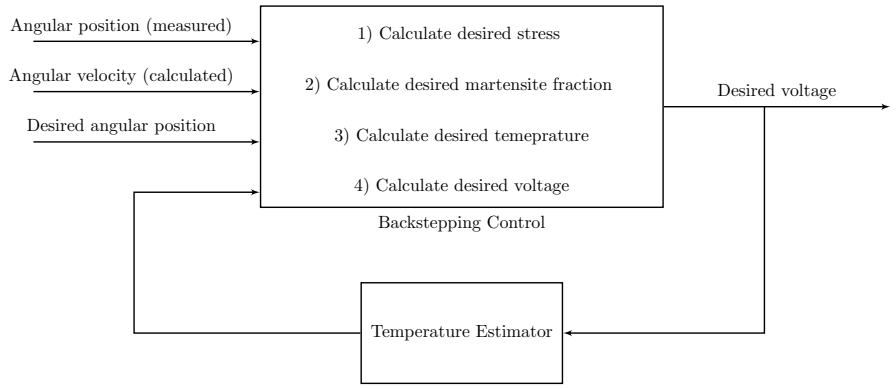

FIGURE 4.1: Backstepping control block diagram [13].

observer-based output-feedback adaptive neural control method is developed to rigorously guarantee closed-loop stability.

4.1.3 Inverse model based control strategies

Inverse model based strategies use an inverse mathematical model of the nonlinear dynamic of the system to cancel its effects. The inverse model is then combined with linear controllers to increase speed and accuracy [63] . In the case of SMAs, the canceled nonlinearity is the hysteresis. For this purpose, models as the Preisach model, Prandtl-Ishlinskii, among others are used. Riccardi *et al* [137], present a control strategy for time-varying hysteretic systems applied to a magnetic SMA system. The controller is based on the combination of a feedforward hysteresis cancellation using a modified Prandtl-Ishlinskii inverse model and a closed-loop control law with adjustable parameter. These parameters are updated online based on a set of learning laws based on Lyapunov design tools. Another adaptive approach is presented by the authors in [138]. Here the authors propose a control for linear systems with unknown input hysteresis, based on an off-line approximated Krasnoselśkii-Pokrovskii (KP) hysteresis model. A Model Reference Control (MRC) is used to compensate for the inaccuracies of the inverse hysteresis model. To ensure the tracking error asymptotically converges to zero, the relation between the tracking error and the KP model parameter errors is used to develop an adaptive control algorithm which updates the KP model parameters.

Similarly, the authors in [97] present an adaptive approach based on recursive identification and adaptive inverse control of hysteresis in SMAs. The hysteresis is modeled using Preisach operator with a piece-wise uniform density function. Two recursive identification techniques are developed and compared, based on output error and output time difference respectively. In addition, we find the control proposed in [139], where an inverse hysteresis model based on a generalized Prandtl Ishlinskii model is applied

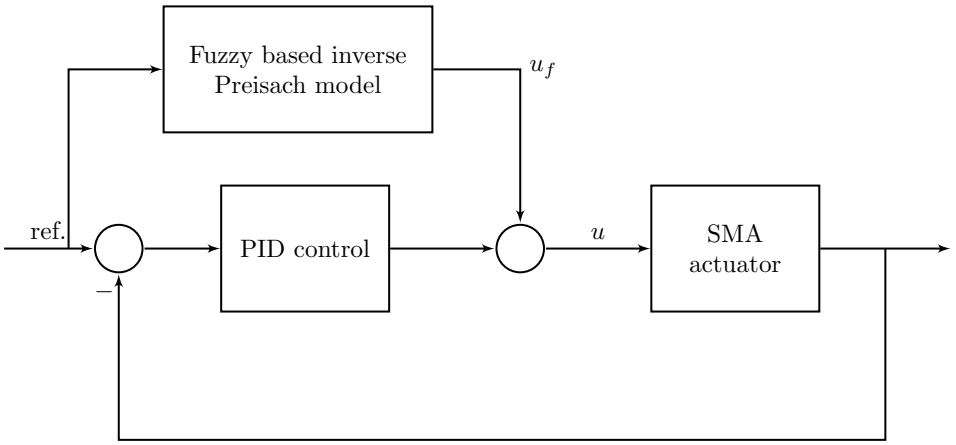

FIGURE 4.2: Fuzzy based inverse Preisach and PID block diagram control [14].

to compensate the hysteretic behavior. Later, a robust dynamic model based control is applied to drive a SMA based micro-actuator to the desired position.

Other than adaptive approaches, in the last decade various works on intelligent control and inverse hysteresis models have been reported. Example of this is the work proposed by the authors in [14]. Here, a fuzzy-based inverse Preisach model is used to cancel the hysteresis in a feedforward control approach. After, a PID control is used to close the loop as feedback controller (see Fig. 4.2).

We can also find Neural Network based techniques, as the one proposed in [140]. Here, the authors propose a neural network open-loop control for position control of a SMA based actuator. A multilayer feedforward neural network is trained to model the variation of voltage as a function of displacement, so it represents the inverse model of the plant.

4.2 Output feedback control for the SMA wire robotic arm

The performance of three different control approaches is compared with for angular position regulation and tracking of the robotic arm.

The controllers selected for this study are: PID control, Sliding Mode Control (SMC) and Adaptive Control (AC). The following subsections describe the design and evaluation of these four controllers.

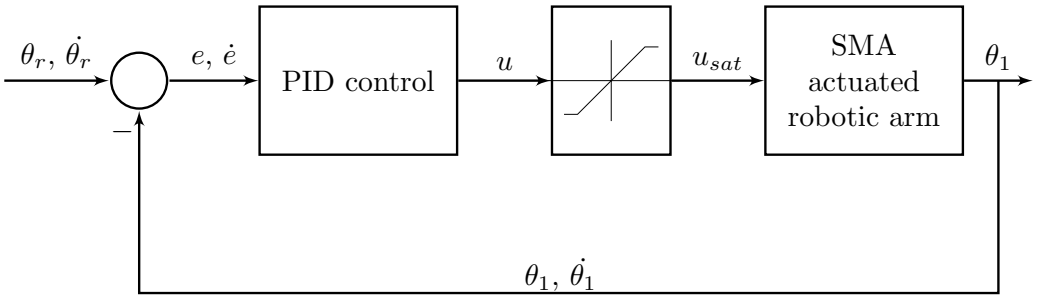

FIGURE 4.3: Block diagram for PID Controller.

4.2.1 PID control

For the purpose of comparison we start with the implementation of a PID control, which is one of the simplest approaches for the control of Robotic joint angular position. The advantages and disadvantages of using a PID approach to control a system with hysteresis are discussed in survey article [141].

Let us define the angular position error (e) as:

$$e = \theta_r - \theta_1 \tag{4.1}$$

where $\theta_r \in \mathbb{R}$ is the desired angular position of the arm with respect to the Z-axis and $\dot{e}$ is defined as the derivative of the error with respect to the time:

$$\dot{e} = \frac{d}{dt}e \tag{4.2}$$

Then, the control law for the PID control is given by:

$$u_j = K_p e + K_i \int e\, dt + K_d \dot{e}, \tag{4.3}$$

where K_p, K_i and K_d represent the proportional, integral and derivative gains respectively.

Figure 4.3 shows the block diagram for the PID controller. In this diagram, the plant is described by the model presented in Eq. (3.21).

4.2.2 Sliding Mode Control

When talking about control of nonlinear systems, the SMC is one of the most applied strategies due to its robustness and fairly easy design. The SMC is a specific type of VSC, which consists of a high-speed switching control law. The SMC aims to drive the

plant states onto a user-defined surface (sliding surface). The structure of the control applied will depend on whether the trajectory of the plant is above or below the sliding surface [27].

The inability of a real actuator to meet the high-speed switching requirements of this type of controller generates a problem known as *chattering*. This problem is perceived as an oscillation around the sliding surface. To overcome this problem a technique called boundary layer is applied, which is a smooth approximation of the switching element [142].

The first step to construct a SMC control is to select the sliding surface, which should represent the desired dynamic of the plant's states in steady state. The sliding surface s selected for this case is a first-order function of the error e, defined in Eq. (4.1) [27]:

$$s = c_p\, e + c_d\, \dot{e}, \tag{4.4}$$

where c_p defines the slope of the sliding surface. Then the control law is established as:

$$v = \begin{cases} M1\, sgn(s) & ,|s| \geq \phi \\ M2\, s & ,|s| < \phi \end{cases}, \tag{4.5}$$

where $M1$ and $M2$ are positive definite constants, ϕ is the value of the boundary layer and $sgn(\cdot)$ defines the sign function as:

$$sgn(\cdot) = \begin{cases} -1, \cdot < 0 \\ 0, \cdot = 0 \\ 1, \cdot > 0 \end{cases} \tag{4.6}$$

The block diagram of this controller is shown in the Figure 4.4.

4.2.3 Adaptive Control

This approach includes a set of different techniques which provide a systematic way of automatically adjusting the control parameters in real time, in order to maintain the desired performance while handling parameter and model uncertainties [28].

Different Adaptive control techniques have been applied for the control of SMA wires. For example in the work presented by [29, 44] a Direct Linear Adaptive control law is developed for a single SMA wire actuated robotic arm. While in [91, 92] an Indirect Adaptive Predictive control using Laguerre functions was used. In [143] and [136]

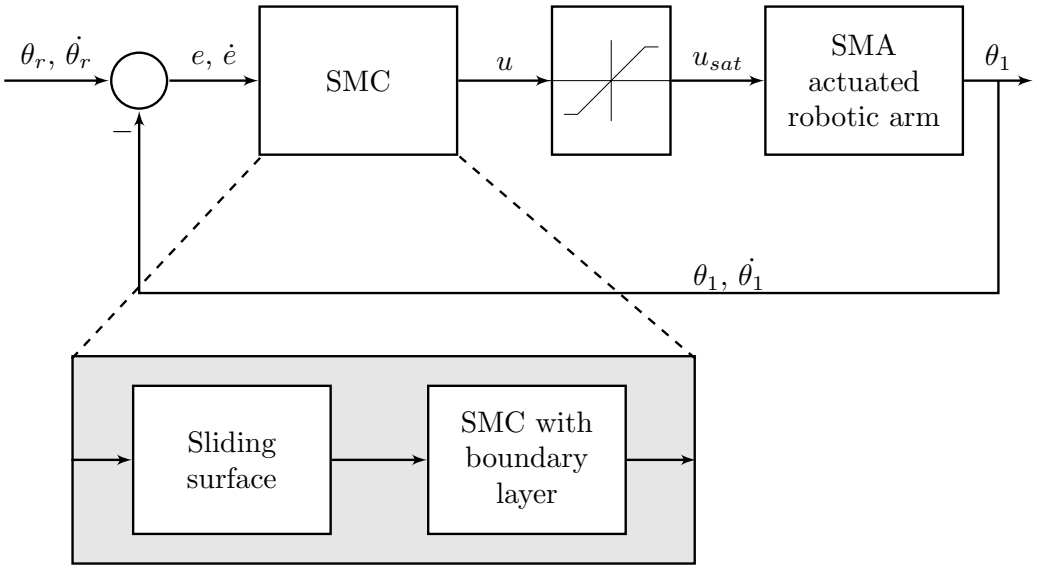

FIGURE 4.4: Block diagram for SMC Controller.

Adaptive nonlinear control has been applied to control the SMA actuator using universal approximators such as Neural-Networks. An adaptive inverse model was implemented in [143] using Dynamic Neural Network (DNN) identifier while, in [136], an observer based output feedback control was implemented using Neural-Network in an Indirect Adaptive method. Similarly, in [144] a Direct adaptive inverse model based controller using a dynamic neural network was implemented. The Adaptive Nonlinear Control based on universal approximators such as Neural-Networks can also be classified under Intelligent Adaptive control. This approach requires the identification of a large number of parameters and the quality of the approximator depends on the number of neurons and persistent excitation condition. The chosen method for this comparative study on output feedback control is the adaptive control presented by the authors in [29]. Contrary to the intelligent adaptive control methods, the authors in [29] use a Direct adaptive control method which requires only one parameter to be tuned in real-time.

For the construction of the adaptive control we consider the general dynamic model for the robotic arm presented as follows:

$$M(\theta)\ddot{\theta} + V_m\left(\theta, \dot{\theta}\right)\dot{\theta} + g(\theta) + F_d\dot{\theta} + \Phi(\theta, \theta_r) = \tau_\omega \tag{4.7}$$

where $\theta, \dot{\theta}, \ddot{\theta}$ represent the position, velocity and acceleration of the couplers, $M(\theta)$ is the inertia matrix, $V_m\left(\theta, \dot{\theta}\right)$ is the centripetal-Coriolis matrix, $g(\theta)$ is considered as the effect of gravity, F_d is the viscous coefficient term, $\Phi(\theta, \theta_r)$ is the nonlinear hysteretic term, τ_ω is the input torque applied to the manipulator joint by the SMA wire.

Based on Eq. (4.1), let us define the filtered error $r(t)$ as:

$$r(t) = \dot{e}(t) + \alpha e(t), \tag{4.8}$$

where α is a known positive gain, different for each SMA wire. After algebraic manipulations, the system dynamic in open loop can be mathematically described as [145]:

$$M(\theta)\dot{r} = -V_m\left(\theta, \dot{\theta}\right) r + \gamma - \tau \tag{4.9}$$

and

$$\gamma = M(\theta)\left(\ddot{\theta}_r + \alpha\dot{e}\right) + V_m\left(\theta, \dot{\theta}\right)\left(\dot{\theta}_r + \alpha e\right) + g(\theta) + F_d\dot{\theta} + \Phi(\theta, \theta_r) \tag{4.10}$$

Based on the open loop dynamics (4.9), we choose the control input as:

$$\tau = \hat{\gamma} + Kr, \tag{4.11}$$

where τ is the control input vector, K is a positive control gain matrix and $\hat{\gamma}$ is the estimate of γ. This value is estimated as follows:

$$\hat{\gamma} = \Gamma^{-1} r, \tag{4.12}$$

where Γ is the positive adaptation gain. Finally the closed-loop dynamic is given by:

$$M(\theta)\dot{r} = -V_m\left(\theta, \dot{\theta}\right) r + Kr + \tilde{\gamma} \tag{4.13}$$

and $\tilde{\gamma} = \gamma - \hat{\gamma}$.

Figure 4.5 shows the block diagram of the closed-loop system with the adaptive control.

4.3 Simulation and experimental results.

The three control approaches presented are tested in simulation and experiments under different scenarios. The operation scenarios include regulation and tracking of desired angular positions and payload conditions as follows:

1. Position regulation. The three controllers are tested under a series of three reference steps: one small step up (0.2 rad), one large step up (0.6 rad) and one step down (0.8 rad), see Fig. 4.6, solid line.

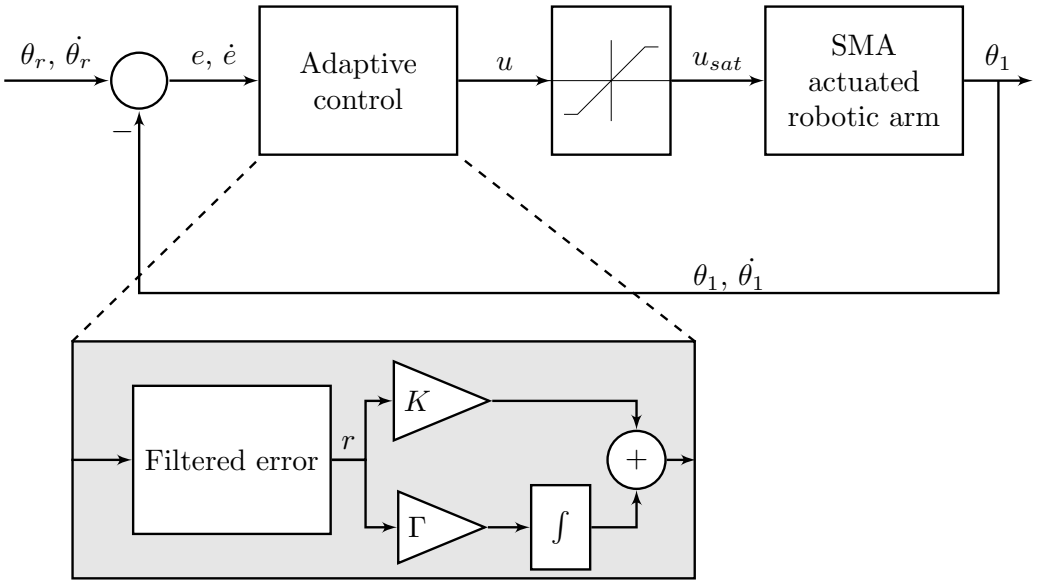

FIGURE 4.5: Block diagram for Adaptive Controller.

2. Position tracking. The three controllers are tested for tracking a sinusoidal reference at three different frequencies (0.1, 0.2 and 0.3 rad/s). See Fig. 4.8, solid lines.

3. Position tracking with payload. The controllers are tested for position tracking of a sinusoidal reference at 0.1 rad/s with a 31 g payload.

For a quantitative comparison, the 3 controllers presented above are analyzed by evaluating different characteristics for regulation and position tracking. For position regulation four characteristics are analyzed: maximum Overshoot (OS), average Settling Time (ST), average Steady State Error (SSE) and relative error (E_r). For position tracking three characteristics are considered: Time to reach and start following the reference, called for practical purposes as Reference Follow Time (FT), Tracking Error (TE) and the relative error (E_r). These parameters are compared in simulation and experiments. The results of the tests are discussed in the following subsections.

4.3.1 Simulation results

The control signal u generated by all the control methods is limited by a saturation block, in order to protect the SMA actuator from over heating. In the same way, the lower voltage is limited to 0 V due to the one way heating control, inherent to the system. The maximum saturation voltage (V_H) is set to $V_H = 5\,V$. The controllers are tuned heuristically with different gains for regulation and tracking as shown in Tab. 4.1.

TABLE 4.1: Controller parameters in simulation.

Control	**Parameters**		
	Regulation		Tracking
PID	*PID1*	*PID2*	
	$K_p = 4.5$	$K_p = 3$	$K_p = 7$
	$K_i = 0.5$	$K_i = 0.2$	$K_i = 3$
	$K_d = 1.5$	$K_d = 1.5$	$K_d = 1.5$
SMC	$\phi = 10$		$\phi = 10$
	$K_p = 10$		$K_p = 10$
	$K_i = 1.3$		$K_i = 3$
	$K_d = 4$		$K_d = 4$
Adaptive	$\alpha = 4$		$\alpha = 7$
	$K = 1.5$		$K = 1.5$

Figures 4.6 to 4.11 show the results of all the tests in simulation. Table 4.2 summarizes the results for position regulation. It is clear that a simple PID control it is not capable of dealing with the nonlinearities of SMA wires. While PID1 has a good performance to follow step up references, the settling time for the step down is over 50 s. On the other hand, PID2 is incapable of reaching the reference for the steps up but has an acceptable performance for step down reference. It has a settling time of 26 s and the smallest steady state error. It becomes clear that a conventional PID approach cannot handle both dynamics for position regulation. The SMC shows a good behavior for both steps up and down. However, the settling time is considerably longer than the one showed by the adaptive control. The adaptive control shows the fastest response and the smallest relative error for position regulation.

Table 4.3 shows the results of position tracking with and without payload. For tracking all three controllers show a similar behavior with and without load for a frequency of 0.1 rad/s. When the frequency increases to 0.2 rad/s, the PID is no longer capable of following the reference and its relative error increases to double of that shown by the SMC and adaptive control. The SMC and adaptive control present a similar behavior for tracking control, although the adaptive control has a slightly better performance with shorter settling times and relative error. However, non of the three controllers is capable of following the 0.3 rad/s sinusoidal reference.

The adaptive control and SMC prove to be capable of dealing with the system nonlinear dynamics for regulation and tracking. The adaptive control presents slightly better results in most of the test. Nevertheless, the real advantage of the adaptive control is the fact that this control will adapt to possible changes in parameters over time, while the SMC will need to be tuned after any change in the system.

TABLE 4.2: Comparative table of output feedback controls performance for position regulation in simulation.

Control	**OS [rad]**	**ST [s]**	**SSE [rad]**	E_r
Small Step up (0.2 rad)				
PID1	0	24.4	0.0152	0.4581
PID2	0	> 40	N/A	0.4911
SMC	0.4775	15	0.0085	0.4492
Adaptive	-1.0458	12.6	-0.0035	0.4463
Large Step up (0.6 rad)				
PID1	12.48	20.2	0.0112	0.4581
PID2	0	> 40	N/A	0.4911
SMC	26.73	25.8	0.0149	0.4492
Adaptive	20.95	16.8	-0.0089	0.4463
Step down (0.8 rad)				
PID1	0	> 50	N/A	0.4581
PID2	0	15.6	-0.0024	0.4911
SMC	0	33.2	0.0033	0.4492
Adaptive	0	14.4	0.0051	0.4463

OS: Overshoot percentage; ST: Settling time; SSE: Steady State Error; E_r: Relative Error.

4.3.2 Experimental results

The conditions for the experimental tests are the same as described for the simulation tests. The control input u is saturated between 0 and 5 V to avoid overheating of the wire. Table 4.4 shows the parameters of the three controllers for regulations and tracking of angular position. The controllers were tuned heuristically based on the gains used in simulation. The gains are moderately different from the ones used in simulation.

The experimental results are shown in Figures 4.12 to 4.17. The Table 4.5 summarizes the results for position regulation. The results obtain in experiments are close to the ones shown in simulation. The controllers PID1 and PID2 present a better performance in experiments. For the small step up test, PID2 reaches the reference at 27.2 s and PID1 reaches at 32 s for the step down test. The SMC presents a faster response and a lower steady state error of the controllers for the step up regulation. However, this controller takes almost double the time, as compare to adaptive control, to reach the reference for the step down. In general the adaptive control shows a better performance for position regulation.

Table 4.6 shows the results for position tracking. For position tracking all three controllers show a good performance for tracking of a sinusoidal reference at 0.1 rad/s,

TABLE 4.3: Comparative table of output feedback controls performance for angular position tracking in simulation.

Control	**FT [s]**	**TE [rad]**	E_r
Sine 0.1 rad/s			
PID	16	0.0159	0.0740
SMC	15	0.0150	0.0637
Adaptive	14.2	0.01558	0.0636
Sine 0.2 rad/s			
PID	4.8	0.0719	0.2230
SMC	9	0.0455	0.1322
Adaptive	9	0.0425	0.1207
Sine 0.3 rad/s			
PID	2.8	0.2532	0.6323
SMC	2.6	0.1208	0.3240
Adaptive	2.4	0.1146	0.3104
Sine 0.1 rad/s, 31g payload			
PID	16.2	0.0173	0.0731
SMC	16	0.0161	0.0639
Adaptive	14.6	0.0167	0.0636

FT: Reference Follow Time; TE: Tracking Error; E_r: Relative Error.

TABLE 4.4: Controller Parameters in experiments.

Control	**Parameters**		
	Regulation		Tracking
PID	*PID1*	*PID2*	
	$K_p = 4.5$	$K_p = 4.8$	$K_p = 7$
	$K_i = 0.5$	$K_i = 0.9$	$K_i = 3$
	$K_d = 1.5$	$K_d = 1.5$	$K_d = 1.5$
SMC	$\phi = 10$		$\phi = 10$
	$K_p = 10$		$K_p = 10$
	$K_i = 1.3$		$K_i = 3$
	$K_d = 4$		$K_d = 4$
Adaptive	$\alpha = 3.8$		$\alpha = 7$
	$K = 1.5$		$K = 1.5$

with and without payload. When the frequency increases, the relative error of the three controllers increases, not being able to follow the reference at 0.3 rad/s. In the case of position tracking adaptive control shows a faster response and a lower relative error as expected based on simulation results.

In conclusion, the adaptive control proved to be the better approach for the kind of system dealt with in this dissertation. Although SMC shows good results, close to those

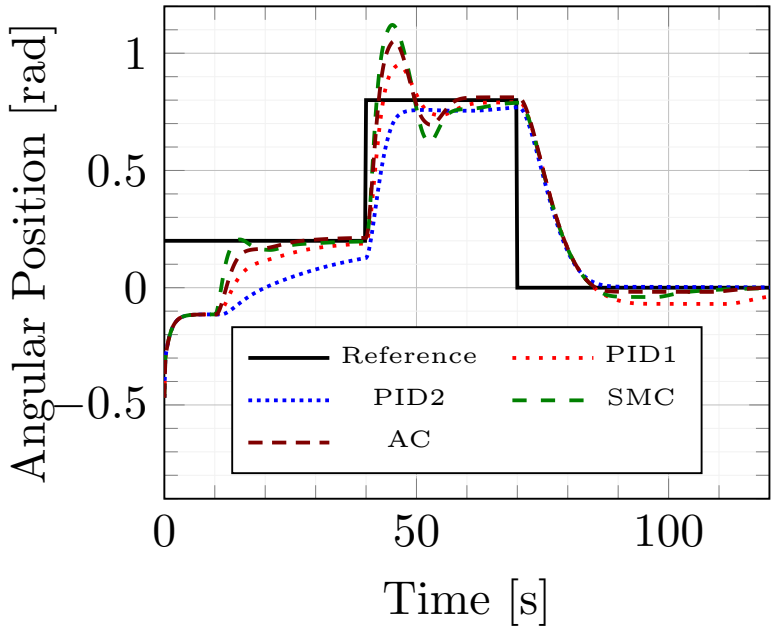

FIGURE 4.6: Output feedback controllers for angular position regulation in simulation.

of the adaptive control, the adaptive control has, as its name suggests, the ability to adapt to changes in ambient and system parameters, such as changes on convection coefficient. This was proven in simulation in [39]. The adaptive capability makes the adaptive control a good control approach for output feedback control.

4.4 Conclusions

The first section of this chapter presents an overview of the different control techniques developed and applied on SMA based actuated systems. Three of this methods, named PID, Sliding Mode Control and a model based Adaptive Control are further explained and applied in simulation and experiments for angular position control of the biased lightweight robotic arm proposed in the previous chapter. The three controllers are tested for position regulation and tracking under different scenarios. The adaptive control showed to be the best, out of the three chosen control techniques, to deal with the nonlinearities of the controlled system. The results of this chapter are used on Chapter 6 for comparative purposes.

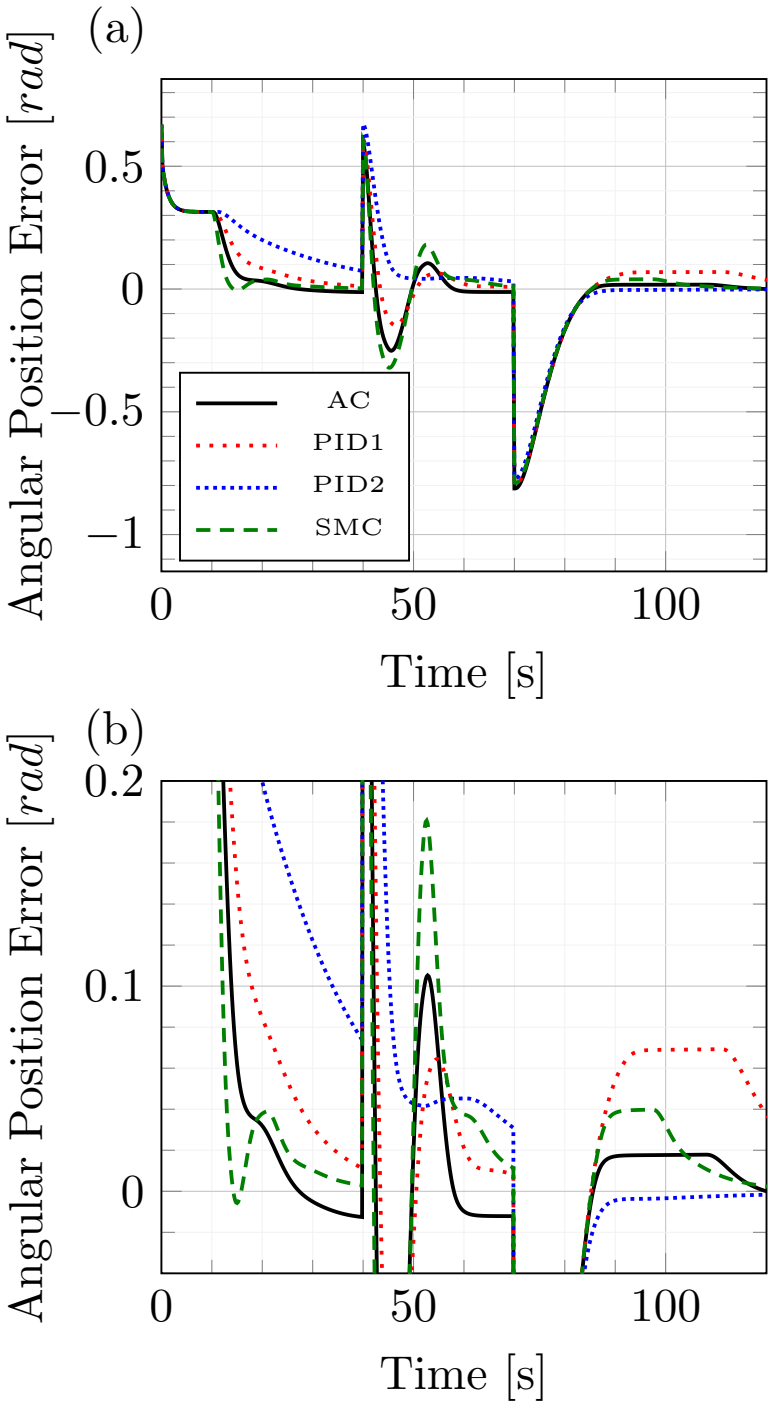

FIGURE 4.7: Output feedback controllers errors in simulation.

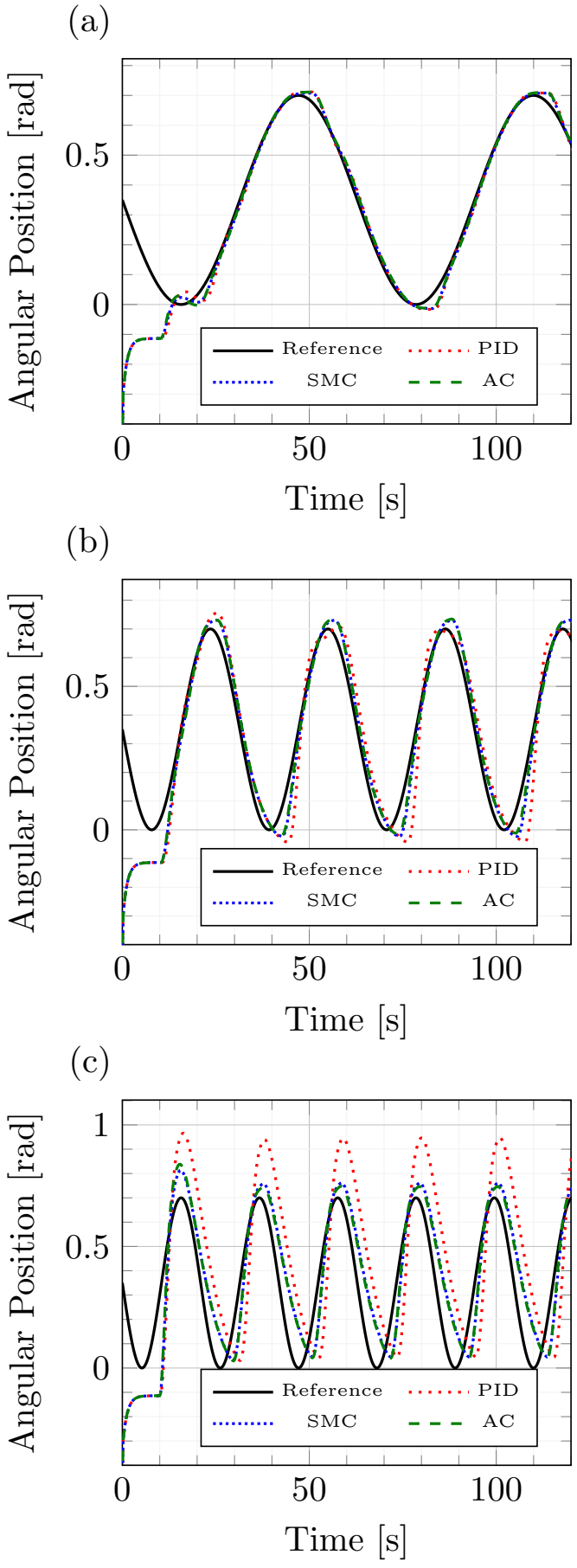

FIGURE 4.8: Output feedback controllers for angular position tracking in simulation, a) 0.1 rad/s sine, b) 0.2 rad/s sine, c) 0.3 rad/s sine.

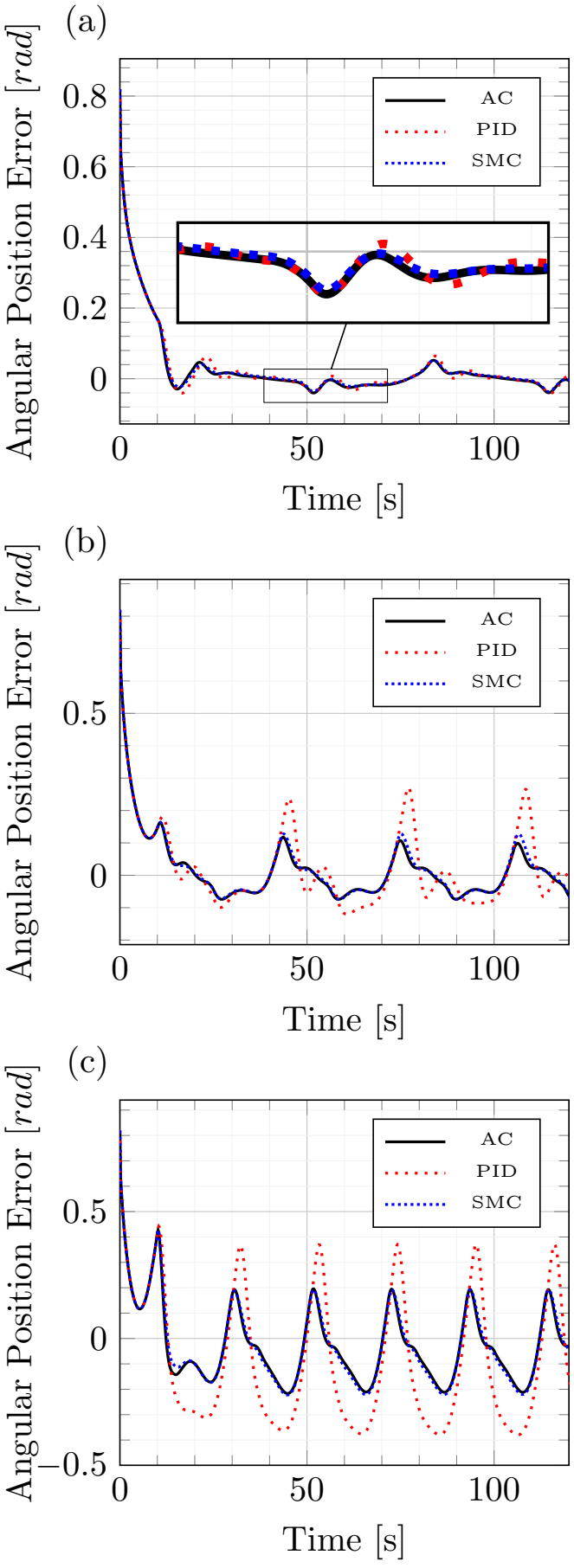

FIGURE 4.9: Output feedback controllers errors for angular position tracking in simulation, a) 0.1 rad/s sine, b) 0.2 rad/s sine, c) 0.3 rad/s sine.

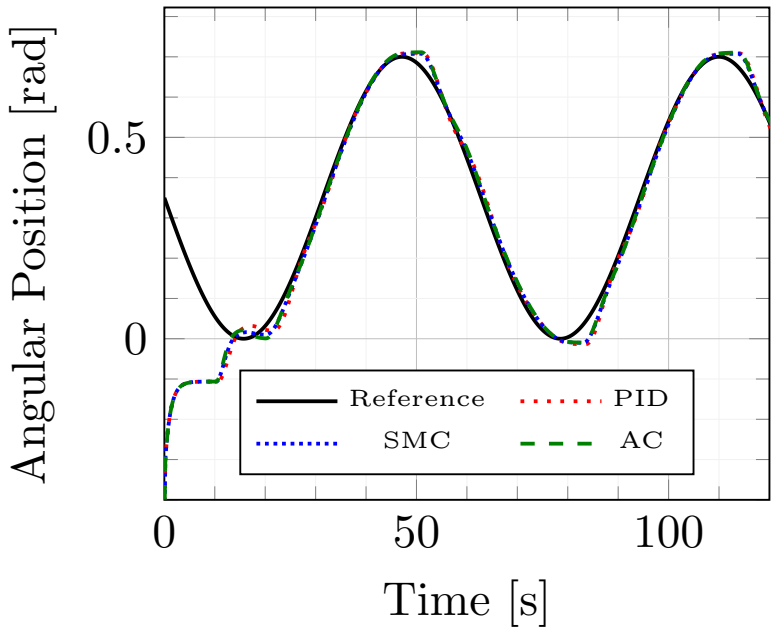

FIGURE 4.10: Output feedback controllers for angular position tracking with 31 g payload in simulation.

TABLE 4.5: Comparative table of output feedback controls performance for position regulation in experiments.

Control	**OS [%]**	**ST [s]**	**SSE [rad]**	E_r
Small Step up (0.2 rad)				
PID1	2.77	7.8	-0.0181	0.3821
PID2	0	> 40	N/A	0.4307
SMC	0.2575	3.4	-0.0013	0.3523
Adaptive	5.3691	19.6	-0.0043	0.3666
Large Step up (0.6 rad)				
PID1	3.0458	22.4	-0.00869	0.3821
PID2	0	27.2	0.0165	0.4307
SMC	2.6275	16.4	-0.0090	0.3523
Adaptive	5.5875	20.8	-0.0112	0.3666
Step down (0.8 rad)				
PID1	0	32.4	0.0006	0.3821
PID2	0	26.4	-0.0013	0.4307
SMC	0	23	0.00273	0.3523
Adaptive	0	13.2	-0.0058	0.3666

OS: Overshoot percentage; ST: Settling time; SSE: Steady State Error; E_r: Relative Error.

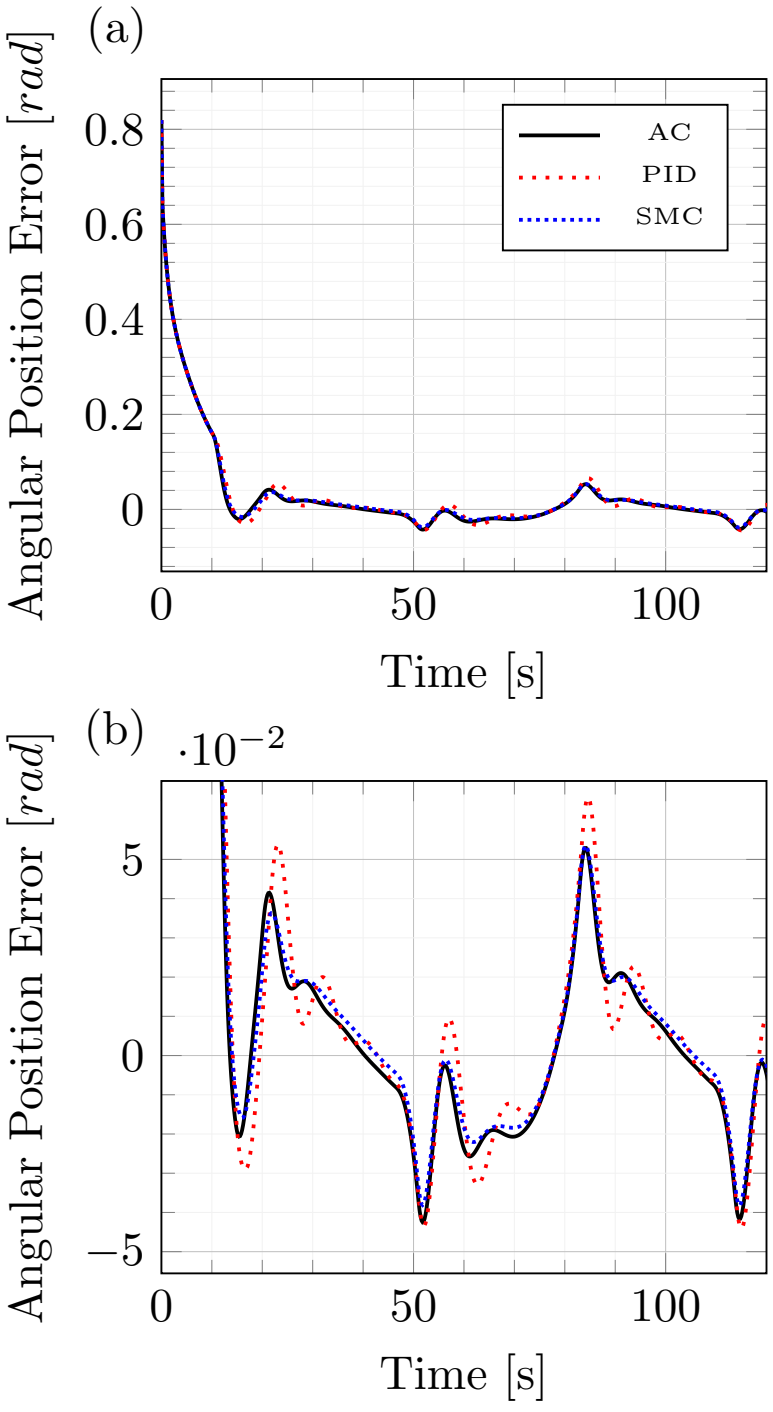

FIGURE 4.11: Output feedback controllers errors with 31 g payload in simulation.

TABLE 4.6: Comparative table of output feedback controls performance for angular position tracking in experiments.

Control	**FT [s]**	**TE [rad]**	E_r
Sine 0.1 rad/s			
`PID`	16.8	0.0157	0.0799
`SMC`	14.2	0.0146	0.0714
`Adaptive`	13.6	0.0141	0.0679
Sine 0.2 rad/s			
`PID`	4.8	0.0399	0.1461
`SMC`	4.6	0.0351	0.1269
`Adaptive`	4	0.0332	0.1155
Sine 0.3 rad/s			
`PID`	3.2	0.1187	0.3552
`SMC`	3.2	0.0791	0.2539
`Adaptive`	2.8	0.0669	0.2210
Sine 0.1 rad/s, 31g payload			
`PID`	9.6	0.0185	0.0774
`SMC`	7.6	0.0179	0.0702
`Adaptive`	7.4	0.0178	0.0712

FT: Reference Follow Time; TE: Tracking Error; E_r: Relative Error.

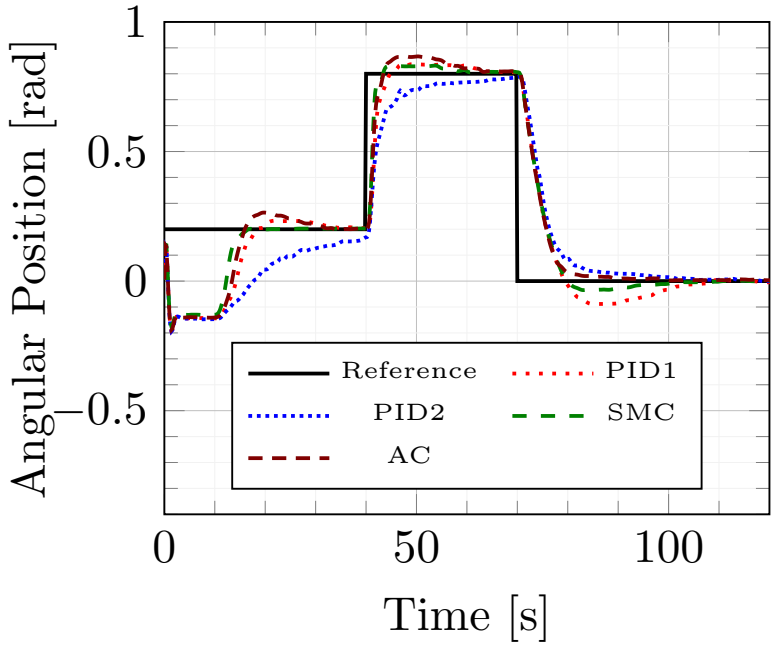

FIGURE 4.12: Output feedback controllers for angular position regulation in experiments.

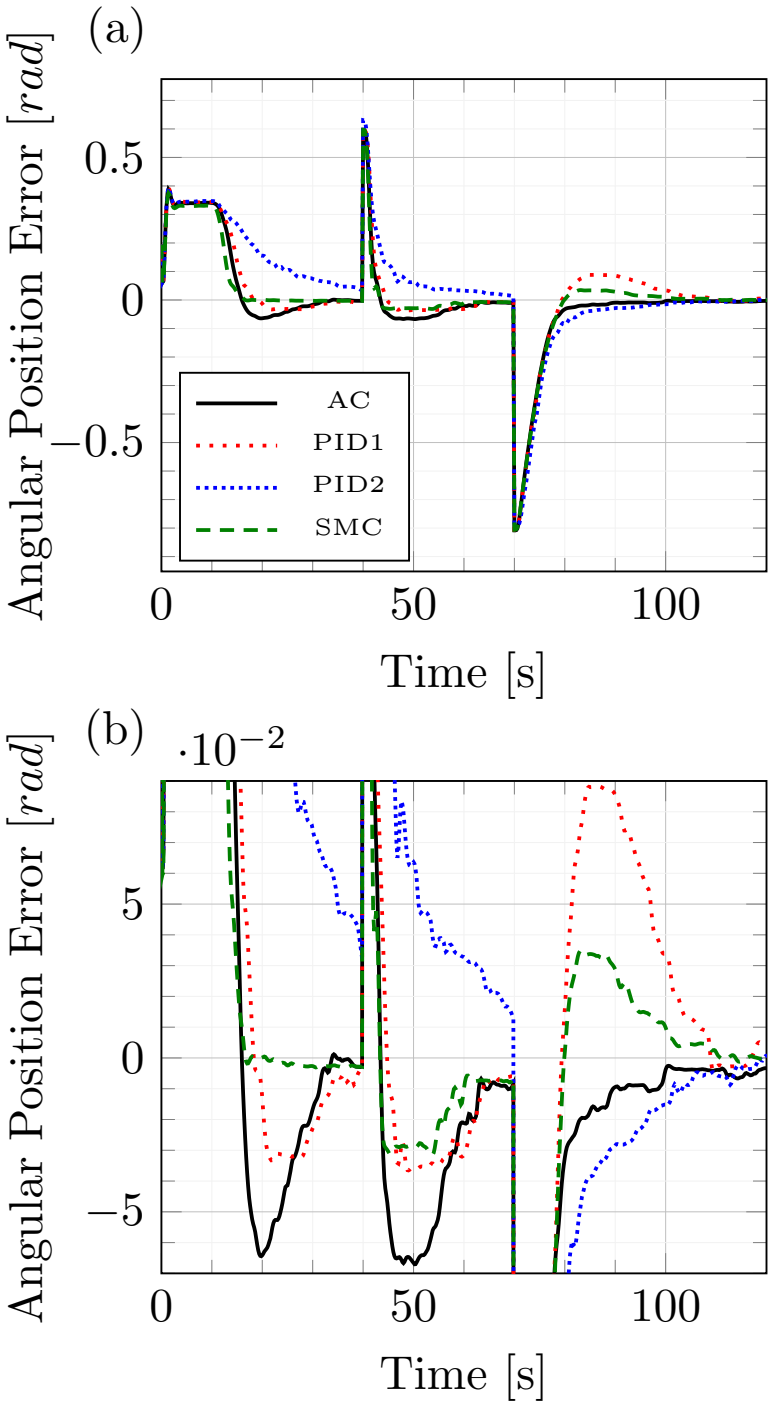

FIGURE 4.13: Output feedback controllers errors for angular position regulation in experiments.

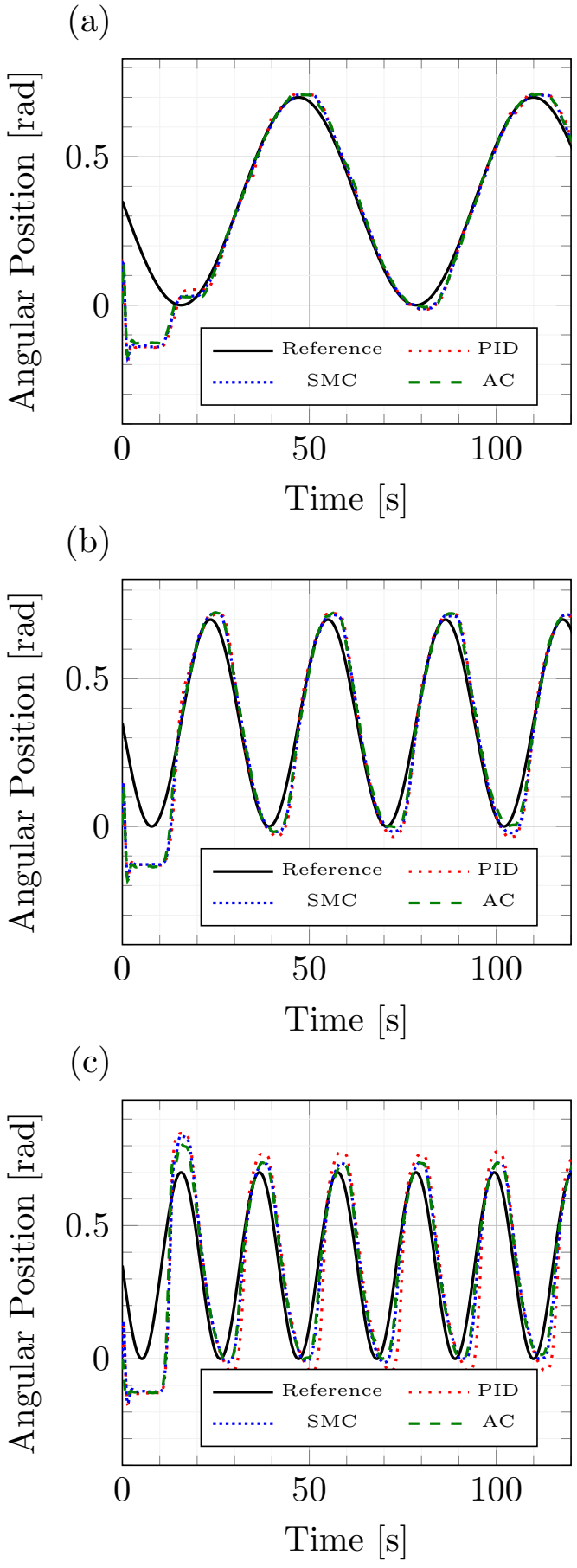

FIGURE 4.14: Output feedback controllers for angular position tracking in experiments, a) 0.1 rad/s sine, b) 0.2 rad/s sine, c) 0.3 rad/s sine.

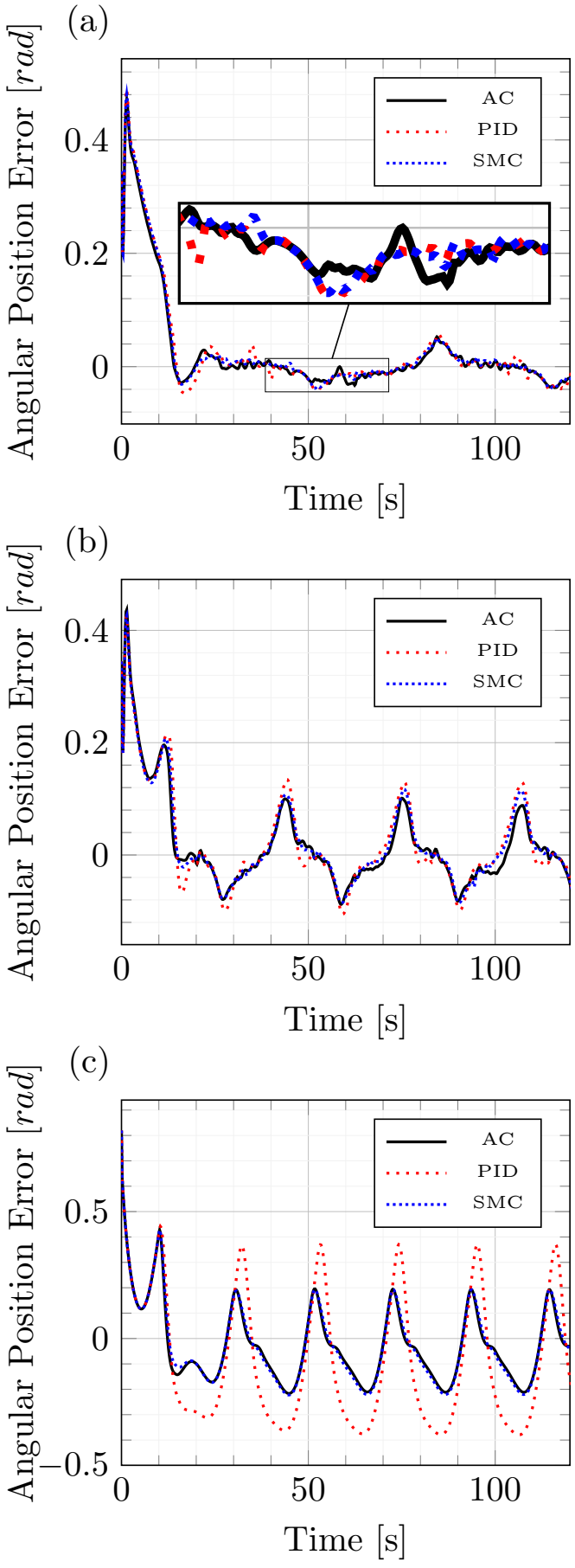

FIGURE 4.15: Output feedback controllers errors for angular position tracking in experiments, a) 0.1 rad/s sine, b) 0.2 rad/s sine, c) 0.3 rad/s sine.

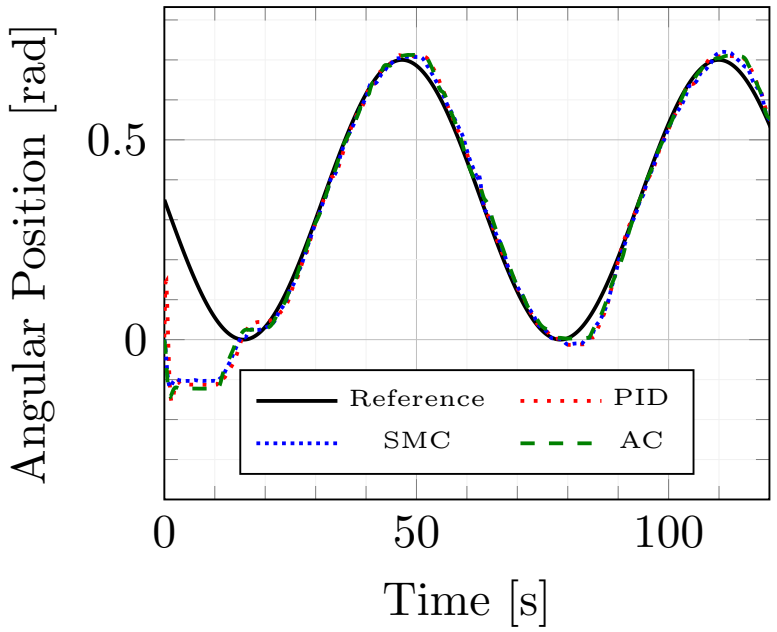

FIGURE 4.16: Output feedback controllers for angular position tracking with 31 g payload in experiments.

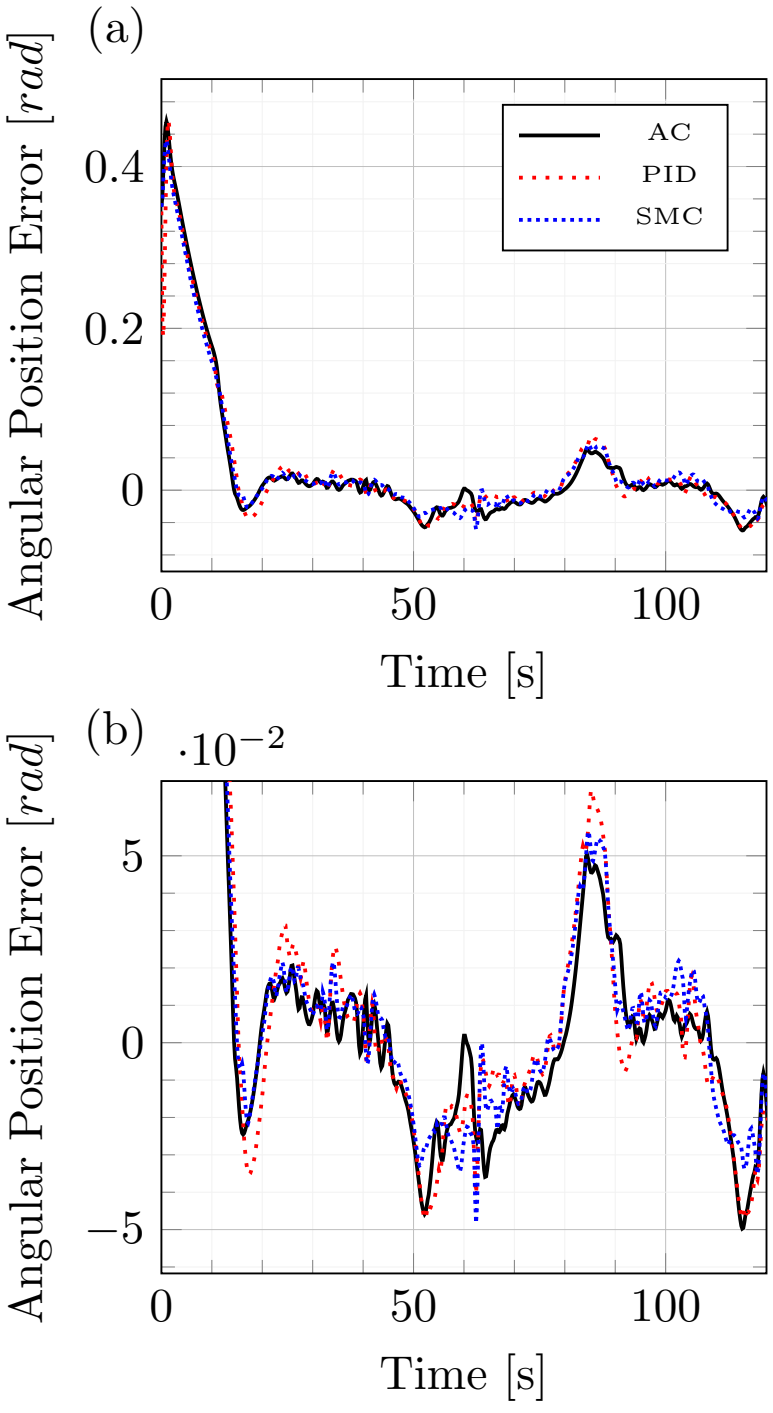

FIGURE 4.17: Output feedback controllers errors for angular position tracking with 31 g payload in experiments.

Chapter 5

Extended Kalman Filter for State and Unknown Input Estimation with Sliding Modes

This chapter presents the development and validation of the proposed observer for state and unknown input estimation. Section 5.1 presents an overview of the observers found in literature for SMA based systems. Section 5.2 describes the development of the observable discrete-time mathematical model for the single SMA wire robotic arm presented in Chapter 3. Section 5.3 presents the proposed Extended Kalman Filter observer for state and unknown input estimation with sliding modes (EKF-UI). Further in this section, the convergence analysis of the proposed observer and its implementation is discussed. Finally, section 5.4 discusses the validation of the experimental results of the observer against simulation results and experimental measurements. The chapter conclusions are presented in section 5.5.

5.1 Literature Overview

When talking about estimation for SMAs, the research found in the literature is limited and mostly focused on the estimation of the mechanical states (position and velocity) of SMA based actuators. We found few observers for estimation of the SMA wire states where the switching dynamic of the SMA is considered. However, more often than not, the works found in literature fail to provide any stability or convergence analysis. The following paragraphs present a review of the state of the art in observers for SMA wire based systems.

The authors in [146] present a non-switching Extended Kalman Filter (EKF) for the estimation of position, velocity, stress and temperature of an SMA wire based actuator. The SMA manipulator state vector is defined as $x = \begin{bmatrix} \theta & \dot{\theta} & \sigma & T \end{bmatrix}$. This proposal avoids the switching in the model by computing the stress from the dynamic equations and not the constitutive model. The model is then discretizied and an Extended Kalman Filter is proposed. It is important to mention that the model proposed in this research is not rank observable.

In [147], the authors present a simple SMA wire rotational actuator with a bias spring. They propose an augmented EKF for the estimation of the temperature and stress of the SMA wire and the bias spring coefficients, where the augmented parameters correspond to these coefficients. The model used for the development of the augmented EKF is a switching model based on a constitutive model. The authors do not provide any observability or stability proof. The authors in [148] develop a position control of a spherical joint using feedback linearization. For the feedback linearization the wire's temperature is needed, thus the authors propose a simple first degree nonlinear switching model for the estimation of the SMA wire temperature as shown in the next equation:

$$\dot{\hat{T}}_{SMA} = \frac{\frac{V^2}{R} - hA_w\left(\hat{T}_{SMA} - T_{amb}\right)}{mC_p + mL_{heat}Q_T\left(\hat{T}_{SMA}\right)/\varepsilon_i} \tag{5.1}$$

where the variable Q represents the coupling between changes in temperature and strain. This variable is described by a switching equation outlined by different equations for heating and cooling respectively.

A Luenberger observer for temperature estimation based on position measurements is introduced in [133] for an antagonistic endoscope like actuator. The authors propose a neural networks to process each position to obtain an equivalent temperature as reference for a Sliding Mode Control (SMC).

In [149], a sliding mode observer for the estimation of temperature, velocity and acceleration of an antagonistic SMA based actuator is presented. A basic observer structure is defined as:

$$\dot{\hat{x}} = \hat{f}(x) - H\left(C\hat{x} - z\right) - Kl_s \tag{5.2}$$

where l_s is an error based sign vector (sliding gain) and H is the gain matrix for a Luenberger observer obtained form the linearization of $\hat{f}(x)$. From the estimated states, a non-stress dependent martensite fraction calculation is applied.

In [150] an EKF is applied to a single SMA wire actuator with biased spring. The EKF is used to estimate the SMA wire temperature and spring displacements from the

measurement of the electric resistance. This estimation is latter used for the training of a couple of Artificial Neural Networks (ANN), in order to estimate the total displacement of the actuator. The authors in [151] present a simple linearized model for a SMA based smart joint for minimally invasive surgeries, which is later used to develop a sliding mode control law with disturbance observer. This observer is used to compensate for the inaccuracies caused by the linearization.

The authors in [136] propose a state observer for a compliant differential SMA based actuator. The estimator is developed for an antagonistic configuration of the actuator, where the state vector is defined as $x_k = \begin{bmatrix} \theta_k & \theta_{k+1} & \sigma_k \end{bmatrix}$, and the temperature is considered an internal dynamic. An adaptive Neural Network (NN) is implemented to estimate the states, based on a fourth-order strict-feedback nonlinear model of the actuator. The authors present an asymptotic stability analysis of the closed-loop system (including an output-feedback adaptive neural control) using the time-separation principle and Lyapunov synthesis. The observer is experimentally tested.

More recently, the authors in [152] proposed an observer based on a Linear Parameter Varying (LPV) model of the SMA wire based on the constitutive model. The proposed observer is a Luenberger observer for state estimation, where the state vector is $x = \begin{bmatrix} \theta & \dot{\theta} & \xi & T \end{bmatrix}$. To the best of our knowledge, this is the only reported observer for martensite fraction estimation (ξ). This observer is developed for a system with constant stress, since it does not consider the effect of the latter in the system. The lack of consideration of the stress effect, could imply this observer will not be suitable for systems with big changes in stress during operation, like the antagonistic configurations or, as is the case of this implementation, a system with changing payloads.

5.2 EKF-UI for biased SMA wire robotic arm

This section describes the modeling process to obtain a non-switching discrete-time observable model of the biased SMA wire robotic arm, suitable for observer development.

From the literature overview, we can see there are not many formal studies on the development of estimation techniques for SMAs. Most of the work found in this field, lack formal proves of model observability or observer stability and convergence when including the switched dynamic of this system. In addition to these issues, all the current approaches require the switching law of the system to be known in order to estimate the system states. This switching law depends on multiple system states (temperature and stress) and parameters (transformation temperatures) which makes it difficult to estimate. With this in mind, a new approach for observer development is proposed.

To address the need of the switching law for state estimation, an unknown input approach is proposed. Considering the switching term ($\dot{\xi}$) as an unknown input, eliminates the switching from the system's model. With this approach, there is no need to determine the switching law of the system. The system becomes a non-switching nonlinear system, allowing the implementation of simpler techniques for estimation and control.

5.2.1 Non-switching single SMA wire system

Consider the nonlinear switching system presented in Eq.(3.21). Taking the martensite fraction rate as the unknown input, let us propose a nonlinear non-switching system as follows:

$$\begin{cases} \dot{x}(t) &= f_1(x(t), u(t)) + \Phi_1(x(t))\, d(x(t), u(t)) \\ y(t) &= h(x(t)) \end{cases} \tag{5.3}$$

where $x(t) \in \mathbb{R}^n$ is the state vector and $u(t) \in \mathbb{R}^m$ is the input vector, which is upper bounded with $ulequ_{max}$ $\forall t$. In addition $d(x,u)$ is an unknown input with distribution vector $\Phi(x(t))$ and upper bound $\overline{d} \geq d$ $\forall t$. The model of the biased SMA actuated robotic arm with martensite fraction as the unknown input is written as follows:

$$f_1(x(t), u(t)) = \begin{bmatrix} x_2 \\ \frac{A_1 r_1}{J_1} x_4 - \frac{b_1}{J_1} x_2 - \frac{m_L g r_{load}}{J_1} \sin(x_1) - \frac{1}{J_1} k_s x_1 - \frac{1}{J_1} b_s x_2 \\ \frac{1}{R_1(x_5) m_{w_1} c_{p_1}} u_1 - \frac{h_1(x_3) A_{w_1}}{m_{w_1} c_{p_1}} (x_3 - T_{amb}) \\ -\frac{E_1 r_1}{l_{1_0}} x_2 + \frac{\Theta_1}{R_1(x_5) m_{w_1} c_{p_1}} u_1 - \frac{\Theta_1 h_1(x_3) A_{w_1}}{m_{w_1} c_{p_1}} (x_3 - T_{amb}) \\ 0 \end{bmatrix} \tag{5.4}$$

$$\Phi_1(x(t)) = \begin{bmatrix} 0 \\ 0 \\ 0 \\ \Omega \\ 1 \end{bmatrix} \tag{5.5}$$

$$d(x(t), u(t)) = \dot{\xi}(t) \tag{5.6}$$

$$h(t) = x_1(t) \tag{5.7}$$

We simplify the Young modulus of the system as follows:

$$E_1 = \frac{1}{2} E_m + \frac{1}{2} E_a \tag{5.8}$$

so the distribution vector of the unknown input ($\Phi_1(x(t))$) is now constant.

5.2.2 Singular Perturbation Model

When the system in Eq. (5.3) is discretized, the simulation of the discrete-time model shows that an extremely fast sampling time (in the order of μs) is needed for the system to agree with the dynamic response of its continuous-time equivalent. This sampling time is experimentally unfeasible with the current equipment, in addition to be unnecessary to capture the actual dynamics of the system. This phenomenon occurs due to the extremely small inertia of the Coupler-1 (J_1), which generates a fast dynamic of the angular velocity in comparison with the rest of the states.

The system in Eq. (5.3) meets the characteristics of a singularly perturbed system, where the angular velocity can be considered as a quasi-static state and its dynamic equation replaced by an algebraic equivalent. This process is laid out in the next paragraphs.

Consider the singularly perturbed system as follows [153]:

$$\begin{cases} \dot{x} &= f_s\left(t, x, z, \epsilon\right) \\ \epsilon\dot{z} &= g\left(t, x, z, \epsilon\right) \end{cases} \tag{5.9}$$

where $f_s\left(t, x, z, \epsilon\right)$ and $g\left(t, x, z, \epsilon\right)$ are nonlinear continuously differentiable functions and ϵ is a small positive parameter. When we set $\epsilon = 0$, the function $\dot{z}$ degenerates into:

$$0 = g\left(t, x, z, 0\right) \tag{5.10}$$

so we obtain a reduced order model:

$$\dot{x} = f_s\left(t, x, h_z\left(t, x\right), 0\right) \tag{5.11}$$

where

$$z = h_{sz}\left(t, x\right) \tag{5.12}$$

Now consider the mechanic and thermal time constants $T_m = \dfrac{J_1}{b}$ and $T_t = \dfrac{m_{w_1} c_{p_1}}{h_1\left(T\right) A_{w_1}}$, of the the system in Eq.(5.4). Where $b = b_1 + b_s$. Based on the parameters in Tab. 3.3, we know $T_t \gg T_m$, so we choose T_t as the time unit introducing the dimensionless time variable $t_r = \dfrac{t}{T_t}$. Let us introduce the normalized state equations of the biased robotic

arm as follows:

$$\begin{aligned}
\frac{d\theta}{dt_r} &= T_t\dot{\theta} \\
\frac{T_m}{T_t}\frac{d\dot{\theta}}{dt_r} &= \frac{A_1 r_1}{b}\sigma - \dot{\theta} - \frac{m_L g r_{load}}{b}\sin(\theta) - \frac{1}{b}k_s\theta \\
\frac{dT}{dt_r} &= T_t\left(\frac{1}{R_1(\xi)\, m_{w_1} c_{p_1}}u_1 - \frac{h_1(T)\, A_{w_1}}{m_{w_1} c_{p_1}}(T - T_{amb})\right) \\
\frac{d\sigma}{dt_r} &= T_t\left(-\frac{E_1 r_1}{l_{1_0}}\dot{\theta} + \frac{\Theta_1}{R_1(\xi)\, m_{w_1} c_{p_1}}u_1 - \frac{\Theta_1 h_1(T)\, A_{w_1}}{m_{w_1} c_{p_1}}(T - T_{amb}) + \Omega d(t)\right) \\
\frac{d\xi}{dt_r} &= T_t d(t)
\end{aligned}$$

In its normalized form, the system presented above can be considered a singularly perturbed system of the form in Eq.(5.9), where:

$$\epsilon = \frac{T_m}{T_t} = \frac{J_1 h_1(T)\, A_{w_1}}{b m_{w_1} c_{p_1}} \approx 0 \tag{5.13}$$

Let us define a new state vector $x_s = \begin{bmatrix} \theta & T & \sigma & \xi \end{bmatrix}$, and the singularly perturbed state space model for the biased SMA wire robotic arm with unknown input as follows:

$$\begin{cases} \dot{x}_s(t) &= f_s(x_s(t), u(t)) + \Phi_s(x_s(t))\, d(x_s(t), u(t)) \\ y_s(t) &= h_s(x_s(t)) \end{cases} \tag{5.14}$$

where

$$f_s(x_s(t), u(t)) = \begin{bmatrix} h_{sz} \\ \frac{1}{R_1(x_{s4}) m_{w_1} c_{p_1}}u_1 - \frac{h_1(x_{s2}) A_{w_1}}{m_{w_1} c_{p_1}}(x_{s2} - T_{amb}) \\ -\frac{E_1 r_1}{l_{1_0}}h_z + \frac{\Theta_1}{R_1(x_{s4}) m_{w_1} c_{p_1}}u_1 - \frac{\Theta_1 h_1(x_{s2}) A_{w_1}}{m_{w_1} c_{p_1}}(x_{s2} - T_{amb}) \\ 0 \end{bmatrix} \tag{5.15}$$

$$\Phi_s(x_s(t)) = \begin{bmatrix} 0 \\ 0 \\ \Omega \\ 1 \end{bmatrix} \tag{5.16}$$

$$d(x_s(t), u(t)) = \dot{\xi}(t) \tag{5.17}$$

$$h_s(t) = x_{s1}(t) \tag{5.18}$$

$$h_{sz} = \frac{A_1 r_1}{b}x_{s3} - \frac{m_L g r_{load}}{b}\sin(x_{s1}) - \frac{1}{b}k_s x_{s1} \tag{5.19}$$

5.2.3 State and Unknown Input Nonlinear observability

Consider a system with unknown inputs of the form given in Eq.(5.37). Now let us define the tensor μ_j^i as follows [30]:

$$\mu_j^i = L_{\Phi^i} h_j, \ \ \forall i, j \tag{5.20}$$

where $i, j = 1, \ldots, \omega$, and ω is the unknown input vector. The matrix $\Phi = \begin{bmatrix} \Phi_1 & \ldots & \Phi_\omega \end{bmatrix}$ and $h = \begin{bmatrix} h_1 & \ldots & h_\omega & \ldots & h_z \end{bmatrix}^T$, where $z \geq \omega$ is the total number of outputs of the system. It is necessary condition for a system to be observable that the tensor μ is not singular on a given neighborhood x_0 [30], meaning the unknown input is observable from the output of the system.

It is clear that the model presented in Eq.(5.14) does not meet this condition, thus the unknown input is not observable from the given output of the system. Assuming that the angular velocity can be "measured", computing the derivative of the measured angular position. Let us define a new output vector $(h_s(t))$ as follows:

$$h_s(t) = \begin{bmatrix} \frac{A_1 r_1}{b} x_{s3} - \frac{m_L g r_{load}}{b} \sin(x_{s1}) - \frac{1}{b} k_s x_{s1} \\ x_{s1}(t) \end{bmatrix} \tag{5.21}$$

Then the tensor $\mu_1^1 = \frac{A_1 r_1}{b} \Omega \neq 0 \ \forall x(t)$. So we can conclude the unknown input is observable from the output at all times and operation points.

Consider the system of the form Eq.(5.14), with the output vector Eq.(5.21). The system is considered locally observable if

$$rank(\Omega_m) = n \tag{5.22}$$

and

$$\frac{\partial x_j}{\partial x} \in \Omega_m, j = 1, ..., n \tag{5.23}$$

where Ω_m is the observable codistribution of the system and $m \leq n + 2$.

The analytic method proposed by the author in [30], is applied to compute the observable codistribution of the biased SMA wire robotic arm in Eq.(5.14) and Eq.(5.21). To apply this method, the system is restructured as a system of the form:

$$\begin{cases} \dot{x}_s = g^0(x_s) + \sum_{i=1}^{m_u} f^i(x_s) u_i + \sum_{j=1}^{m_w} g^j(x_s) w_j \\ y_z = h_s(x_s) \end{cases} \tag{5.24}$$

where u is the known inputs vector defined as $u \triangleq [u_1, \cdots, u_{m_u}]^\top$ and w the unknown input vector ($w \triangleq [w_1, \cdots, w_{m_w}]^\top$). The function $h_z(x_s)$, $z = 1, \cdots, m_z$ is a set of scalar functions, with m_z being the number of outputs of the system. Considering $u = \begin{bmatrix} V_1^2 & T_{amb} \end{bmatrix}^\top$ and $w = \dot{\xi}$. We apply the mentioned method as follows [30]:

1. Select a set of m_w scalar functions in h_s such that $\mu_j^i \triangleq L_{\Phi^i} h_j \neq 0 \ \forall i, j$.

$$\mu_1^1 = L_{g^1} h_1 = \frac{A_1 r_1}{b} \Omega \tag{5.25}$$

2. Step 2

$$\hat{g}^\alpha = \nu_\beta^\alpha g^\beta \tag{5.26}$$

$$\hat{g}^0 = \nu_0^0 g^0 + \nu_1^0 g^1 =$$

$$= \begin{bmatrix} \dfrac{-ks\theta + A_1 r_1 \sigma - m_L g r_{load} \sin(\theta)}{b} \\ -\frac{A_{w_1} x_3}{m_{w_1} c_{p_1}} \left(-h_0 - h_2 x_3^2\right) \\ \frac{A_{w_1} x_3 \Theta}{m_{w_1} c_{p_1}} \left(h_0 + h_2 x_3^2\right) - \Omega - \dfrac{E_1 r_1}{l_0} \dfrac{-ks\theta + A_1 r_1 \sigma - m_L g r_{load} \sin(\theta)}{b} \\ -1 \end{bmatrix} \tag{5.27}$$

$$\hat{g}^1 = \nu_0^1 g^0 + \nu_1^1 g^1 = \begin{bmatrix} 0 \\ 0 \\ \dfrac{b}{A_1 r_1} \\ \dfrac{b}{A_1 r_1 \Omega} \end{bmatrix} \tag{5.28}$$

3. Step 3

$$\Omega_0 = span\left\{\frac{\partial h(x)}{\partial x}\right\} = \tag{5.29}$$

$$= \left\{ \begin{pmatrix} \dfrac{-ks - m_L g r_{load} \sin(\theta)}{b} & 0 & \dfrac{A_1 r_1}{b} & 0 \end{pmatrix}, \begin{pmatrix} 1 & 0 & 0 & 0 \end{pmatrix} \right\}$$

$$\Omega_1 = \left\{ \begin{pmatrix} \dfrac{-ks - m_L g r_{load} \sin(\theta)}{b} & 0 & \dfrac{A_1 r_1}{b} & 0 \end{pmatrix}, \begin{pmatrix} 1 & 0 & 0 & 0 \end{pmatrix}, \right.$$
$$\left. \begin{pmatrix} 0 & 0 & -\dfrac{A_1 r_1 \Theta (R_m - R_a)}{b m_{w_1} c_{p_1} \left(R_m x_5 + (1 - x_5) R_a\right)^2} & 0 \end{pmatrix}, \begin{pmatrix} 0 & \dfrac{A_1 r_1 A_{w_1} h_2 \Theta x_2}{b m_{w_1} c_{p_1}} & 0 & 0 \end{pmatrix} \right\} \tag{5.30}$$

4. Calculate Ω_m for $m \geq 2$.

$$\Omega_2 = \left\{ \begin{pmatrix} \frac{-ks - m_L g r_{load} \sin(\theta)}{b} & 0 & \frac{A_1 r_1}{b} & 0 \end{pmatrix}, \begin{pmatrix} 1 & 0 & 0 & 0 \end{pmatrix}, \begin{pmatrix} 0 & 0 & -\frac{A_1 r_1 \Theta (R_m - R_a)}{b m_{w_1} c_{p_1} (R_m x_5 + (1 - x_5) R_a)^2} & 0 \end{pmatrix}, \begin{pmatrix} 0 & \frac{A_1 r_1 A_{w_1} h_2 \Theta x_2}{b m_{w_1} c_{p_1}} & 0 & 0 \end{pmatrix} \right\} \tag{5.31}$$

5. After computation we can conclude that any new vector in Ω_2 or higher, is a linear combination of the vectors in Ω_1. Such that $\Omega^* = \Omega_1$

6. The observable codistribution Ω_1 has full rank and all the state differentials belong to it. In conclusion the presented system is weakly locally observable.

5.2.4 Model discretization

Discretizing the model presented in Eq.(5.14) by first order Euler approximation, we have the following non-linear discrete system:

$$\begin{cases} x_{k+1} &= x_k + (f_k(x_k, u_k) + \Phi_k(x_k) d(x_k, u_k)) T_s \\ y_k &= h_k(x_k) \end{cases} \tag{5.32}$$

where T_s is the sampling time and

$$f_k(x_k, u_k) = \begin{bmatrix} \omega_k \\ \frac{1}{R_1(x_{4_k}) m_{w_1} c_{p_1}} u_1 - \frac{h_1(x_{2_k}) A_{w_1}}{m_{w_1} c_{p_1}} (x_{2_k} - T_{amb}) \\ -\frac{E_1 r_1}{l_{1_0}} h_{zk} + \frac{\Theta_1}{R_1(x_{4_k}) m_{w_1} c_{p_1}} u_1 - \frac{\Theta_1 h_1(x_{2_k}) A_{w_1}}{m_{w_1} c_{p_1}} (x_{2_k} - T_{amb}) \\ 0 \end{bmatrix} \tag{5.33}$$

$$\Phi_k(x_k) = \begin{bmatrix} 0 \\ 0 \\ \Omega \\ 1 \end{bmatrix} \tag{5.34}$$

$$h_k(t) = \begin{bmatrix} \omega_k \\ x_{1_k}(t) \end{bmatrix} \tag{5.35}$$

$$\omega_k = \frac{A_1 r_1}{b} x_{3_k} - \frac{m_L g r_{load}}{b} \sin(x_{1_k}) - \frac{1}{b} k_s x_{1_k} \tag{5.36}$$

Sampling Time selection

The sampling period is chosen based on two factors. First, the indicative values for different kind of systems recommended in [15] (See Tab. 5.1). The system here presented

is a combination between the thermal model of the SMA wire (Temperature) and the dynamics of the robotic arm (Servo-mechanisms). Based on this criteria and the values on the Tab. 5.1, the recommended sampling time is between 0.001 and 0.05 s, which is the fastest between the two kind of systems. The second factor is based on the capabilities of the computer used for the realization of this project. The interface and calculations were implemented using Matlab/Simulink and the Matlab Desktop Real-Time library. The fastest sampling time achieve during testing was 0.02 s. This sampling time allows to observe the complete dynamics of the system, since the action force is provided by a thermal system (SMA wire) with a considerably slower dynamic.

TABLE 5.1: Choice of sampling period for digital control systems (indicative values) [15].

Type of variable (or plant)	Sampling period (s)
Flow rate	1 - 3
Level	5 - 10
Pressure	1 - 5
Temperature	10 - 180
Distillation	10 - 180
Servo-mechanisms	0.001-0.05
Catalytic reactors	10 - 45
Cement plants	20 - 45
Dryers	20 - 45

5.3 Extended Kalman Filter with Unknown Input

For state and unknown input estimation of a system of the type dealt with in this dissertation, we propose an Extended Kalman Filter with sliding modes for unknown input estimation. Consider the following discrete non-linear system:

$$\begin{aligned} x_{k+1} &= f(x_k, u_k, r_k) + \phi(x_k)\, d(x_k, u_k) \\ y_k &= h(x_k, w_k) \end{aligned} \tag{5.37}$$

where $x_k = \begin{bmatrix} x_{1k} & x_{2k} & \dots & x_{nk} \end{bmatrix}^T \in \mathbb{R}^n$ is the state vector at instant k, $u_k \in \mathbb{R}^r$ and $y_k \in \mathbb{R}^p$ are the input and output vectors at time instant k, $d(x_k, u_k)$ is the unknown input and $\phi(x_k)$ is the distribution matrix of unknown inputs, r_k is the system noise caused by the parameters inaccuracy and w_k is the measurement noise. Both, system and measurement noise matrices are modeled as Gaussian noises with zero mean and completely independent.

Assuming the function $f(x_k, u_k)$ is bounded with respect to its own arguments and system in Eq.(5.37) is uniformly observable while the unknown input is also bounded as $|d(\cdot)| \leq \overline{d}$. The Extended Kalman Filter with Unknown Input (EKF-UI) observer is proposed as follows:

1. Measurement update

$$\hat{x}_{k+1} = \hat{x}_{k+1/k} + K_{k+1} e_{k+1} \tag{5.38}$$

$$K_{k+1} = P_{k+1/k} H_{k+1}^{\top} \left(H_{k+1} P_{k+1/k} H_{k+1}^{\top} + R_{k+1} \right)^{-1} \tag{5.39}$$

$$P_{k+1} = \left(I - K_{k+1} H_{k+1} \right) P_{k+1/k} \tag{5.40}$$

2. Time update

$$\hat{x}_{k+1/k} = f\left(\hat{x}_k, u_k\right) + \phi\left(\hat{x}_k\right) \hat{d}\left(x_k, u_k\right) \tag{5.41}$$

$$P_{k+1/k} = F_k P_k F_k^{\top} + Q_k \tag{5.42}$$

Where

$$e_{k+1} = y_{k+1} - h\left(\hat{x}_{k+1/k}, w_{k+1}\right) \tag{5.43}$$

$$F_k = F\left(\hat{x}_k, u_k\right) = \left. \frac{\partial f\left(x_k, u_k\right)}{\partial x_k} \right|_{x_k = \hat{x}_k} \tag{5.44}$$

$$H_{k+1} = H\left(\hat{x}_{k+1/k}\right) = \left. \frac{\partial h\left(x_{k+1}, w_{k+1}\right)}{\partial x_{k+1}} \right|_{x_{k+1} = \hat{x}_{k+1/k}} \tag{5.45}$$

here Q_k and R_k are diagonal matrices, which represent the covariance matrices of the system (r_k) and measurement (w_k) noises respectively. These matrices satisfy:

$$\begin{cases} Q = cov(r) = E\left[rr^{\top}\right] \\ R = cov(w) = E\left[ww^{\top}\right] \end{cases} \tag{5.46}$$

The Unknown Input is estimated with a sliding mode based estimator. This approach is based on the work presented in [154], where a high-gain observer with sliding mode for state and unknown input estimations is developed with stability discussion. Using this approach the unknown input can be estimated using a sliding surface defined as a function of the error term used to estimate the given unknown input (e_{i_k}) as follows [154]:

$$\hat{d}\left(x_k, u_k\right) = -\rho sign\left(e_{i_k}\right) \tag{5.47}$$

where ρ is the sliding mode gain. From Eq.(5.43), we can define e_{i_k} for $i = 1, \cdots, d$ as follows:

$$e_k = \begin{bmatrix} e_{1_k} \\ \vdots \\ e_{d_k} \end{bmatrix} \tag{5.48}$$

and $d < p$ is the number of unknown inputs in the system.

To avoid the chattering caused by the $sign(\cdot)$ function (characteristic challenge of sliding mode technique), this function is replaced by a $sat(\cdot, \epsilon)$, defined as [155]:

$$sat\left(\cdot, \epsilon\right) = \begin{cases} \cdot/\epsilon, & \text{if } |\cdot| \leq \epsilon, \\ sign\left(\cdot\right), & \text{if } |\cdot| > \epsilon. \end{cases} \tag{5.49}$$

5.3.1 Convergence analysis

Let us denote by $\tilde{x}_{k+1}$ and $\tilde{x}_{k+1/k}$ the first order euler linearization of the state estimation and state prediction error vectors respectively defined by

$$\tilde{x}_{k+1} = x_{k+1} - \hat{x}_{k+1} = \left[I - K_{k+1}H_{k+1}\right]\tilde{x}_{k+1/k} \tag{5.50}$$

and

$$\tilde{x}_{k+1/k} = x_{k+1} - \hat{x}_{k+1/k} = \alpha_k F_k \tilde{x}_k + \beta_k \Phi_k \tilde{d}_k \tag{5.51}$$

where α_k and β_k are unknown time-varying diagonal matrices of appropriate dimensions accounting for the errors due to the linearization process. In addition, $\tilde{d}_k = d_k - \hat{d}_k$ is the unknown input estimation error and ϕ_k is defined as:

$$\phi\left(\hat{x}_k\right) = \Phi_k \tag{5.52}$$

Defining an unknown time-varying matrix of appropriate dimensions γ_k, such that

$$\beta_k \Phi_k \tilde{d}_k = \alpha_k \gamma_k \tilde{x}_k \tag{5.53}$$

so it is possible to write

$$\tilde{x}_{k+1/k} = x_{k+1} - \hat{x}_{k+1/k} = \alpha_k \left[F_k + \gamma_k\right]\tilde{x}_k = \alpha_k Z_k \tilde{x}_k \tag{5.54}$$

We can write the state estimation error as

$$\tilde{x}_{k+1} = \left[I - K_{k+1}H_{k+1}\right]\alpha_k Z_k \tilde{x}_k \tag{5.55}$$

Assumption 1. *The system in Eq.(5.37) is locally uniformly rank observable. So the matrix P_k is bounded and positive definite.*

Assumption 2. *The matrix F_k is bounded and non singular.*

Considering the following theorem proposed in [156], we can establish sufficient condition for local asymptotical stability of the proposed EKF-UI.

Theorem 5.1. *[156] If assumption 1 and 2 are satisfied, consider the Rayleigh quotient such that $\underline{\varphi}(X) \leq \frac{\tilde{x}_k^\top X \tilde{x}_k}{\tilde{x}_k^\top \tilde{x}_k} \leq \overline{\varphi}(X)$ and*

$$\overline{\varphi}(\alpha_k) \leq \left[\frac{\underline{\varphi}(\alpha_k)^2 \, \underline{\varphi}\left(Z_k^\top Z_k\right) \underline{\varphi}\left(H_k^\top H_k\right) \underline{\varphi}\left(P_{k+1/k}\right)}{\overline{\varphi}\left(H_{k+1} P_{k+1/k} H_{k+1}^\top + R_{k+1}\right) \overline{\varphi}\left(Z_k^\top Z_k\right)} + \frac{\underline{\varphi}\left(P_{k+1/k}\right)}{\overline{\varphi}\left(Z_k^\top Z_k\right) \overline{\varphi}\left(P_k\right)} \right]^{1/2} \tag{5.56}$$

then the proposed Extended Kalman Filter observer with sliding mode unknown input estimation is locally asymptotically stable.

Let us discuss the proof presented in [156] for Theorem 5.1. Consider the the candidate Lyapunov function V_{k+1} as

$$V_{k+1} = \tilde{x}_{k+1}^\top P_{k+1}^{-1} \tilde{x}_{k+1} \tag{5.57}$$

and

$$V_k = \tilde{x}_k^\top P_k^{-1} \tilde{x}_k \tag{5.58}$$

Substituting Eq.(5.55) into Eq.(5.57) gives

$$V_{k+1} = \tilde{x}_k^\top Z_k^\top \alpha_k \left[I - H_{k+1}^\top K_{k+1}^\top \right] P_{k+1}^{-1} \left[I - K_{k+1} H_{k+1} \right] \alpha_k Z_k \tilde{x}_k \tag{5.59}$$

From Eq.(5.40), we can write

$$\left[I - H_{k+1}^\top K_{k+1}^\top \right] = P_{k+1/k}^{-1} P_{k+1} \tag{5.60}$$

Substituting Eq.(5.39) into Eq.(5.60):

$$\begin{aligned} &[I - K_{k+1} H_{k+1}] = \\ &= \left(I - P_{k+1/k} H_{k+1}^\top \left(H_{k+1} P_{k+1/k} H_{k+1}^\top + R_{k+1} \right)^{-1} \right) H_{k+1} = P_{k+1/k}^{-1} P_{k+1} \end{aligned} \tag{5.61}$$

substituting Eq.(5.61) and Eq.(5.55) into the proposed Lyapunov function in Eq.(5.57), after algebraical manipulation we have:

$$V_{k+1} = \tilde{x}_k^\top Z_k^\top \alpha_k \left[P_{k+1/k}^{-1} - H_{k+1}^\top \left(H_{k+1} P_{k+1/k} H_{k+1}^\top + R_{k+1} \right)^{-1} H_{k+1} \right] \alpha_k Z_k \tilde{x}_k \tag{5.62}$$

To determine conditions for which is a decreasing sequence,

$$V_{k+1} - V_k \leq 0 \tag{5.63}$$

From Eq.(5.58) and Eq.(5.62), the inequality can be expressed as

$$\tilde{x}_k^\top \left[Z_k^\top \alpha_k \left[P_{k+1/k}^{-1} - H_{k+1}^\top \left(H_{k+1} P_{k+1/k} H_{k+1}^\top + R_{k+1} \right)^{-1} H_{k+1} \right] \alpha_k Z_k - \right. \tag{5.64}$$
$$\left. - P_k^{-1} \right] \tilde{x}_k \leq 0$$

Applying the bounds of the Rayleigh quotient for $X \succeq 0$, i.e., $\underline{\varphi}(X) \leq \frac{\tilde{x}_k^\top X \tilde{x}_k}{\tilde{x}_k^\top \tilde{x}_k} \leq \overline{\varphi}(X)$, the inequality in Eq.(5.64) can be written as:

$$\overline{\varphi}\left(Z_k^\top \alpha_k P_{k+1/k}^{-1} \alpha_k Z_k \right) - \tag{5.65}$$
$$- \underline{\varphi}\left(Z_k^\top \alpha_k H_{k+1}^\top \left(H_{k+1} P_{k+1/k} H_{k+1}^\top + R_{k+1} \right)^{-1} H_{k+1} \alpha_k Z_k \right) - \underline{\varphi}\left(P_k^{-1} \right) \leq 0$$

from here we can deduce the following inequalities

$$\overline{\varphi}\left(Z_k^\top \alpha_k P_{k+1/k}^{-1} \alpha_k Z_k \right) \leq \overline{\varphi}(\alpha_k)^2 \, \overline{\varphi}\left(Z_k^\top Z_k \right) \overline{\varphi}\left(P_{k+1/k}^{-1} \right) \tag{5.66}$$

$$\underline{\varphi}\left(Z_k^\top \alpha_k H_{k+1}^\top \left(H_{k+1} P_{k+1/k} H_{k+1}^\top + R_{k+1} \right)^{-1} H_{k+1} \alpha_k Z_k \right) \leq \tag{5.67}$$
$$\leq \frac{\underline{\varphi}(\alpha_k)^2 \, \underline{\varphi}\left(Z_k^\top Z_k \right) \underline{\varphi}\left(H_k^\top H_k \right)}{\overline{\varphi}\left(H_{k+1} P_{k+1/k} H_{k+1}^\top + R_{k+1} \right)}$$

we can conclude that the inequality in Eq.(5.65) is satisfied if

$$\overline{\varphi}(\alpha_k)^2 \leq \frac{\underline{\varphi}(\alpha_k)^2 \, \underline{\varphi}\left(Z_k^\top Z_k \right) \underline{\varphi}\left(H_k^\top H_k \right) \underline{\varphi}\left(P_{k+1/k} \right)}{\overline{\varphi}\left(H_{k+1} P_{k+1/k} H_{k+1}^\top + R_{k+1} \right) \overline{\varphi}\left(Z_k^\top Z_k \right)} + \frac{\underline{\varphi}\left(P_{k+1/k} \right)}{\overline{\varphi}\left(Z_k^\top Z_k \right) \overline{\varphi}\left(P_k \right)} \tag{5.68}$$

Thus, if the condition in Eq.(5.68) is satisfied, then $\langle V_k \rangle_{k=1\ldots}$ is a decreasing sequence and the proposed observer ensures local asymptotic convergence.

5.3.2 EKF-UI implementation

Consider the model presented in Eq.(5.32), developing a state and unknown input observer of the form proposed in section 5.3 for this system we have:

$$F_k = \begin{bmatrix} 1+a_{11} & 0 & a_{13} & 0 \\ 0 & 1+a_{22} & 0 & a_{24} \\ a_{31} & a_{32} & 1+a_{33} & a_{34} \\ 0 & 0 & 0 & 1 \end{bmatrix} \tag{5.69}$$

$$\phi_k = \begin{bmatrix} 0 \\ 0 \\ \Omega T_s \\ T_s \end{bmatrix} \tag{5.70}$$

$$H_k = \begin{bmatrix} -\frac{m_L g r_{load}}{b}\cos\left(x_{1_k}\right) - \frac{1}{b}k_s & 0 & \frac{A_1 r_1}{b} & 0 \\ 1 & & 0 & 0 & 0 \end{bmatrix} \tag{5.71}$$

$$\tag{5.72}$$

where

$$\begin{aligned}
a_{11} &= \left(-\frac{m_L g r_{load}}{b}\cos\left(x_{1_k}\right) - \frac{1}{b}k_s\right) T_s \\
a_{13} &= \frac{A_1 r_1}{b} T_s \\
a_{22} &= -\frac{A_{w_1}}{m_{w_1} c_{p_1}}\left(2h_2 x_{2_k}\left(x_{2_k} - T_{amb}\right) + \left(h_0 + h_2^2 x_{2_k}^2\right)\right) T_s \\
a_{24} &= \frac{V_1^2\left(R_m - R_a\right)}{m_{w_1} c_{p_1}\left(R_a\left(1 - x_{4_k}\right) + R_m x_{4_k}\right)^2} T_s \\
a_{31} &= -\frac{E_1 r_1}{l_{1_0}} a_{11} \\
a_{32} &= \Theta a_{22} \\
a_{33} &= -\frac{E_1 r_1}{l_{1_0}} a_{13} \\
a_{34} &= \Theta a_{24}
\end{aligned}$$

From Theorem 5.1, and considering that the presented system fulfills assumptions 1 and 2, the EKF-UI for state and unknown input estimation of the biased SMA wire robotic arm is locally asymptotically stable.

5.4 Observer validation

This section presents the validation of state and unknown input observer proposed in equations from Eq.(5.38) to Eq.(5.42) and Eq.(5.69) to Eq.(5.71). Table 5.2 shows the observer gains used to obtain the results discussed in this section.

TABLE 5.2: Observer Parameters.

State estimation
$Q = \begin{bmatrix} 5 & 0 & 0 & 0 \\ 0 & 1 & 0 & 0 \\ 0 & 0 & 1 & 0 \\ 0 & 0 & 0 & 1 \end{bmatrix}$
$R = \begin{bmatrix} 0.01 & 0 \\ 0 & 20 \end{bmatrix}$
Unknown input estimation
$\rho = 85$
$\epsilon = 1$

The observer validation is performed under three different operation conditions. The observer is validated in simulation and experiments. The system was tested under the following conditions:

1. No load. First the system was tested with no added payload under two different input signals:
   (a) Steps. The system was tested at several consecutive steps signals of different amplitudes . Figure 3.17 shows the voltage signal used for this test.
   (b) Sine. The system was tested under a sinusoidal voltage with 2.6 V peak-peak voltage and 0.1 rad/s frequency. The sine waves are shown in Fig. 3.18, solid line.
2. Load test. The arm was tested under a 31 g payload with a sinusoidal voltage input (see Fig. 3.18, solid line).

The following subsections discuss the results of the mentioned tests.

5.4.1 The influence of gain on unknown input estimation

Four different parameters can be tuned to achieve a better estimation of states and unknown input from the proposed EKF-UI observer. One of these parameters is of

particular interest for experimental implementation, since it is highly affected by the measurements noise. This parameter is the gain ρ for the unknown input estimation.

Figure 5.1 shows the behavior of the observer under step input voltages for different values of ρ, in simulation (with and without added noise to the system output) and experiments . This value affects the accuracy of the unknown input estimation. Table 5.3 condenses the results shown in Fig. 5.1. The system was tested for three different values of ρ (10, 40 and 85). In simulation, without added noise, we can see the accuracy of the unknown input (d_k) estimation increases significantly with $\rho = 40$ as compared to $\rho = 10$. The increment in accuracy for the unknown input is not as drastic with the increment of $\rho = 85$. However, the accuracy of state estimation ξ_k increases from a BFP=93% to BFP=97%. It is important to mention that the accuracy in estimation of the rest of the states is also affected by this gain, but not as drastically as for ξ_k.

The results obtained for the simulation test with added noise and the experiments were similar. When tested experimentally, the susceptibility of the unknown input estimation to measurement noise became clear. While a gain of $\rho = 10$ achieves good accuracy with BFP=92% for experiments, the accuracy in state estimation is considerably lower at BFP=68% and BFP=70.5% for simulation with added noise. With the increment of ρ, the BFP percentage in the state estimation increases significantly while the for the unknown input reaches extremely low (even negative in the experimental case) values. This effect is caused by the measurement noise, as demonstrated by comparing the results from simulation test with and without added noise. In Fig. 5.1, d) we can see how the estimation of the unknown input becomes noisy with the increase of ρ in the presence of measurement noise.

Despite the low percentage of estimation of the unknown input with noise outputs, we can see the estimated value follows the dynamic of the system and after filtering we obtain estimations up to BFP=49% (d_{f_k}). As it will be discussed in the next subsection, even with this low BFP for the unknown input estimation, the observer shows a good accuracy for state estimation. The estimated unknown input shows the correct dynamic, so this estimation can be later used for control purposes, since the only information necessary from this parameter is its sign, as will be discussed in Chapter 6.

5.4.2 Simulation and experimental results for EKF-UI

The three scenarios presented at the beginning of this section were tested in simulation (with and without added output noise) and experiments. Figures from5.2 to 5.7 show the results of these tests. Tables 5.4 and 5.6 summarize the results of the tests performed for the observer validation. The observer is started at t=3 s, to allow the system to start

TABLE 5.3: EKF-UI Results at different gains for unknown input estimation.

ρ	State	Sim No Noise		Sim Noise		Experimental	
		SD [%]	BFP [%]	SD [%]	BFP [%]	SD [%]	BFP [%]
10	ξ_k	4.70	66.7	4.34	70.6	4.59	68.0
	d_k	10.65	46.8	7.93	60.4	1.58	92.0
	d_{f_k}	10.01	50.0	9.80	51.1	3.88	80.4
40	ξ_k	1.31	93.0	1.54	94.5	3.56	86.2
	d_k	0.72	96.3	7.69	61.5	15.49	22.7
	d_{f_k}	3.45	82.6	7.16	64.2	10.09	49.6
85	ξ_k	0.85	97.4	1.32	95.8	3.58	89.2
	d_k	0.72	96.3	8.61	57.0	-23.36	-123.6
	d_{f_k}	3.43	82.7	7.12	64.4	10.18	49.2

SD: Standard Deviation, BFP: Best Fit Percentage.

the data acquisition during the experimental test. The observer shows a convergence time of less than 5 sample times for all three tests.

Table 5.4 shows the results for state and unknown input estimation in simulation without added output noise. All the states and unknown input show an estimation accuracy above BFP=96% for all three scenarios. Based on these results, the observer is clearly capable of estimating the states with no previous knowledge of the switching dynamics of the SMA wire model. Table 5.5 shows the results for state and unknown input estimation in simulation with added output noise. The performance of the observer in simulation in the presence of output noise is close to the experimental results, discussed on the next paragraph.

Table 5.6 shows the results for state and unknown input estimation in experiments. The accuracy of the non-measured states and unknown input is computed against the simulation values. As discussed in the previous subsection, the BFP for the unknown input in all three scenarios is about 50%. Most of the states show an accuracy in estimation above BFP=90%. The stress shows the higher error in estimation with an average BFP=80%.

Looking at the plots of the estimated states, it is clear that a part of this error in estimation comes from the mathematical model. For example, in Fig. 5.2 a), we can observe a difference between the measured position and the value in simulation around t=17 s and again around t=100 s. This difference in value is similar to the one observed in the stress estimation at these same points in time, and in a lesser extent in the rest of the states. The same kind of behavior is observed during the three different tested scenarios, which lead us to conclude the observer is compensating for the error in model and estimating a value closer to the real system.

In conclusion, the proposed Extended Kalman Filter with sliding mode unknown input estimation (EKF-UI) is capable to deal with the measurement noise with a less accurate estimation on the unknown input, without affecting the state estimation accuracy. It shows a fast convergence and a good accuracy under different scenarios with and without payload. The performance of the proposed observer could be improved with a better measurement of the angular velocity, since this is not actually measured but computed from the measured angular position.

TABLE 5.4: EKF-UI Simulation Results.

Test	State	Units	EM	E_r	MxE	SD (%)	BFP [%]
Steps	$\boldsymbol{\theta_k}$	rad	-8.2E-6	0.0020	0.0041	0.0012 (0.10)	99.7
	$\boldsymbol{\omega_k}$	rad/s	9.13E-6	0.0100	0.0042	0.0006 (0.28)	98.9
	$\boldsymbol{T_k}$	^oC	0.4044	0.0103	5.8396	0.7242 (0.45)	98.2
	$\boldsymbol{\sigma_k}$	MPa	0.4734	0.0043	6.0926	0.5090 (0.11)	99.5
	$\boldsymbol{\xi_k}$		0.0025	0.0126	0.0175	0.0085 (0.85)	97.4
	$\boldsymbol{d_k}$	1/s	4.63E-5	0.0360	0.0324	0.0018 (0.72)	96.3
Sine	$\boldsymbol{\theta_k}$	rad	-1.5E-4	0.0013	0.0021	0.0010 (0.08)	99.8
	$\boldsymbol{\omega_k}$	rad/s	7.7E-5	0.0025	0.0016	0.0004 (0.43)	99.0
	$\boldsymbol{T_k}$	^oC	0.1036	0.0025	0.6184	0.2025 (0.13)	99.6
	$\boldsymbol{\sigma_k}$	MPa	0.2885	0.0032	0.9254	0.4437 (0.14)	99.6
	$\boldsymbol{\xi_k}$		0.0027	0.0199	0.0203	0.0120 (1.20)	96.9
	$\boldsymbol{d_k}$	1/s	-0.0001	0.0236	0.0110	0.0010 (1.40)	97.6
Load sine	$\boldsymbol{\theta_k}$	rad	-1.1E-4	0.0014	0.0018	0.0008 (0.09)	99.8
	$\boldsymbol{\omega_k}$	rad/s	7.1E-5	0.0110	0.0015	0.0004 (0.53)	98.8
	$\boldsymbol{T_k}$	^oC	-0.0027	0.0015	0.3286	0.1429 (0.09)	99.6
	$\boldsymbol{\sigma_k}$	MPa	-1.9009	0.0190	4.8041	2.5224 (0.85)	98.0
	$\boldsymbol{\xi_k}$		0.0084	0.0197	0.0212	0.0091 (0.91)	97.0
	$\boldsymbol{d_k}$	1/s	-5.5E-5	0.0251	0.0170	0.0011 (1.42)	97.4

EM: Error Mean, E_r: Relative error, MxE: Maximum Error, SD: Standard Deviation, BFP: Best Fit Percentage.

5.5 Conclusions

In the first section of this chapter, an overview of the different estimation techniques found in the literature for SMA based system is presented. Following, the modeling process to obtain a non-switching nonlinear model of the biased configuration of the lightweight robotic arm is detailed. This process includes the implementation of a singular perturbation model and the consideration of the martensite fraction rate ($\dot{\xi}$) as an unknown input. A nonlinear observability analysis for the system with unknown input is presented and the observability of the model proved. A first order Euler approximation is applied to discretize the observable model.

TABLE 5.5: EKF-UI Simulation with added noise results.

Test	State	Units	EM	E_r	MxE	SD (%)	BFP [%]
Steps	$\boldsymbol{\theta_k}$	rad	-1.2E-5	0.0020	0.0042	0.0012 (0.10)	99.7
	$\boldsymbol{\omega_k}$	rad/s	5.31E-6	0.0099	0.0025	0.0006 (0.29)	99.0
	$\boldsymbol{T_k}$	^oC	0.7329	0.0170	8.6150	1.1601 (0.73)	97.1
	$\boldsymbol{\sigma_k}$	MPa	0.1536	0.0773	100.76	12.2502 (2.88)	92.1
	$\boldsymbol{\xi_k}$		0.0059	0.0207	0.0861	0.0133 (1.32)	95.8
	$\boldsymbol{d_{f_k}}$	1/s	-0.0011	0.3560	0.1582	0.0181 (7.12)	62.1
Sine	$\boldsymbol{\theta_k}$	rad	-1.6E-4	0.0013	0.0022	0.0010 (0.09)	99.8
	$\boldsymbol{\omega_k}$	rad/s	8.1E-5	0.0102	0.0014	0.0005 (0.45)	98.7
	$\boldsymbol{T_k}$	^oC	-0.1566	0.0024	0.5000	0.1621 (0.10)	99.5
	$\boldsymbol{\sigma_k}$	MPa	-0.3341	0.0410	37.71	6.5992 (2.19)	95.8
	$\boldsymbol{\xi_k}$		0.0137	0.0286	0.0347	0.0112 (1.12)	95.7
	$\boldsymbol{d_{f_k}}$	1/s	0.0004	0.2467	0.0799	0.0106 (14.7)	75.2
Load sine	$\boldsymbol{\theta_k}$	rad	-1.2E-4	0.0014	0.0019	0.0008 (0.09)	99.8
	$\boldsymbol{\omega_k}$	rad/s	7.3E-5	0.0116	0.0013	0.0005 (0.53)	98.8
	$\boldsymbol{T_k}$	^oC	-0.1033	0.0017	0.4220	0.1212 (0.08)	99.6
	$\boldsymbol{\sigma_k}$	MPa	-2.5075	0.0471	41.26	7.3922 (2.51)	95.2
	$\boldsymbol{\xi_k}$		0.0111	0.0258	0.0325	0.0119 (1.19)	96.1
	$\boldsymbol{d_{f_k}}$	1/s	0.0004	0.2557	0.0777	0.0113 (14.5)	74.4

EM: Error Mean, E_r: Relative error, MxE: Maximum Error, SD: Standard Deviation, BFP: Best Fit Percentage.

In section 5.3, an Extended Kalman Filter for state and unknown input estimation with sliding mode is proposed and its convergence analysis presented. Subsequently, the proposed observer is implemented on the previously presented observable model. Finally, the validation of the observer is presented in simulation and experimental. This observer is implemented experimentally in the next chapter, in order to test the State-Dependent Riccati Equation control approach.

Table 5.6: EKF-UI Experimental Results.

Test	State	Units	EM	E_r	MxE	SD (%)	BFP [%]
Steps	$\boldsymbol{\theta_k}$	rad	-1.5E-6	0.0020	0.0049	0.0012 (0.10)	99.7
	$\boldsymbol{\omega_k}$	rad/s	-1.5E-5	0.0177	0.0097	0.0013 (0.10)	97.8
	$\boldsymbol{T_k}$	^oC	0.8570	0.0177	5.2154	1.1369 (0.71)	96.9
	$\boldsymbol{\sigma_k}$	MPa	0.5190	0.1683	128.2054	26.6415 (6.27)	82.9
	$\boldsymbol{\xi_k}$		-0.0114	0.0535	0.1084	0.0358 (3.58)	89.2
	$\boldsymbol{d_{f_k}}$	1/s	-4.4E-5	0.50794	0.2381	0.0259 (10.18)	49.2
Sine	$\boldsymbol{\theta_k}$	rad	-1.6E-4	0.0013	0.0029	0.0009 (0.08)	99.8
	$\boldsymbol{\omega_k}$	rad/s	9.7E-5	0.0164	0.0094	0.0008 (0.56)	98.3
	$\boldsymbol{T_k}$	^oC	0.2250	0.0056	1.5278	0.4566 (0.30)	98.8
	$\boldsymbol{\sigma_k}$	MPa	4.0695	0.1580	73.3636	25.09 (8.36)	83.9
	$\boldsymbol{\xi_k}$		-0.0127	0.0547	0.0947	0.0315 (3.15)	91.7
	$\boldsymbol{d_{f_k}}$	1/s	0.0006	0.4324	0.0691	0.0185 (25.8)	56.5
Load sine	$\boldsymbol{\theta_k}$	rad	-1.1E-4	0.0013	0.0023	0.0008 (0.08)	99.8
	$\boldsymbol{\omega_k}$	rad/s	6.9E-5	0.0115	0.0016	0.0004 (0.41)	98.8
	$\boldsymbol{T_k}$	^oC	0.3105	0.1335	1.5612	0.5161 (0.34)	98.6
	$\boldsymbol{\sigma_k}$	MPa	2.8120	0.1335	91.2916	21.9317 (7.45)	86.3
	$\boldsymbol{\xi_k}$		-0.0168	0.0632	0.1300	0.0361 (3.61)	90.4
	$\boldsymbol{d_{f_k}}$	1/s	0.0002	0.4762	0.1054	0.0211 (27.02)	52.3

EM: Error Mean, E_r: Relative error, MxE: Maximum Error, SD: Standard Deviation, BFP: Best Fit Percentage.

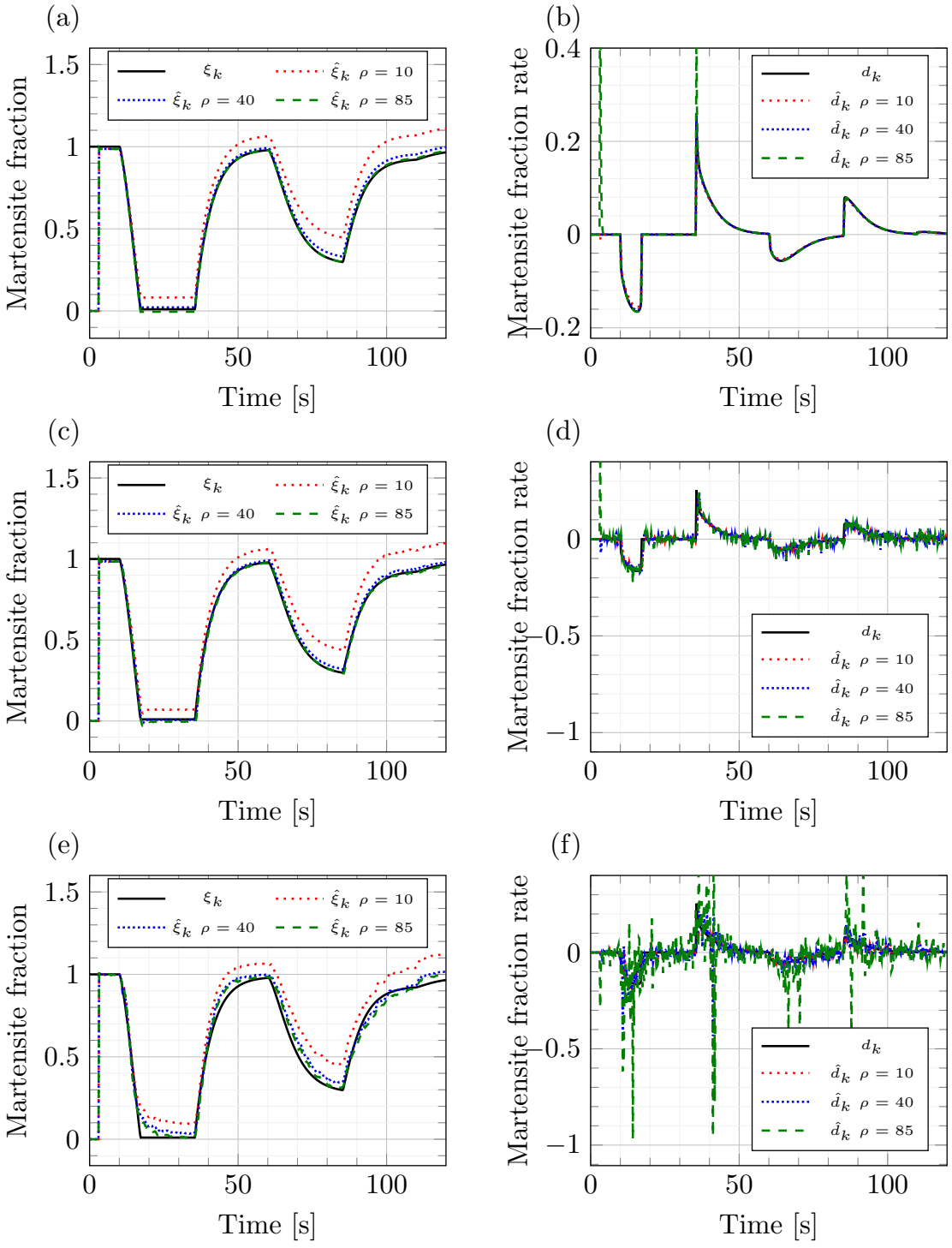

FIGURE 5.1: Observer behavior in simulation and experiments at different gains for unknown input estimation, a)Martensite fraction at different values of ρ in simulation, b) Martensite fraction rate at different values of ρ in simulation, c)Martensite fraction at different values of ρ in simulation with added noise, d) Martensite fraction rate at different values of ρ in simulation with added noise, e)Martensite fraction at different values of ρ in experiments, f) Martensite fraction rate at different values of ρ in experiments.

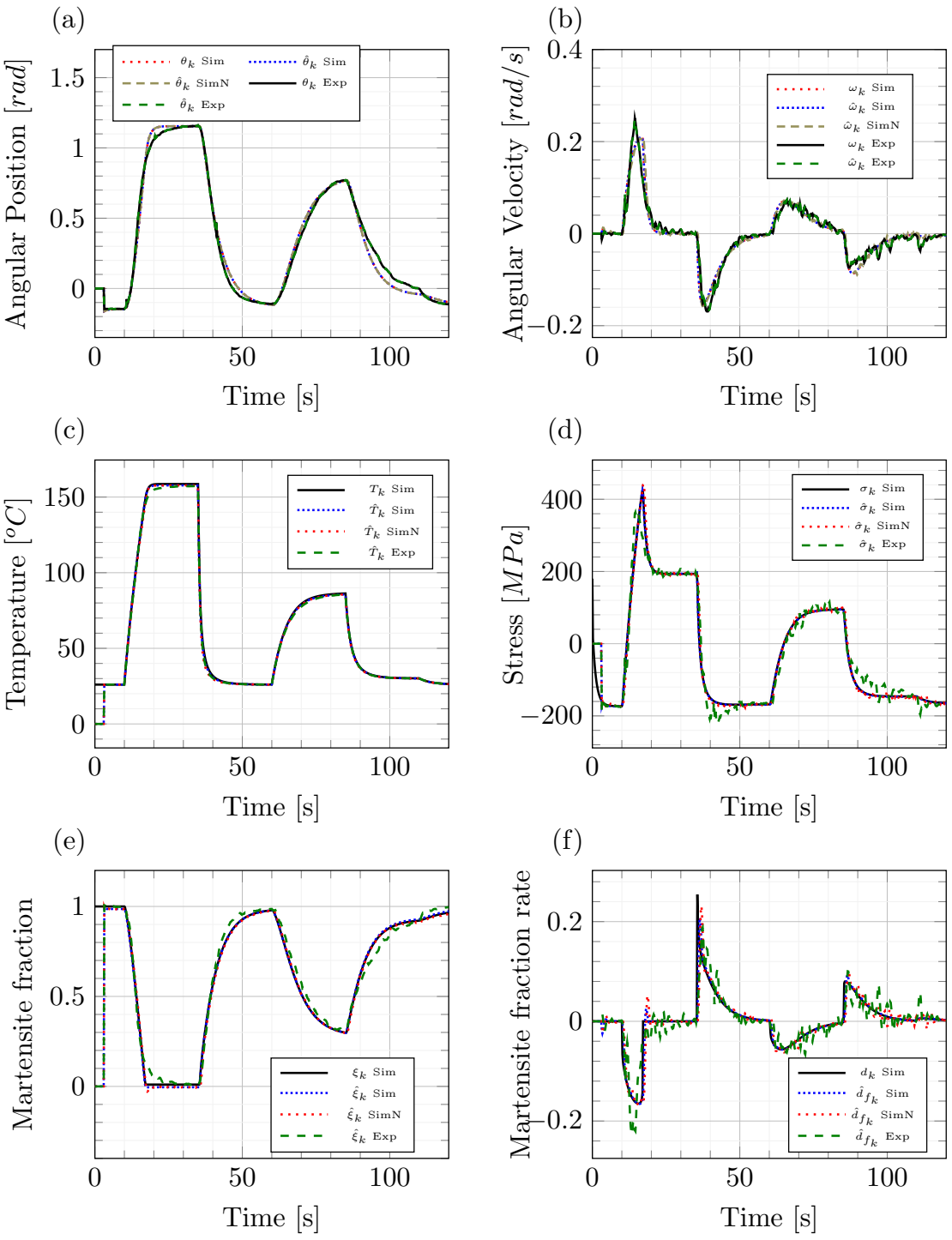

FIGURE 5.2: Estimated states and unknown input with step voltage input. Simulation and experimental results, a) Angular position, b) Angular velocity, c) Temperature, d) SMA wire stress, e) Martensite fraction, f) Martensite fraction rate.
Sim - Simulation results without added noise; SimN - simulation results with added noise to the output.

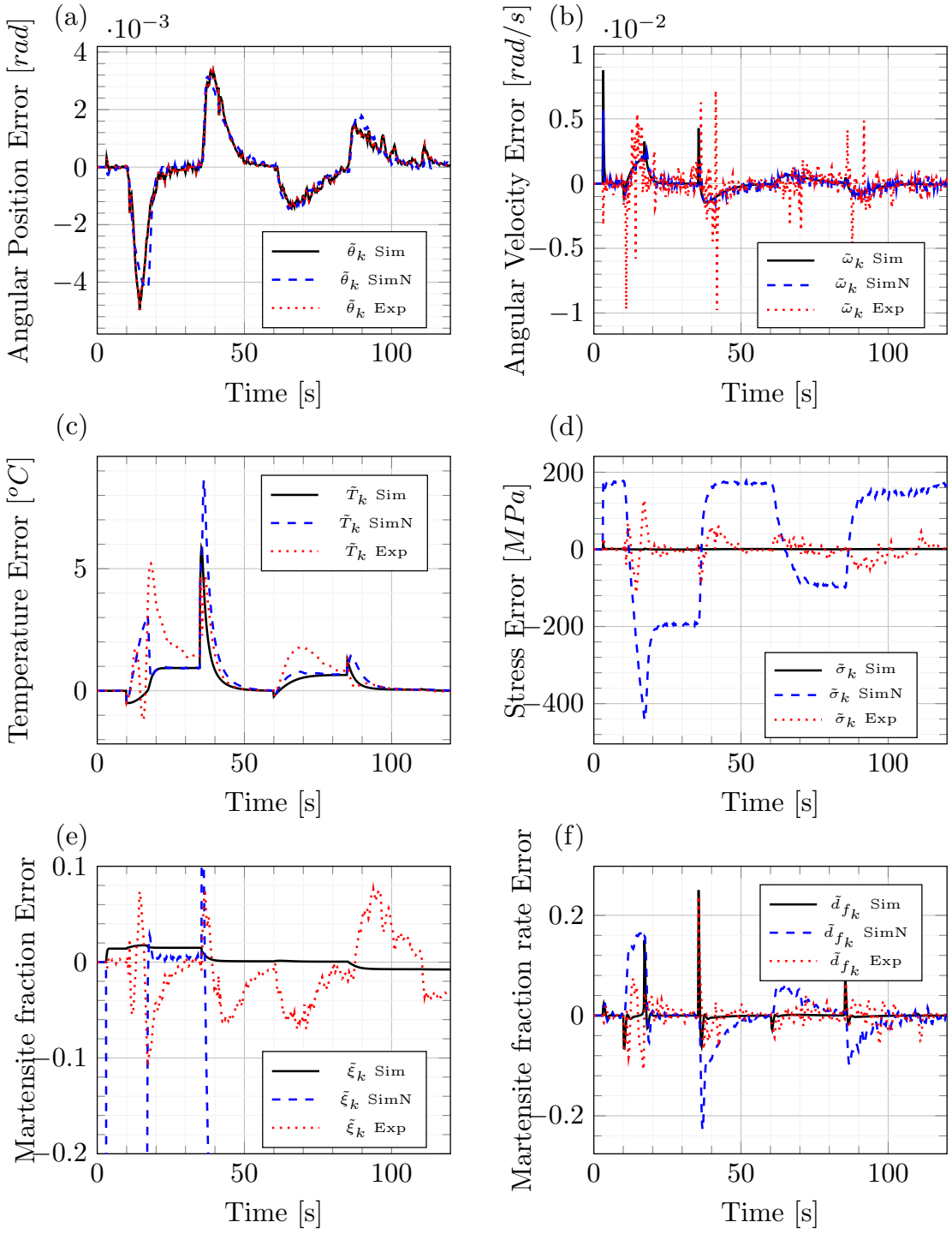

FIGURE 5.3: Estimation error for states and unknown input with step voltage input. Simulation and experimental results, a) Angular position, b) Angular velocity, c) Temperature, d) SMA wire stress, e) Martensite fraction, f) Martensite fraction rate. Sim - Simulation results without added noise; SimN - simulation results with added noise to the output.

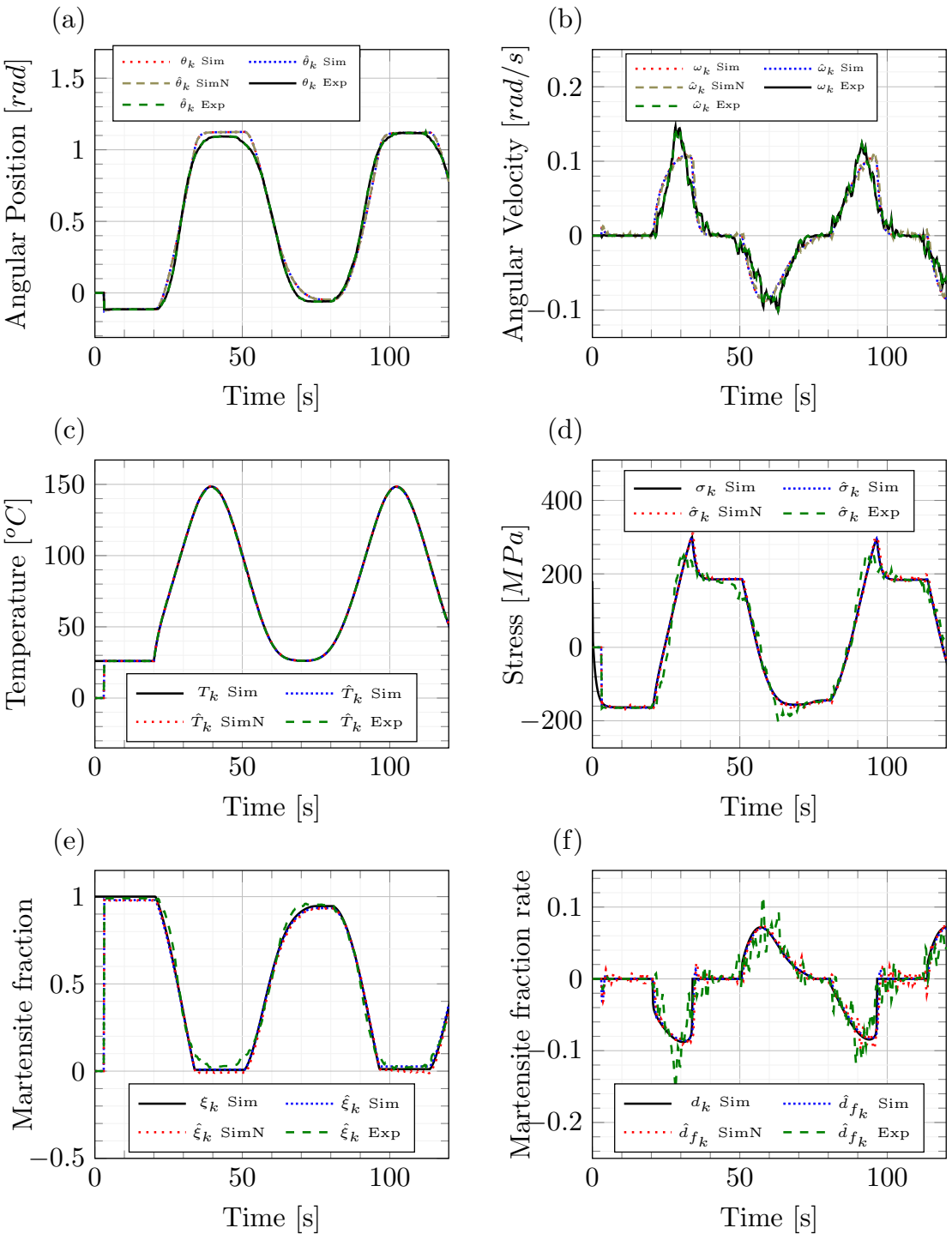

FIGURE 5.4: Estimated states and unknown input with 0.01 Hz sinusoidal voltage. Simulation and experimental results, a) Angular position, b) Angular velocity, c) Temperature, d) SMA wire stress, e) Martensite fraction, f) Martensite fraction rate. Sim - Simulation results without added noise; SimN - simulation results with added noise to the output.

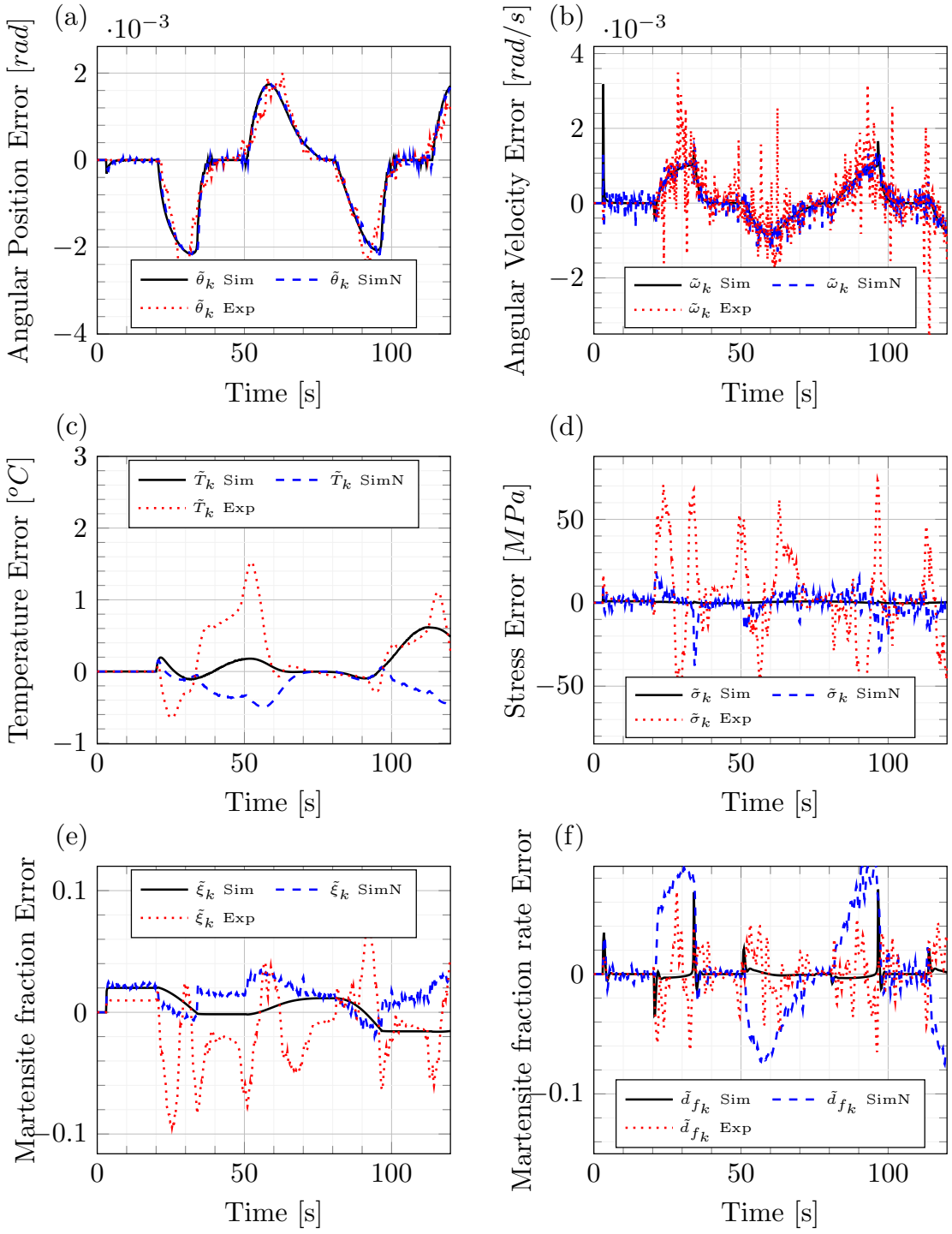

FIGURE 5.5: Estimation error for states and unknown input with 0.01 Hz sinusoidal voltage. Simulation and experimental results, a) Angular position, b) Angular velocity, c) Temperature, d) SMA wire stress, e) Martensite fraction, f) Martensite fraction rate. Sim - Simulation results without added noise; SimN - simulation results with added noise to the output.

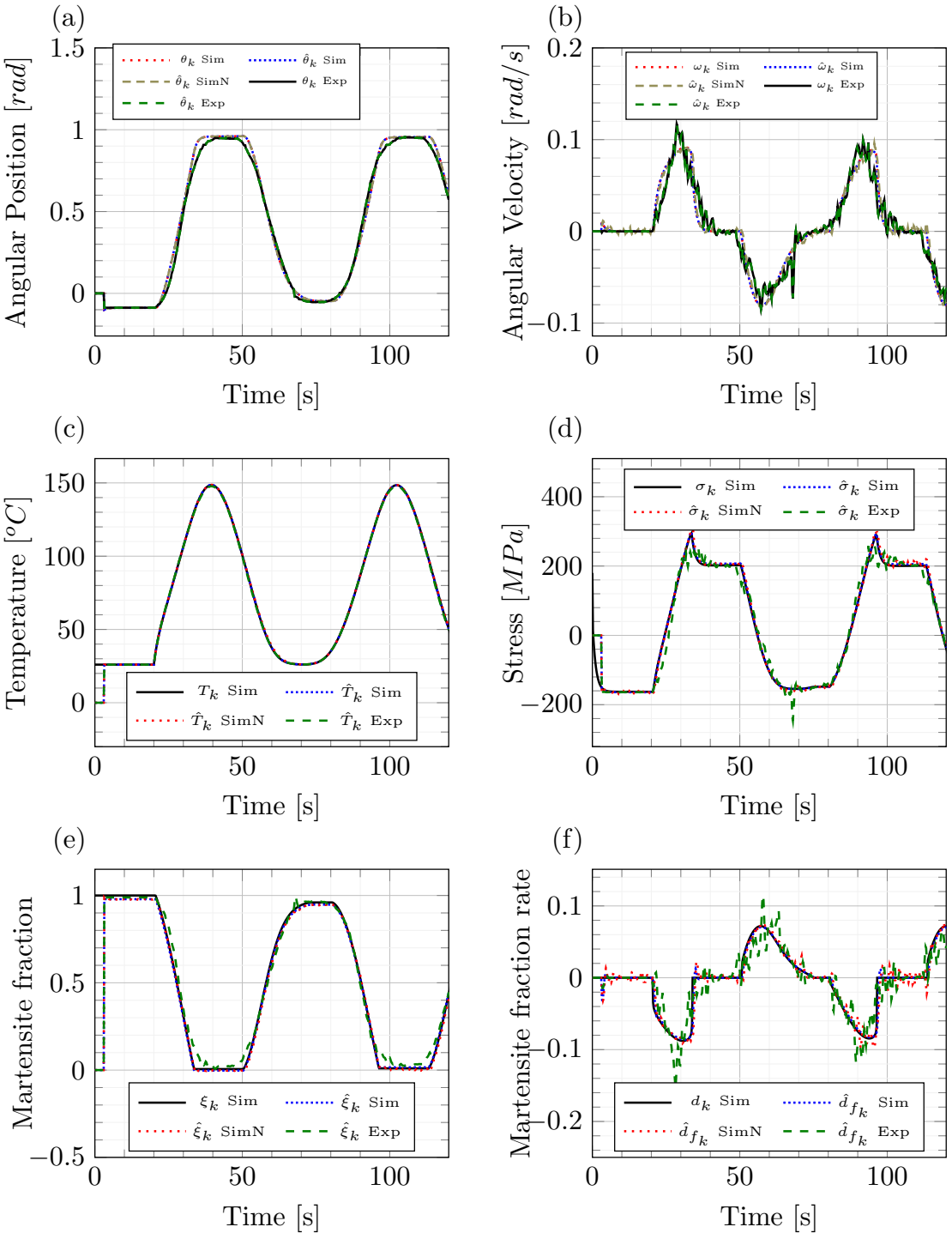

FIGURE 5.6: Estimated states and unknown input with 0.01 Hz sinusoidal voltage and 31 g payload. Simulation and experimental results, a) Angular position, b) Angular velocity, c) Temperature, d) SMA wire stress, e) Martensite fraction, f) Martensite fraction rate.

Sim - Simulation results without added noise; SimN - simulation results with added noise to the output.

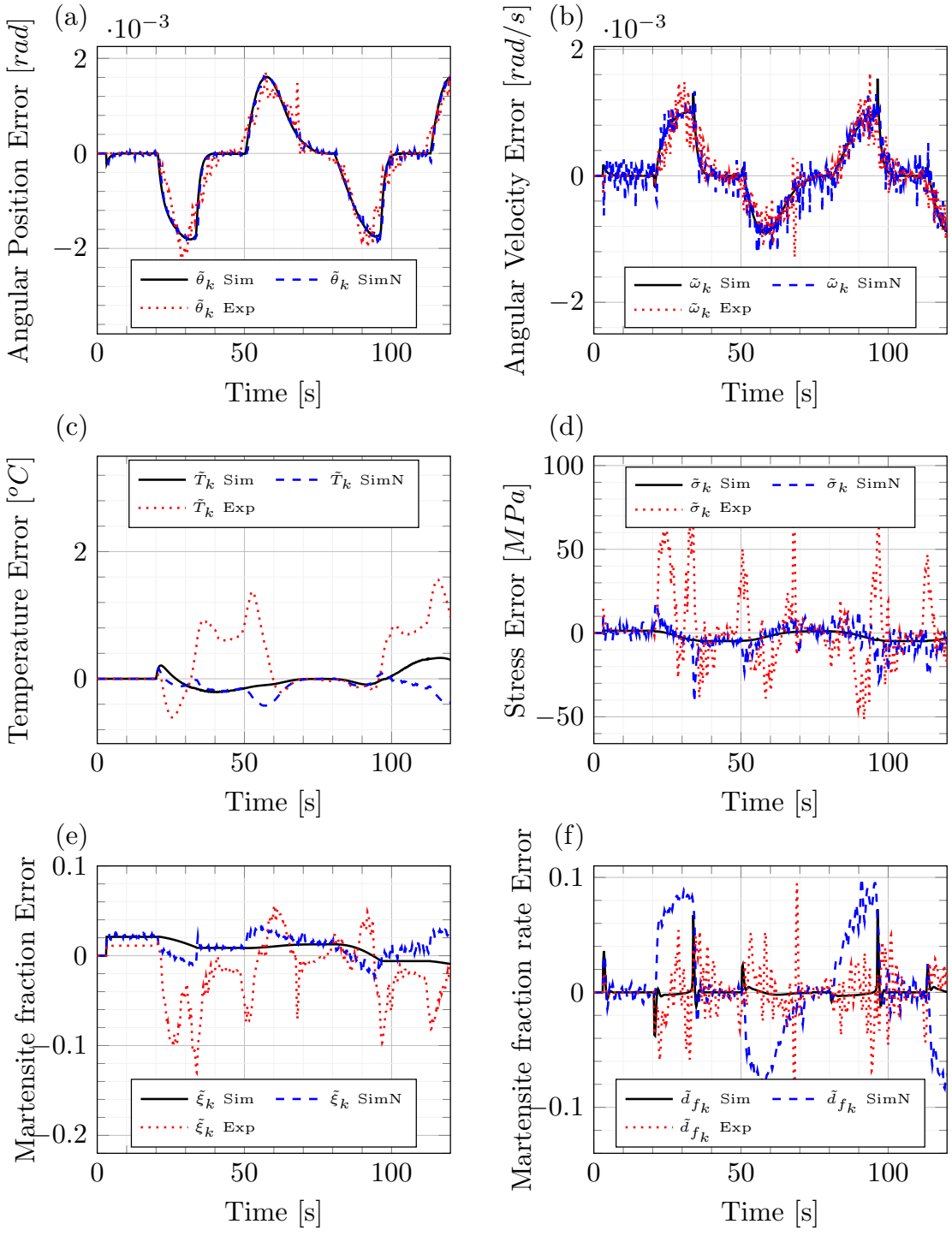

FIGURE 5.7: Estimation error for states and unknown input with 0.01 Hz sinusoidal voltage and 31 g payload. Simulation and experimental results, a) Angular position, b) Angular velocity, c) Temperature, d) SMA wire stress, e) Martensite fraction, f) Martensite fraction rate.

Sim - Simulation results without added noise; SimN - simulation results with added noise to the output.

Chapter 6

State Feedback Control

This chapter presents the development, implementation and performance analysis of state feedback control for regulation and tracking of angular position of the bias SMA wire actuated robotic arm presented in Chapter 3. A State-Dependent Ricatti Equation (SDRE) and a Discrete-time State-Dependent Ricatti Equation (DSDRE) controls are implemented. The results of these approaches are compared in simulation and experiments over different scenarios with the adaptive control proposed in Chapter 4. Section 6.1 presents an overview of the SDRE and DSDRE control techniques and existing implementation on SMA wire based systems. Section 6.2 describes the controllable continuously differentiable model for the bias SMA wire actuated robotic arm, followed by the implementation of the SDRE control for the mentioned system. Followed by the modeling and implementation of the discrete-time variation of the SDRE approach in section 6.3. Finally, section 6.4 discusses the results in simulation and experiments of the two proposed state feedback control *vs.* the Adaptive Control discussed in Chapter 4. In this section, an implementation scenario, where the SMA based robotic arm reaches a desired position, grasps and object and goes to transportation position is also presented. The chapter conclusions are presented in section 6.5.

6.1 Literature Overview

6.1.1 SDRE Control

The State-Dependent Riccati Equation (SDRE) strategy for control, is a nonlinear optimal regulation technique. The SDRE method entails the factorization (parametrization) of the nonlinear system into the product of a matrix-valued function (state-dependent)

and the state vector. This factorization brings the system to a point-wise linear structure with State-Dependent Coefficients (SDC) matrices [31].

Consider the deterministic, infinite-horizon nonlinear optimal regulation problem, where the system is autonomous, nonlinear in the state, full-state observable and affine in the input of the form [31]:

$$\dot{x}(t) = f(x) + B(x)\,u(t), \quad x(0) = x_0 \tag{6.1}$$

where $x \in \mathbb{R}^n$ is the state vector, $u(t)\,\mathbb{R}^m$ the unconstrained input vector, $t \in [0, \infty)$. The functions $f : \mathbb{R}^n \to \mathbb{R}^n \times \mathbb{R}^n$, and $B : \mathbb{R}^n \to \mathbb{R}^n \times \mathbb{R}^m$ are functions of the class $\mathcal{C}^1$ and $B(x) \neq 0\ \forall x$. Assuming the origin $x = 0$ as an equilibrium point, such that $f(0) = 0$, the minimization of the infinite-time performance criterion

$$J(x_0, u(\cdot)) = \frac{1}{2}\int_0^\infty \{x^\top(t)\,Q(x)\,x(t) + u^\top(t)\,R(x)\,u(t)\}dt \tag{6.2}$$

is considered, which is non-quadratic in x but quadratic in u. The weighting matrices are state-dependent such that $Q : \mathbb{R}^n \to \mathbb{R}^n \times \mathbb{R}^n$ and $R : \mathbb{R}^n \to \mathbb{R}^m \times \mathbb{R}^m$. Where $Q(x) \geq 0$ and $R(x) \geq 0\ \forall x$. So we define the control law:

$$u(x) = -k(x)\,x = -R^{-1}(x)\,B^\top(x)\,P(x)\,x, \tag{6.3}$$

where $P(x)$ is the unique, symmetric, positive-definite solution of the state-dependent Riccati equation

$$P(x)\,A(x) + A^\top(x)\,P(x) - P(x)\,B(x)\,R^{-1}(x)\,B^\top(x)\,P(x) + Q(x) = 0 \tag{6.4}$$

for a parametrized system of the form:

$$\dot{x} = A(x)\,x + B(x)\,u \tag{6.5}$$

and $Q(x) = C(x)\,C^\top(x)$, where the pairs $\{A(x), B(x)\}$ and $\{C(x), A(x)\}$ are point-wise stabilizable and detectable, respectively, in the linear sense for all x.

6.1.1.1 SDRE control for SMA based systems

There exist few reported research on the implementation of SDRE control for SMA based system. The difficulty for measuring the SMA wire states, and the requirement of a full state feedback makes this technique difficult to be implemented experimentally. In the work presented in [157], the aeroelastic control of a cantilever wing with embedded shape memory alloy wires and piezoelectric actuators is carried out. The authors implement a

SDRE control for the piezoelectric actuators, while the SMA wires are actuated through passive control by increasing the stiffness of the system. Although the dynamics of the SMA wire are considered for the development of this approach, they are not directly controlled. The authors present and discuss simulation results.

The authors in [18] propose a vibration and position control of a flexible structural beam driven by a DC motor. In this work, SMA actuators are used as a mean of vibration control of the flexible beam. Two SDRE controls are applied to the system in a cascade configuration. The first SDRE control commands the DC motor to control position, while the second one controls the SMA wire to eliminate the vibration. The proposed system is tested in simulation and numerical results are discussed. The simulation results show the effectiveness of the SDRE control to deal with the highly nonlinear system of a SMA based actuator. However, experimental implementation could be challenging, thus the required states are not always available for SMA based systems.

In [19] the authors propose a similar approach to the one presented in [18] for control of position and vibration of a 3 link flexible manipulator. The Falk's SMA wire model ([104]) is used, where the free energy is considered in a polynomial form and only the temperature (T) and the deformation (ϵ) are considered as states. A SDRE control is developed to control the DC motor for position regulation and the SMA wire for vibration control. Simulation results are presented and discussed, showing the effectiveness of the SDRE control. The use of the Falk's model allows the implementation of this approach with the estimation of the temperature only. However, no experimental results are presented.

Based on the literature overview, we propose the implementation of the SDRE control approach for angular position regulation and tracking of the biased SMA wire based robotic arm presented in Chapter 3. An observer based approach is used to provide the full state vector for the SDRE control loop. The next sections describe the development of a controllable model for the proposed robotic arm, the SDRE implementation and results are discussed.

6.1.2 DSDRE Control

The Discrete-time State-Dependent Riccati Equation (DSDRE) strategy for control, is a variation of the SDRE control strategy, applied to discrete nonlinear systems. This approach uses the solution of the Discrete Algebraic Riccati Equation (DARE) to find a sub-optimal control input, minimizing an infinite horizon quadratic performance index

[158]. Consider the discrete nonlinear system as follows:

$$x_{k+1} = \ f_k\left(x_k\right) + B_k\left(x_k\right) u_k \tag{6.6}$$

Let us rewrite the system in a state-dependent parametrized form as follows [158]:

$$x_{k+1} = A_k\left(x_k\right) x_k + B_k\left(x_k\right) u_k \tag{6.7}$$

where the pair $\{A_k\left(x_k\right), B_k\left(x_k\right)\}$ is point-wise controllable. Now consider the discrete cost function:

$$J_k = \frac{1}{2}\sum_{i=k}^{\infty}\left\{x_i^\top Q x_i + u_i^\top R u_i\right\} \tag{6.8}$$

The sub-optimal solution for this minimization is obtained solving the Discrete-time State Dependent Riccati Equation given by the following equation:

$$\begin{aligned} P\left(x_k\right) = A_k\left(x_k\right)^\top \Big[P\left(x_k\right) - P_k\left(x_k\right) B_k\left(x_k\right)^\top \times \\ \times \left(R + B_k\left(x_k\right)^\top P\left(x_k\right) B_k\left(x_k\right)\right)^{-1} B_k\left(x_k\right)^\top P\left(x_k\right)\Big] A_k\left(x_k\right) + Q \end{aligned} \tag{6.9}$$

where $Q\left(x_k\right) = C_k\left(x_k\right) C_k^\top\left(x_k\right)$ so the pair $\{C_k\left(x_k\right), A_k\left(x_k\right)\}$ is point-wise detectable in the linear sense for all x_k. The nonlinear control action is computed as follows [158]:

$$u_k = -K_k x_k \tag{6.10}$$

where

$$K_k = \left(R + B_k\left(x_k\right)^\top P\left(x_k\right) B_k\left(x_k\right)\right)^{-1} B_k\left(x_k\right)^\top P\left(x_k\right) A_k\left(x_k\right) \tag{6.11}$$

Finally, the solution of the DSDRE for the system in Eq.(6.6) subject to Eq.(6.8) results in a locally stabilizing control [158].

6.2 SDRE Control of SMA robotic arm

In the following subsections, the process to obtain a non-switching controllable continuous nonlinear model, suitable for SDRE control is detailed.

6.2.1 Continuously differentiable model

The implementation of the SDRE control techniques requires a controllable nonlinear system of the class $\mathcal{C}^1$, i.e. continuously differentiable. Consider the nonlinear system

as follows:

$$\dot{x}(t) = f(x, u) \tag{6.12}$$

where the state vector $x = \begin{bmatrix} \theta & \dot{\theta} & T & \sigma \end{bmatrix}^\top$ and the input vector $u = V_1^2$

$$f(x, u) = \begin{bmatrix} x_2 \\ \left(A_1 r_1 x_4 - b x_2 - m_{load} g r_{load} \sin(x_1) - k_s x_1\right)\left(\frac{1}{J_1}\right) \\ -\frac{h_1(x_3) A_{w_1}}{m_{w_1} c_{p_1}}(x_3 - T_{amb}) + \frac{1}{R_1(\xi) m_{w_1} c_{p_1}} u_1 \\ f_{x_4}(x, u) \end{bmatrix} \tag{6.13}$$

and $f_{x_4}(x, u)$ is obtained by substituting the SMA wire transformation model in Eq.(3.6) into the constitutive model in Eq.(3.9). After algebraical manipulation we have:

$$f_{x_4}(x, u) = \frac{-\frac{E_1 r_1}{l_{1_0}} x_2 + \Theta T_r(x_3, u) + \Omega \xi_T(x_3, x_4) T_r(x_3, u)}{1 - \Omega \xi_\sigma(x_3, x_4)} \tag{6.14}$$

where

$$T_r(x_3, u) = -\frac{h_1(x_3) A_{w_1}}{m_{w_1} c_{p_1}}(x_3 - T_{amb}) + \frac{1}{R_1(\xi) m_{w_1} c_{p_1}} u \tag{6.15}$$

The nonlinear system in Eq.(6.13), as discussed in subsection 3.2.1, is a switching model where the switching law depends on several factors, such as transformation temperatures, SMA wire temperature and stress as well as their respective time derivatives. This switching law determines if the SMA wire is going through a forward or a reverse transformation. The SMA wire going through a forward or reverse transformation entails an increase or decrease of the martensite fraction value respectively. With this in mind, it is possible to infer the switching law directly from the sign of the martensite fraction time derivative $\left(\dot{\xi}\right)$. Thus, we can reformulate Eq.(3.7) and Eq.(3.8) as follows:

$$\xi_T(T, \sigma) = \begin{cases} -\frac{\xi_M}{2} \sin\left(a_A\left(T - A_s - \frac{1}{c_M}\sigma\right)\right) a_A, & \text{if } \dot{\xi} < 0 \\ -\frac{1 - \xi_A}{2} \sin\left(a_M\left(T - M_f - \frac{1}{c_A}\sigma\right)\right) a_M, & \text{if } \dot{\xi} > 0 \\ 0, & \text{if } \dot{\xi} = 0 \end{cases} \tag{6.16}$$

$$\xi_\sigma(T, \sigma) = \begin{cases} -\frac{1}{c_A}\xi_T(T, \sigma), & \text{if } \dot{\xi} < 0 \\ -\frac{1}{c_M}\xi_T(T, \sigma), & \text{if } \dot{\xi} > 0 \\ 0, & \text{if } \dot{\xi} = 0 \end{cases} \tag{6.17}$$

Let us express the switching function in Eq.(6.14) as follows:

$$f_{x_4}(x,u) = \begin{cases} f_{x_4}^1(x,u), & \text{if } \dot{\xi} < 0 \\ f_{x_4}^2(x,u), & \text{if } \dot{\xi} > 0 \\ f_{x_4}^3(x,u), & \text{if } \dot{\xi} = 0 \end{cases} \tag{6.18}$$

where

$$f_{x_4}^1(x,u) = \frac{-\frac{E_1 r_1}{l_{1_0}} x_2 + \Theta T_r(x_3,u) + \Omega \xi_T^1(x_3,x_4) T_r(x_3,u)}{1 - \Omega \xi_\sigma^1(x_3,x_4)}$$
$$f_{x_4}^2(x,u) = \frac{-\frac{E_1 r_1}{l_{1_0}} x_2 + \Theta T_r(x_3,u) + \Omega \xi_T^2(x_3,x_4) T_r(x_3,u)}{1 - \Omega \xi_\sigma^2(x_3,x_4)}$$
$$f_{x_4}^3(x,u) = -\frac{E_1 r_1}{l_{1_0}} x_2 + \Theta T_r(x_3,u)$$

and

$$\xi_T^1(x_3,x_4) = -\frac{\xi_M}{2} \sin\left(a_A\left(x_3 - A_s - \frac{1}{c_M}x_4\right)\right) a_A$$
$$\xi_T^2(x_3,x_4) = -\frac{1-\xi_A}{2} \sin\left(a_M\left(x_3 - M_f - \frac{1}{c_A}x_4\right)\right) a_M$$
$$\xi_\sigma^1(x_3,x_4) = -\frac{1}{c_A}\xi_T^1(x_3,x_4)$$
$$\xi_\sigma^2(x_3,x_4) = -\frac{1}{c_M}\xi_T^2(x_3,x_4)$$

The switching function presented in Eq.(6.18) can be approximated to a continuous differentiable function $\overline{f}_{x_4}(x,u) \in \mathcal{C}^1$, such that:

$$\overline{f}_{x_4}(x,u) = f_{x_4}^1(x,u) Z_1\left(\dot{\xi}\right) + f_{x_4}^2(x,u) Z_2\left(\dot{\xi}\right) + f_{x_4}^3(x,u) Z_3\left(\dot{\xi}\right) \tag{6.19}$$

where

$$Z_1\left(\dot{\xi}\right) = \left(\arctan\left(\delta\left(\dot{\xi} - \epsilon\right)\right) + \frac{\pi}{2}\right)\left(\frac{1}{\pi}\right) \tag{6.20}$$
$$Z_2\left(\dot{\xi}\right) = \left(\arctan\left(-\delta\left(\dot{\xi} + \epsilon\right)\right) + \frac{\pi}{2}\right)\left(\frac{1}{\pi}\right) \tag{6.21}$$
$$Z_3\left(\dot{\xi}\right) = \left(\arctan\left(\delta\left(\dot{\xi} + \epsilon\right)\right) + \arctan\left(-\delta\left(\dot{\xi} - \epsilon\right)\right)\right)\left(\frac{1}{\pi}\right) \tag{6.22}$$

This function yields a continuous derivable approximation which is arbitrarily close to the switching function in Eq.(6.18), depending on the choice of δ, where δ is a positive constant which determines the softness of the transition. In addition, the positive small

constant $\epsilon \leq 0.01$ sets a boundary layer to avoid overlapping of active states at the switching point $\dot{\xi} = 0$. Finally, from the system in Eq.(6.13), substituting the approximated function Eq.(6.19), let us redefine the model for a biased SMA wire robotic arm as a non-switched system as follows:

$$\overline{f}\left(x,u\right) = \begin{bmatrix} x_2 \\ \left(A_1 r_1 x_4 - b x_2 - m_{load} g r_{load} \sin\left(x_1\right) - k_s x_1\right)\left(\frac{1}{J_1}\right) \\ -\frac{h_1(x_3) A_{w_1}}{m_{w_1} c_{p_1}}\left(x_3 - T_{amb}\right) + \frac{1}{R_1(\xi) m_{w_1} c_{p_1}} u \\ \overline{f}_{x_4}\left(x,u\right) \end{bmatrix} \tag{6.23}$$

6.2.2 Nonlinear Controllability

Consider the nonlinear system presented in Eq.(6.23). The dependency of the angular position (x_1) over the temperature (x_3) and stress (x_4), renders impossible to control these states separately. This condition leads to a partially controllable system. Now let us divide the state vector into controllable (x_c) and non-controllable states (η). Consider the new controllable state vector $x_c = \begin{bmatrix} \theta & \dot{\theta} & \sigma \end{bmatrix}^\top$ and the non-controllable state vector $\eta = T$. We rewrite the model in Eq.(6.23) as follows:

$$\dot{x}_c = \overline{f}_c\left(x_c,\eta\right) + g\left(x_c,\eta\right) u \tag{6.24}$$

where

$$\overline{f}_c\left(x_c,\eta\right) = \begin{bmatrix} x_{c_2} \\ \left(A_1 r_1 x_{c_3} - b x_{c_2} - m_{load} g r_{load} \sin\left(x_{c_1}\right) - k_s x_{c_1}\right)\left(\frac{1}{J_1}\right) \\ \overline{f}_{c_3}\left(x_c,\eta\right) \end{bmatrix} \tag{6.25}$$

$$g\left(x_c,\eta\right) = \begin{bmatrix} 0 \\ 0 \\ \overline{g}_{c_3}\left(x_c,\eta\right) \end{bmatrix} \tag{6.26}$$

$$\dot{\eta}\left(\eta,u\right) = \begin{bmatrix} -\frac{h_1(\eta) A_{w_1}}{m_{w_1} c_{p_1}}\left(\eta - T_{amb}\right) + \frac{1}{R_1(\xi) m_{w_1} c_{p_1}} u \end{bmatrix} \tag{6.27}$$

$$\overline{f}_{c_3}\left(x_c,\eta\right) = f_c^1\left(x_c,\eta\right) Z_1\left(\dot{\xi}\right) + f_c^2\left(x_c,\eta\right) Z_2\left(\dot{\xi}\right) + f_c^3\left(x_c,\eta\right) Z_3\left(\dot{\xi}\right) \tag{6.28}$$

$$\overline{g}_{c_3}\left(x_c,\eta\right) = g_c^1\left(x_c,\eta\right) Z_1\left(\dot{\xi}\right) + g_c^2\left(x_c,\eta\right) Z_2\left(\dot{\xi}\right) + g_c^3\left(x_c,\eta\right) Z_3\left(\dot{\xi}\right) \tag{6.29}$$

and

$$
\begin{aligned}
f_c^1(x_c,\eta) &= \frac{-\dfrac{E_1 r_1}{l_{1_0}} x_{c_2} + \left(\Theta + \Omega\xi_T^1(x_{c_3},\eta)\right)\left(-\frac{h_1(\eta)A_{w_1}}{m_{w_1}c_{p_1}}(\eta - T_{amb})\right)}{1-\Omega\xi_\sigma^1(x_{c_3},\eta)} \\
f_c^2(x_c,\eta) &= \frac{-\dfrac{E_1 r_1}{l_{1_0}} x_{c_2} + \left(\Theta + \Omega\xi_T^2(x_{c_3},\eta)\right)\left(-\frac{h_1(\eta)A_{w_1}}{m_{w_1}c_{p_1}}(\eta - T_{amb})\right)}{1-\Omega\xi_\sigma^2(x_{c_3},\eta)} \\
f_c^3(x_c,\eta) &= -\frac{E_1 r_1}{l_{1_0}} x_{c_2} + \Theta\left(-\frac{h_1(\eta)A_{w_1}}{m_{w_1}c_{p_1}}(\eta - T_{amb})\right) \\
g_c^1(x_c,\eta) &= \frac{\left(\Theta + \Omega\xi_T^1(x_{c_3},\eta)\right)}{1-\Omega\xi_\sigma^1(x_{c_3},\eta)}\frac{1}{R_1(\xi)\,m_{w_1}c_{p_1}} \\
g_c^2(x_c,\eta) &= \frac{\left(\Theta + \Omega\xi_T^2(x_{c_3},\eta)\right)}{1-\Omega\xi_\sigma^2(x_{c_3},\eta)}\frac{1}{R_1(\xi)\,m_{w_1}c_{p_1}} \\
g_c^3(x_c,\eta) &= \frac{\Theta}{R_1(\xi)\,m_{w_1}c_{p_1}}
\end{aligned}
$$

Notice that the non-controllable subsystem $\dot{\eta}$ is input (u)-to-state (η) stable.

Consider the system in Eq.(6.24). Performing a change of variable to avoid zero crossing in the first state (x_{c_1}), let us define the new state vector $\overline{x}_c = \begin{bmatrix} \overline{x}_{c_1} & \dot{\theta} & \sigma \end{bmatrix}^\top$, where:

$$
\overline{x}_{c_1} = \theta - \theta_m \tag{6.30}
$$

and $\theta > \theta_m \ \forall t$. We define the system with the new state vector as follows:

$$
\dot{\overline{x}}_c = \tilde{f}_c(\overline{x}_c,\eta) + g(\overline{x}_c,\eta)\,u \tag{6.31}
$$

where

$$
\tilde{f}_c(\overline{x}_c,\eta) = \begin{bmatrix} \overline{x}_{c_2} \\ \dfrac{A_1 r_1}{J_1}\overline{x}_{c_3} - \dfrac{b}{J_1}\overline{x}_{c_2} - \dfrac{m_{load}g r_{load}}{J_1}\sin(\overline{x}_{c_1}+\theta_m) - \dfrac{k_s}{J_1}(\overline{x}_{c_1}+\theta_m) \\ \overline{f}_{c_3}(\overline{x}_c,\eta) \end{bmatrix} \tag{6.32}
$$

Let us define the accessibility distribution C_a as the distribution generated by the accessibility algebra $\mathcal{C}_a$ as follows:

$$
C_a(\overline{x}_c) = span\left\{X(x_c) \ \middle|\ X \text{vector field in } \mathcal{C}_a\right\}, \quad x_c \in X \tag{6.33}
$$

and the accessibility algebra $\mathcal{C}_a$ are the linear combinations of repeated Lie brackets as follows:

$$
[X_k,[X_{k-1},[\cdots,[X_2,X_1]\cdots]]], \quad k = 1,2,\ldots, \tag{6.34}
$$

where X_i is a vector field in the set $\{\overline{f}_c, g\}$. In addition the Lie bracket of any two vectors $[W, V]$ is defined as:

$$[W, V] = \frac{\partial V}{\partial x} W - \frac{\partial W}{\partial x} V \tag{6.35}$$

After computing the accessibility algebra, the system in Eq.(6.32) is proven to be accessible in the nonlinear sense for all $\overline{x}_c$. The full nonlinear controllability analysis is provided in Appendix B.2.

6.2.3 SDC parametrization

Different parametrizations of the form in Eq.(6.5) were tested for the system presented in Eq.(6.31). We propose the following parametrization:

$$A(\overline{x}_c) = \begin{bmatrix} 0 & 1 & 0 \\ a_{21} & -\frac{b}{J_1} & \frac{A_1 r_1}{J_1} \\ a_{31} & a_{32} & a_{33} \end{bmatrix} \tag{6.36}$$

$$B(\overline{x}_c) = \begin{bmatrix} 0 \\ 0 \\ b_{31} \end{bmatrix} \tag{6.37}$$

where

$$a_{21} = -\frac{k_s}{J_1} - \frac{m_{load} g r_{load} \left(\sin\left(\overline{x}_1 - \theta_m\right) - \sin\left(\theta_m\right)\right)}{J_1 \overline{x}_1} + \frac{k_s \theta_m}{J_1 \overline{x}_1} - \\ - \frac{m_{load} g r_{load} \left(\sin\left(\theta_m\right)\right)}{J_1 \overline{x}_1}$$

$$a_{31} = \left(\frac{\Theta_1 + \xi_T^1\left(\overline{x}_{c_3}, \eta\right)}{1 - \Omega \xi_\sigma^1\left(\overline{x}_{c_3}, \eta\right)} Z_1\left(\dot{\xi}\right) + \frac{\Theta_1 + \xi_T^2\left(\overline{x}_{c_3}, \eta\right)}{1 - \Omega \xi_\sigma^2\left(\overline{x}_{c_3}, \eta\right)} Z_2\left(\dot{\xi}\right) + \right. \\ \left. + \Theta_1 Z_3\left(\dot{\xi}\right)\right)\left(-\frac{h_1(\eta) A_{w_1}}{m_{w_1} c_{p_1}}\left(\eta - T_{amb}\right)\right)\frac{1}{\overline{x}_1}$$

$$a_{32} = \left(-\frac{E_1 r_1}{l_{1_0}\left(1 - \Omega \xi_\sigma^1\left(\overline{x}_{c_3}, \eta\right)\right)} Z_1\left(\dot{\xi}\right) - \frac{E_1 r_1}{l_{1_0}\left(1 - \Omega \xi_\sigma^2\left(\overline{x}_{c_3}, \eta\right)\right)} Z_2\left(\dot{\xi}\right)\right)\alpha - \\ - \frac{E_1 r_1}{l_{1_0}} Z_3\left(\dot{\xi}\right)$$

$$a_{33} = \left(-\frac{E_1 r_1 x_{c_2}}{l_{1_0}\left(1 - \Omega \xi_\sigma^1\left(\overline{x}_{c_3}, \eta\right)\right)} Z_1\left(\dot{\xi}\right) - \frac{E_1 r_1 x_{c_2}}{l_{1_0}\left(1 - \Omega \xi_\sigma^2\left(\overline{x}_{c_3}, \eta\right)\right)} Z_2\left(\dot{\xi}\right)\right)\frac{1 - \alpha}{\overline{x}_{c_3}}$$

$$b_{31} = \left(\frac{\Theta_1 + \xi_T^1\left(\overline{x}_{c_3}, \eta\right)}{1 - \Omega \xi_\sigma^1\left(\overline{x}_{c_3}, \eta\right)} Z_1\left(\dot{\xi}\right) + \frac{\Theta_1 + \xi_T^2\left(\overline{x}_{c_3}, \eta\right)}{1 - \Omega \xi_\sigma^2\left(\overline{x}_{c_3}, \eta\right)} Z_2\left(\dot{\xi}\right) + \Theta_1 Z_3\left(\dot{\xi}\right)\right)\frac{1}{R_1(\xi) m_{w_1} c_{p_1}}$$

The system in Eq.(6.32) is proven to be reachable for all $\overline{x}_c$ in the nonlinear sense (See Appendix B.2), thus the pair $\{A(\overline{x}_c), B(\overline{x}_c)\}$ is ensured to be pointwise stabilizable in the linear sense for all $\overline{x}_c$. In addition, if $Q(\overline{x}_c) = C(\overline{x}_c) C^\top(\overline{x}_c) \geq 0$, the pair $\{C(\overline{x}_c), A(\overline{x}_c)\}$ is ensured to be pointwise detectable in the linear sense for all $\overline{x}_c$. As demonstrated in [159], the feedback control in Eq.(6.3) is proven to stabilize the proposed parametrized system.

6.2.4 SDRE Integral Servomechanism

In order to perform regulation and tracking we implement the SDRE controller as an integral servomechanism as proposed in [160]. Let us decompose the state vector as $\overline{x}_c = \begin{bmatrix} X_R^\top & X_N^\top \end{bmatrix}$ and define the augmented state vector $x_{IS} = \begin{bmatrix} X_I^\top & X_R^\top & X_N^\top \end{bmatrix}^\top$, where the vector $X_R^\top$ tracks the reference command vector r_c and $X_I^\top$ is the integral of the state $X_R^\top$. The augmented system is given by:

$$\dot{x}_{IS} = \tilde{A}(x_{IS})\, x_{IS} + \tilde{B}(x_{IS})\, u \tag{6.38}$$

where

$$\tilde{A}(x_{IS}) = \left[\begin{array}{c|cc} \mathbf{0} & \mathbf{I} & \mathbf{0} \\ \hline \mathbf{0} & A(\overline{x}_c) & \end{array}\right]$$

$$\tilde{B}(x_{IS}) = \begin{bmatrix} \mathbf{0} \\ B(\overline{x}_c) \end{bmatrix}$$

The SDRE integral servo controller is given by

$$u = -\tilde{R}^{-1}(x_{IS})\, \tilde{B}^T(x_{IS})\, \tilde{P}(x_{IS}) \begin{bmatrix} X_I - \int r_c dt \\ X_R - r_c \\ x_N \end{bmatrix} \tag{6.39}$$

where $x_R = \overline{x}_{c_1}$, $r_c = \theta_d + \theta_m$ and $x_N = \begin{bmatrix} \dot{\theta} & \sigma \end{bmatrix}^\top$.

6.3 DSDRE Control of SMA robotic arm

In the following subsections, the process to obtain a non-switching controllable discrete-time nonlinear model, suitable for DSDRE control implementation is detailed.

6.3.1 Singular perturbation controllable model

Consider the nonlinear continuously differentiable controllable system in Eq.(6.31). The system can be written as a singularly perturbed system in the form of Eq.(5.9), with

$$\epsilon = \frac{T_m}{T_t} = \frac{J_1 h_1(T) A_{w_1}}{b m_{w_1} c_{p_1}} \approx 0 \tag{6.40}$$

Let us define the new state vector $x_p = \begin{bmatrix} \overline{x}_{c_1} & \sigma \end{bmatrix}^\top$ and the algebraic equation derived from the singularly perturbed system:

$$\frac{T_m}{T_t}\frac{d\dot{\theta}}{dt_r} = h_p = \frac{A_1 r_1}{b} x_{p_2} - \frac{m_L g r_{load}}{b}\sin(x_{p_1} + \theta_m) - \frac{1}{b} k_s (x_{p_1} - \theta_m) \approx 0 \tag{6.41}$$

so we can write the system in Eq.(6.31) as follows:

$$\dot{x}_p = f_p(x_p, \eta) + g_p(x_p, \eta)\, u \tag{6.42}$$

where

$$f_p(x_p, \eta) = \begin{bmatrix} h_p \\ f_{p_2}(x_p, \eta) \end{bmatrix} \tag{6.43}$$

$$g_p(x_p, \eta) = \begin{bmatrix} 0 \\ g_{p_2}(x_p, \eta) \end{bmatrix} \tag{6.44}$$

$$f_{p_2}(x_p, \eta) = f_p^1(x_p, \eta) Z_1\left(\dot{\xi}\right) + f_p^2(x_p, \eta) Z_2\left(\dot{\xi}\right) + f_p^3(x_p, \eta) Z_3\left(\dot{\xi}\right) \tag{6.45}$$

$$g_{p_2}(x_p, \eta) = g_p^1(x_p, \eta) Z_1\left(\dot{\xi}\right) + g_p^2(x_p, \eta) Z_2\left(\dot{\xi}\right) + g_p^3(x_p, \eta) Z_3\left(\dot{\xi}\right) \tag{6.46}$$

and

$$f_p^1(x_p, \eta) = \frac{-\frac{E_1 r_1}{l_{1_0}} h_p + \left(\Theta + \Omega\xi_T^1(x_{p_2}, \eta)\right)\left(-\frac{h_1(\eta) A_{w_1}}{m_{w_1} c_{p_1}}(\eta - T_{amb})\right)}{1 - \Omega\xi_\sigma^1(x_{p_2}, \eta)}$$

$$f_p^2(x_p, \eta) = \frac{-\frac{E_1 r_1}{l_{1_0}} h_p + \left(\Theta + \Omega\xi_T^2(x_{p_2}, \eta)\right)\left(-\frac{h_1(\eta) A_{w_1}}{m_{w_1} c_{p_1}}(\eta - T_{amb})\right)}{1 - \Omega\xi_\sigma^2(x_{p_2}, \eta)}$$

$$f_p^3(x_p, \eta) = -\frac{E_1 r_1}{l_{1_0}} h_p + \Theta\left(-\frac{h_1(\eta) A_{w_1}}{m_{w_1} c_{p_1}}(\eta - T_{amb})\right)$$

$$g_p^1(x_p, \eta) = \frac{\left(\Theta + \Omega\xi_T^1(x_{p_2}, \eta)\right)}{1 - \Omega\xi_\sigma^1(x_{p_2}, \eta)} \frac{1}{R_1(\xi) m_{w_1} c_{p_1}}$$

$$g_p^2(x_p, \eta) = \frac{\left(\Theta + \Omega\xi_T^2(x_{p_2}, \eta)\right)}{1 - \Omega\xi_\sigma^2(x_{p_2}, \eta)} \frac{1}{R_1(\xi) m_{w_1} c_{p_1}}$$

$$g_p^3(x_p, \eta) = \frac{\Theta}{R_1(\xi) m_{w_1} c_{p_1}}$$

6.3.2 Controllable model discretization

Discretizing the model in Eq.(6.42) by first order Euler approximation, we have the discrete system as follows:

$$x_{p_{k+1}} = x_{p_k} + \left(f_{p_k}\left(x_{p_k}, \eta_k\right) + g_{p_k}\left(x_{p_k}, \eta_k\right) u_k \right) T_s \tag{6.47}$$

where

$$f_{p_k}\left(x_{p_k}, \eta_k\right) = \begin{bmatrix} h_{p_k} \\ f_{p_{k2}}\left(x_{p_k}, \eta_k\right) \end{bmatrix} \tag{6.48}$$

$$g_{p_k}\left(x_{p_k}, \eta_k\right) = \begin{bmatrix} 0 \\ g_{p_{k2}}\left(x_{p_k}, \eta_k\right) \end{bmatrix} \tag{6.49}$$

$$\eta_{k+1}\left(\eta_k, u_k\right) = \eta_k + \left(-\frac{h_1\left(\eta_k\right) A_{w_1}}{m_{w_1} c_{p_1}} \left(\eta_k - T_{amb}\right) + \frac{1}{R_1\left(\xi_k\right) m_{w_1} c_{p_1}} u_k \right) T_s \tag{6.50}$$

$$f_{p_{k2}}\left(x_{p_k}, \eta_k\right) = \sum_{i=1}^{3} f_{p_k}^i\left(x_{p_k}, \eta_k\right) Z_i\left(\xi_{k+1}\right) \tag{6.51}$$

$$g_{p_{k2}}\left(x_{p_k}, \eta_k\right) = \sum_{i=1}^{3} g_{p_k}^i\left(x_p, \eta\right) Z_i\left(\xi_{k+1}\right) \tag{6.52}$$

$$h_{p_k} = \frac{A_1 r_1}{b} x_{p_{k2}} - \frac{m_L g r_{load}}{b} \sin\left(x_{p_{k1}} + \theta_m\right) - \frac{1}{b} k_s \left(x_{p_{k1}} - \theta_m\right) \tag{6.53}$$

and

$$f_{p_k}^1\left(x_{p_k}, \eta_k\right) = \frac{-\frac{E_1 r_1}{l_{1_0}} h_{p_k} + \left(\Theta + \Omega \xi_T^1\left(x_{p_{k2}}, \eta\right)\right) \left(-\frac{h_1(\eta_k) A_{w_1}}{m_{w_1} c_{p_1}} \left(\eta_k - T_{amb}\right) \right)}{1 - \Omega \xi_\sigma^1\left(x_{p_{k2}}, \eta_k\right)}$$

$$f_{p_k}^2\left(x_{p_k}, \eta_k\right) = \frac{-\frac{E_1 r_1}{l_{1_0}} h_{p_k} + \left(\Theta + \Omega \xi_T^2\left(x_{p_{k2}}, \eta_k\right)\right) \left(-\frac{h_1(\eta_k) A_{w_1}}{m_{w_1} c_{p_1}} \left(\eta_k - T_{amb}\right) \right)}{1 - \Omega \xi_\sigma^2\left(x_{p_{k2}}, \eta_k\right)}$$

$$f_{p_k}^3\left(x_{p_k}, \eta_k\right) = -\frac{E_1 r_1}{l_{1_0}} h_{p_k} + \Theta \left(-\frac{h_1\left(\eta_k\right) A_{w_1}}{m_{w_1} c_{p_1}} \left(\eta_k - T_{amb}\right) \right)$$

$$g_{p_k}^1\left(x_{p_k}, \eta_k\right) = \frac{\left(\Theta + \Omega \xi_T^1\left(x_{p_{k2}}, \eta_k\right)\right)}{1 - \Omega \xi_\sigma^1\left(x_{p_{k2}}, \eta_k\right)} \frac{1}{R_1\left(\xi_k\right) m_{w_1} c_{p_1}}$$

$$g_{p_k}^2\left(x_{p_k}, \eta_k\right) = \frac{\left(\Theta + \Omega \xi_T^2\left(x_{p_{k2}}, \eta_k\right)\right)}{1 - \Omega \xi_\sigma^2\left(x_{p_{k2}}, \eta_k\right)} \frac{1}{R_1\left(\xi_k\right) m_{w_1} c_{p_1}}$$

$$g_{p_k}^3\left(x_{p_k}, \eta_k\right) = \frac{\Theta}{R_1\left(\xi_k\right) m_{w_1} c_{p_1}}$$

where $T_s = 0.02s$ is the sampling time chosen as described in Chapter 5.

6.3.3 Discrete SDC parametrization

Different parametrizations of the form in Eq.(6.7) were tested for the system presented in Eq.(6.47). We propose the following parametrization:

$$A_k\left(x_{p_k}\right) = \begin{bmatrix} 1 + a_{11}T_s & a_{12}T_s \\ a_{21}T_s & 1 + a_{22}T_s \end{bmatrix} \tag{6.54}$$

$$B_k\left(x_{p_k}\right) = \begin{bmatrix} 0 \\ b_{21}T_s \end{bmatrix} \tag{6.55}$$

where

$$a_{11} = -\frac{k_s}{b} - \frac{m_{load} g r_{load}\left(\sin\left(x_{p_{k_1}} - \theta_m\right) - \sin\left(\theta_m\right)\right)}{b\ x_{p_{k_1}}} + \frac{k_s\theta_m}{b\ x_{p_{k_1}}} - \\ - \frac{m_{load} g r_{load}\left(\sin\left(\theta_m\right)\right)}{b\ x_{p_{k_1}}}$$

$$a_{12} = \frac{A_1 r_1}{b}$$

$$a_{21} = \left(\frac{\Theta_1 + \xi_T^1\left(x_{p_{k_2}}, \eta_k\right)}{1 - \Omega\xi_\sigma^1\left(x_{p_{k_2}}, \eta_k\right)} Z_1\left(\xi_{k+1}\right) + \frac{\Theta_1 + \xi_T^2\left(x_{p_{k_2}}, \eta_k\right)}{1 - \Omega\xi_\sigma^2\left(x_{p_{k_2}}, \eta_k\right)} Z_2\left(\xi_{k+1}\right) + \right. \\ \left. + \Theta_1 Z_3\left(\xi_{k+1}\right)\right)\left(-\frac{h_1\left(\eta_k\right) A_{w_1}}{m_{w_1} c_{p_1}}\left(\eta_k - T_{amb}\right)\right)\frac{1}{x_{p_{k_1}}} - \\ - \frac{E_1 r_1}{l_{1_0}} a_{11}\left(\frac{Z_1\left(\xi_{k+1}\right)}{1 - \Omega\xi_\sigma^1\left(x_{p_{k_2}}, \eta_k\right)} + \frac{Z_2\left(\xi_{k+1}\right)}{1 - \Omega\xi_\sigma^2\left(x_{p_{k_2}}, \eta_k\right)} + Z_3\left(\xi_{k+1}\right)\right)$$

$$a_{22} = -\frac{E_1 r_1}{l_{1_0}} a_{12}\left(\frac{Z_1\left(\xi_{k+1}\right)}{1 - \Omega\xi_\sigma^1\left(x_{p_{k_2}}, \eta_k\right)} + \frac{Z_2\left(\xi_{k+1}\right)}{1 - \Omega\xi_\sigma^2\left(x_{p_{k_2}}, \eta_k\right)} + Z_3\left(\xi_{k+1}\right)\right)$$

$$b_{21} = \left(\frac{\Theta_1 + \xi_T^1\left(x_{p_{k_2}}, \eta_k\right)}{1 - \Omega\xi_\sigma^1\left(x_{p_{k_2}}, \eta_k\right)} Z_1\left(\xi_{k+1}\right) + \frac{\Theta_1 + \xi_T^2\left(x_{p_{k_2}}, \eta_k\right)}{1 - \Omega\xi_\sigma^2\left(x_{p_{k_2}}, \eta_k\right)} Z_2\left(\xi_{k+1}\right) + \right. \\ \left. + \Theta_1 Z_3\left(\xi_{k+1}\right)\right)\frac{1}{R_1\left(\xi_k\right) m_{w_1} c_{p_1}}$$

The system in Eq.(6.47) is proven to be reachable for all x_{p_k} in the nonlinear sense (See Appendix B.2), thus the pair $\{A_k\left(x_{p_k}\right), B_k\left(x_{p_k}\right)\}$ is ensured to be pointwise stabilizable in the linear sense for all x_{p_k}. In addition, if $Q\left(x_{p_k}\right) = C\left(x_{p_k}\right) C^\top\left(x_{p_k}\right) \geq 0$, the pair $\{C_k\left(x_{p_k}\right), A_k\left(x_{p_k}\right)\}$ is ensured to be pointwise detectable in the linear sense for all x_{p_k}. As demonstrated in [158], the feedback control in Eq.(6.10) is proven to stabilize the proposed parametrized system.

6.3.4 DSDRE Integral Servomechanism

In order to perform regulation and tracking we implement the DSDRE controller as an integral servomechanism as proposed in [160], employing this approach in its discrete version. Let us decompose the state vector as $x_{p_k} = \begin{bmatrix} X_{r_k}^\top & X_{N_k}^\top \end{bmatrix}$ and define the augmented state vector $x_{IS} = \begin{bmatrix} X_{I_k}^\top & X_{R_k}^\top & X_{N_k}^\top \end{bmatrix}^\top$, where the vector $X_{R_k}^\top$ tracks the reference command vector r_{c_k} and $X_{I_k}^\top$ is the integral of the state $X_{R_k}^\top$. The augmented system is given by:

$$x_{IS_{k+1}} = \tilde{A}\left(x_{IS_k}\right) x_{IS_k} + \tilde{B}\left(x_{IS_k}\right) u_k \tag{6.56}$$

where

$$\tilde{A}_k\left(x_{IS_k}\right) = \left[\begin{array}{c|cc} \mathbf{I} & \mathbf{I}\, T_s & \mathbf{0} \\ \hline \mathbf{0} & A\left(x_{p_k}\right) & \end{array}\right]$$

$$\tilde{B}_k\left(x_{IS_k}\right) = \begin{bmatrix} \mathbf{0} \\ B_k\left(x_{p_k}\right) \end{bmatrix}$$

The DSDRE integral servocontroller is given by

$$u_k = -\left(\tilde{R} + \tilde{B}_k\left(x_{IS_k}\right)^\top P\left(x_{IS_k}\right) \tilde{B}_k\left(x_{IS_k}\right)\right)^{-1} \tilde{B}_k\left(x_{IS_k}\right)^\top \tilde{P}\left(x_{IS_k}\right) \tilde{A}_k\left(x_{IS_k}\right) \begin{bmatrix} X_{I_k} - \sum_{k=0}^{\infty} r_{c_k} \\ X_{R_k} - r_{c_k} \\ x_{N_k} \end{bmatrix} \tag{6.57}$$

where $x_{R_k} = x_{p_{1\,k}}$, $r_{c_k} = \theta_d + \theta_m$ and $x_{N_k} = \sigma_k$.

6.4 Simulation and experimental results

The proposed SDRE and DSDRE controls for the biased SMA robotic arm are tested for the same scenarios used for the output feedback control, presented in section 4.3. The SDRE and DSDRE controls are tested in simulation and experiments. The results of these tests are compared with the results of the adaptive control presented in Chapter 4, which is the output feedback control with the best performance of the three tested controllers. The next subsections present the results of this comparison in simulation and experiments. In the final subsection, a programmed task using the DSDRE control approach, for a grasping and carrying scenario, is presented.

6.4.1 Simulation results

The control signals u and u_k are, for all the tests, constrained to avoid voltages over the limit, which can overheat the wire and destroy its shape memory. In the same way, the lower voltage is limited to 0 V due to the one way heating control inherent to the system. The maximum saturation voltage (V_H) is set to $V_H = 5$ V. This limitation of voltage can be performed as part of the design of the SDRE or DSDRE control itself, so the condition is taken into account for the computation of the control input. However, this case was not considered during the design. The controllers are tuned heuristically with different gains for regulation and tracking as follows:

SDRE Regulation:

$$Q = \begin{bmatrix} 0.07 & 0 & 0 & 0 \\ 0 & 0.04 & 0 & 0 \\ 0 & 0 & 0.006 & 0 \\ 0 & 0 & 0 & 1E-6 \end{bmatrix}$$

$$R = 0.001$$

SDRE Tracking:

$$Q = \begin{bmatrix} 10 & 0 & 0 & 0 \\ 0 & 0.4 & 0 & 0 \\ 0 & 0 & 0.6 & 0 \\ 0 & 0 & 0 & 1E-5 \end{bmatrix}$$

$$R = 0.001$$

DSDRE Regulation:

$$Q = \begin{bmatrix} 5.2 & 0 & 0 \\ 0 & 13 & 0 \\ 0 & 0 & 1E-5 \end{bmatrix}$$

$$R = 0.001$$

DSDRE Tracking:

$$Q = \begin{bmatrix} 1 & 0 & 0 \\ 0 & 3 & 0 \\ 0 & 0 & 1E-5 \end{bmatrix}$$

$$R = 0.001$$

The gains for the adaptive control are the same as those used in Chapter 4. Figures 6.1 to 6.6 show the results of all the tests for the SDRE, DSDRE and adaptive controls in simulation. Table 6.1 summarizes the results for position regulation in simulation. We can see that the three control approaches have a good behavior for position regulation. From the three controllers, the DSDRE presents a better performance in comparison with the SDRE and the adaptive control. The DSDRE presents no overshoot and the fastest settling time for step up references. Although the relative error is almost the same for the three approaches, the DSDRE has a better overall behavior.

Table 6.2 shows the results of position tracking with and without payload, for the SDRE, DSDRE and adaptive controls in simulation. For the tracking of the sinusoidal reference at 0.1 rad/s, the best adaptive control shows a faster response and a lower relative error, which is attributed to the extremely low overshoot achieved by this controller. However, the lowest tracking error, after reaching the reference, is the one presented by

TABLE 6.1: Comparative table of output feedback control *vs.* state feedback control performance for position regulation in simulation.

Control	**OS [rad]**	**ST [s]**	**SSE [rad]**	E_r
Small Step up (0.2 rad)				
SDRE	7.2908	10.8	0.0007	0.4116
DSDRE	0	4.6	0.0047	0.4433
Adaptive	-1.0458	12.6	-0.0035	0.4463
Large Step up (0.6 rad)				
SDRE	5.6550	13	0.0002	0.4116
DSDRE	0	8.2	0.0040	0.4433
Adaptive	20.95	16.8	-0.0089	0.4463
Step down (0.8 rad)				
SDRE	0	12.8	0.0111	0.4116
DSDRE	0	14.2	0.0007	0.4433
Adaptive	0	14.4	0.0051	0.4463

OS: Overshoot percentage; ST: Settling time; SSE: Steady State Error; E_r: Relative Error.

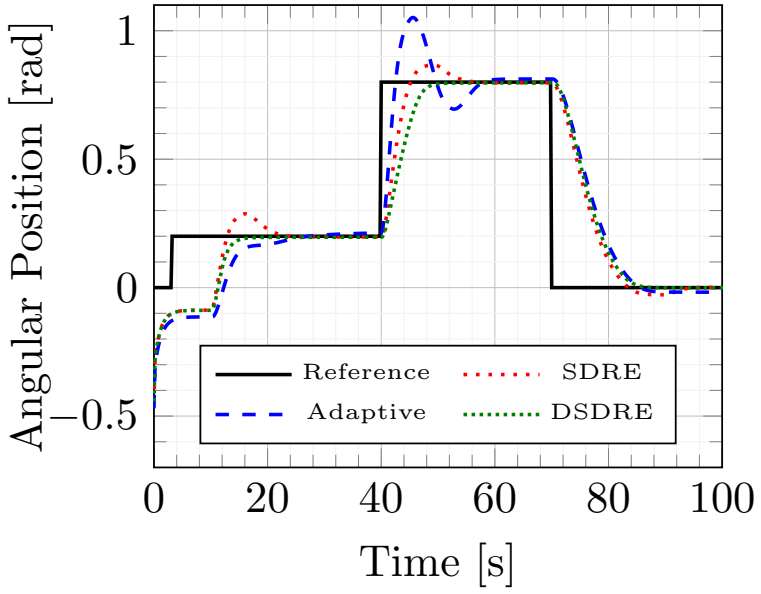

FIGURE 6.1: Adaptive control *vs.* state feedback control for angular position regulation in simulation.

the DSDRE. In addition, at higher frequencies, the DSDRE has the lowest relative error and tracking error. This takes us to conclude that the DSDRE has an overall better performance for tracking task at low and high frequencies.

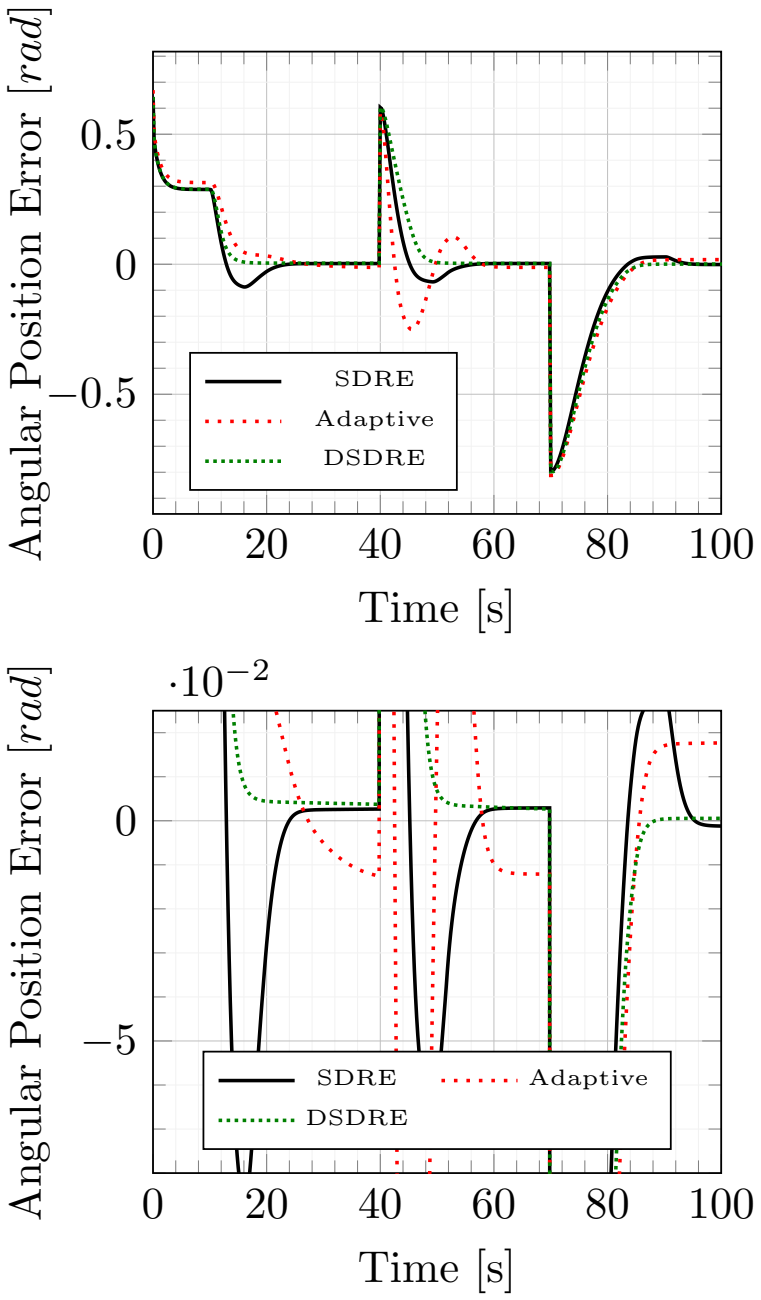

FIGURE 6.2: Adaptive control *vs.* state feedback control errors in simulation.

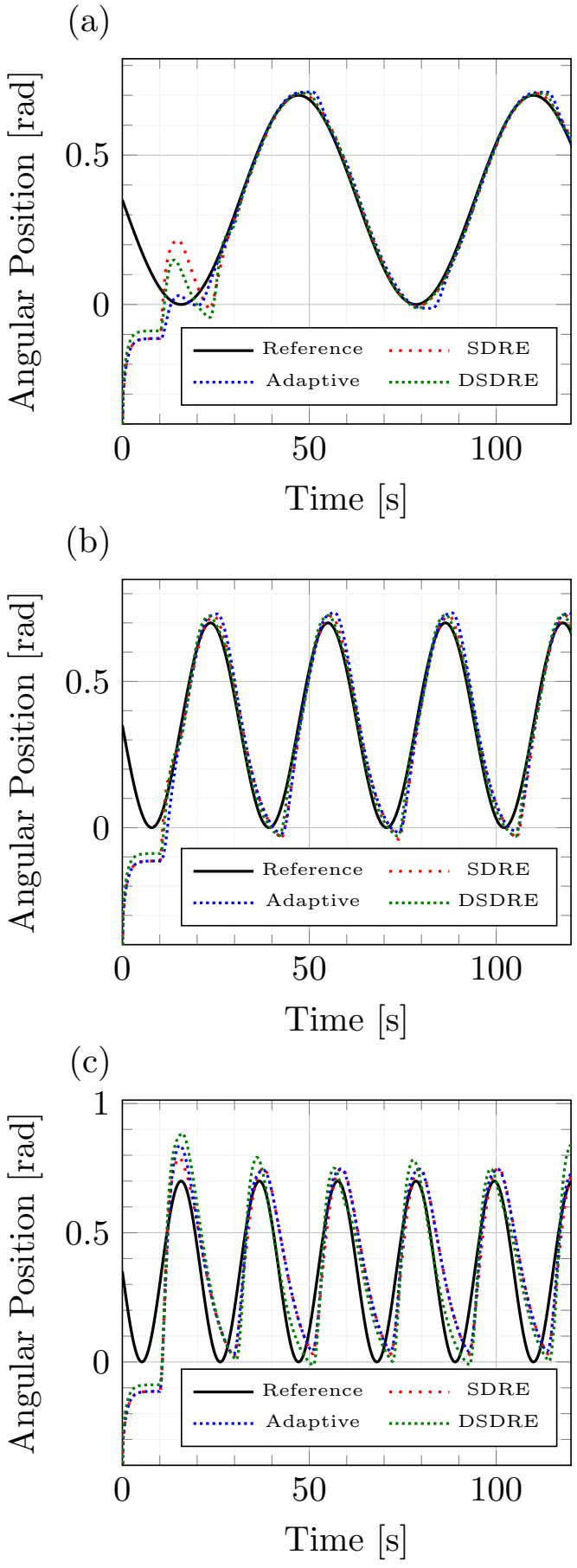

FIGURE 6.3: Adaptive control *vs.* state feedback control for angular position tracking in simulation, a) 0.1 rad/s sine, b) 0.2 rad/s sine, c) 0.3 rad/s sine.

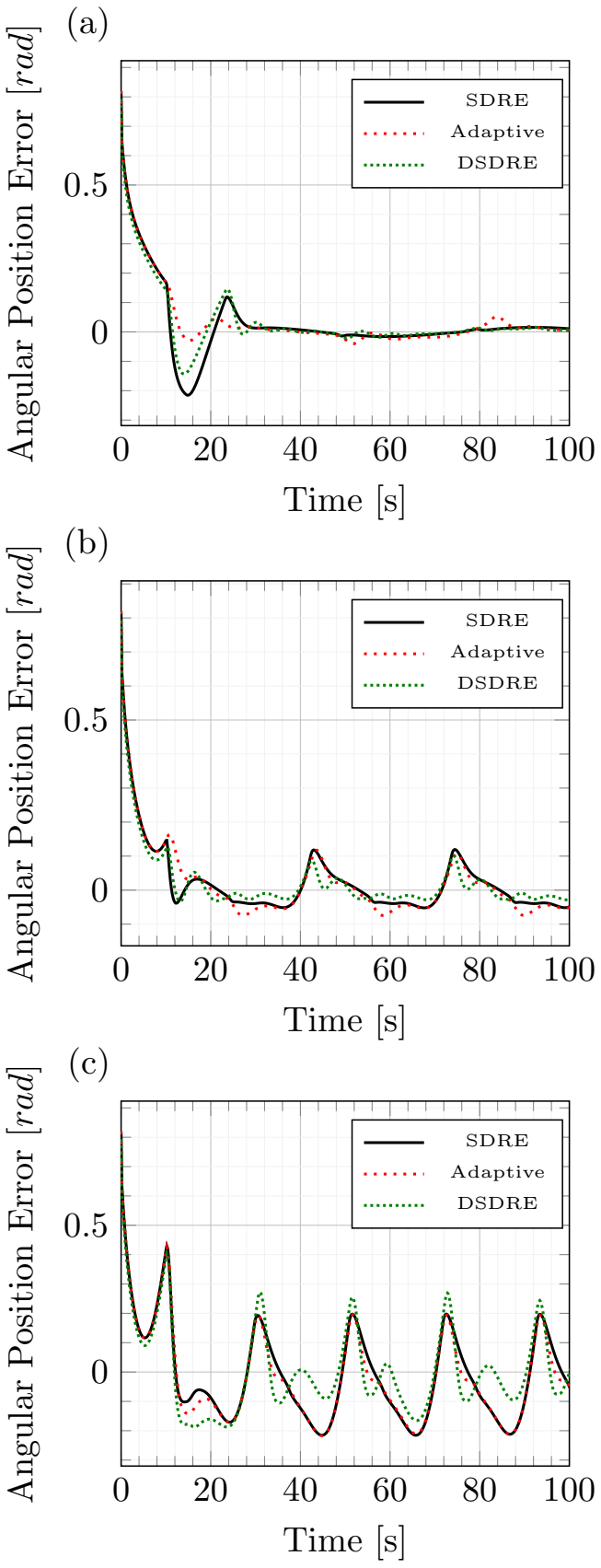

FIGURE 6.4: Adaptive control *vs.* state feedback control errors for angular position tracking in simulation, a) 0.1 rad/s sine, b) 0.2 rad/s sine, c) 0.3 rad/s sine.

TABLE 6.2: Comparative table of output feedback control *vs.* state feedback control performance for position tracking in simulation

Control	**FT [s]**	**TE [rad]**	E_r
Sine 0.1 rad/s			
SDRE	18.2	0.0105	0.1129
DSDRE	16.0	0.0080	0.0843
Adaptive	14.2	0.0155	0.0636
Sine 0.2 rad/s			
SDRE	9.6	0.0397	0.1096
DSDRE	8.2	0.0247	0.0760
Adaptive	9	0.0425	0.1207
Sine 0.3 rad/s			
SDRE	2.2	0.1187	0.3166
DSDRE	1.8	0.0982	0.2821
Adaptive	2.4	0.1146	0.3104
Sine 0.1 rad/s, 31g payload			
SDRE	18.4	0.0119	0.1006
DSDRE	16.8	0.0079	0.0938
Adaptive	14.6	0.0167	0.0636

FT: Reference Follow Time; TE: Tracking Error; E_r: Relative Error.

6.4.2 Experimental results

For the experimental tests, a virtual sensor is implemented to measure the system states and to have a full state feedback for both, the SDRE and DSDRE controls. The SDRE control, is a continuous control approach. However, it is not possible to apply a continuous control or to have continuous state feedback in a real environment. For this tests, it is considered that the control action and measurement are continuous. Although, this assumption is not completely mathematically correct, it is possible to do it thanks to the fast sampling time of the system. The conditions tested experimentally are the same described for the simulation tests. The control input u and u_k are saturated between 0 and 5 V to avoid overheating of the wire. The controllers are tuned heuristically with different gains for regulation and tracking. The gains have slight changes as compared to those used in simulation, as follows:

SDRE Regulation:

$$Q = \begin{bmatrix} 0.07 & 0 & 0 & 0 \\ 0 & 0.04 & 0 & 0 \\ 0 & 0 & 0.006 & 0 \\ 0 & 0 & 0 & 1E-6 \end{bmatrix}$$

$R = 0.001$

SDRE Tracking:

$$Q = \begin{bmatrix} 4 & 0 & 0 & 0 \\ 0 & 0.6 & 0 & 0 \\ 0 & 0 & 0.6 & 0 \\ 0 & 0 & 0 & 1E-5 \end{bmatrix}$$

$R = 0.001$

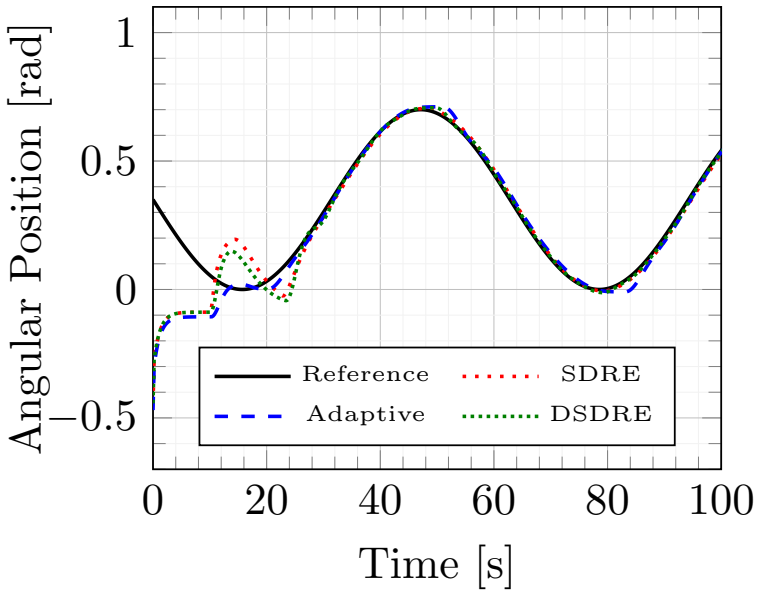

FIGURE 6.5: Adaptive control *vs.* state feedback control for angular position tracking with 31 g payload in simulation.

DSDRE Regulation:

$$Q = \begin{bmatrix} 5.1 & 0 & 0 \\ 0 & 13 & 0 \\ 0 & 0 & 1E-5 \end{bmatrix}$$

$$R = 0.001$$

DSDRE Tracking:

$$Q = \begin{bmatrix} 3 & 0 & 0 \\ 0 & 2 & 0 \\ 0 & 0 & 1E-5 \end{bmatrix}$$

$$R = 0.001$$

The gains for the adaptive control are the same as those used in Chapter 4. Figures 6.7 to 6.12 show the results of all the tests for the SDRE, DSDRE and adaptive controls experimentally. Table 6.3 summarizes the results for position regulation in experiments. The experimental results are similar to those obtained in simulation. The DSDRE control presents the fastest response and the lowest relative error of all three controllers. However, this control shows a high overshoot in comparison to the SDRE and adaptive approaches. In the overall the DSDRE control has the best performance followed by the SDRE control, which has the second fastest response and the lowest steady state error.

Table 6.4 shows the results of position tracking with and without payload, for the SDRE, DSDRE and adaptive controls in experiments. For position tracking all three controllers show a good performance for tracking of a sinusoidal reference at 0.1 rad/s, with and without payload. The DSDRE control, once again, shows the fastest response and the lowest tracking error. When the frequency increases, the relative error of the SDRE and adaptive control increases. The DSDRE is capable of following the sinusoidal reference at 0.2 rad/s with a low tracking error. When the frequency increases to 0.3 rad/s none

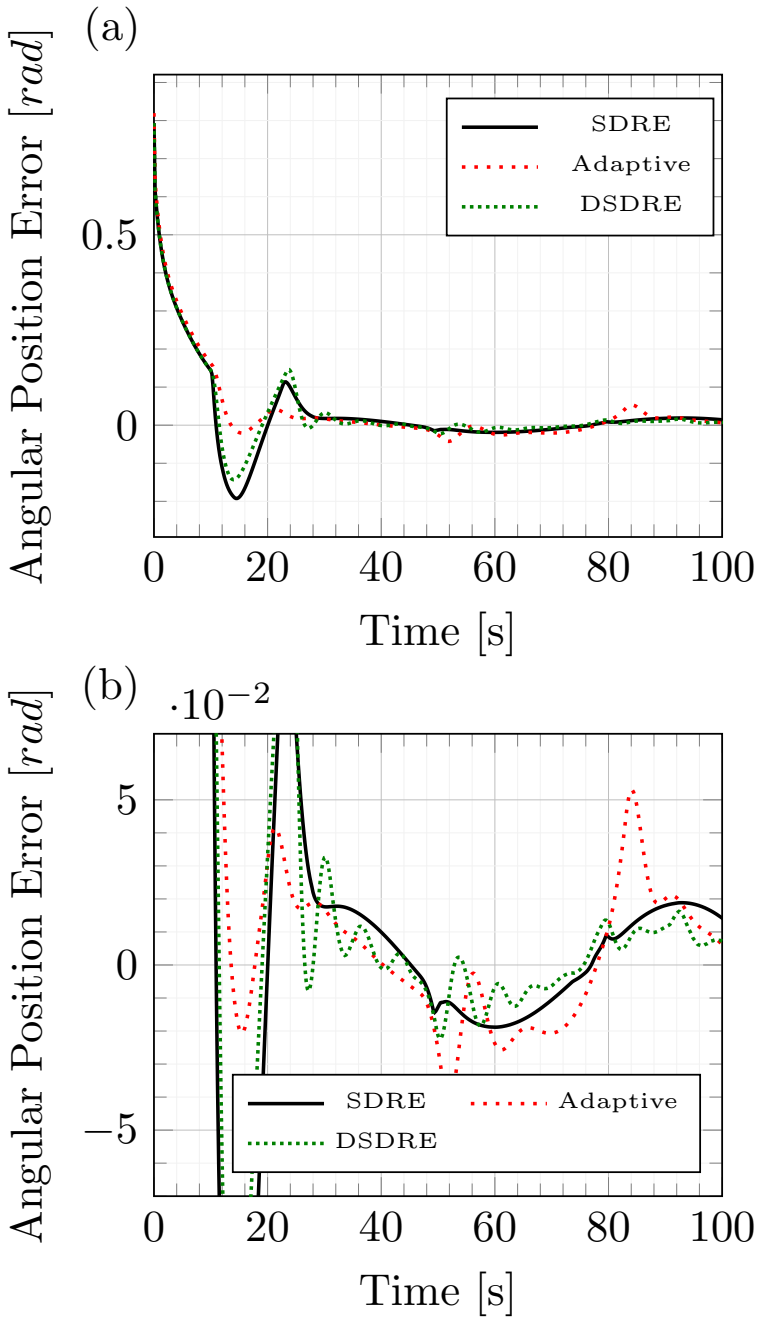

FIGURE 6.6: Adaptive control *vs.* state feedback control errors for angular position tracking with 31 g payload in simulation.

TABLE 6.3: Comparative table of output feedback control *vs.* state feedback control performance for position regulation in experiments.

Control	**OS [%]**	**ST [s]**	**SSE [rad]**	E_r
Small Step up (0.2 rad)				
SDRE	7.2908	10.8	0.0007	0.4116
DSDRE	15.2808	8.2	0.0013	0.3497
Adaptive	5.3691	19.6	-0.0043	0.3666
Large Step up (0.6 rad)				
SDRE	5.6550	13	0.0002	0.4116
DSDRE	12.0900	9.4	0.0006	0.3497
Adaptive	5.5875	20.8	-0.0112	0.3666
Step down (0.8 rad)				
SDRE	0	12.8	0.0026	0.4116
DSDRE	0	14.2	0.0004	0.3497
Adaptive	0	13.2	-0.0058	0.3666

OS: Overshoot percentage; ST: Settling time; SSE: Steady State Error; E_r: Relative Error.

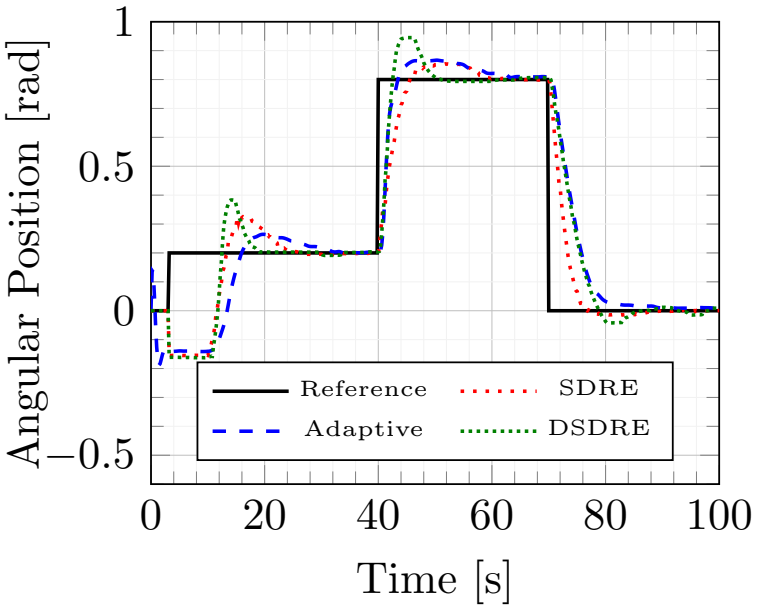

FIGURE 6.7: Adaptive control *vs.* state feedback control for angular position regulation in experiments.

of the controllers is able to follow the reference accurately. In the case of position tracking DSDRE shows a faster response and a lower relative error as expected based on simulation results. In conclusion, the DSDRE control proved to be the best approach for regulation and tracking of angular position of the system dealt in this project.

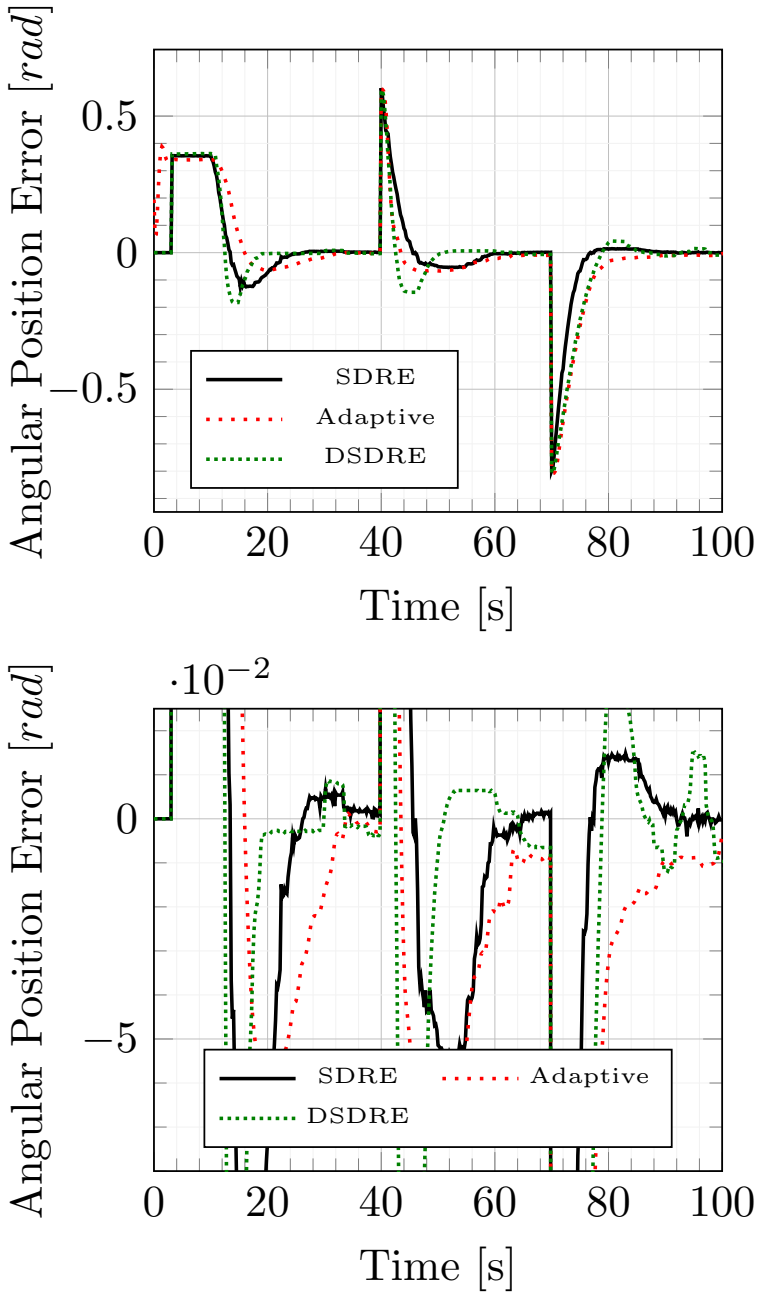

FIGURE 6.8: Adaptive control *vs.* state feedback control errors in experiments.

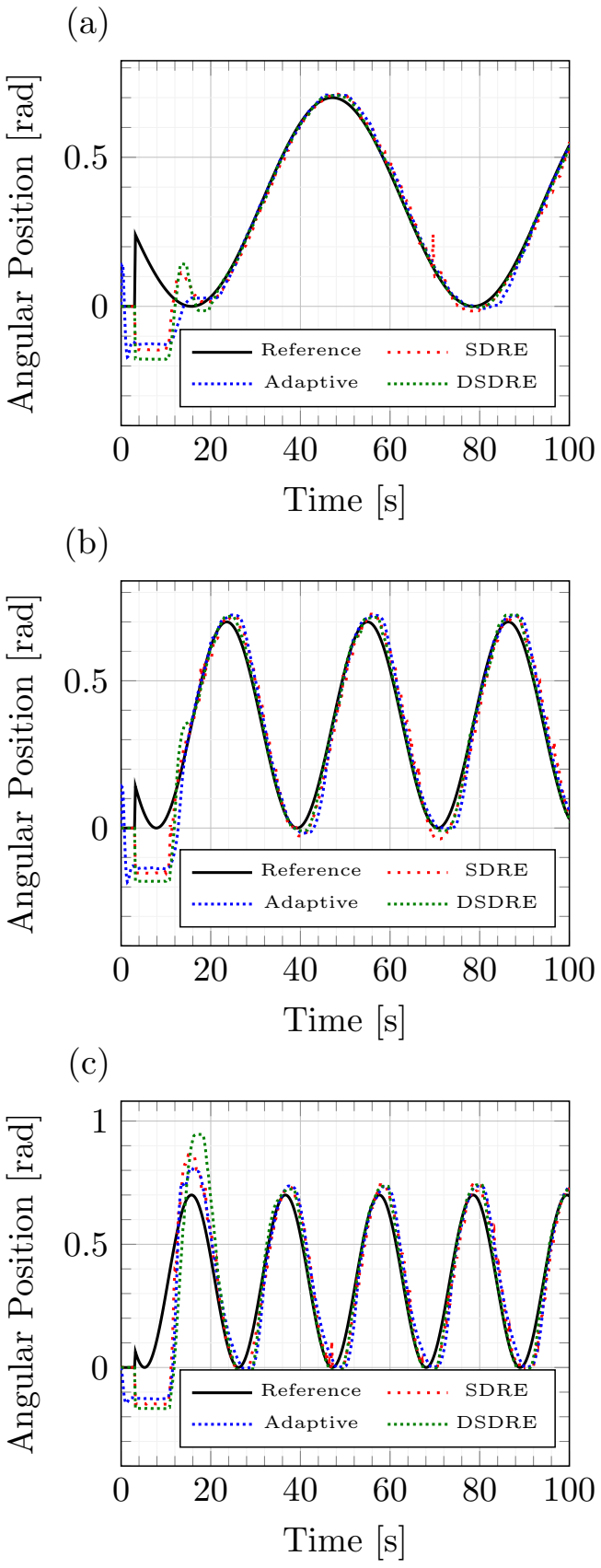

FIGURE 6.9: Adaptive control *vs.* state feedback control for angular position tracking in experiments, a) 0.1 rad/s sine, b) 0.2 rad/s sine, c) 0.3 rad/s sine.

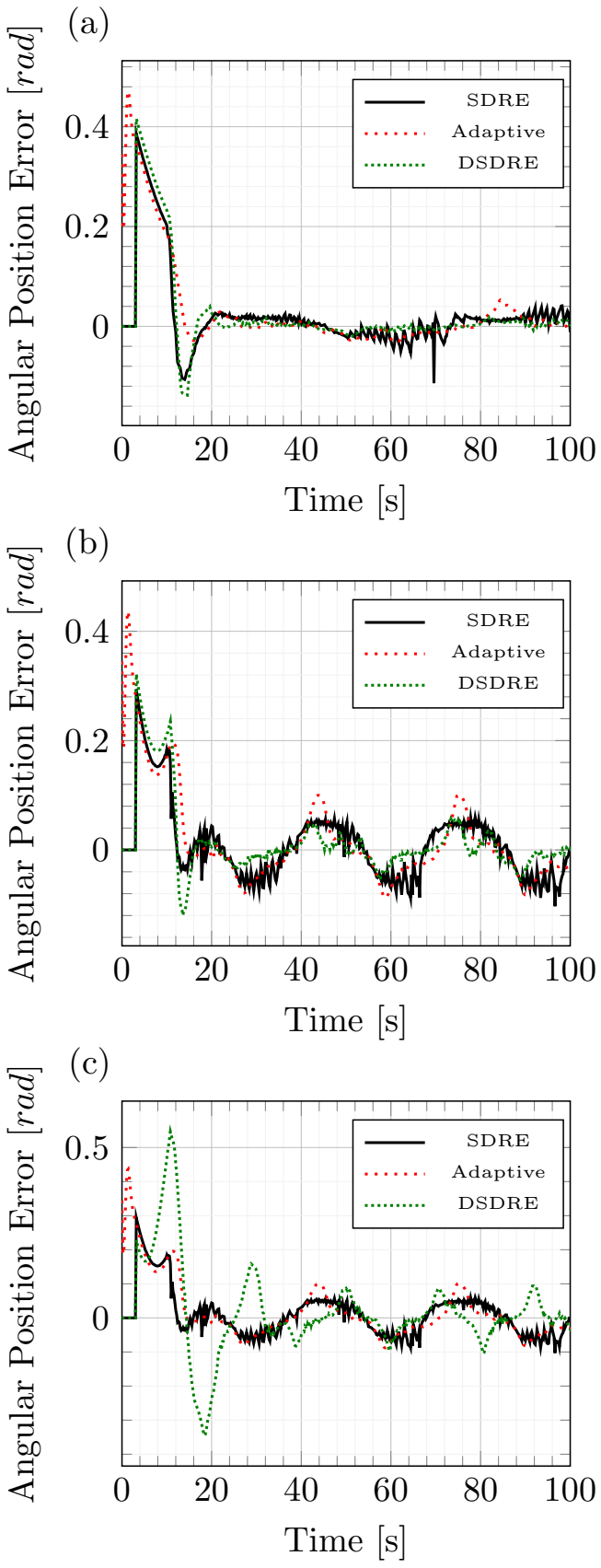

FIGURE 6.10: Adaptive control *vs.* state feedback control errors in experiments, a) 0.1 rad/s sine, b) 0.2 rad/s sine, c) 0.3 rad/s sine.

TABLE 6.4: Comparative table of output feedback control *vs.* state feedback control performance for position tracking in experiments

Control	**FT [s]**	**TE [rad]**	E_r
Sine 0.1 rad/s			
SDRE	13.6	0.0162	0.0842
DSDRE	10.6	0.0063	0.0721
Adaptive	13.6	0.0141	0.0679
Sine 0.2 rad/s			
SDRE	3.4	0.0379	0.1051
DSDRE	5.8	0.0160	0.0789
Adaptive	4	0.0332	0.1155
Sine 0.3 rad/s			
SDRE	2.4	0.0793	0.2180
DSDRE	3.8	0.0668	0.2315
Adaptive	2.8	0.0669	0.2210
Sine 0.1 rad/s, 31g payload			
SDRE	7.8	0.1457	0.0915
DSDRE	6.6	0.0084	0.0719
Adaptive	7.4	0.0178	0.0712

FT: Reference Follow Time; TE: Tracking Error; E_r: Relative Error.

6.4.3 Programmed arm task: Grasping and carrying

The biased SMA wire based robotic arm is tested on a final scenario where grasping and transportation tasks are performed. This final scenario is composed of different individual tasks, which emulate the grasping and transportation scenario likely to occur when the robotic arm is implemented as an aerial manipulator. The scenario is as follows:

1. Reach desired angular position (θ_{d_1}) according to the location of the object to be grasped and UAV position (P_{d_1}). Position regulation task.

2. Once in place, open gripper. Assuming the UAV will take the arm to the needed position to perform grasping (P_{d_2}), close the gripper after reaching grasping position.

3. Lift grasped object to avoid collision with surrounding surfaces (θ_{d_2}). Position regulation task.

4. Assuming UAV will take the arm to a free collision zone (P_{d_3}), reach transportation position (θ_{d_3}). This position is designed to minimize the disturbance to the UAV

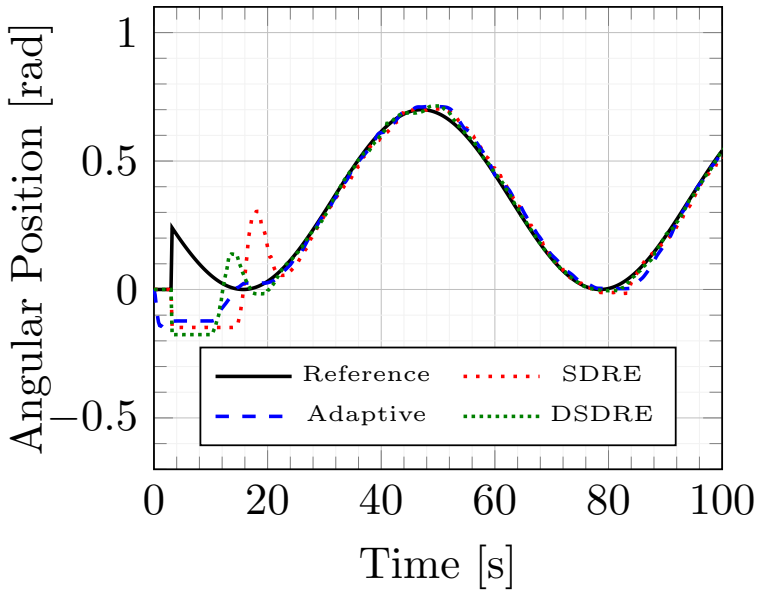

FIGURE 6.11: Adaptive control *vs.* state feedback control for angular position tracking with 31 g payload in experiments.

center of mass, considering the mass of the arm and additional payload. Position regulation task.

5. After reaching final position, release payload (open gripper).

6. Close gripper and go to resting position ($V_1 = 0$).

The position regulation tasks are carried out using the DSDRE control discussed in the current Chapter. For the gripper, a simple ON/OFF control is implemented. Figure 6.14 shows a sequence of the experimental performance of the grasping and carrying task.

6.5 Conclusions

In the first section of this chapter, a literature overview of the State-Dependent Riccati Equation strategy for control applied to SMA based system is presented. Following, a continuous differentiable continuous-time controllable model is derived for the biased lightweight robotic arm presented in previous chapters. The system is rendered differentiable at all instants using an approximation by arctan based functions. The controllability of the system in the nonlinear sense is demonstrated and the system parametrized to implement a SDRE control for angular position.

Subsequently a discrete-time controllable model is derived in order to apply a discrete-time SDRE control. The discrete model is derived using a singular perturbation model.

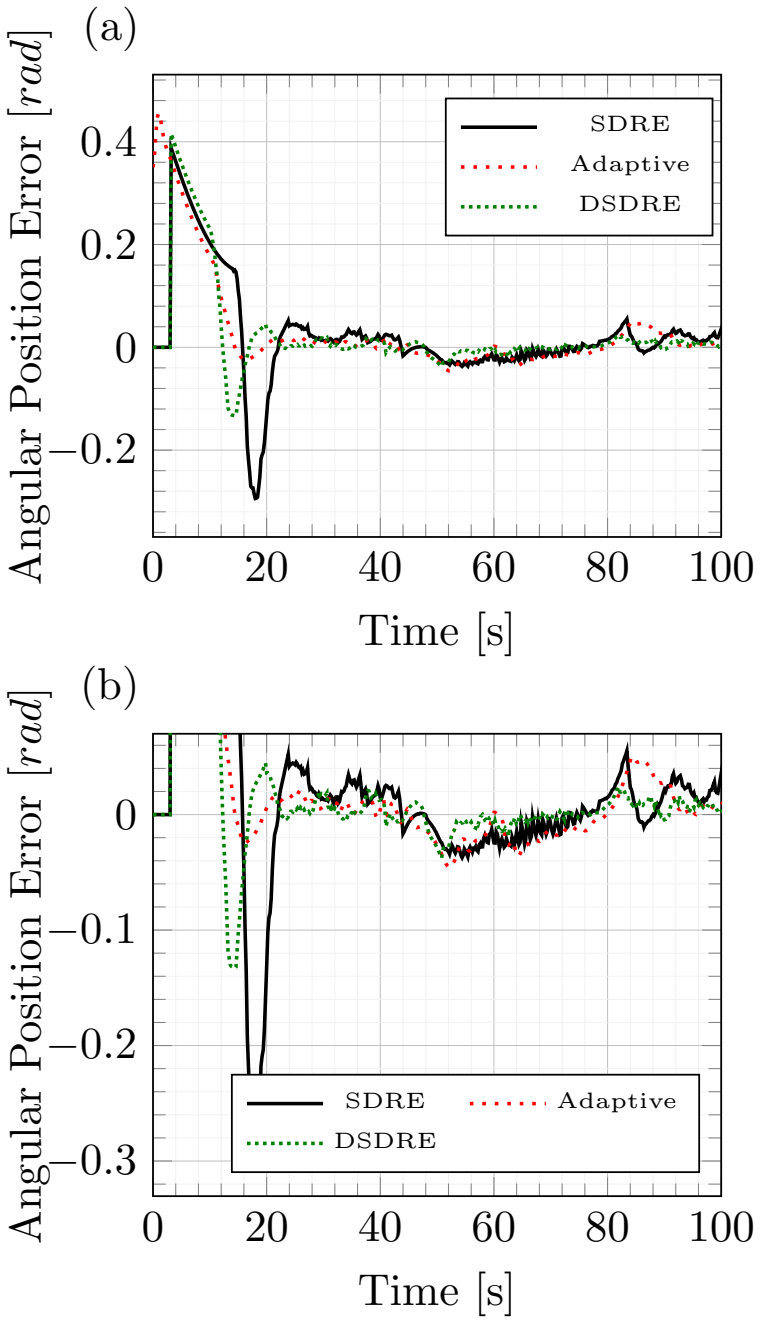

FIGURE 6.12: Adaptive control *vs.* state feedback control errors with 31 g payload in experiments.

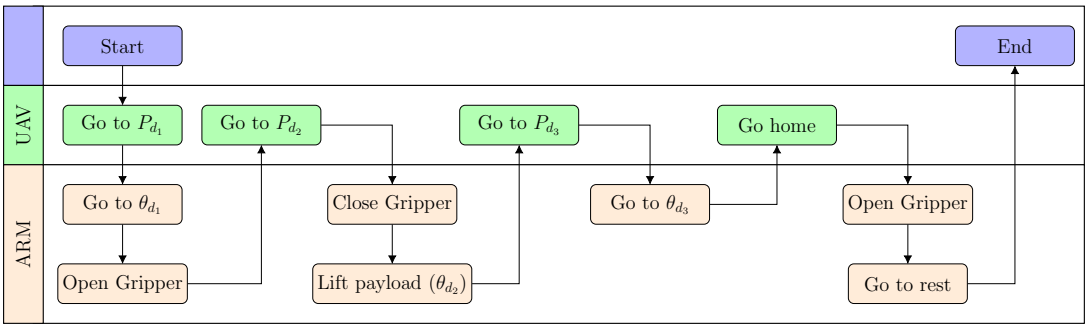

FIGURE 6.13: Grasping and carrying task block diagram.
P_{d_1} - UAV desired position for arm positioning; θ_{d_1} - Arm desired position for grasping; P_{d_2} - UAV desired position for grasping; θ_{d_2} - Arm position for avoiding collision; P_{d_3} - UAV desired position for arm transportation positioning; θ_{d_3} - Arm transportation position.

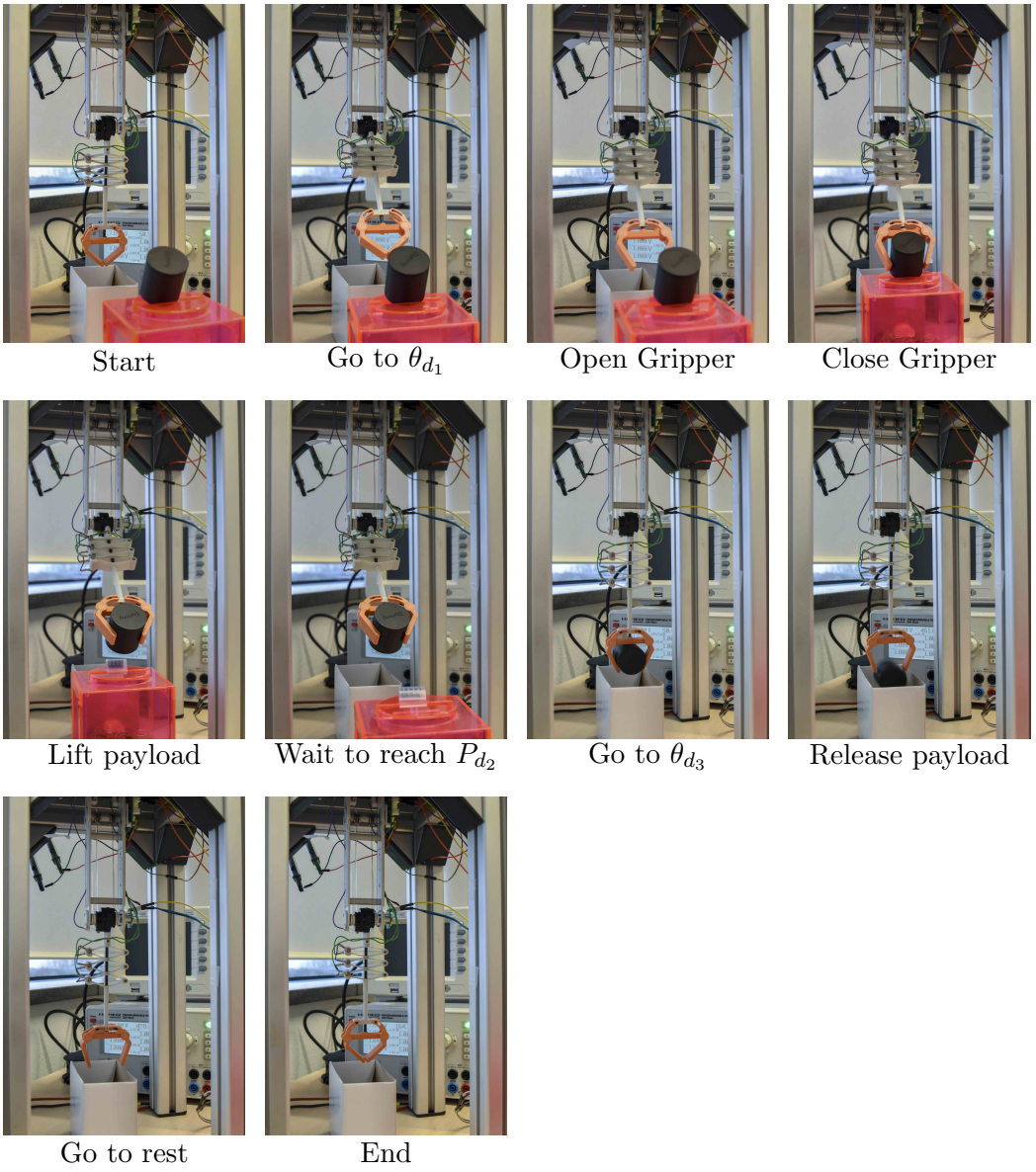

FIGURE 6.14: Grasping and carrying experimental sequence.

A servo-integral mechanism is implemented in both continuous and discrete-time approaches to eliminate the steady state error.

Finally, both control approaches are tested for regulation and tracking of the angular position of the lightweight robotic arm. The obtained results are compared with the results of the Adaptive Control previously presented. The DSDRE control results show a faster and more accurate response for position regulation and tracking. Different types of state feedback control approach could be tested as future work to achieve even faster and more accurate responses.

Chapter 7

Conclusions and future Outlook

This chapter presents an overview of the findings and contributions presented in this research work, followed by the future outlook of the project in section 7.2.

7.1 Conclusions

This research presented the experimental implementation of a state feedback control approach for angular position of a lightweight robotic arm (LWRA) actuated by Shape Memory Alloy (SMA) wires.

Firstly, in Chapter 3, the mechanical design of a LWRA actuated by SMA wires was introduced as an alternative lighter manipulator design. Although initially oriented to be implemented as an aerial manipulator, this lightweight design can be applied to a wide range of fields, where the size and weight available for the manipulator are limited. In this same chapter, the mathematical model of the proposed LWRA was developed based on a constitutive model of the SMA wire. Following, the model was validated in simulation and experimentally under different conditions of operation, such as, step and sinusoidal voltage inputs and different payloads.

In Chapter 5, an observable model of the LWRA is developed applying the singular perturbation theory. The proposed model is a non-switched nonlinear model with four states and one unknown input. An observability analysis for nonlinear systems with unknown inputs is carried out, and the proposed model proven to be observable. Subsequently, the developed model is discretized by a first Euler approximation and an Extended Kalman Filter with Unknown Input (EKF-UI) was introduced. The proposed EKF-UI uses the EKF technique to estimate the states of the system while a sliding mode approach was implemented to estimate the unknown input from the outputs of

the system. To conclude this chapter, the EKF-UI was validated in simulation and experimentally under different scenarios.

In Chapter 6 a controllable continuously differentiable model was developed using arctangent based functions to join and smooth the three separate function integrating the switching dynamics of the SMA wire hysteresis, using the martensite fraction derivative sign as the reference inflection point. A nonlinear controllability tests was performed and the model proven to be controllable. Following, the controllable model was parametrized and a State-Dependent Riccati Equation (SDRE) control technique was implemented using the parametrized model. The same system was then discretized with a first order Euler approximation and parametrized to develop a Discrete-time State-Dependent Riccati Equation (DSDRE) control. A servo-integral mechanism was implemented to allow for position tracking and regulation in both controls, eliminating the steady state error.

Three different approaches for output feedback control were tested and compared in their performance in Chapter 4. The controller with the best performance out of the three tested controllers, was then used to carry out a comparative analysis of the implemented state feedback control, presented in Chapter 6. This analysis was qualitative and quantitative, comparing the performance of the tested controllers in terms of accuracy and response time. All the implemented controllers were tested experimentally and in simulation under a variety of scenarios, including position regulation and tracking, and conditions with and without added payload. The DSDRE control approach proved to be the best control approach to deal with the nonlinearities of the SMA wires. This control approach presented the fastest time response and the lowest regulation and tracking errors, respectively, in most of the performed tests. Finally, a grasping an carrying scenario was tested experimentally using the DSDRE control. This scenario shows a series of tasks performed by the arm, assuming independent control for arm and UAV.

The experimental implementation of state feedback control approaches has been limited for the lack of access to SMA wire states. These set of control techniques allow to obtain better results in terms of accuracy and response time in control, according to the results obtained in this research. The implementation of the proposed EKF-UI opens the possibility for the experimental implementation of this type of approaches, thus the development of faster and more accurate control approaches for SMA based systems.

7.2 Future Outlook

Future work can be divided into two different aspects of the research: practical and theoretical. From the practical point of view, two main points can be studied. Firstly,

it is possible to extend the proposed prototype to a two wires configuration as explained in Chapter 3. This will allow a faster response of the system, at the expense of a greater energy cost and more complex control requirements. These aspects will need to be analyzed further, to determine the overall advantages of the two wires configuration.

Secondly, the proposed prototype can be tested in flying condition, by attaching it to a small UAV. For this aspect, multiple factors have to be solved and addressed. The implementation on flying conditions will require a control capable of thermal disturbance rejection. For this, further work of this research will focus on thermal disturbance rejection test of the proposed controller,and possible other types of state feedback control, such as Model Predictive Control (MPC).

From the theoretical point of view, the proposed observer can be extended to consider multiple unknown inputs. A second unknown input, for the system presented in this research, will allow the estimation of the states even when none of the variables of the second coupler are being measured. This technique can be extended to multiple wires interacting, so the need of multiple sensors can be reduced, and the states of the full system estimated.

Finally, recent research on auto-sensing of SMA wires based on electric resistance measurement have been explored. This research could be applied to the proposed prototype as an alternative to estimate the states of a second wire on a two wire configuration, or possibly a multiple configuration for different implementations.

Appendix A

Control Board Code

The microcontroller ESP-12E on the control board was programmed using arduino interface. This is the code used to communicate the board with matlab via serial interface and ADC ADS1115 via I2C.

```
#include <SPI.h>
#include <cstdint>
#include <array>
#include <Wire.h>
#include <Adafruit_ADS1015.h>

 Adafruit_ADS1115 ads;  /* Use this for the 16-bit version */

void begin(
  int sda,
  int scl
  );

// named pins
const int ledPin = 2;


// mosfet pins
std::array<int, 3> mosfetPins = { 16, 5, 15 }; // OUT1 [GRIPPER
   ], OUT2 [ARM], OUT3 [ARM]


void setup(void)
```

```
23 {
24   analogWriteFreq(1000);  // PWM frequency (100Hz-1kHz)
25   for (auto pin : mosfetPins) {   // set mosfet pins as output
26     pinMode(pin, OUTPUT);
27     digitalWrite(pin, LOW);
28   }
29
30   // set ADC chip-select pin as output
31   digitalWrite(adcCS, HIGH);
32
33   // Position reset
34   analogWrite(mosfetPins[2], 300);
35   delay(10000);
36   analogWrite(mosfetPins[2], 0);
37   delay(10000);
38   analogWrite(mosfetPins[1], 300);
39   delay(10000);
40   analogWrite(mosfetPins[1], 0);
41   delay(10000);
42
43   Serial.begin(115200);
44  -------  -------
45    ads.setGain(GAIN_ONE);// 1x gain   +/- 4.096V  1 bit = 2mV
          0.125mV
46   Wire.begin(2,0);
47   ads.begin();
48 }
49
50 struct Output {
51   float rawdat = 0.0f;
52 };
53
54 struct Input {
55   int32_t dutyCycle0 = 0;
56   int32_t dutyCycle1 = 0;
57   int32_t dutyCycle2 = 0;
58 };
59
60   Output out;
```

```
61
62 void loop(void)
63 {
64
65 // Send data to Matlab
66
67   out.rawdat = ads.readADC_Differential_0_1();
68
69   Serial.printf("BEG");
70   //Serial.print(rawdat);
71   Serial.write(reinterpret_cast<byte*>(&out), sizeof(Output));
      // send data
72   Serial.printf("\n");
73
74 // Receive data from Matlab
75 // Received header?
76   if (Serial.find("BEG")) {
77     // then the following bytes can be interpreted as Input
78     Input in;
79     Serial.readBytes(reinterpret_cast<byte*>(&in), sizeof(in));
80
81     in.dutyCycle0 = constrain(in.dutyCycle0, 0, PWMRANGE);
82     in.dutyCycle1 = constrain(in.dutyCycle1, 0, PWMRANGE);
83     in.dutyCycle2 = constrain(in.dutyCycle2, 0, PWMRANGE);
84     analogWrite(mosfetPins[0], in.dutyCycle0);
85     analogWrite(mosfetPins[1], in.dutyCycle1);
86     analogWrite(mosfetPins[2], in.dutyCycle2);
87     }
88
89   delay(0);
90 }
```

Listing A.1: Arduino Code for serial and I2C communication.

Appendix B

Wolfram Mathematica Code for Nonlinear Observability and Controllability calculations

B.1 Nonlinear Observability

The nonlinear observability co-distribution of the nonlinear continuous-time system with unknown input presented in in Eq.(5.14) and Eq.(5.21) was computed using Wolfram Mathematica, and is provided in the following pages.

```
(*NonlinearObservabilityproofforsystemwithunknowninputs.Continuousmodel*)
x = {θ, T, σ, ξ};
u = {{V^2}, {Tamb}};
w = {dξ};
b = bs + b1;
h[x_]:=h0 + h2x[[2]]^2;
R[x_]:=Rmx[[4]] + (1 − x[[4]])Ra;
x2[x_]:=(Arx[[3]] − mlgrlSin[x[[1]]] − ks(x[[1]] − Tin))/b;

f1[x_]:={{0}, {(Kt^2)/(R[x]mwcp)}, {Θ(Kt^2)/(R[x]mwcp)}, {0}}
f2[x_]:={{0}, {h[x]Aw/(mwcp)}, {Θh[x]Aw/(mwcp)}, {0}}
g1[w_]:={{0}, {0}, {Ω}, {1}}
```

```
g0[x_]:={{x2[x]}, {-h[x]Awx[[2]]/(mwcp)}, {(-E1r/l0)x2[x] + Θ(-h[x]Awx[[2]]/(mwcp))}, {0}}
h1[x_]:=x[[1]] - ((-l0/(E1r))((x[[3]] - x30) - Θ(x[[2]] - x20) - Ω(x[[4]] - x50)) + x10)
h2[x_]:=x[[1]]
h3[x_]:=x2[x]

Print["Step 1: Compute μ11. Test outputs for unknown input observability"]
Print["For h1"]
μ11 = D[h1[x], {x}].g1[w]; μ11 = μ11[[1]]
Print["For h2"]
μ11 = D[h2[x], {x}].g1[w];
Print["For h3"]
μ11 = D[h3[x], {x}].g1[w]; μ11 = μ11[[1]]

Print["**********************************************************************"]
Print["Step 2: Compute tensors μ, ν and"g^α]
μ00 = 1;
μ10 = 0;
μ01 = D[h3[x], {x}].g0[x]; μ01 = μ01[[1]];
Print["Tensor μ"]
μ = {{μ00, μ01}, {μ10, μ11}}

v11 = 1/μ11;
v00 = 1;
v10 = 0;
v01 = -v11μ01; v01 = v01[[1]];
Print["Tensor υ"]
υ = {{v00, v01}, {v10, v11}}

Print["Field "hg^α]
Print["hg^0"]
hg0 = v00g0[x] + avg1[w];
```

```
%/.av → v01
Print["hg^1"]
hg1 = v10g0[x] + v11g1[w]

Print["**********************************************************************"]
Print["Step 3: Compute the codistribution Ω0 and Ω1"]
Print["Ω0"]
Ω0 = {D[h2[x], {x}], D[h3[x], {x}]}

Print["LfiΩ0"]
Lf1Ω01 = D[Ω0[[1]].f1[x], {x}]; Lf1Ω01 = Lf1Ω01[[1]];
Lf1Ω02 = D[Ω0[[2]].f1[x], {x}]; Lf1Ω02 = Lf1Ω02[[1]];
Lf2Ω01 = D[Ω0[[1]].f2[x], {x}]; Lf2Ω01 = Lf2Ω01[[1]];
Lf2Ω02 = D[Ω0[[2]].f2[x], {x}]; Lf2Ω02 = Lf2Ω02[[1]];
LfiΩ0 = {Lf1Ω02, Lf2Ω02}

Print["LgαΩ0"]
Lg0Ω01 = D[Ω0[[1]].g0[x], {x}]; Lg0Ω01 = Lg0Ω01[[1]];
Lg1Ω01 = D[Ω0[[1]].g1[w], {x}]; Lg1Ω01 = Lg1Ω01[[1]];
Lg0Ω02 = D[Ω0[[2]].g0[x], {x}]; Lg0Ω02 = Lg0Ω02[[1]];
Lg1Ω02 = D[Ω0[[2]].g1[w], {x}]; Lg1Ω02 = Lg1Ω02[[1]];
LgαΩ0 = {Lg0Ω01, Lg0Ω02}

(*Print["iϕ0"]*)
ϕ10 = f1[x];
ϕ20 = f2[x];

Print["Liϕ0hl"]
L1ϕ0h1 = D[Ω0[[1]].ϕ10, {x}]; L1ϕ0h1 = L1ϕ0h1[[1]];
L1ϕ0h2 = D[Ω0[[2]].ϕ10, {x}]; L1ϕ0h2 = L1ϕ0h2[[1]];
L2ϕ0h1 = D[Ω0[[1]].ϕ20, {x}]; L2ϕ0h1 = L2ϕ0h1[[1]];
```

```
L2ϕ0h2 = D[Ω0[[2]].ϕ20, {x}]; L2ϕ0h2 = L2ϕ0h2[[1]];
Liϕ0hl = {L1ϕ0h2, L2ϕ0h2}

Print["Ω1"]
Ω1 = {Ω0[[1]], Ω0[[2]], Lf1Ω02, Lf2Ω02}

Print["Ω0 at x(0) and Rank"]
Ω00 = Ω0/.{θ → 0, T → 28, σ → 0, ξ → 1}
MatrixRank[Ω00]

Print["Ω1 at x(0) and Rank"]
Ω10 = Ω1/.{θ → 0, T → 28, σ → 0, ξ → 1}
MatrixRank[Ω10]

Print["**********************************************************************"]
Print["Step 4: Check Lemma 14"]

(* To compute Ω2*)
Print["LfiΩ1"]
Lf1Ω11 = D[Ω1[[1]].f1[x], {x}]; Lf1Ω11 = Lf1Ω11[[1]];
Lf1Ω12 = D[Ω1[[2]].f1[x], {x}]; Lf1Ω12 = Lf1Ω12[[1]];
Lf1Ω13 = D[Ω1[[3]].f1[x], {x}]; Lf1Ω13 = Lf1Ω13[[1]];
Lf2Ω11 = D[Ω1[[1]].f2[x], {x}]; Lf2Ω11 = Lf2Ω11[[1]];
Lf2Ω12 = D[Ω1[[2]].f2[x], {x}]; Lf2Ω12 = Lf2Ω12[[1]];
Lf2Ω13 = D[Ω1[[3]].f2[x], {x}]; Lf2Ω13 = Lf2Ω13[[1]];
LfiΩ1 = {Lf1Ω12, Lf2Ω12}

Print["LgαΩ1"]
Lg0Ω11 = D[Ω1[[1]].g0[x], {x}]; Lg0Ω11 = Lg0Ω11[[1]];
Lg1Ω11 = D[Ω1[[1]].g1[w], {x}]; Lg1Ω11 = Lg1Ω11[[1]];
Lg0Ω12 = D[Ω1[[2]].g0[x], {x}]; Lg0Ω12 = Lg0Ω12[[1]];
```

```
Lg1Ω12 = D[Ω1[[2]].g1[w], {x}]; Lg1Ω12 = Lg1Ω12[[1]];
Lg0Ω13 = D[Ω1[[3]].g0[x], {x}]; Lg0Ω13 = Lg0Ω13[[1]];
Lg1Ω13 = D[Ω1[[3]].g1[w], {x}]; Lg1Ω13 = Lg1Ω13[[1]];
LgαΩ1 = {Lg0Ω11, Lg0Ω12, Lg1Ω13}

(*Print["iϕ1α"]*)
(*ϕim*)

a0b0 = v00(D[g0[x], {x}].ϕ10 − D[ϕ10, {x}].g0[x]);
a0b1 = v01(D[g1[w], {x}].ϕ10 − D[ϕ10, {x}].g1[x]);
a1b0 = v10(D[g0[x], {x}].ϕ10 − D[ϕ10, {x}].g0[x]);
a1b1 = v11(D[g1[w], {x}].ϕ10 − D[ϕ10, {x}].g1[x]);
ϕ11 = a0b0 + a0b1 + a1b0 + a1b1;
ϕ11 = {ϕ11[[1, 1]], ϕ11[[2, 1]], ϕ11[[3, 1]], ϕ11[[4, 1]]};

a0b0 = v00(D[g0[x], {x}].ϕ20 − D[ϕ20, {x}].g0[x]);
a0b1 = v01(D[g1[w], {x}].ϕ20 − D[ϕ20, {x}].g1[x]);
a1b0 = v10(D[g0[x], {x}].ϕ20 − D[ϕ20, {x}].g0[x]);
a1b1 = v11(D[g1[w], {x}].ϕ20 − D[ϕ20, {x}].g1[x]);
ϕ21 = a0b0 + a0b1 + a1b0 + a1b1;
ϕ21 = {ϕ21[[1, 1]], ϕ21[[2, 1]], ϕ21[[3, 1]], ϕ21[[4, 1]]};

Print["Liϕ1hl"]
L1ϕ1h1 = D[Ω0[[1]].ϕ11, {x}]; L1ϕ1h1 = L1ϕ1h1[[1]];
L1ϕ1h2 = D[Ω0[[2]].ϕ11, {x}]; L1ϕ1h2 = L1ϕ1h2[[1]];
L2ϕ1h1 = D[Ω0[[1]].ϕ21, {x}]; L2ϕ1h1 = L2ϕ1h1[[1]];
L2ϕ1h2 = D[Ω0[[2]].ϕ21, {x}]; L2ϕ1h2 = L2ϕ1h2[[1]];
Liϕ1hl = {L1ϕ1h2, L2ϕ1h2}

Print["Ω2"]
Ω2 = {Ω1[[1]], Ω1[[2]], Ω1[[3]], Ω1[[4]]}
```

Print[“Ω2 at x(0) and Rank”]

$\Omega 20 = \Omega 2/.\{\theta \to 0, T \to 28, \sigma \to 98, \xi \to 1\}$

MatrixRank[Ω20]

Print[“********”]**

Print[“Step 7: check if Ωm+1=Ω”]

Print[“Ω2=Ω1”]

Print[

"Step 8: The differential of all the states belongs to Ω1 in a given neighbourhood of x(0). The state x is wekly locally observable for the given neighbourhood."]

Step 1: Compute $\mu 11$. Test outputs for unknown input observability

For h1

0

For h2

For h3

$\frac{Ar\Omega}{\mathrm{b1+bs}}$

****

Controllability Matrix

Construction the Accesibility algebra C

Step 2: Compute tensors μ, ν and g^{α}

Tensor μ

$$\left\{\left\{1, \frac{(-ks - g\,ml\,rl\,Cos[\theta])\,(-ks\,(-Tin+\theta) + A\,r\,\sigma - g\,ml\,rl\,Sin[\theta])}{(b1+bs)^2} + \frac{A\,r\left(\frac{Aw\,T\,(-h0-h2\,T^2)\,\Theta}{cp\,mw} - \frac{E1\,r\,(-ks\,(-Tin+\theta)+A\,r\,\sigma-g\,ml\,rl\,Sin[\theta])}{(b1+bs)\,l0}\right)}{b1+bs}\right\}, \left\{0, \frac{A\,r\,\Omega}{b1+bs}\right\}\right\}$$

Tensor υ

$$\left\{\{1, -1\}, \left\{0, \frac{b1+bs}{A\,r\,\Omega}\right\}\right\}$$

Field hg^{α}

hg^0

$$\left\{\left\{\frac{-ks\,(-Tin+\theta) + A\,r\,\sigma - g\,ml\,rl\,Sin[\theta]}{b1+bs}\right\}, \left\{\frac{Aw\,T\left(-h0-h2\,T^2\right)}{cp\,mw}\right\}, \left\{\frac{Aw\,T\left(-h0-h2\,T^2\right)\Theta}{cp\,mw} - \Omega - \frac{E1\,r\,(-ks\,(-Tin+\theta) + A\,r\,\sigma - g\,ml\,rl\,Sin[\theta])}{(b1+bs)\,l0}\right\}, \{-1\}\right\}$$

hg^1

$$\left\{\{0\}, \{0\}, \left\{\frac{b1+bs}{A\,r}\right\}, \left\{\frac{b1+bs}{A\,r\,\Omega}\right\}\right\}$$

****

Step 3: Compute the codistribution $\Omega 0$ and $\Omega 1$

$\Omega 0$

$$\left\{\{1, 0, 0, 0\}, \left\{\frac{-ks - g\,ml\,rl\,Cos[\theta]}{b1+bs}, 0, \frac{A\,r}{b1+bs}, 0\right\}\right\}$$

LfiΩ0

$$\left\{\left\{0, 0, 0, -\frac{A\,Kt^2\,r\,(-Ra+Rm)\,\Theta}{(b1+bs)\,cp\,mw\,(Ra\,(1-\xi)+Rm\,\xi)^2}\right\}, \left\{0, \frac{2\,A\,Aw\,h2\,r\,T\,\Theta}{(b1+bs)\,cp\,mw}, 0, 0\right\}\right\}$$

Lg$\alpha\Omega$0

$$\left\{\left\{\frac{-ks - g\,ml\,rl\,Cos[\theta]}{b1+bs}, 0, \frac{A\,r}{b1+bs}, 0\right\}, \left\{-\frac{A\,E1\,r^2\,(-ks - g\,ml\,rl\,Cos[\theta])}{(b1+bs)^2\,l0} + \frac{(-ks - g\,ml\,rl\,Cos[\theta])^2}{(b1+bs)^2} + \frac{g\,ml\,rl\,Sin[\theta]\,(-ks\,(-Tin+\theta) + A\,r\,\sigma - g\,ml\,rl\,Sin[\theta])}{(b1+bs)^2}, \frac{A\,r\left(-\frac{2\,Aw\,h2\,T^2\,\Theta}{cp\,mw} + \frac{Aw\,(-h0-h2\,T^2)\,\Theta}{cp\,mw}\right)}{b1+bs}, -\frac{A^2\,E1\,r^3}{(b1+bs)^2\,l0} + \frac{A\,r\,(-ks - g\,ml\,rl\,Cos[\theta])}{(b1+bs)^2}, 0\right\}\right\}$$

Liϕ0hl

$$\left\{\left\{0,\ 0,\ 0,\ -\frac{A\,Kt^2\,r\,(-Ra+Rm)\,\Theta}{(b1+bs)\,cp\,mw\,(Ra\,(1-\xi)+Rm\,\xi)^2}\right\},\right.$$
$$\left.\left\{0,\ \frac{2\,A\,Aw\,h2\,r\,T\,\Theta}{(b1+bs)\,cp\,mw},\ 0,\ 0\right\}\right\}$$

Ω1

$$\left\{\{1,\ 0,\ 0,\ 0\},\ \left\{\frac{-ks-g\,ml\,rl\,\mathrm{Cos}[\theta]}{b1+bs},\ 0,\ \frac{A\,r}{b1+bs},\ 0\right\},\right.$$
$$\left\{0,\ 0,\ 0,\ -\frac{A\,Kt^2\,r\,(-Ra+Rm)\,\Theta}{(b1+bs)\,cp\,mw\,(Ra\,(1-\xi)+Rm\,\xi)^2}\right\},$$
$$\left.\left\{0,\ \frac{2\,A\,Aw\,h2\,r\,T\,\Theta}{(b1+bs)\,cp\,mw},\ 0,\ 0\right\}\right\}$$

Ω0 at x(0) and Rank

$$\left\{\{1,\ 0,\ 0,\ 0\},\ \left\{\frac{-ks-g\,ml\,rl}{b1+bs},\ 0,\ \frac{A\,r}{b1+bs},\ 0\right\}\right\}$$

2

Ω1 at x(0) and Rank

$$\left\{\{1,\ 0,\ 0,\ 0\},\ \left\{\frac{-ks-g\,ml\,rl}{b1+bs},\ 0,\ \frac{A\,r}{b1+bs},\ 0\right\},\right.$$
$$\left.\left\{0,\ 0,\ 0,\ -\frac{A\,Kt^2\,r\,(-Ra+Rm)\,\Theta}{(b1+bs)\,cp\,mw\,Rm^2}\right\},\ \left\{0,\ \frac{56\,A\,Aw\,h2\,r\,\Theta}{(b1+bs)\,cp\,mw},\ 0,\ 0\right\}\right\}$$

4

****

Step 4: Check Lemma 14

LfiΩ1

$$\left\{\left\{0,\ 0,\ 0,\ -\frac{A\,Kt^2\,r\,(-Ra+Rm)\,\Theta}{(b1+bs)\,cp\,mw\,(Ra\,(1-\xi)+Rm\,\xi)^2}\right\},\right.$$
$$\left.\left\{0,\ \frac{2\,A\,Aw\,h2\,r\,T\,\Theta}{(b1+bs)\,cp\,mw},\ 0,\ 0\right\}\right\}$$

LgαΩ1

$$\left\{\left\{\frac{-ks-g\,ml\,rl\,\mathrm{Cos}[\theta]}{b1+bs},\ 0,\ \frac{A\,r}{b1+bs},\ 0\right\},\right.$$
$$\left\{-\frac{A\,E1\,r^2\,(-ks-g\,ml\,rl\,\mathrm{Cos}[\theta])}{(b1+bs)^2\,l0}+\frac{(-ks-g\,ml\,rl\,\mathrm{Cos}[\theta])^2}{(b1+bs)^2}+\right.$$
$$\left.\frac{1}{(b1+bs)^2}g\,ml\,rl\,\mathrm{Sin}[\theta]\,(-ks\,(-Tin+\theta)+A\,r\,\sigma-g\,ml\,rl\,\mathrm{Sin}[\theta]),\right.$$
$$\left.\frac{A\,r\left(-\frac{2\,Aw\,h2\,T^2\,\Theta}{cp\,mw}+\frac{Aw\,(-h0-h2\,T^2)\,\Theta}{cp\,mw}\right)}{b1+bs},\right.$$
$$\left.-\frac{A^2\,E1\,r^3}{(b1+bs)^2\,l0}+\frac{A\,r\,(-ks-g\,ml\,rl\,\mathrm{Cos}[\theta])}{(b1+bs)^2},\ 0\right\},$$
$$\left.\left\{0,\ 0,\ 0,\ \frac{2\,A\,Kt^2\,r\,(-Ra+Rm)^2\,\Theta}{(b1+bs)\,cp\,mw\,(Ra\,(1-\xi)+Rm\,\xi)^3}\right\}\right\}$$

Liϕ1hl

$$\left\{\left\{\frac{A\,g\,Kt^2\,ml\,r\,rl\,\Theta\,Sin[\theta]}{(b1+bs)^2\,cp\,mw\,(Ra\,(1-\xi)+Rm\,\xi)},\right.\right.$$
$$-\frac{6\,A\,Aw\,h2\,Kt^2\,r\,T\,\Theta}{(b1+bs)\,cp^2\,mw^2\,(Ra\,(1-\xi)+Rm\,\xi)},\ 0,\ \frac{1}{b1+bs}$$
$$A\,r\left(\frac{2\,Kt^2\,(-Ra+Rm)^2\,\Theta}{cp\,mw\,(Ra\,(1-\xi)+Rm\,\xi)^3}+\frac{A\,E1\,Kt^2\,r^2\,(-Ra+Rm)\,\Theta}{(b1+bs)\,cp\,l0\,mw\,(Ra\,(1-\xi)+Rm\,\xi)^2}-\right.$$
$$\frac{Kt^2\,(-Ra+Rm)\left(-\frac{2\,Aw\,h2\,T^2\,\Theta}{cp\,mw}+\frac{Aw\,(-h0-h2\,T^2)\,\Theta}{cp\,mw}\right)}{cp\,mw\,(Ra\,(1-\xi)+Rm\,\xi)^2}-$$
$$\left.\left.\frac{2\,(b1+bs)\,Kt^2\,(-Ra+Rm)^2\,\Theta}{A\,cp\,mw\,r\,(Ra\,(1-\xi)+Rm\,\xi)^3\,\Omega}\right)-\right.$$
$$\left.\frac{A\,Kt^2\,r\,(-Ra+Rm)\,\Theta\,(-ks-g\,ml\,rl\,Cos[\theta])}{(b1+bs)^2\,cp\,mw\,(Ra\,(1-\xi)+Rm\,\xi)^2}\right\},$$
$$\left\{\frac{A\,Aw\,g\,ml\,r\,rl\left(h0+h2\,T^2\right)\Theta\,Sin[\theta]}{(b1+bs)^2\,cp\,mw},\ \frac{1}{b1+bs}\right.$$
$$A\,r\left(-\frac{2\,A\,Aw\,E1\,h2\,r^2\,T\,\Theta}{(b1+bs)\,cp\,l0\,mw}+\frac{4\,Aw^2\,h2^2\,T^3\,\Theta}{cp^2\,mw^2}-\frac{4\,Aw^2\,h2\,T\left(-h0-h2\,T^2\right)\Theta}{cp^2\,mw^2}-\right.$$
$$\left.\frac{6\,Aw^2\,h2\,T\left(h0+h2\,T^2\right)\Theta}{cp^2\,mw^2}+\frac{2\,Aw\,h2\,T\left(-\frac{2\,Aw\,h2\,T^2\,\Theta}{cp\,mw}+\frac{Aw\,(-h0-h2\,T^2)\,\Theta}{cp\,mw}\right)}{cp\,mw}\right)+$$
$$\left.\left.\frac{2\,A\,Aw\,h2\,r\,T\,\Theta\,(-ks-g\,ml\,rl\,Cos[\theta])}{(b1+bs)^2\,cp\,mw},\ 0,\ 0\right\}\right\}$$

Ω2

$$\left\{\{1,\ 0,\ 0,\ 0\},\ \left\{\frac{-ks-g\,ml\,rl\,Cos[\theta]}{b1+bs},\ 0,\ \frac{A\,r}{b1+bs},\ 0\right\},\right.$$
$$\left\{0,\ 0,\ 0,\ -\frac{A\,Kt^2\,r\,(-Ra+Rm)\,\Theta}{(b1+bs)\,cp\,mw\,(Ra\,(1-\xi)+Rm\,\xi)^2}\right\},$$
$$\left.\left\{0,\ \frac{2\,A\,Aw\,h2\,r\,T\,\Theta}{(b1+bs)\,cp\,mw},\ 0,\ 0\right\}\right\}$$

Ω2 at x(0) and Rank

$$\left\{\{1,\ 0,\ 0,\ 0\},\ \left\{\frac{-ks-g\,ml\,rl}{b1+bs},\ 0,\ \frac{A\,r}{b1+bs},\ 0\right\},\right.$$
$$\left.\left\{0,\ 0,\ 0,\ -\frac{A\,Kt^2\,r\,(-Ra+Rm)\,\Theta}{(b1+bs)\,cp\,mw\,Rm^2}\right\},\ \left\{0,\ \frac{56\,A\,Aw\,h2\,r\,\Theta}{(b1+bs)\,cp\,mw},\ 0,\ 0\right\}\right\}$$

4

****

Step 7: check if Ωm+1=Ω

Ω2=Ω1

Step 8: The differential of all the states belongs
to Ω1 in a given neighbourhood of x(0). The state x is
wekly locally observable for the given neighbourhood.

B.2 Nonlinear Controllability

The nonlinear controllability of the continuous and discrete-time models used to design the SDRE an DSDRE control is proven using the Lie algebra. The computation of the controllability matrix is done with the aid of Wolfram Mathematica.

B.2.1 Continuous Nonlinear Controllability

The nonlinear controllability proof for the continuous-time system presented in Eq. (6.32) was computed using Wolfram Mathematica, and is provided in the following pages.

```
x = {θ, dθ, σ};
u = {V^2};
b = bs + b1;

ξT1[x_]:=(ξM/2)Sin[aA(T − As − (1/cM)x[[3]])]aA
ξσ1[x_]:= − (1/cM)ξT[x]
ξT2[x_]:=((1 − ξA)/2)Sin[aM(T − Mf − (1/cA)x[[3]])]aM
ξσ2[x_]:= − (1/cA)ξT[x]

f1[x_]:=((−E1r1/l10)x[[2]] + (Θ + ΩξT1[x])(−(T − Ta)h0Aw1/(mw1cp1)))/(1 − Ωξσ1[x])
g1[x_]:=(Θ + ΩξT1[x])(1/(R1mw1cp1))/(1 − Ωξσ1[x])
f2[x_]:=((−E1r1/l10)x[[2]] + (Θ + ΩξT2[x])(−(T − Ta)h0Aw1/(mw1cp1)))/(1 − Ωξσ2[x])
g2[x_]:=(Θ + ΩξT2[x])(1/(R1mw1cp1))/(1 − Ωξσ2[x])
f3[x_]:=(−E1r1/l10)x[[2]] + Θ(−(T − Ta)h0Aw1/(mw1cp1))
g3[x_]:=(Θ)(1/(R1mw1cp1))

Z1[dξ_]:=(ArcTan[δ(dξ − ϵ)] + Pi/2)(1/Pi)
Z2[dξ_]:=(ArcTan[−δ(dξ + ϵ)] + Pi/2)(1/Pi)
Z3[dξ_]:=(ArcTan[δ(dξ + ϵ)] + ArcTan[−δ(dξ − ϵ)])(1/Pi)

fx4[dξ_]:=f1[x]Z1[dξ] + f2[x]Z2[dξ] + f3[x]Z3[dξ]
```

```
g4[dξ_]:=g1[x]Z1[dξ] + g2[x]Z2[dξ] + g3[x]Z3[dξ]

f[x_]:={{x[[2]]}, {(A1r1(x[[3]]) − mlgrlCos[x[[1]]] − ksx[[1]] − bx[[2]])/J}, {fx4[dξ]}}
g[x_]:={{0}, {0}, {g4[dξ]}}

Print["Controllability Matrix"]
Print["Construction the Accesibility algebra C"]

C11 = D[g[x], {x}].f[x]; C11 = {C11[[1, 1]], C11[[2, 1]], C11[[3, 1]]};
C12 = D[f[x], {x}].g[x]; C12 = {C12[[1, 1]], C12[[2, 1]], C12[[3, 1]]};
C1 = C11 − C12;
C21 = D[C1, {x}].f[x]; C21 = {C21[[1, 1]], C21[[2, 1]], C21[[3, 1]]};
C22 = D[f[x], {x}].C1; C22 = {C22[[1, 1]], C22[[2, 1]], C22[[3, 1]]};
C2 = C21 − C22;
C31 = D[g[x], {x}].C2; C31 = {C31[[1, 1]], C31[[2, 1]], C31[[3, 1]]};
C32 = D[C2, {x}].g[x]; C32 = {C32[[1, 1]], C32[[2, 1]], C32[[3, 1]]};
C3 = C31 − C32;

a = Transpose[f[x]]; a = a[[1]];
b = Transpose[g[x]]; b = b[[1]];
c = Transpose[C1]; c = c[[1]];
d = Transpose[C2]; d = d[[1]];
e = Transpose[C3]; e = e[[1]];
aC = {a, b, d}
(*aC0 = aC/.{θ → 0, dθ → 0, T → 25, Ta → 25, σ → 0, β1 → 0, β2 → 0, β3 → 0, β4 → 0}*)
MatrixRank[aC]
Print[
"Due to the constraints over the control input, although the controllability matrix is
full rank for all x, the system is proved to be reachable."]
```

```
Controllability Matrix

Construction the Accesibility algebra C
```

$$\Big\{\Big\{d\theta,\ \frac{-(b1+bs)\ d\theta-ks\,\theta+A1\ r1\ \sigma-g\ ml\ rl\ Cos[\theta]}{J},$$

$$\frac{1}{\pi}\Big(-\frac{d\theta\ E1\ r1}{l10}+\frac{Aw1\ h0\ (-T+Ta)\ \Theta}{cp1\ mw1}\Big)$$

$$(-ArcTan[\delta\ (d\xi-\epsilon)]+ArcTan[\delta\ (d\xi+\epsilon)])+$$

$$\Big(\Big(\frac{\pi}{2}-ArcTan[\delta\ (d\xi+\epsilon)]\Big)\Big(-\frac{d\theta\ E1\ r1}{l10}+\frac{1}{cp1\ mw1}$$

$$Aw1\ h0\ (-T+Ta)\ \Big(\Theta+\frac{1}{2}\ aM\ (1-\xi A)\ \Omega\ Sin\Big[aM\ \Big(-Mf+T-\frac{\sigma}{cA}\Big)\Big]\Big)\Big)\Big)\Big/$$

$$\Big(\pi\ \Big(1+\frac{\Omega\ \xi T[\{\theta,\ d\theta,\ \sigma\}]}{cA}\Big)\Big)+\Big(\Big(\frac{\pi}{2}+ArcTan[\delta\ (d\xi-\epsilon)]\Big)\Big(-\frac{d\theta\ E1\ r1}{l10}+$$

$$\frac{1}{cp1\ mw1}Aw1\ h0\ (-T+Ta)\ \Big(\Theta+\frac{1}{2}\ aA\ \xi M\ \Omega\ Sin\Big[aA\ \Big(-As+T-\frac{\sigma}{cM}\Big)\Big]\Big)\Big)\Big)\Big/$$

$$\Big(\pi\ \Big(1+\frac{\Omega\ \xi T[\{\theta,\ d\theta,\ \sigma\}]}{cM}\Big)\Big)\Big\},\ \{0,\ 0,$$

$$\frac{\Theta\ (-ArcTan[\delta\ (d\xi-\epsilon)]+ArcTan[\delta\ (d\xi+\epsilon)])}{cp1\ mw1\ \pi\ R1}+$$

$$\Big(\Big(\frac{\pi}{2}-ArcTan[\delta\ (d\xi+\epsilon)]\Big)\Big(\Theta+\frac{1}{2}\ aM\ (1-\xi A)\ \Omega\ Sin\Big[aM\ \Big(-Mf+T-\frac{\sigma}{cA}\Big)\Big]\Big)\Big)\Big/$$

$$\Big(cp1\ mw1\ \pi\ R1\ \Big(1+\frac{\Omega\ \xi T[\{\theta,\ d\theta,\ \sigma\}]}{cA}\Big)\Big)+$$

$$\Big(\Big(\frac{\pi}{2}+ArcTan[\delta\ (d\xi-\epsilon)]\Big)\Big(\Theta+\frac{1}{2}\ aA\ \xi M\ \Omega\ Sin\Big[aA\ \Big(-As+T-\frac{\sigma}{cM}\Big)\Big]\Big)\Big)\Big/$$

$$\Big(cp1\ mw1\ \pi\ R1\ \Big(1+\frac{\Omega\ \xi T[\{\theta,\ d\theta,\ \sigma\}]}{cM}\Big)\Big)\Big\},$$

$$\Big\{\frac{1}{J}A1\ r1\ \Big(\frac{\Theta\ (-ArcTan[\delta\ (d\xi-\epsilon)]+ArcTan[\delta\ (d\xi+\epsilon)])}{cp1\ mw1\ \pi\ R1}+$$

$$\Big(\Big(\frac{\pi}{2}-ArcTan[\delta\ (d\xi+\epsilon)]\Big)$$

$$\Big(\Theta+\frac{1}{2}\ aM\ (1-\xi A)\ \Omega\ Sin\Big[aM\ \Big(-Mf+T-\frac{\sigma}{cA}\Big)\Big]\Big)\Big)\Big/$$

$$\Big(cp1\ mw1\ \pi\ R1\ \Big(1+\frac{\Omega\ \xi T[\{\theta,\ d\theta,\ \sigma\}]}{cA}\Big)\Big)+$$

$$\Big(\Big(\frac{\pi}{2}+ArcTan[\delta\ (d\xi-\epsilon)]\Big)\Big(\Theta+\frac{1}{2}\ aA\ \xi M\ \Omega\ Sin\Big[aA\ \Big(-As+T-\frac{\sigma}{cM}\Big)\Big]\Big)\Big)\Big/$$

$$\Big(cp1\ mw1\ \pi\ R1\ \Big(1+\frac{\Omega\ \xi T[\{\theta,\ d\theta,\ \sigma\}]}{cM}\Big)\Big)\Big),$$

$$\frac{1}{J^2}A1\ (-b1-bs)\ r1\ \Big(\frac{\Theta\ (-ArcTan[\delta\ (d\xi-\epsilon)]+ArcTan[\delta\ (d\xi+\epsilon)])}{cp1\ mw1\ \pi\ R1}+$$

$$\Big(\Big(\frac{\pi}{2}-ArcTan[\delta\ (d\xi+\epsilon)]\Big)$$

$$\Big(\Theta+\frac{1}{2}\ aM\ (1-\xi A)\ \Omega\ Sin\Big[aM\ \Big(-Mf+T-\frac{\sigma}{cA}\Big)\Big]\Big)\Big)\Big/$$

$$\Big(cp1\ mw1\ \pi\ R1\ \Big(1+\frac{\Omega\ \xi T[\{\theta,\ d\theta,\ \sigma\}]}{cA}\Big)\Big)+$$

$$\Big(\Big(\frac{\pi}{2}+ArcTan[\delta\ (d\xi-\epsilon)]\Big)\Big(\Theta+\frac{1}{2}\ aA\ \xi M\ \Omega\ Sin\Big[aA\ \Big(-As+T-\frac{\sigma}{cM}\Big)\Big]\Big)\Big)\Big/$$

$$\Big(cp1\ mw1\ \pi\ R1\ \Big(1+\frac{\Omega\ \xi T[\{\theta,\ d\theta,\ \sigma\}]}{cM}\Big)\Big)\Big)-$$

$$\frac{1}{J}A1\ r1\ \Big(\frac{1}{\pi}\Big(-\frac{d\theta\ E1\ r1}{l10}+\frac{Aw1\ h0\ (-T+Ta)\ \Theta}{cp1\ mw1}\Big)$$

$$(-ArcTan[\delta\ (d\xi-\epsilon)]+ArcTan[\delta\ (d\xi+\epsilon)])+$$

$$\left(\left(\frac{\pi}{2}-\text{ArcTan}[\delta\ (\text{d}\xi+\epsilon)]\right)\left(-\frac{\text{d}\theta\ \text{E1}\ \text{r1}}{\text{l10}}+\frac{1}{\text{cp1}\ \text{mw1}}\text{Aw1}\ \text{h0}\ (-\text{T}+\text{Ta})\right.\right.$$
$$\left.\left.\left(\Theta+\frac{1}{2}\ \text{aM}\ (1-\xi\text{A})\ \Omega\ \text{Sin}\left[\text{aM}\left(-\text{Mf}+\text{T}-\frac{\sigma}{\text{cA}}\right)\right]\right)\right)\Bigg/$$
$$\left(\pi\left(1+\frac{\Omega\ \xi\text{T}[\{\theta,\ \text{d}\theta,\ \sigma\}]}{\text{cA}}\right)\right)+\left(\left(\frac{\pi}{2}+\text{ArcTan}[\delta\ (\text{d}\xi-\epsilon)]\right)\right.$$
$$\left(-\frac{\text{d}\theta\ \text{E1}\ \text{r1}}{\text{l10}}+\frac{1}{\text{cp1}\ \text{mw1}}\text{Aw1}\ \text{h0}\ (-\text{T}+\text{Ta})\ \left(\Theta+\frac{1}{2}\ \text{aA}\ \xi\text{M}\ \Omega\ \text{Sin}\right.\right.\Big[$$
$$\left.\left.\left.\text{aA}\left(-\text{As}+\text{T}-\frac{\sigma}{\text{cM}}\right)\right]\right)\right)\Bigg/\left(\pi\left(1+\frac{\Omega\ \xi\text{T}[\{\theta,\ \text{d}\theta,\ \sigma\}]}{\text{cM}}\right)\right)$$
$$\left(-\left(\left(\text{aM}^2\ (1-\xi\text{A})\ \Omega\left(\frac{\pi}{2}-\text{ArcTan}[\delta\ (\text{d}\xi+\epsilon)]\right)\text{Cos}\left[\text{aM}\left(-\text{Mf}+\text{T}-\frac{\sigma}{\text{cA}}\right)\right]\right)\Bigg/\right.\right.$$
$$\left.\left.\left(2\ \text{cA}\ \text{cp1}\ \text{mw1}\ \pi\ \text{R1}\left(1+\frac{\Omega\ \xi\text{T}[\{\theta,\ \text{d}\theta,\ \sigma\}]}{\text{cA}}\right)\right)\right)-$$
$$\left(\text{aA}^2\ \xi\text{M}\ \Omega\left(\frac{\pi}{2}+\text{ArcTan}[\delta\ (\text{d}\xi-\epsilon)]\right)\text{Cos}\left[\text{aA}\left(-\text{As}+\text{T}-\frac{\sigma}{\text{cM}}\right)\right]\right)\Bigg/$$
$$\left(2\ \text{cM}\ \text{cp1}\ \text{mw1}\ \pi\ \text{R1}\left(1+\frac{\Omega\ \xi\text{T}[\{\theta,\ \text{d}\theta,\ \sigma\}]}{\text{cM}}\right)\right)-$$
$$\left(\Omega\left(\frac{\pi}{2}-\text{ArcTan}[\delta\ (\text{d}\xi+\epsilon)]\right)\left(\Theta+\frac{1}{2}\ \text{aM}\ (1-\xi\text{A})\ \Omega\right.\right.$$
$$\left.\left.\text{Sin}\left[\text{aM}\left(-\text{Mf}+\text{T}-\frac{\sigma}{\text{cA}}\right)\right]\right)\xi\text{T}^{(\{0,0,1\})}[\{\theta,\ \text{d}\theta,\ \sigma\}]\right)\Bigg/$$
$$\left(\text{cA}\ \text{cp1}\ \text{mw1}\ \pi\ \text{R1}\left(1+\frac{\Omega\ \xi\text{T}[\{\theta,\ \text{d}\theta,\ \sigma\}]}{\text{cA}}\right)^2\right)-$$
$$\left(\Omega\left(\frac{\pi}{2}+\text{ArcTan}[\delta\ (\text{d}\xi-\epsilon)]\right)\left(\Theta+\frac{1}{2}\ \text{aA}\ \xi\text{M}\ \Omega\ \text{Sin}\left[\text{aA}\left(-\text{As}+\text{T}-\frac{\sigma}{\text{cM}}\right)\right]\right)\right.$$
$$\left.\xi\text{T}^{(\{0,0,1\})}[\{\theta,\ \text{d}\theta,\ \sigma\}]\right)\Bigg/$$
$$\left.\left(\text{cM}\ \text{cp1}\ \text{mw1}\ \pi\ \text{R1}\left(1+\frac{\Omega\ \xi\text{T}[\{\theta,\ \text{d}\theta,\ \sigma\}]}{\text{cM}}\right)^2\right)\right)-\frac{1}{\text{J}^2}$$
$$\text{A1}\ \text{r1}\ (-(\text{b1}+\text{bs})\ \text{d}\theta-\text{ks}\ \theta+\text{A1}\ \text{r1}\ \sigma-\text{g}\ \text{ml}\ \text{rl}\ \text{Cos}[\theta])$$
$$\left(-\left(\left(\Omega\left(\frac{\pi}{2}-\text{ArcTan}[\delta\ (\text{d}\xi+\epsilon)]\right)\left(\Theta+\frac{1}{2}\ \text{aM}\ (1-\xi\text{A})\ \Omega\right.\right.\right.\right.$$
$$\left.\left.\left.\left.\text{Sin}\left[\text{aM}\left(-\text{Mf}+\text{T}-\frac{\sigma}{\text{cA}}\right)\right]\right)\xi\text{T}^{(\{0,1,0\})}[\{\theta,\ \text{d}\theta,\ \sigma\}]\right)\Bigg/\right.\right.$$
$$\left.\left.\left(\text{cA}\ \text{cp1}\ \text{mw1}\ \pi\ \text{R1}\left(1+\frac{\Omega\ \xi\text{T}[\{\theta,\ \text{d}\theta,\ \sigma\}]}{\text{cA}}\right)^2\right)\right)-$$
$$\left(\Omega\left(\frac{\pi}{2}+\text{ArcTan}[\delta\ (\text{d}\xi-\epsilon)]\right)\left(\Theta+\frac{1}{2}\ \text{aA}\ \xi\text{M}\ \Omega\ \text{Sin}\left[\text{aA}\left(-\text{As}+\text{T}-\frac{\sigma}{\text{cM}}\right)\right]\right)\right.$$
$$\left.\xi\text{T}^{(\{0,1,0\})}[\{\theta,\ \text{d}\theta,\ \sigma\}]\right)\Bigg/$$
$$\left.\left(\text{cM}\ \text{cp1}\ \text{mw1}\ \pi\ \text{R1}\left(1+\frac{\Omega\ \xi\text{T}[\{\theta,\ \text{d}\theta,\ \sigma\}]}{\text{cM}}\right)^2\right)\right)-\frac{1}{\text{J}}$$
$$\text{A1}\ \text{d}\theta\ \text{r1}\left(-\left(\left(\Omega\left(\frac{\pi}{2}-\text{ArcTan}[\delta\ (\text{d}\xi+\epsilon)]\right)\left(\Theta+\frac{1}{2}\ \text{aM}\ (1-\xi\text{A})\ \Omega\right.\right.\right.\right.$$
$$\left.\left.\left.\left.\text{Sin}\left[\text{aM}\left(-\text{Mf}+\text{T}-\frac{\sigma}{\text{cA}}\right)\right]\right)\xi\text{T}^{(\{1,0,0\})}[\{\theta,\ \text{d}\theta,\ \sigma\}]\right)\Bigg/\right.\right.$$
$$\left.\left.\left(\text{cA}\ \text{cp1}\ \text{mw1}\ \pi\ \text{R1}\left(1+\frac{\Omega\ \xi\text{T}[\{\theta,\ \text{d}\theta,\ \sigma\}]}{\text{cA}}\right)^2\right)\right)-$$
$$\left(\Omega\left(\frac{\pi}{2}+\text{ArcTan}[\delta\ (\text{d}\xi-\epsilon)]\right)\left(\Theta+\frac{1}{2}\ \text{aA}\ \xi\text{M}\ \Omega\ \text{Sin}\left[\text{aA}\left(-\text{As}+\text{T}-\frac{\sigma}{\text{cM}}\right)\right]\right)\right.$$
$$\left.\xi\text{T}^{(\{1,0,0\})}[\{\theta,\ \text{d}\theta,\ \sigma\}]\right)\Bigg/$$

$$\left(\text{cM cp1 mw1 }\pi\text{ R1 }\left(1+\frac{\Omega\,\xi T[\{\theta,\,d\theta,\,\sigma\}]}{\text{cM}}\right)^2\right)\Bigg)-$$
$$\frac{1}{J}\text{A1 r1}\left(\left(\frac{1}{\pi}\left(-\frac{d\theta\,\text{E1 r1}}{\text{l10}}+\frac{\text{Aw1 h0 }(-\text{T}+\text{Ta})\,\Theta}{\text{cp1 mw1}}\right)\right.\right.$$
$$(-\text{ArcTan}[\delta\,(d\xi-\epsilon)]+\text{ArcTan}[\delta\,(d\xi+\epsilon)])+$$
$$\left(\left(\frac{\pi}{2}-\text{ArcTan}[\delta\,(d\xi+\epsilon)]\right)\left(-\frac{d\theta\,\text{E1 r1}}{\text{l10}}+\frac{1}{\text{cp1 mw1}}\text{Aw1 h0}\right.\right.$$
$$\left.\left.(-\text{T}+\text{Ta})\left(\Theta+\frac{1}{2}\,\text{aM}\,(1-\xi\text{A})\,\Omega\,\text{Sin}\left[\text{aM}\left(-\text{Mf}+\text{T}-\frac{\sigma}{\text{cA}}\right)\right]\right)\right)\Bigg)\Bigg/$$
$$\left(\pi\left(1+\frac{\Omega\,\xi T[\{\theta,\,d\theta,\,\sigma\}]}{\text{cA}}\right)\right)+\left(\left(\frac{\pi}{2}+\text{ArcTan}[\delta\,(d\xi-\epsilon)]\right)\right.$$
$$\left(-\frac{d\theta\,\text{E1 r1}}{\text{l10}}+\frac{1}{\text{cp1 mw1}}\text{Aw1 h0 }(-\text{T}+\text{Ta})\left(\Theta+\frac{1}{2}\,\text{aA}\,\xi\text{M}\,\Omega\,\text{Sin}\left[\right.\right.\right.$$
$$\left.\left.\left.\text{aA}\left(-\text{As}+\text{T}-\frac{\sigma}{\text{cM}}\right)\right]\right)\right)\Bigg)\Bigg/\left(\pi\left(1+\frac{\Omega\,\xi T[\{\theta,\,d\theta,\,\sigma\}]}{\text{cM}}\right)\right)\Bigg)$$
$$\left(-\left(\left(\text{aM}^2\,(1-\xi\text{A})\,\Omega\left(\frac{\pi}{2}-\text{ArcTan}[\delta\,(d\xi+\epsilon)]\right)\text{Cos}\left[\text{aM}\left(-\text{Mf}+\text{T}-\right.\right.\right.\right.\right.$$
$$\left.\left.\left.\left.\left.\frac{\sigma}{\text{cA}}\right)\right]\right)\Bigg/\left(2\,\text{cA cp1 mw1}\,\pi\,\text{R1}\left(1+\frac{\Omega\,\xi T[\{\theta,\,d\theta,\,\sigma\}]}{\text{cA}}\right)\right)\right)-$$
$$\left(\text{aA}^2\,\xi\text{M}\,\Omega\left(\frac{\pi}{2}+\text{ArcTan}[\delta\,(d\xi-\epsilon)]\right)\text{Cos}\left[\text{aA}\left(-\text{As}+\text{T}-\frac{\sigma}{\text{cM}}\right)\right]\right)\Bigg/$$
$$\left(2\,\text{cM cp1 mw1}\,\pi\,\text{R1}\left(1+\frac{\Omega\,\xi T[\{\theta,\,d\theta,\,\sigma\}]}{\text{cM}}\right)\right)-$$
$$\left(\Omega\left(\frac{\pi}{2}-\text{ArcTan}[\delta\,(d\xi+\epsilon)]\right)\left(\Theta+\frac{1}{2}\,\text{aM}\,(1-\xi\text{A})\,\Omega\,\text{Sin}\left[\right.\right.\right.$$
$$\left.\left.\left.\text{aM}\left(-\text{Mf}+\text{T}-\frac{\sigma}{\text{cA}}\right)\right]\right)\xi T^{(\{0,0,1\})}[\{\theta,\,d\theta,\,\sigma\}]\right)\Bigg/$$
$$\left(\text{cA cp1 mw1}\,\pi\,\text{R1}\left(1+\frac{\Omega\,\xi T[\{\theta,\,d\theta,\,\sigma\}]}{\text{cA}}\right)^2\right)-$$
$$\left(\Omega\left(\frac{\pi}{2}+\text{ArcTan}[\delta\,(d\xi-\epsilon)]\right)\left(\Theta+\frac{1}{2}\,\text{aA}\,\xi\text{M}\,\Omega\,\text{Sin}\left[\right.\right.\right.$$
$$\left.\left.\left.\text{aA}\left(-\text{As}+\text{T}-\frac{\sigma}{\text{cM}}\right)\right]\right)\xi T^{(\{0,0,1\})}[\{\theta,\,d\theta,\,\sigma\}]\right)\Bigg/$$
$$\left(\text{cM cp1 mw1}\,\pi\,\text{R1}\left(1+\frac{\Omega\,\xi T[\{\theta,\,d\theta,\,\sigma\}]}{\text{cM}}\right)^2\right)\Bigg)-$$
$$\left(\left(\Theta\,(-\text{ArcTan}[\delta\,(d\xi-\epsilon)]+\text{ArcTan}[\delta\,(d\xi+\epsilon)])\right)/(\text{cp1 mw1}\,\pi\,\text{R1})+\right.$$
$$\left(\left(\frac{\pi}{2}-\text{ArcTan}[\delta\,(d\xi+\epsilon)]\right)\right.$$
$$\left.\left.\left(\Theta+\frac{1}{2}\,\text{aM}\,(1-\xi\text{A})\,\Omega\,\text{Sin}\left[\text{aM}\left(-\text{Mf}+\text{T}-\frac{\sigma}{\text{cA}}\right)\right]\right)\right)\Bigg/\left(\text{cp1 mw1}\right.$$
$$\left.\pi\,\text{R1}\left(1+\frac{\Omega\,\xi T[\{\theta,\,d\theta,\,\sigma\}]}{\text{cA}}\right)\right)+\left(\left(\frac{\pi}{2}+\text{ArcTan}[\delta\,(d\xi-\epsilon)]\right)\right.$$
$$\left.\left(\Theta+\frac{1}{2}\,\text{aA}\,\xi\text{M}\,\Omega\,\text{Sin}\left[\text{aA}\left(-\text{As}+\text{T}-\frac{\sigma}{\text{cM}}\right)\right]\right)\right)\Bigg/$$
$$\left.\left(\text{cp1 mw1}\,\pi\,\text{R1}\left(1+\frac{\Omega\,\xi T[\{\theta,\,d\theta,\,\sigma\}]}{\text{cM}}\right)\right)\right)$$
$$\left(-\left(\left(\text{aM}^2\,\text{Aw1 h0 }(-\text{T}+\text{Ta})\,(1-\xi\text{A})\,\Omega\left(\frac{\pi}{2}-\text{ArcTan}[\delta\,(d\xi+\epsilon)]\right)\right.\right.\right.$$
$$\left.\left.\left.\text{Cos}\left[\text{aM}\left(-\text{Mf}+\text{T}-\frac{\sigma}{\text{cA}}\right)\right]\right)\Bigg/\left(2\,\text{cA cp1 mw1}\,\pi\right.\right.\right.$$
$$\left.\left.\left.\left(1+\frac{\Omega\,\xi T[\{\theta,\,d\theta,\,\sigma\}]}{\text{cA}}\right)\right)\right)-\left(\text{aA}^2\,\text{Aw1 h0 }(-\text{T}+\text{Ta})\,\xi\text{M}\,\Omega\right.$$

$$\left(\frac{\pi}{2}+\text{ArcTan}[\delta\ (\text{d}\xi-\epsilon)]\right)\text{Cos}\left[\text{aA}\left(-\text{As}+\text{T}-\frac{\sigma}{\text{cM}}\right)\right]\Big)\Big/$$
$$\left(2\ \text{cM}\ \text{cp1}\ \text{mw1}\ \pi\left(1+\frac{\Omega\ \xi\text{T}[\{\theta,\ \text{d}\theta,\ \sigma\}]}{\text{cM}}\right)\right)-$$
$$\left(\Omega\left(\frac{\pi}{2}-\text{ArcTan}[\delta\ (\text{d}\xi+\epsilon)]\right)\left(-\frac{\text{d}\theta\ \text{E1}\ \text{r1}}{\text{l10}}+\frac{1}{\text{cp1}\ \text{mw1}}\text{Aw1}\ \text{h0}\right.\right.$$
$$(-\text{T}+\text{Ta})\left(\Theta+\frac{1}{2}\text{aM}\ (1-\xi\text{A})\ \Omega\ \text{Sin}\left[\text{aM}\left(-\text{Mf}+\text{T}-\frac{\sigma}{\text{cA}}\right)\right]\right)\Big)$$
$$\xi\text{T}^{(\{0,0,1\})}[\{\theta,\ \text{d}\theta,\ \sigma\}]\Big)\Big/\left(\text{cA}\,\pi\left(1+\frac{\Omega\ \xi\text{T}[\{\theta,\ \text{d}\theta,\ \sigma\}]}{\text{cA}}\right)^2\right)-$$
$$\left(\Omega\left(\frac{\pi}{2}+\text{ArcTan}[\delta\ (\text{d}\xi-\epsilon)]\right)\left(-\frac{\text{d}\theta\ \text{E1}\ \text{r1}}{\text{l10}}+\frac{1}{\text{cp1}\ \text{mw1}}\right.\right.$$
$$\text{Aw1}\ \text{h0}\ (-\text{T}+\text{Ta})\left(\Theta+\frac{1}{2}\text{aA}\ \xi\text{M}\ \Omega\ \text{Sin}\left[\text{aA}\left(-\text{As}+\text{T}-\frac{\sigma}{\text{cM}}\right)\right]\right)\Big)$$
$$\xi\text{T}^{(\{0,0,1\})}[\{\theta,\ \text{d}\theta,\ \sigma\}]\Big)\Big/\left(\text{cM}\,\pi\left(1+\frac{\Omega\ \xi\text{T}[\{\theta,\ \text{d}\theta,\ \sigma\}]}{\text{cM}}\right)^2\right)\Big)+$$
$$\frac{1}{\text{J}}(-(\text{b1}+\text{bs})\ \text{d}\theta-\text{ks}\ \theta+\text{A1}\ \text{r1}\ \sigma-\text{g}\ \text{ml}\ \text{rl}\ \text{Cos}[\theta])$$
$$\left(-\left(\left(\Omega\left(\frac{\pi}{2}-\text{ArcTan}[\delta\ (\text{d}\xi+\epsilon)]\right)\left(\Theta+\frac{1}{2}\text{aM}\ (1-\xi\text{A})\ \Omega\right.\right.\right.\right.$$
$$\left.\left.\left.\text{Sin}\left[\text{aM}\left(-\text{Mf}+\text{T}-\frac{\sigma}{\text{cA}}\right)\right]\right)\xi\text{T}^{(\{0,1,0\})}[\{\theta,\ \text{d}\theta,\ \sigma\}]\right)\Big/$$
$$\left.\left(\text{cA}\ \text{cp1}\ \text{mw1}\ \pi\ \text{R1}\left(1+\frac{\Omega\ \xi\text{T}[\{\theta,\ \text{d}\theta,\ \sigma\}]}{\text{cA}}\right)^2\right)\right)-$$
$$\left(\Omega\left(\frac{\pi}{2}+\text{ArcTan}[\delta\ (\text{d}\xi-\epsilon)]\right)\left(\Theta+\frac{1}{2}\text{aA}\ \xi\text{M}\ \Omega\ \text{Sin}\left[\right.\right.\right.$$
$$\left.\left.\left.\text{aA}\left(-\text{As}+\text{T}-\frac{\sigma}{\text{cM}}\right)\right]\right)\xi\text{T}^{(\{0,1,0\})}[\{\theta,\ \text{d}\theta,\ \sigma\}]\right)\Big/$$
$$\left.\left(\text{cM}\ \text{cp1}\ \text{mw1}\ \pi\ \text{R1}\left(1+\frac{\Omega\ \xi\text{T}[\{\theta,\ \text{d}\theta,\ \sigma\}]}{\text{cM}}\right)^2\right)\right)+$$
$$\text{d}\theta\left(-\left(\left(\Omega\left(\frac{\pi}{2}-\text{ArcTan}[\delta\ (\text{d}\xi+\epsilon)]\right)\left(\Theta+\frac{1}{2}\text{aM}\ (1-\xi\text{A})\ \Omega\right.\right.\right.\right.$$
$$\left.\left.\left.\text{Sin}\left[\text{aM}\left(-\text{Mf}+\text{T}-\frac{\sigma}{\text{cA}}\right)\right]\right)\xi\text{T}^{(\{1,0,0\})}[\{\theta,\ \text{d}\theta,\ \sigma\}]\right)\Big/$$
$$\left.\left(\text{cA}\ \text{cp1}\ \text{mw1}\ \pi\ \text{R1}\left(1+\frac{\Omega\ \xi\text{T}[\{\theta,\ \text{d}\theta,\ \sigma\}]}{\text{cA}}\right)^2\right)\right)-$$
$$\left(\Omega\left(\frac{\pi}{2}+\text{ArcTan}[\delta\ (\text{d}\xi-\epsilon)]\right)\left(\Theta+\frac{1}{2}\text{aA}\ \xi\text{M}\ \Omega\ \text{Sin}\left[\right.\right.\right.$$
$$\left.\left.\left.\text{aA}\left(-\text{As}+\text{T}-\frac{\sigma}{\text{cM}}\right)\right]\right)\xi\text{T}^{(\{1,0,0\})}[\{\theta,\ \text{d}\theta,\ \sigma\}]\right)\Big/$$
$$\left.\left.\left(\text{cM}\ \text{cp1}\ \text{mw1}\ \pi\ \text{R1}\left(1+\frac{\Omega\ \xi\text{T}[\{\theta,\ \text{d}\theta,\ \sigma\}]}{\text{cM}}\right)^2\right)\right)\right)\Big),$$
$$\frac{1}{\text{J}}\text{A1}\ \text{r1}\left(\frac{\Theta\ (-\text{ArcTan}[\delta\ (\text{d}\xi-\epsilon)]+\text{ArcTan}[\delta\ (\text{d}\xi+\epsilon)])}{\text{cp1}\ \text{mw1}\ \pi\ \text{R1}}+\right.$$
$$\left(\left(\frac{\pi}{2}-\text{ArcTan}[\delta\ (\text{d}\xi+\epsilon)]\right)\right.$$
$$\left.\left(\Theta+\frac{1}{2}\text{aM}\ (1-\xi\text{A})\ \Omega\ \text{Sin}\left[\text{aM}\left(-\text{Mf}+\text{T}-\frac{\sigma}{\text{cA}}\right)\right]\right)\right)\Big/$$
$$\left(\text{cp1}\ \text{mw1}\ \pi\ \text{R1}\left(1+\frac{\Omega\ \xi\text{T}[\{\theta,\ \text{d}\theta,\ \sigma\}]}{\text{cA}}\right)\right)+$$
$$\left(\left(\frac{\pi}{2}+\text{ArcTan}[\delta\ (\text{d}\xi-\epsilon)]\right)\left(\Theta+\frac{1}{2}\text{aA}\ \xi\text{M}\ \Omega\ \text{Sin}\left[\text{aA}\left(-\text{As}+\text{T}-\frac{\sigma}{\text{cM}}\right)\right]\right)\right)\Big/$$
$$\left.\left.\left(\text{cp1}\ \text{mw1}\ \pi\ \text{R1}\left(1+\frac{\Omega\ \xi\text{T}[\{\theta,\ \text{d}\theta,\ \sigma\}]}{\text{cM}}\right)\right)\right)\right)$$

$$\left(-\frac{1}{l10\,\pi}E1\,r1\,(-\text{ArcTan}[\delta\,(d\xi-\epsilon)]+\text{ArcTan}[\delta\,(d\xi+\epsilon)])-\right.$$
$$\frac{E1\,r1\,\left(\frac{\pi}{2}-\text{ArcTan}[\delta\,(d\xi+\epsilon)]\right)}{l10\,\pi\left(1+\frac{\Omega\,\xi T[\{\theta,d\theta,\sigma\}]}{cA}\right)}-$$
$$\frac{E1\,r1\,\left(\frac{\pi}{2}+\text{ArcTan}[\delta\,(d\xi-\epsilon)]\right)}{l10\,\pi\left(1+\frac{\Omega\,\xi T[\{\theta,d\theta,\sigma\}]}{cM}\right)}-$$
$$\left(\Omega\left(\frac{\pi}{2}-\text{ArcTan}[\delta\,(d\xi+\epsilon)]\right)\left(-\frac{d\theta\,E1\,r1}{l10}+\frac{1}{cp1\,mw1}\right.\right.$$
$$Aw1\,h0\,(-T+Ta)\left(\Theta+\frac{1}{2}aM\,(1-\xi A)\,\Omega\,\text{Sin}\left[aM\left(-Mf+T-\frac{\sigma}{cA}\right)\right]\right)\Big)$$
$$\left.\xi T^{(\{0,1,0\})}[\{\theta,\,d\theta,\,\sigma\}]\right)\Big/\left(cA\,\pi\left(1+\frac{\Omega\,\xi T[\{\theta,\,d\theta,\,\sigma\}]}{cA}\right)^2\right)-$$
$$\left(\Omega\left(\frac{\pi}{2}+\text{ArcTan}[\delta\,(d\xi-\epsilon)]\right)\left(-\frac{d\theta\,E1\,r1}{l10}+\frac{1}{cp1\,mw1}\right.\right.$$
$$Aw1\,h0\,(-T+Ta)\left(\Theta+\frac{1}{2}aA\,\xi M\,\Omega\,\text{Sin}\left[aA\left(-As+T-\frac{\sigma}{cM}\right)\right]\right)\Big)$$
$$\left.\left.\xi T^{(\{0,1,0\})}[\{\theta,\,d\theta,\,\sigma\}]\right)\Big/\left(cM\,\pi\left(1+\frac{\Omega\,\xi T[\{\theta,\,d\theta,\,\sigma\}]}{cM}\right)^2\right)\right)-$$
$$\left(-\left(\left(aM^2\,Aw1\,h0\,(-T+Ta)\,(1-\xi A)\,\Omega\left(\frac{\pi}{2}-\text{ArcTan}[\delta\,(d\xi+\epsilon)]\right)\right.\right.\right.$$
$$\left.\left.\text{Cos}\left[aM\left(-Mf+T-\frac{\sigma}{cA}\right)\right]\right)\Big/$$
$$\left.\left(2\,cA\,cp1\,mw1\,\pi\left(1+\frac{\Omega\,\xi T[\{\theta,\,d\theta,\,\sigma\}]}{cA}\right)\right)\right)-$$
$$\left(aA^2\,Aw1\,h0\,(-T+Ta)\,\xi M\,\Omega\left(\frac{\pi}{2}+\text{ArcTan}[\delta\,(d\xi-\epsilon)]\right)\right.$$
$$\text{Cos}\left[aA\left(-As+T-\frac{\sigma}{cM}\right)\right]\Big)\Big/$$
$$\left(2\,cM\,cp1\,mw1\,\pi\left(1+\frac{\Omega\,\xi T[\{\theta,\,d\theta,\,\sigma\}]}{cM}\right)\right)-$$
$$\left(\Omega\left(\frac{\pi}{2}-\text{ArcTan}[\delta\,(d\xi+\epsilon)]\right)\left(-\frac{d\theta\,E1\,r1}{l10}+\frac{1}{cp1\,mw1}\right.\right.$$
$$Aw1\,h0\,(-T+Ta)\left(\Theta+\frac{1}{2}aM\,(1-\xi A)\,\Omega\,\text{Sin}\left[aM\left(-Mf+T-\frac{\sigma}{cA}\right)\right]\right)\Big)$$
$$\left.\xi T^{(\{0,0,1\})}[\{\theta,\,d\theta,\,\sigma\}]\right)\Big/\left(cA\,\pi\left(1+\frac{\Omega\,\xi T[\{\theta,\,d\theta,\,\sigma\}]}{cA}\right)^2\right)-$$
$$\left(\Omega\left(\frac{\pi}{2}+\text{ArcTan}[\delta\,(d\xi-\epsilon)]\right)\left(-\frac{d\theta\,E1\,r1}{l10}+\frac{1}{cp1\,mw1}\right.\right.$$
$$Aw1\,h0\,(-T+Ta)\left(\Theta+\frac{1}{2}aA\,\xi M\,\Omega\,\text{Sin}\left[aA\left(-As+T-\frac{\sigma}{cM}\right)\right]\right)\Big)$$
$$\left.\left.\xi T^{(\{0,0,1\})}[\{\theta,\,d\theta,\,\sigma\}]\right)\Big/\left(cM\,\pi\left(1+\frac{\Omega\,\xi T[\{\theta,\,d\theta,\,\sigma\}]}{cM}\right)^2\right)\right)$$
$$\left(\left(\frac{1}{\pi}\left(-\frac{d\theta\,E1\,r1}{l10}+\frac{Aw1\,h0\,(-T+Ta)\,\Theta}{cp1\,mw1}\right)\right.\right.$$
$$(-\text{ArcTan}[\delta\,(d\xi-\epsilon)]+\text{ArcTan}[\delta\,(d\xi+\epsilon)])+$$
$$\left(\left(\frac{\pi}{2}-\text{ArcTan}[\delta\,(d\xi+\epsilon)]\right)\left(-\frac{d\theta\,E1\,r1}{l10}+\frac{1}{cp1\,mw1}Aw1\,h0\right.\right.$$
$$\left.\left.\left.\left.(-T+Ta)\left(\Theta+\frac{1}{2}aM\,(1-\xi A)\,\Omega\,\text{Sin}\left[aM\left(-Mf+T-\frac{\sigma}{cA}\right)\right]\right)\right)\right)\right)\Big/$$

$$\left(\pi\left(1+\frac{\Omega\,\xi T[\{\theta,\,d\theta,\,\sigma\}]}{cA}\right)\right)+\left(\left(\frac{\pi}{2}+\text{ArcTan}[\delta\,(d\xi-\epsilon)]\right)\right.$$
$$\left(-\frac{d\theta\,E1\,r1}{l10}+\frac{1}{cp1\,mw1}Aw1\,h0\,(-T+Ta)\left(\Theta+\frac{1}{2}\,aA\,\xi M\,\Omega\,\text{Sin}\Big[\right.\right.$$
$$\left.\left.aA\left(-As+T-\frac{\sigma}{cM}\right)\Big]\right)\right)\Big/\left(\pi\left(1+\frac{\Omega\,\xi T[\{\theta,\,d\theta,\,\sigma\}]}{cM}\right)\right)\Big)$$
$$\left(-\left(\left(aM^2\,(1-\xi A)\,\Omega\left(\frac{\pi}{2}-\text{ArcTan}[\delta\,(d\xi+\epsilon)]\right)\text{Cos}\Big[aM\left(-Mf+T-\right.\right.\right.\right.$$
$$\left.\left.\left.\left.\frac{\sigma}{cA}\right)\Big]\right)\Big/\left(2\,cA\,cp1\,mw1\,\pi\,R1\left(1+\frac{\Omega\,\xi T[\{\theta,\,d\theta,\,\sigma\}]}{cA}\right)\right)\right)-$$
$$\left(aA^2\,\xi M\,\Omega\left(\frac{\pi}{2}+\text{ArcTan}[\delta\,(d\xi-\epsilon)]\right)\text{Cos}\Big[aA\left(-As+T-\frac{\sigma}{cM}\right)\Big]\right)\Big/$$
$$\left(2\,cM\,cp1\,mw1\,\pi\,R1\left(1+\frac{\Omega\,\xi T[\{\theta,\,d\theta,\,\sigma\}]}{cM}\right)\right)-$$
$$\left(\Omega\left(\frac{\pi}{2}-\text{ArcTan}[\delta\,(d\xi+\epsilon)]\right)\left(\Theta+\frac{1}{2}\,aM\,(1-\xi A)\,\Omega\,\text{Sin}\Big[\right.\right.$$
$$\left.\left.aM\left(-Mf+T-\frac{\sigma}{cA}\right)\Big]\right)\xi T^{(\{0,0,1\})}[\{\theta,\,d\theta,\,\sigma\}]\right)\Big/$$
$$\left(cA\,cp1\,mw1\,\pi\,R1\left(1+\frac{\Omega\,\xi T[\{\theta,\,d\theta,\,\sigma\}]}{cA}\right)^2\right)-$$
$$\left(\Omega\left(\frac{\pi}{2}+\text{ArcTan}[\delta\,(d\xi-\epsilon)]\right)\left(\Theta+\frac{1}{2}\,aA\,\xi M\,\Omega\,\text{Sin}\Big[\right.\right.$$
$$\left.\left.aA\left(-As+T-\frac{\sigma}{cM}\right)\Big]\right)\xi T^{(\{0,0,1\})}[\{\theta,\,d\theta,\,\sigma\}]\right)\Big/$$
$$\left(cM\,cp1\,mw1\,\pi\,R1\left(1+\frac{\Omega\,\xi T[\{\theta,\,d\theta,\,\sigma\}]}{cM}\right)^2\right)\Big)-$$
$$\left((\Theta\,(-\text{ArcTan}[\delta\,(d\xi-\epsilon)]+\text{ArcTan}[\delta\,(d\xi+\epsilon)]))\,/\,(cp1\,mw1\,\pi\,R1)+\right.$$
$$\left(\left(\frac{\pi}{2}-\text{ArcTan}[\delta\,(d\xi+\epsilon)]\right)\right.$$
$$\left.\left(\Theta+\frac{1}{2}\,aM\,(1-\xi A)\,\Omega\,\text{Sin}\Big[aM\left(-Mf+T-\frac{\sigma}{cA}\right)\Big]\right)\Big/\left(cp1\,mw1\right.$$
$$\left.\pi\,R1\left(1+\frac{\Omega\,\xi T[\{\theta,\,d\theta,\,\sigma\}]}{cA}\right)\right)+\left(\left(\frac{\pi}{2}+\text{ArcTan}[\delta\,(d\xi-\epsilon)]\right)\right.$$
$$\left.\left.\left(\Theta+\frac{1}{2}\,aA\,\xi M\,\Omega\,\text{Sin}\Big[aA\left(-As+T-\frac{\sigma}{cM}\right)\Big]\right)\right)\Big/$$
$$\left.\left(cp1\,mw1\,\pi\,R1\left(1+\frac{\Omega\,\xi T[\{\theta,\,d\theta,\,\sigma\}]}{cM}\right)\right)\right)$$
$$\left(-\left(\left(aM^2\,Aw1\,h0\,(-T+Ta)\,(1-\xi A)\,\Omega\left(\frac{\pi}{2}-\text{ArcTan}[\delta\,(d\xi+\epsilon)]\right)\right.\right.\right.$$
$$\left.\left.\text{Cos}\Big[aM\left(-Mf+T-\frac{\sigma}{cA}\right)\Big]\right)\Big/\left(2\,cA\,cp1\,mw1\,\pi\right.$$
$$\left.\left.\left(1+\frac{\Omega\,\xi T[\{\theta,\,d\theta,\,\sigma\}]}{cA}\right)\right)\right)-\left(aA^2\,Aw1\,h0\,(-T+Ta)\,\xi M\,\Omega\right.$$
$$\left.\left(\frac{\pi}{2}+\text{ArcTan}[\delta\,(d\xi-\epsilon)]\right)\text{Cos}\Big[aA\left(-As+T-\frac{\sigma}{cM}\right)\Big]\right)\Big/$$
$$\left(2\,cM\,cp1\,mw1\,\pi\left(1+\frac{\Omega\,\xi T[\{\theta,\,d\theta,\,\sigma\}]}{cM}\right)\right)-$$
$$\left(\Omega\left(\frac{\pi}{2}-\text{ArcTan}[\delta\,(d\xi+\epsilon)]\right)\left(-\frac{d\theta\,E1\,r1}{l10}+\frac{1}{cp1\,mw1}Aw1\,h0\right.\right.$$
$$\left.\left.(-T+Ta)\left(\Theta+\frac{1}{2}\,aM\,(1-\xi A)\,\Omega\,\text{Sin}\Big[aM\left(-Mf+T-\frac{\sigma}{cA}\right)\Big]\right)\right)$$
$$\left.\xi T^{(\{0,0,1\})}[\{\theta,\,d\theta,\,\sigma\}]\right)\Big/\left(cA\,\pi\left(1+\frac{\Omega\,\xi T[\{\theta,\,d\theta,\,\sigma\}]}{cA}\right)^2\right)-$$

$$\left(\Omega\left(\frac{\pi}{2}+\text{ArcTan}[\delta\ (d\xi-\epsilon)]\right)\left(-\frac{d\theta\ E1\ r1}{l10}+\frac{1}{cp1\ mw1}\right.\right.$$
$$\left.\left.Aw1\ h0\ (-T+Ta)\left(\Theta+\frac{1}{2}\,aA\,\xi M\,\Omega\,\text{Sin}\left[aA\left(-As+T-\frac{\sigma}{cM}\right)\right]\right)\right)$$
$$\left.\xi T^{(\{0,0,1\})}[\{\theta,\ d\theta,\ \sigma\}]\right)\Big/\left(cM\,\pi\left(1+\frac{\Omega\,\xi T[\{\theta,\ d\theta,\ \sigma\}]}{cM}\right)^2\right)\Bigg)+$$
$$\frac{1}{J}(-(b1+bs)\ d\theta-ks\,\theta+A1\ r1\,\sigma-g\ ml\ rl\ \text{Cos}[\theta])$$
$$\left(-\left(\left(\Omega\left(\frac{\pi}{2}-\text{ArcTan}[\delta\ (d\xi+\epsilon)]\right)\left(\Theta+\frac{1}{2}\,aM\ (1-\xi A)\ \Omega\right.\right.\right.\right.$$
$$\left.\left.\left.\left.\text{Sin}\left[aM\left(-Mf+T-\frac{\sigma}{cA}\right)\right]\right)\xi T^{(\{0,1,0\})}[\{\theta,\ d\theta,\ \sigma\}]\right)\Big/\right.$$
$$\left.\left(cA\ cp1\ mw1\ \pi\ R1\left(1+\frac{\Omega\,\xi T[\{\theta,\ d\theta,\ \sigma\}]}{cA}\right)^2\right)\right)-$$
$$\left(\Omega\left(\frac{\pi}{2}+\text{ArcTan}[\delta\ (d\xi-\epsilon)]\right)\left(\Theta+\frac{1}{2}\,aA\,\xi M\,\Omega\,\text{Sin}\left[\right.\right.\right.$$
$$\left.\left.\left.aA\left(-As+T-\frac{\sigma}{cM}\right)\right]\right)\xi T^{(\{0,1,0\})}[\{\theta,\ d\theta,\ \sigma\}]\right)\Big/$$
$$\left(cM\ cp1\ mw1\ \pi\ R1\left(1+\frac{\Omega\,\xi T[\{\theta,\ d\theta,\ \sigma\}]}{cM}\right)^2\right)\Bigg)+$$
$$d\theta\left(-\left(\left(\Omega\left(\frac{\pi}{2}-\text{ArcTan}[\delta\ (d\xi+\epsilon)]\right)\left(\Theta+\frac{1}{2}\,aM\ (1-\xi A)\ \Omega\right.\right.\right.\right.$$
$$\left.\left.\left.\left.\text{Sin}\left[aM\left(-Mf+T-\frac{\sigma}{cA}\right)\right]\right)\xi T^{(\{1,0,0\})}[\{\theta,\ d\theta,\ \sigma\}]\right)\Big/\right.$$
$$\left.\left(cA\ cp1\ mw1\ \pi\ R1\left(1+\frac{\Omega\,\xi T[\{\theta,\ d\theta,\ \sigma\}]}{cA}\right)^2\right)\right)-$$
$$\left(\Omega\left(\frac{\pi}{2}+\text{ArcTan}[\delta\ (d\xi-\epsilon)]\right)\left(\Theta+\frac{1}{2}\,aA\,\xi M\,\Omega\,\text{Sin}\left[\right.\right.\right.$$
$$\left.\left.\left.aA\left(-As+T-\frac{\sigma}{cM}\right)\right]\right)\xi T^{(\{1,0,0\})}[\{\theta,\ d\theta,\ \sigma\}]\right)\Big/$$
$$\left(cM\ cp1\ mw1\ \pi\ R1\left(1+\frac{\Omega\,\xi T[\{\theta,\ d\theta,\ \sigma\}]}{cM}\right)^2\right)\Bigg)\Bigg)+$$
$$\left(\frac{1}{\pi}\left(-\frac{d\theta\ E1\ r1}{l10}+\frac{Aw1\ h0\ (-T+Ta)\ \Theta}{cp1\ mw1}\right)(-\text{ArcTan}[\delta\ (d\xi-\epsilon)]+\right.$$
$$\left.\text{ArcTan}[\delta\ (d\xi+\epsilon)])+\right.$$
$$\left(\left(\frac{\pi}{2}-\text{ArcTan}[\delta\ (d\xi+\epsilon)]\right)\left(-\frac{d\theta\ E1\ r1}{l10}+\frac{1}{cp1\ mw1}Aw1\ h0\right.\right.$$
$$\left.\left.(-T+Ta)\left(\Theta+\frac{1}{2}\,aM\ (1-\xi A)\ \Omega\,\text{Sin}\left[aM\left(-Mf+T-\frac{\sigma}{cA}\right)\right]\right)\right)\Big/$$
$$\left(\pi\left(1+\frac{\Omega\,\xi T[\{\theta,\ d\theta,\ \sigma\}]}{cA}\right)\right)+\left(\left(\frac{\pi}{2}+\text{ArcTan}[\delta\ (d\xi-\epsilon)]\right)\right.$$
$$\left(-\frac{d\theta\ E1\ r1}{l10}+\frac{1}{cp1\ mw1}\right.$$
$$\left.\left.Aw1\ h0\ (-T+Ta)\left(\Theta+\frac{1}{2}\,aA\,\xi M\,\Omega\,\text{Sin}\left[aA\left(-As+T-\frac{\sigma}{cM}\right)\right]\right)\right)\Big/$$
$$\left.\left(\pi\left(1+\frac{\Omega\,\xi T[\{\theta,\ d\theta,\ \sigma\}]}{cM}\right)\right)\right)$$
$$\left(\left(\frac{1}{\pi}\left(-\frac{d\theta\ E1\ r1}{l10}+\frac{Aw1\ h0\ (-T+Ta)\ \Theta}{cp1\ mw1}\right)\right.\right.$$
$$\left.(-\text{ArcTan}[\delta\ (d\xi-\epsilon)]+\text{ArcTan}[\delta\ (d\xi+\epsilon)])+\right.$$
$$\left.\left(\left(\frac{\pi}{2}-\text{ArcTan}[\delta\ (d\xi+\epsilon)]\right)\left(-\frac{d\theta\ E1\ r1}{l10}+\frac{1}{cp1\ mw1}Aw1\ h0\right.\right.\right.$$

$$
\begin{aligned}
&(-\mathrm{T}+\mathrm{Ta})\left(\Theta+\frac{1}{2}\,\mathrm{aM}\,(1-\xi\mathrm{A})\,\Omega\,\mathrm{Sin}\left[\mathrm{aM}\left(-\mathrm{Mf}+\mathrm{T}-\frac{\sigma}{\mathrm{cA}}\right)\right]\right)\Bigg)\Bigg)\Bigg/\\
&\left(\pi\left(1+\frac{\Omega\,\xi\mathrm{T}[\{\theta,\,\mathrm{d}\theta,\,\sigma\}]}{\mathrm{cA}}\right)\right)+\left(\left(\frac{\pi}{2}+\mathrm{ArcTan}[\delta\,(\mathrm{d}\xi-\epsilon)]\right)\right.\\
&\left(-\frac{\mathrm{d}\theta\,\mathrm{E1}\,\mathrm{r1}}{\mathrm{l10}}+\frac{1}{\mathrm{cp1}\,\mathrm{mw1}}\mathrm{Aw1}\,\mathrm{h0}\,(-\mathrm{T}+\mathrm{Ta})\left(\Theta+\frac{1}{2}\,\mathrm{aA}\,\xi\mathrm{M}\,\Omega\,\mathrm{Sin}\left[\right.\right.\right.\\
&\left.\left.\left.\left.\mathrm{aA}\left(-\mathrm{As}+\mathrm{T}-\frac{\sigma}{\mathrm{cM}}\right)\right]\right)\right)\Bigg)\Bigg/\left(\pi\left(1+\frac{\Omega\,\xi\mathrm{T}[\{\theta,\,\mathrm{d}\theta,\,\sigma\}]}{\mathrm{cM}}\right)\right)\Bigg)\\
&\left(-\left(\left(\mathrm{aM}^3\,(1-\xi\mathrm{A})\,\Omega\left(\frac{\pi}{2}-\mathrm{ArcTan}[\delta\,(\mathrm{d}\xi+\epsilon)]\right)\mathrm{Sin}\left[\mathrm{aM}\right.\right.\right.\right.\\
&\left.\left.\left.\left.\left(-\mathrm{Mf}+\mathrm{T}-\frac{\sigma}{\mathrm{cA}}\right)\right]\right)\Bigg/\\
&\left.\left.\left(2\,\mathrm{cA}^2\,\mathrm{cp1}\,\mathrm{mw1}\,\pi\,\mathrm{R1}\left(1+\frac{\Omega\,\xi\mathrm{T}[\{\theta,\,\mathrm{d}\theta,\,\sigma\}]}{\mathrm{cA}}\right)\right)\right)-\right.\\
&\left(\mathrm{aA}^3\,\xi\mathrm{M}\,\Omega\left(\frac{\pi}{2}+\mathrm{ArcTan}[\delta\,(\mathrm{d}\xi-\epsilon)]\right)\mathrm{Sin}\left[\mathrm{aA}\left(-\mathrm{As}+\mathrm{T}-\frac{\sigma}{\mathrm{cM}}\right)\right]\right)\Bigg/\\
&\left(2\,\mathrm{cM}^2\,\mathrm{cp1}\,\mathrm{mw1}\,\pi\,\mathrm{R1}\left(1+\frac{\Omega\,\xi\mathrm{T}[\{\theta,\,\mathrm{d}\theta,\,\sigma\}]}{\mathrm{cM}}\right)\right)+\\
&\left(\mathrm{aM}^2\,(1-\xi\mathrm{A})\,\Omega^2\left(\frac{\pi}{2}-\mathrm{ArcTan}[\delta\,(\mathrm{d}\xi+\epsilon)]\right)\right.\\
&\left.\mathrm{Cos}\left[\mathrm{aM}\left(-\mathrm{Mf}+\mathrm{T}-\frac{\sigma}{\mathrm{cA}}\right)\right]\xi\mathrm{T}^{(\{0,0,1\})}[\{\theta,\,\mathrm{d}\theta,\,\sigma\}]\right)\Bigg/\\
&\left(\mathrm{cA}^2\,\mathrm{cp1}\,\mathrm{mw1}\,\pi\,\mathrm{R1}\left(1+\frac{\Omega\,\xi\mathrm{T}[\{\theta,\,\mathrm{d}\theta,\,\sigma\}]}{\mathrm{cA}}\right)^2\right)+\\
&\left(\mathrm{aA}^2\,\xi\mathrm{M}\,\Omega^2\left(\frac{\pi}{2}+\mathrm{ArcTan}[\delta\,(\mathrm{d}\xi-\epsilon)]\right)\right.\\
&\left.\mathrm{Cos}\left[\mathrm{aA}\left(-\mathrm{As}+\mathrm{T}-\frac{\sigma}{\mathrm{cM}}\right)\right]\xi\mathrm{T}^{(\{0,0,1\})}[\{\theta,\,\mathrm{d}\theta,\,\sigma\}]\right)\Bigg/\\
&\left(\mathrm{cM}^2\,\mathrm{cp1}\,\mathrm{mw1}\,\pi\,\mathrm{R1}\left(1+\frac{\Omega\,\xi\mathrm{T}[\{\theta,\,\mathrm{d}\theta,\,\sigma\}]}{\mathrm{cM}}\right)^2\right)+\\
&\left(2\,\Omega^2\left(\frac{\pi}{2}-\mathrm{ArcTan}[\delta\,(\mathrm{d}\xi+\epsilon)]\right)\left(\Theta+\frac{1}{2}\,\mathrm{aM}\,(1-\xi\mathrm{A})\,\Omega\,\mathrm{Sin}\left[\right.\right.\right.\\
&\left.\left.\left.\mathrm{aM}\left(-\mathrm{Mf}+\mathrm{T}-\frac{\sigma}{\mathrm{cA}}\right)\right]\right)\xi\mathrm{T}^{(\{0,0,1\})}[\{\theta,\,\mathrm{d}\theta,\,\sigma\}]^2\Bigg)\Bigg/\\
&\left(\mathrm{cA}^2\,\mathrm{cp1}\,\mathrm{mw1}\,\pi\,\mathrm{R1}\left(1+\frac{\Omega\,\xi\mathrm{T}[\{\theta,\,\mathrm{d}\theta,\,\sigma\}]}{\mathrm{cA}}\right)^3\right)+\\
&\left(2\,\Omega^2\left(\frac{\pi}{2}+\mathrm{ArcTan}[\delta\,(\mathrm{d}\xi-\epsilon)]\right)\left(\Theta+\frac{1}{2}\,\mathrm{aA}\,\xi\mathrm{M}\,\Omega\,\mathrm{Sin}\left[\right.\right.\right.\\
&\left.\left.\left.\mathrm{aA}\left(-\mathrm{As}+\mathrm{T}-\frac{\sigma}{\mathrm{cM}}\right)\right]\right)\xi\mathrm{T}^{(\{0,0,1\})}[\{\theta,\,\mathrm{d}\theta,\,\sigma\}]^2\Bigg)\Bigg/\\
&\left(\mathrm{cM}^2\,\mathrm{cp1}\,\mathrm{mw1}\,\pi\,\mathrm{R1}\left(1+\frac{\Omega\,\xi\mathrm{T}[\{\theta,\,\mathrm{d}\theta,\,\sigma\}]}{\mathrm{cM}}\right)^3\right)-\\
&\left(\Omega\left(\frac{\pi}{2}-\mathrm{ArcTan}[\delta\,(\mathrm{d}\xi+\epsilon)]\right)\left(\Theta+\frac{1}{2}\,\mathrm{aM}\,(1-\xi\mathrm{A})\,\Omega\,\mathrm{Sin}\left[\right.\right.\right.\\
&\left.\left.\left.\mathrm{aM}\left(-\mathrm{Mf}+\mathrm{T}-\frac{\sigma}{\mathrm{cA}}\right)\right]\right)\xi\mathrm{T}^{(\{0,0,2\})}[\{\theta,\,\mathrm{d}\theta,\,\sigma\}]\Bigg)\Bigg/\\
&\left(\mathrm{cA}\,\mathrm{cp1}\,\mathrm{mw1}\,\pi\,\mathrm{R1}\left(1+\frac{\Omega\,\xi\mathrm{T}[\{\theta,\,\mathrm{d}\theta,\,\sigma\}]}{\mathrm{cA}}\right)^2\right)-\\
&\left(\Omega\left(\frac{\pi}{2}+\mathrm{ArcTan}[\delta\,(\mathrm{d}\xi-\epsilon)]\right)\left(\Theta+\frac{1}{2}\,\mathrm{aA}\,\xi\mathrm{M}\,\Omega\,\mathrm{Sin}\left[\right.\right.\right.\\
&\left.\left.\left.\mathrm{aA}\left(-\mathrm{As}+\mathrm{T}-\frac{\sigma}{\mathrm{cM}}\right)\right]\right)\xi\mathrm{T}^{(\{0,0,2\})}[\{\theta,\,\mathrm{d}\theta,\,\sigma\}]\Bigg)\Bigg/\\
&\left.\left(\mathrm{cM}\,\mathrm{cp1}\,\mathrm{mw1}\,\pi\,\mathrm{R1}\left(1+\frac{\Omega\,\xi\mathrm{T}[\{\theta,\,\mathrm{d}\theta,\,\sigma\}]}{\mathrm{cM}}\right)^2\right)\right)-
\end{aligned}
$$

$$\Bigg(\left(\Theta\left(-\text{ArcTan}\left[\delta\left(d\xi-\epsilon\right)\right]+\text{ArcTan}\left[\delta\left(d\xi+\epsilon\right)\right]\right)\right)/\left(cp1\,mw1\,\pi\,R1\right)+\left(\left(\frac{\pi}{2}-\text{ArcTan}\left[\delta\left(d\xi+\epsilon\right)\right]\right)\left(\Theta+\frac{1}{2}\,aM\left(1-\xi A\right)\Omega\,\text{Sin}\left[aM\left(-Mf+T-\frac{\sigma}{cA}\right)\right]\right)\right)\Big/\left(cp1\,mw1\,\pi\,R1\left(1+\frac{\Omega\,\xi T\left[\left\{\theta,\,d\theta,\,\sigma\right\}\right]}{cA}\right)\right)+\left(\left(\frac{\pi}{2}+\text{ArcTan}\left[\delta\left(d\xi-\epsilon\right)\right]\right)\left(\Theta+\frac{1}{2}\,aA\,\xi M\,\Omega\,\text{Sin}\left[aA\left(-As+T-\frac{\sigma}{cM}\right)\right]\right)\right)\Big/\left(cp1\,mw1\,\pi\,R1\left(1+\frac{\Omega\,\xi T\left[\left\{\theta,\,d\theta,\,\sigma\right\}\right]}{cM}\right)\right)\Bigg)$$

$$\Bigg(-\left(\left(aM^3\,Aw1\,h0\left(-T+Ta\right)\left(1-\xi A\right)\Omega\left(\frac{\pi}{2}-\text{ArcTan}\left[\delta\left(d\xi+\epsilon\right)\right]\right)\text{Sin}\left[aM\left(-Mf+T-\frac{\sigma}{cA}\right)\right]\right)\Big/\left(2\,cA^2\,cp1\,mw1\,\pi\left(1+\frac{\Omega\,\xi T\left[\left\{\theta,\,d\theta,\,\sigma\right\}\right]}{cA}\right)\right)\right)-\left(aA^3\,Aw1\,h0\left(-T+Ta\right)\xi M\,\Omega\left(\frac{\pi}{2}+\text{ArcTan}\left[\delta\left(d\xi-\epsilon\right)\right]\right)\text{Sin}\left[aA\left(-As+T-\frac{\sigma}{cM}\right)\right]\right)\Big/\left(2\,cM^2\,cp1\,mw1\,\pi\left(1+\frac{\Omega\,\xi T\left[\left\{\theta,\,d\theta,\,\sigma\right\}\right]}{cM}\right)\right)+\left(aM^2\,Aw1\,h0\left(-T+Ta\right)\left(1-\xi A\right)\Omega^2\left(\frac{\pi}{2}-\text{ArcTan}\left[\delta\left(d\xi+\epsilon\right)\right]\right)\text{Cos}\left[aM\left(-Mf+T-\frac{\sigma}{cA}\right)\right]\xi T^{(\{0,0,1\})}\left[\left\{\theta,\,d\theta,\,\sigma\right\}\right]\right)\Big/\left(cA^2\,cp1\,mw1\,\pi\left(1+\frac{\Omega\,\xi T\left[\left\{\theta,\,d\theta,\,\sigma\right\}\right]}{cA}\right)^2\right)+\left(aA^2\,Aw1\,h0\left(-T+Ta\right)\xi M\,\Omega^2\left(\frac{\pi}{2}+\text{ArcTan}\left[\delta\left(d\xi-\epsilon\right)\right]\right)\text{Cos}\left[aA\left(-As+T-\frac{\sigma}{cM}\right)\right]\xi T^{(\{0,0,1\})}\left[\left\{\theta,\,d\theta,\,\sigma\right\}\right]\right)\Big/\left(cM^2\,cp1\,mw1\,\pi\left(1+\frac{\Omega\,\xi T\left[\left\{\theta,\,d\theta,\,\sigma\right\}\right]}{cM}\right)^2\right)+\left(2\,\Omega^2\left(\frac{\pi}{2}-\text{ArcTan}\left[\delta\left(d\xi+\epsilon\right)\right]\right)\left(-\frac{d\theta\,E1\,r1}{l10}+\frac{1}{cp1\,mw1}Aw1\,h0\left(-T+Ta\right)\left(\Theta+\frac{1}{2}\,aM\left(1-\xi A\right)\Omega\,\text{Sin}\left[aM\left(-Mf+T-\frac{\sigma}{cA}\right)\right]\right)\right)\xi T^{(\{0,0,1\})}\left[\left\{\theta,\,d\theta,\,\sigma\right\}\right]^2\right)\Big/\left(cA^2\,\pi\left(1+\frac{\Omega\,\xi T\left[\left\{\theta,\,d\theta,\,\sigma\right\}\right]}{cA}\right)^3\right)+\left(2\,\Omega^2\left(\frac{\pi}{2}+\text{ArcTan}\left[\delta\left(d\xi-\epsilon\right)\right]\right)\left(-\frac{d\theta\,E1\,r1}{l10}+\frac{1}{cp1\,mw1}Aw1\,h0\left(-T+Ta\right)\left(\Theta+\frac{1}{2}\,aA\,\xi M\,\Omega\,\text{Sin}\left[aA\left(-As+T-\frac{\sigma}{cM}\right)\right]\right)\right)\xi T^{(\{0,0,1\})}\left[\left\{\theta,\,d\theta,\,\sigma\right\}\right]^2\right)\Big/\left(cM^2\,\pi\left(1+\frac{\Omega\,\xi T\left[\left\{\theta,\,d\theta,\,\sigma\right\}\right]}{cM}\right)^3\right)-\left(\Omega\left(\frac{\pi}{2}-\text{ArcTan}\left[\delta\left(d\xi+\epsilon\right)\right]\right)\left(-\frac{d\theta\,E1\,r1}{l10}+\frac{1}{cp1\,mw1}Aw1\,h0\left(-T+Ta\right)\left(\Theta+\frac{1}{2}\,aM\left(1-\xi A\right)\Omega\,\text{Sin}\left[aM\left(-Mf+T-\frac{\sigma}{cA}\right)\right]\right)\right)\xi T^{(\{0,0,2\})}\left[\left\{\theta,\,d\theta,\,\sigma\right\}\right]\right)\Big/\left(cA\,\pi\left(1+\frac{\Omega\,\xi T\left[\left\{\theta,\,d\theta,\,\sigma\right\}\right]}{cA}\right)^2\right)-$$

$$\left(\Omega\left(\frac{\pi}{2}+\text{ArcTan}[\delta\ (d\xi-\epsilon)]\right)\left(-\frac{d\theta\ E1\ r1}{l10}+\frac{1}{cp1\ mw1}\right.\right.$$
$$\left.\left.Aw1\ h0\ (-T+Ta)\left(\Theta+\frac{1}{2}\,aA\,\xi M\,\Omega\,\text{Sin}\left[aA\left(-As+T-\frac{\sigma}{cM}\right)\right]\right)\right)$$
$$\left.\xi T^{(\{0,0,2\})}[\{\theta,\ d\theta,\ \sigma\}]\right)\Big/\left(cM\,\pi\left(1+\frac{\Omega\,\xi T[\{\theta,\ d\theta,\ \sigma\}]}{cM}\right)^2\right)\Bigg)+$$
$$\frac{1}{J}A1\ r1\left(-\left(\left(\Omega\left(\frac{\pi}{2}-\text{ArcTan}[\delta\ (d\xi+\epsilon)]\right)\left(\Theta+\frac{1}{2}\,aM\ (1-\xi A)\ \Omega\right.\right.\right.\right.$$
$$\left.\left.\left.\left.\text{Sin}\left[aM\left(-Mf+T-\frac{\sigma}{cA}\right)\right]\right)\xi T^{(\{0,1,0\})}[\{\theta,\ d\theta,\ \sigma\}]\right)\Big/\right.$$
$$\left.\left(cA\ cp1\ mw1\ \pi\ R1\left(1+\frac{\Omega\,\xi T[\{\theta,\ d\theta,\ \sigma\}]}{cA}\right)^2\right)\right)-$$
$$\left(\Omega\left(\frac{\pi}{2}+\text{ArcTan}[\delta\ (d\xi-\epsilon)]\right)\left(\Theta+\frac{1}{2}\,aA\,\xi M\,\Omega\,\text{Sin}\left[\right.\right.\right.$$
$$\left.\left.\left.aA\left(-As+T-\frac{\sigma}{cM}\right)\right]\right)\xi T^{(\{0,1,0\})}[\{\theta,\ d\theta,\ \sigma\}]\right)\Big/$$
$$\left(cM\ cp1\ mw1\ \pi\ R1\left(1+\frac{\Omega\,\xi T[\{\theta,\ d\theta,\ \sigma\}]}{cM}\right)^2\right)\Bigg)+\frac{1}{J}$$
$$(-(b1+bs)\ d\theta-ks\,\theta+A1\ r1\,\sigma-g\ ml\ rl\ \text{Cos}[\theta])$$
$$\left(\left(aM^2\ (1-\xi A)\ \Omega^2\left(\frac{\pi}{2}-\text{ArcTan}[\delta\ (d\xi+\epsilon)]\right)\right.\right.$$
$$\left.\left.\text{Cos}\left[aM\left(-Mf+T-\frac{\sigma}{cA}\right)\right]\xi T^{(\{0,1,0\})}[\{\theta,\ d\theta,\ \sigma\}]\right)\Big/$$
$$\left(2\ cA^2\ cp1\ mw1\ \pi\ R1\left(1+\frac{\Omega\,\xi T[\{\theta,\ d\theta,\ \sigma\}]}{cA}\right)^2\right)+$$
$$\left(aA^2\ \xi M\,\Omega^2\left(\frac{\pi}{2}+\text{ArcTan}[\delta\ (d\xi-\epsilon)]\right)\right.$$
$$\left.\text{Cos}\left[aA\left(-As+T-\frac{\sigma}{cM}\right)\right]\xi T^{(\{0,1,0\})}[\{\theta,\ d\theta,\ \sigma\}]\right)\Big/$$
$$\left(2\ cM^2\ cp1\ mw1\ \pi\ R1\left(1+\frac{\Omega\,\xi T[\{\theta,\ d\theta,\ \sigma\}]}{cM}\right)^2\right)+$$
$$\left(2\,\Omega^2\left(\frac{\pi}{2}-\text{ArcTan}[\delta\ (d\xi+\epsilon)]\right)\right.$$
$$\left(\Theta+\frac{1}{2}\,aM\ (1-\xi A)\ \Omega\,\text{Sin}\left[aM\left(-Mf+T-\frac{\sigma}{cA}\right)\right]\right)$$
$$\left.\xi T^{(\{0,0,1\})}[\{\theta,\ d\theta,\ \sigma\}]\,\xi T^{(\{0,1,0\})}[\{\theta,\ d\theta,\ \sigma\}]\right)\Big/$$
$$\left(cA^2\ cp1\ mw1\ \pi\ R1\left(1+\frac{\Omega\,\xi T[\{\theta,\ d\theta,\ \sigma\}]}{cA}\right)^3\right)+$$
$$\left(2\,\Omega^2\left(\frac{\pi}{2}+\text{ArcTan}[\delta\ (d\xi-\epsilon)]\right)\right.$$
$$\left(\Theta+\frac{1}{2}\,aA\,\xi M\,\Omega\,\text{Sin}\left[aA\left(-As+T-\frac{\sigma}{cM}\right)\right]\right)$$
$$\left.\xi T^{(\{0,0,1\})}[\{\theta,\ d\theta,\ \sigma\}]\,\xi T^{(\{0,1,0\})}[\{\theta,\ d\theta,\ \sigma\}]\right)\Big/$$
$$\left(cM^2\ cp1\ mw1\ \pi\ R1\left(1+\frac{\Omega\,\xi T[\{\theta,\ d\theta,\ \sigma\}]}{cM}\right)^3\right)-$$
$$\left(\Omega\left(\frac{\pi}{2}-\text{ArcTan}[\delta\ (d\xi+\epsilon)]\right)\left(\Theta+\frac{1}{2}\,aM\ (1-\xi A)\ \Omega\,\text{Sin}\left[\right.\right.\right.$$
$$\left.\left.\left.aM\left(-Mf+T-\frac{\sigma}{cA}\right)\right]\right)\xi T^{(\{0,1,1\})}[\{\theta,\ d\theta,\ \sigma\}]\right)\Big/$$
$$\left(cA\ cp1\ mw1\ \pi\ R1\left(1+\frac{\Omega\,\xi T[\{\theta,\ d\theta,\ \sigma\}]}{cA}\right)^2\right)-$$

$$\left(\Omega\left(\frac{\pi}{2}+\text{ArcTan}[\delta\ (\text{d}\xi-\epsilon)]\right)\left(\Theta+\frac{1}{2}\,\text{aA}\,\xi\text{M}\,\Omega\,\text{Sin}\Big[\text{aA}\left(-\text{As}+\text{T}-\frac{\sigma}{\text{cM}}\right)\Big]\right)\xi\text{T}^{(\{0,1,1\})}[\{\theta,\text{d}\theta,\sigma\}]\right)\Big/\left(\text{cM}\,\text{cp1}\,\text{mw1}\,\pi\,\text{R1}\left(1+\frac{\Omega\,\xi\text{T}[\{\theta,\text{d}\theta,\sigma\}]}{\text{cM}}\right)^2\right)+$$

$$\text{d}\theta\left(\left(\text{aM}^2\ (1-\xi\text{A})\ \Omega^2\left(\frac{\pi}{2}-\text{ArcTan}[\delta\ (\text{d}\xi+\epsilon)]\right)\text{Cos}\Big[\text{aM}\left(-\text{Mf}+\text{T}-\frac{\sigma}{\text{cA}}\right)\Big]\xi\text{T}^{(\{1,0,0\})}[\{\theta,\text{d}\theta,\sigma\}]\right)\Big/\left(2\,\text{cA}^2\,\text{cp1}\,\text{mw1}\,\pi\,\text{R1}\left(1+\frac{\Omega\,\xi\text{T}[\{\theta,\text{d}\theta,\sigma\}]}{\text{cA}}\right)^2\right)+\left(\text{aA}^2\,\xi\text{M}\,\Omega^2\left(\frac{\pi}{2}+\text{ArcTan}[\delta\ (\text{d}\xi-\epsilon)]\right)\text{Cos}\Big[\text{aA}\left(-\text{As}+\text{T}-\frac{\sigma}{\text{cM}}\right)\Big]\xi\text{T}^{(\{1,0,0\})}[\{\theta,\text{d}\theta,\sigma\}]\right)\Big/\left(2\,\text{cM}^2\,\text{cp1}\,\text{mw1}\,\pi\,\text{R1}\left(1+\frac{\Omega\,\xi\text{T}[\{\theta,\text{d}\theta,\sigma\}]}{\text{cM}}\right)^2\right)+\left(2\,\Omega^2\left(\frac{\pi}{2}-\text{ArcTan}[\delta\ (\text{d}\xi+\epsilon)]\right)\left(\Theta+\frac{1}{2}\,\text{aM}\ (1-\xi\text{A})\,\Omega\,\text{Sin}\Big[\text{aM}\left(-\text{Mf}+\text{T}-\frac{\sigma}{\text{cA}}\right)\Big]\right)\xi\text{T}^{(\{0,0,1\})}[\{\theta,\text{d}\theta,\sigma\}]\,\xi\text{T}^{(\{1,0,0\})}[\{\theta,\text{d}\theta,\sigma\}]\right)\Big/\left(\text{cA}^2\,\text{cp1}\,\text{mw1}\,\pi\,\text{R1}\left(1+\frac{\Omega\,\xi\text{T}[\{\theta,\text{d}\theta,\sigma\}]}{\text{cA}}\right)^3\right)+\left(2\,\Omega^2\left(\frac{\pi}{2}+\text{ArcTan}[\delta\ (\text{d}\xi-\epsilon)]\right)\left(\Theta+\frac{1}{2}\,\text{aA}\,\xi\text{M}\,\Omega\,\text{Sin}\Big[\text{aA}\left(-\text{As}+\text{T}-\frac{\sigma}{\text{cM}}\right)\Big]\right)\xi\text{T}^{(\{0,0,1\})}[\{\theta,\text{d}\theta,\sigma\}]\,\xi\text{T}^{(\{1,0,0\})}[\{\theta,\text{d}\theta,\sigma\}]\right)\Big/\left(\text{cM}^2\,\text{cp1}\,\text{mw1}\,\pi\,\text{R1}\left(1+\frac{\Omega\,\xi\text{T}[\{\theta,\text{d}\theta,\sigma\}]}{\text{cM}}\right)^3\right)-\left(\Omega\left(\frac{\pi}{2}-\text{ArcTan}[\delta\ (\text{d}\xi+\epsilon)]\right)\left(\Theta+\frac{1}{2}\,\text{aM}\ (1-\xi\text{A})\,\Omega\,\text{Sin}\Big[\text{aM}\left(-\text{Mf}+\text{T}-\frac{\sigma}{\text{cA}}\right)\Big]\right)\xi\text{T}^{(\{1,0,1\})}[\{\theta,\text{d}\theta,\sigma\}]\right)\Big/\left(\text{cA}\,\text{cp1}\,\text{mw1}\,\pi\,\text{R1}\left(1+\frac{\Omega\,\xi\text{T}[\{\theta,\text{d}\theta,\sigma\}]}{\text{cA}}\right)^2\right)-\left(\Omega\left(\frac{\pi}{2}+\text{ArcTan}[\delta\ (\text{d}\xi-\epsilon)]\right)\left(\Theta+\frac{1}{2}\,\text{aA}\,\xi\text{M}\,\Omega\,\text{Sin}\Big[\text{aA}\left(-\text{As}+\text{T}-\frac{\sigma}{\text{cM}}\right)\Big]\right)\xi\text{T}^{(\{1,0,1\})}[\{\theta,\text{d}\theta,\sigma\}]\right)\Big/\left(\text{cM}\,\text{cp1}\,\text{mw1}\,\pi\,\text{R1}\left(1+\frac{\Omega\,\xi\text{T}[\{\theta,\text{d}\theta,\sigma\}]}{\text{cM}}\right)^2\right)\right)\right)+$$

$$\frac{1}{\text{J}}(-(\text{b1}+\text{bs})\ \text{d}\theta-\text{ks}\,\Theta+\text{A1}\ \text{r1}\,\sigma-\text{g}\,\text{ml}\,\text{rl}\,\text{Cos}[\theta])$$

$$\left(\frac{1}{\text{J}}\right.$$

$$(-\text{b1}-\text{bs})$$

$$\left(-\left(\left(\Omega\left(\frac{\pi}{2}-\text{ArcTan}[\delta\ (\text{d}\xi+\epsilon)]\right)\left(\Theta+\frac{1}{2}\,\text{aM}\ (1-\xi\text{A})\ \Omega\right.\right.\right.\right.$$
$$\left.\left.\left.\text{Sin}\left[\text{aM}\left(-\text{Mf}+\text{T}-\frac{\sigma}{\text{cA}}\right)\right]\right)\xi\text{T}^{(\{0,1,0\})}[\{\theta,\ \text{d}\theta,\ \sigma\}]\right)\Big/$$
$$\left.\left.\left(\text{cA}\ \text{cp1}\ \text{mw1}\ \pi\ \text{R1}\left(1+\frac{\Omega\,\xi\text{T}[\{\theta,\ \text{d}\theta,\ \sigma\}]}{\text{cA}}\right)^2\right)\right)-$$
$$\left(\Omega\left(\frac{\pi}{2}+\text{ArcTan}[\delta\ (\text{d}\xi-\epsilon)]\right)\left(\Theta+\frac{1}{2}\,\text{aA}\,\xi\text{M}\,\Omega\,\text{Sin}\right.\right.$$
$$\left.\left.\left[\text{aA}\left(-\text{As}+\text{T}-\frac{\sigma}{\text{cM}}\right)\right]\right)\xi\text{T}^{(\{0,1,0\})}[\{\theta,\ \text{d}\theta,\ \sigma\}]\right)\Big/$$
$$\left.\left(\text{cM}\ \text{cp1}\ \text{mw1}\ \pi\ \text{R1}\left(1+\frac{\Omega\,\xi\text{T}[\{\theta,\ \text{d}\theta,\ \sigma\}]}{\text{cM}}\right)^2\right)\right)-$$
$$\left(-\left(\left(\text{aM}^2\ \text{Aw1}\ \text{h0}\ (-\text{T}+\text{Ta})\ (1-\xi\text{A})\ \Omega\left(\frac{\pi}{2}-\text{ArcTan}[\delta\ (\text{d}\xi+\epsilon)]\right)\right.\right.\right.$$
$$\left.\left.\left.\text{Cos}\left[\text{aM}\left(-\text{Mf}+\text{T}-\frac{\sigma}{\text{cA}}\right)\right]\right)\Big/$$
$$\left.\left.\left(2\ \text{cA}\ \text{cp1}\ \text{mw1}\ \pi\left(1+\frac{\Omega\,\xi\text{T}[\{\theta,\ \text{d}\theta,\ \sigma\}]}{\text{cA}}\right)\right)\right)-$$
$$\left(\text{aA}^2\ \text{Aw1}\ \text{h0}\ (-\text{T}+\text{Ta})\ \xi\text{M}\,\Omega\left(\frac{\pi}{2}+\text{ArcTan}[\delta\ (\text{d}\xi-\epsilon)]\right)\right.$$
$$\left.\text{Cos}\left[\text{aA}\left(-\text{As}+\text{T}-\frac{\sigma}{\text{cM}}\right)\right]\right)\Big/$$
$$\left(2\ \text{cM}\ \text{cp1}\ \text{mw1}\ \pi\left(1+\frac{\Omega\,\xi\text{T}[\{\theta,\ \text{d}\theta,\ \sigma\}]}{\text{cM}}\right)\right)-$$
$$\left(\Omega\left(\frac{\pi}{2}-\text{ArcTan}[\delta\ (\text{d}\xi+\epsilon)]\right)\left(-\frac{\text{d}\theta\ \text{E1}\ \text{r1}}{\text{l10}}+\frac{1}{\text{cp1}\ \text{mw1}}\text{Aw1}\ \text{h0}\right.\right.$$
$$\left.\left.(-\text{T}+\text{Ta})\left(\Theta+\frac{1}{2}\,\text{aM}\ (1-\xi\text{A})\ \Omega\,\text{Sin}\left[\text{aM}\left(-\text{Mf}+\text{T}-\frac{\sigma}{\text{cA}}\right)\right]\right)\right)$$
$$\left.\xi\text{T}^{(\{0,0,1\})}[\{\theta,\ \text{d}\theta,\ \sigma\}]\right)\Big/\left(\text{cA}\,\pi\left(1+\frac{\Omega\,\xi\text{T}[\{\theta,\ \text{d}\theta,\ \sigma\}]}{\text{cA}}\right)^2\right)-$$
$$\left(\Omega\left(\frac{\pi}{2}+\text{ArcTan}[\delta\ (\text{d}\xi-\epsilon)]\right)\left(-\frac{\text{d}\theta\ \text{E1}\ \text{r1}}{\text{l10}}+\frac{1}{\text{cp1}\ \text{mw1}}\right.\right.$$
$$\left.\left.\text{Aw1}\ \text{h0}\ (-\text{T}+\text{Ta})\left(\Theta+\frac{1}{2}\,\text{aA}\,\xi\text{M}\,\Omega\,\text{Sin}\left[\text{aA}\left(-\text{As}+\text{T}-\frac{\sigma}{\text{cM}}\right)\right]\right)\right)$$
$$\left.\xi\text{T}^{(\{0,0,1\})}[\{\theta,\ \text{d}\theta,\ \sigma\}]\right)\Big/\left(\text{cM}\,\pi\left(1+\frac{\Omega\,\xi\text{T}[\{\theta,\ \text{d}\theta,\ \sigma\}]}{\text{cM}}\right)^2\right)\Big)$$
$$\left(-\left(\left(\Omega\left(\frac{\pi}{2}-\text{ArcTan}[\delta\ (\text{d}\xi+\epsilon)]\right)\left(\Theta+\frac{1}{2}\,\text{aM}\ (1-\xi\text{A})\ \Omega\right.\right.\right.\right.$$
$$\left.\left.\left.\text{Sin}\left[\text{aM}\left(-\text{Mf}+\text{T}-\frac{\sigma}{\text{cA}}\right)\right]\right)\xi\text{T}^{(\{0,1,0\})}[\{\theta,\ \text{d}\theta,\ \sigma\}]\right)\Big/$$
$$\left.\left.\left(\text{cA}\ \text{cp1}\ \text{mw1}\ \pi\ \text{R1}\left(1+\frac{\Omega\,\xi\text{T}[\{\theta,\ \text{d}\theta,\ \sigma\}]}{\text{cA}}\right)^2\right)\right)-$$
$$\left(\Omega\left(\frac{\pi}{2}+\text{ArcTan}[\delta\ (\text{d}\xi-\epsilon)]\right)\left(\Theta+\frac{1}{2}\,\text{aA}\,\xi\text{M}\,\Omega\,\text{Sin}\right.\right.$$
$$\left.\left.\left[\text{aA}\left(-\text{As}+\text{T}-\frac{\sigma}{\text{cM}}\right)\right]\right)\xi\text{T}^{(\{0,1,0\})}[\{\theta,\ \text{d}\theta,\ \sigma\}]\right)\Big/$$
$$\left.\left(\text{cM}\ \text{cp1}\ \text{mw1}\ \pi\ \text{R1}\left(1+\frac{\Omega\,\xi\text{T}[\{\theta,\ \text{d}\theta,\ \sigma\}]}{\text{cM}}\right)^2\right)\right)+$$
$$\left(-\left(\left(\text{aM}^2\ (1-\xi\text{A})\ \Omega\left(\frac{\pi}{2}-\text{ArcTan}[\delta\ (\text{d}\xi+\epsilon)]\right)\text{Cos}\left[\text{aM}\left(-\text{Mf}+\text{T}-\right.\right.\right.\right.\right.$$
$$\left.\left.\left.\left.\left.\frac{\sigma}{\text{cA}}\right)\right]\right)\Big/\left(2\ \text{cA}\ \text{cp1}\ \text{mw1}\ \pi\ \text{R1}\left(1+\frac{\Omega\,\xi\text{T}[\{\theta,\ \text{d}\theta,\ \sigma\}]}{\text{cA}}\right)\right)\right)-$$
$$\left(\text{aA}^2\ \xi\text{M}\,\Omega\left(\frac{\pi}{2}+\text{ArcTan}[\delta\ (\text{d}\xi-\epsilon)]\right)\text{Cos}\left[\text{aA}\left(-\text{As}+\text{T}-\frac{\sigma}{\text{cM}}\right)\right]\right)\Big/$$

$$\left(2\,\text{cM}\,\text{cp1}\,\text{mw1}\,\pi\,\text{R1}\left(1+\frac{\Omega\,\xi\text{T}[\{\theta,\,\text{d}\theta,\,\sigma\}]}{\text{cM}}\right)\right)-$$
$$\left(\Omega\left(\frac{\pi}{2}-\text{ArcTan}[\delta\,(\text{d}\xi+\epsilon)]\right)\left(\Theta+\frac{1}{2}\,\text{aM}\,(1-\xi\text{A})\,\Omega\,\text{Sin}\Big[\right.\right.$$
$$\left.\left.\text{aM}\left(-\text{Mf}+\text{T}-\frac{\sigma}{\text{cA}}\right)\Big]\right)\xi\text{T}^{(\{0,0,1\})}[\{\theta,\,\text{d}\theta,\,\sigma\}]\right)\Big/$$
$$\left(\text{cA}\,\text{cp1}\,\text{mw1}\,\pi\,\text{R1}\left(1+\frac{\Omega\,\xi\text{T}[\{\theta,\,\text{d}\theta,\,\sigma\}]}{\text{cA}}\right)^2\right)-$$
$$\left(\Omega\left(\frac{\pi}{2}+\text{ArcTan}[\delta\,(\text{d}\xi-\epsilon)]\right)\left(\Theta+\frac{1}{2}\,\text{aA}\,\xi\text{M}\,\Omega\,\text{Sin}\Big[\right.\right.$$
$$\left.\left.\text{aA}\left(-\text{As}+\text{T}-\frac{\sigma}{\text{cM}}\right)\Big]\right)\xi\text{T}^{(\{0,0,1\})}[\{\theta,\,\text{d}\theta,\,\sigma\}]\right)\Big/$$
$$\left(\text{cM}\,\text{cp1}\,\text{mw1}\,\pi\,\text{R1}\left(1+\frac{\Omega\,\xi\text{T}[\{\theta,\,\text{d}\theta,\,\sigma\}]}{\text{cM}}\right)^2\right)\Bigg)$$
$$\Bigg(-\frac{1}{\text{l10}\,\pi}\text{E1}\,\text{r1}\,(-\text{ArcTan}[\delta\,(\text{d}\xi-\epsilon)]+\text{ArcTan}[\delta\,(\text{d}\xi+\epsilon)])-$$
$$\frac{\text{E1}\,\text{r1}\left(\frac{\pi}{2}-\text{ArcTan}[\delta\,(\text{d}\xi+\epsilon)]\right)}{\text{l10}\,\pi\left(1+\frac{\Omega\,\xi\text{T}[\{\theta,\text{d}\theta,\sigma\}]}{\text{cA}}\right)}-\frac{\text{E1}\,\text{r1}\left(\frac{\pi}{2}+\text{ArcTan}[\delta\,(\text{d}\xi-\epsilon)]\right)}{\text{l10}\,\pi\left(1+\frac{\Omega\,\xi\text{T}[\{\theta,\text{d}\theta,\sigma\}]}{\text{cM}}\right)}-$$
$$\left(\Omega\left(\frac{\pi}{2}-\text{ArcTan}[\delta\,(\text{d}\xi+\epsilon)]\right)\left(-\frac{\text{d}\theta\,\text{E1}\,\text{r1}}{\text{l10}}+\frac{1}{\text{cp1}\,\text{mw1}}\text{Aw1}\,\text{h0}\right.\right.$$
$$\left.\left.(-\text{T}+\text{Ta})\left(\Theta+\frac{1}{2}\,\text{aM}\,(1-\xi\text{A})\,\Omega\,\text{Sin}\Big[\text{aM}\left(-\text{Mf}+\text{T}-\frac{\sigma}{\text{cA}}\right)\Big]\right)\right)$$
$$\xi\text{T}^{(\{0,1,0\})}[\{\theta,\,\text{d}\theta,\,\sigma\}]\Big)\Big/\left(\text{cA}\,\pi\left(1+\frac{\Omega\,\xi\text{T}[\{\theta,\,\text{d}\theta,\,\sigma\}]}{\text{cA}}\right)^2\right)-$$
$$\left(\Omega\left(\frac{\pi}{2}+\text{ArcTan}[\delta\,(\text{d}\xi-\epsilon)]\right)\left(-\frac{\text{d}\theta\,\text{E1}\,\text{r1}}{\text{l10}}+\frac{1}{\text{cp1}\,\text{mw1}}\right.\right.$$
$$\left.\left.\text{Aw1}\,\text{h0}\,(-\text{T}+\text{Ta})\left(\Theta+\frac{1}{2}\,\text{aA}\,\xi\text{M}\,\Omega\,\text{Sin}\Big[\text{aA}\left(-\text{As}+\text{T}-\frac{\sigma}{\text{cM}}\right)\Big]\right)\right)$$
$$\xi\text{T}^{(\{0,1,0\})}[\{\theta,\,\text{d}\theta,\,\sigma\}]\Big)\Big/\left(\text{cM}\,\pi\left(1+\frac{\Omega\,\xi\text{T}[\{\theta,\,\text{d}\theta,\,\sigma\}]}{\text{cM}}\right)^2\right)\Bigg)+$$
$$\left(\frac{1}{\pi}\left(-\frac{\text{d}\theta\,\text{E1}\,\text{r1}}{\text{l10}}+\frac{\text{Aw1}\,\text{h0}\,(-\text{T}+\text{Ta})\,\Theta}{\text{cp1}\,\text{mw1}}\right)(-\text{ArcTan}[\delta\,(\text{d}\xi-\epsilon)]+\right.$$
$$\left.\text{ArcTan}[\delta\,(\text{d}\xi+\epsilon)])+$$
$$\left(\left(\frac{\pi}{2}-\text{ArcTan}[\delta\,(\text{d}\xi+\epsilon)]\right)\left(-\frac{\text{d}\theta\,\text{E1}\,\text{r1}}{\text{l10}}+\frac{1}{\text{cp1}\,\text{mw1}}\text{Aw1}\,\text{h0}\right.\right.$$
$$\left.\left.(-\text{T}+\text{Ta})\left(\Theta+\frac{1}{2}\,\text{aM}\,(1-\xi\text{A})\,\Omega\,\text{Sin}\Big[\text{aM}\left(-\text{Mf}+\text{T}-\frac{\sigma}{\text{cA}}\right)\Big]\right)\right)\Big)\Big/$$
$$\left(\pi\left(1+\frac{\Omega\,\xi\text{T}[\{\theta,\,\text{d}\theta,\,\sigma\}]}{\text{cA}}\right)\right)+\left(\left(\frac{\pi}{2}+\text{ArcTan}[\delta\,(\text{d}\xi-\epsilon)]\right)\right.$$
$$\left(-\frac{\text{d}\theta\,\text{E1}\,\text{r1}}{\text{l10}}+\frac{1}{\text{cp1}\,\text{mw1}}\text{Aw1}\,\text{h0}\,(-\text{T}+\text{Ta})\left(\Theta+\frac{1}{2}\,\text{aA}\,\xi\text{M}\,\Omega\,\text{Sin}\Big[\right.\right.$$
$$\left.\left.\left.\text{aA}\left(-\text{As}+\text{T}-\frac{\sigma}{\text{cM}}\right)\Big]\right)\right)\Big)\Big/\left(\pi\left(1+\frac{\Omega\,\xi\text{T}[\{\theta,\,\text{d}\theta,\,\sigma\}]}{\text{cM}}\right)\right)\Big)$$
$$\left(\left(\text{aM}^2\,(1-\xi\text{A})\,\Omega^2\left(\frac{\pi}{2}-\text{ArcTan}[\delta\,(\text{d}\xi+\epsilon)]\right)\text{Cos}\Big[\text{aM}\left(-\text{Mf}+\text{T}-\frac{\sigma}{\text{cA}}\right)\Big]\right.\right.$$
$$\left.\xi\text{T}^{(\{0,1,0\})}[\{\theta,\,\text{d}\theta,\,\sigma\}]\right)\Big/$$
$$\left(2\,\text{cA}^2\,\text{cp1}\,\text{mw1}\,\pi\,\text{R1}\left(1+\frac{\Omega\,\xi\text{T}[\{\theta,\,\text{d}\theta,\,\sigma\}]}{\text{cA}}\right)^2\right)+$$

$$\left(aA^2\ \xi M\ \Omega^2\ \left(\frac{\pi}{2}+\text{ArcTan}[\delta\ (d\xi-\epsilon)]\right)\right.$$
$$\left.\text{Cos}\left[aA\ \left(-As+T-\frac{\sigma}{cM}\right)\right]\ \xi T^{(\{0,1,0\})}[\{\theta,\ d\theta,\ \sigma\}]\right)\Big/$$
$$\left(2\ cM^2\ cp1\ mw1\ \pi\ R1\ \left(1+\frac{\Omega\ \xi T[\{\theta,\ d\theta,\ \sigma\}]}{cM}\right)^2\right)+$$
$$\left(2\ \Omega^2\ \left(\frac{\pi}{2}-\text{ArcTan}[\delta\ (d\xi+\epsilon)]\right)\right.$$
$$\left(\Theta+\frac{1}{2}\ aM\ (1-\xi A)\ \Omega\ \text{Sin}\left[aM\ \left(-Mf+T-\frac{\sigma}{cA}\right)\right]\right)$$
$$\left.\xi T^{(\{0,0,1\})}[\{\theta,\ d\theta,\ \sigma\}]\ \xi T^{(\{0,1,0\})}[\{\theta,\ d\theta,\ \sigma\}]\right)\Big/$$
$$\left(cA^2\ cp1\ mw1\ \pi\ R1\ \left(1+\frac{\Omega\ \xi T[\{\theta,\ d\theta,\ \sigma\}]}{cA}\right)^3\right)+$$
$$\left(2\ \Omega^2\ \left(\frac{\pi}{2}+\text{ArcTan}[\delta\ (d\xi-\epsilon)]\right)\right.$$
$$\left(\Theta+\frac{1}{2}\ aA\ \xi M\ \Omega\ \text{Sin}\left[aA\ \left(-As+T-\frac{\sigma}{cM}\right)\right]\right)$$
$$\left.\xi T^{(\{0,0,1\})}[\{\theta,\ d\theta,\ \sigma\}]\ \xi T^{(\{0,1,0\})}[\{\theta,\ d\theta,\ \sigma\}]\right)\Big/$$
$$\left(cM^2\ cp1\ mw1\ \pi\ R1\ \left(1+\frac{\Omega\ \xi T[\{\theta,\ d\theta,\ \sigma\}]}{cM}\right)^3\right)-$$
$$\left(\Omega\ \left(\frac{\pi}{2}-\text{ArcTan}[\delta\ (d\xi+\epsilon)]\right)\ \left(\Theta+\frac{1}{2}\ aM\ (1-\xi A)\ \Omega\ \text{Sin}\left[\right.\right.\right.$$
$$\left.\left.\left.aM\ \left(-Mf+T-\frac{\sigma}{cA}\right)\right]\right)\ \xi T^{(\{0,1,1\})}[\{\theta,\ d\theta,\ \sigma\}]\right)\Big/$$
$$\left(cA\ cp1\ mw1\ \pi\ R1\ \left(1+\frac{\Omega\ \xi T[\{\theta,\ d\theta,\ \sigma\}]}{cA}\right)^2\right)-$$
$$\left(\Omega\ \left(\frac{\pi}{2}+\text{ArcTan}[\delta\ (d\xi-\epsilon)]\right)\ \left(\Theta+\frac{1}{2}\ aA\ \xi M\ \Omega\ \text{Sin}\left[\right.\right.\right.$$
$$\left.\left.\left.aA\ \left(-As+T-\frac{\sigma}{cM}\right)\right]\right)\ \xi T^{(\{0,1,1\})}[\{\theta,\ d\theta,\ \sigma\}]\right)\Big/$$
$$\left.\left(cM\ cp1\ mw1\ \pi\ R1\ \left(1+\frac{\Omega\ \xi T[\{\theta,\ d\theta,\ \sigma\}]}{cM}\right)^2\right)\right)-$$
$$\left((\Theta\ (-\text{ArcTan}[\delta\ (d\xi-\epsilon)]+\text{ArcTan}[\delta\ (d\xi+\epsilon)]))\ /\ (cp1\ mw1\ \pi\ R1)+\right.$$
$$\left(\left(\frac{\pi}{2}-\text{ArcTan}[\delta\ (d\xi+\epsilon)]\right)\right.$$
$$\left.\left(\Theta+\frac{1}{2}\ aM\ (1-\xi A)\ \Omega\ \text{Sin}\left[aM\ \left(-Mf+T-\frac{\sigma}{cA}\right)\right]\right)\right)\Big/$$
$$\left(cp1\ mw1\ \pi\ R1\ \left(1+\frac{\Omega\ \xi T[\{\theta,\ d\theta,\ \sigma\}]}{cA}\right)\right)+$$
$$\left(\left(\frac{\pi}{2}+\text{ArcTan}[\delta\ (d\xi-\epsilon)]\right)\right.$$
$$\left.\left(\Theta+\frac{1}{2}\ aA\ \xi M\ \Omega\ \text{Sin}\left[aA\ \left(-As+T-\frac{\sigma}{cM}\right)\right]\right)\right)\Big/$$
$$\left.\left(cp1\ mw1\ \pi\ R1\ \left(1+\frac{\Omega\ \xi T[\{\theta,\ d\theta,\ \sigma\}]}{cM}\right)\right)\right)$$
$$\left(\left(E1\ r1\ \Omega\ \left(\frac{\pi}{2}-\text{ArcTan}[\delta\ (d\xi+\epsilon)]\right)\ \xi T^{(\{0,0,1\})}[\{\theta,\ d\theta,\ \sigma\}]\right)\Big/\right.$$
$$\left(cA\ l10\ \pi\ \left(1+\frac{\Omega\ \xi T[\{\theta,\ d\theta,\ \sigma\}]}{cA}\right)^2\right)+$$

$$\left(\text{E1 r1}\,\Omega\left(\frac{\pi}{2}+\text{ArcTan}[\delta\,(\text{d}\xi-\epsilon)]\right)\xi\text{T}^{(\{0,0,1\})}[\{\theta,\text{d}\theta,\sigma\}]\right)\Big/$$
$$\left(\text{cM l10}\,\pi\left(1+\frac{\Omega\,\xi\text{T}[\{\theta,\text{d}\theta,\sigma\}]}{\text{cM}}\right)^2\right)+$$
$$\left(\text{aM}^2\,\text{Aw1 h0}\,(-\text{T}+\text{Ta})\,(1-\xi\text{A})\,\Omega^2\left(\frac{\pi}{2}-\text{ArcTan}[\delta\,(\text{d}\xi+\epsilon)]\right)\right.$$
$$\left.\text{Cos}\left[\text{aM}\left(-\text{Mf}+\text{T}-\frac{\sigma}{\text{cA}}\right)\right]\xi\text{T}^{(\{0,1,0\})}[\{\theta,\text{d}\theta,\sigma\}]\right)\Big/$$
$$\left(2\,\text{cA}^2\,\text{cp1 mw1}\,\pi\left(1+\frac{\Omega\,\xi\text{T}[\{\theta,\text{d}\theta,\sigma\}]}{\text{cA}}\right)^2\right)+$$
$$\left(\text{aA}^2\,\text{Aw1 h0}\,(-\text{T}+\text{Ta})\,\xi\text{M}\,\Omega^2\left(\frac{\pi}{2}+\text{ArcTan}[\delta\,(\text{d}\xi-\epsilon)]\right)\right.$$
$$\left.\text{Cos}\left[\text{aA}\left(-\text{As}+\text{T}-\frac{\sigma}{\text{cM}}\right)\right]\xi\text{T}^{(\{0,1,0\})}[\{\theta,\text{d}\theta,\sigma\}]\right)\Big/$$
$$\left(2\,\text{cM}^2\,\text{cp1 mw1}\,\pi\left(1+\frac{\Omega\,\xi\text{T}[\{\theta,\text{d}\theta,\sigma\}]}{\text{cM}}\right)^2\right)+$$
$$\frac{1}{\text{cA}^2\,\pi\left(1+\frac{\Omega\,\xi\text{T}[\{\theta,\text{d}\theta,\sigma\}]}{\text{cA}}\right)^3}$$
$$2\,\Omega^2\left(\frac{\pi}{2}-\text{ArcTan}[\delta\,(\text{d}\xi+\epsilon)]\right)\left(-\frac{\text{d}\theta\,\text{E1 r1}}{\text{l10}}+\frac{1}{\text{cp1 mw1}}\right.$$
$$\left.\text{Aw1 h0}\,(-\text{T}+\text{Ta})\left(\Theta+\frac{1}{2}\,\text{aM}\,(1-\xi\text{A})\,\Omega\,\text{Sin}\left[\text{aM}\left(-\text{Mf}+\text{T}-\frac{\sigma}{\text{cA}}\right)\right]\right)\right)$$
$$\xi\text{T}^{(\{0,0,1\})}[\{\theta,\text{d}\theta,\sigma\}]\,\xi\text{T}^{(\{0,1,0\})}[\{\theta,\text{d}\theta,\sigma\}]+$$
$$\frac{1}{\text{cM}^2\,\pi\left(1+\frac{\Omega\,\xi\text{T}[\{\theta,\text{d}\theta,\sigma\}]}{\text{cM}}\right)^3}$$
$$2\,\Omega^2\left(\frac{\pi}{2}+\text{ArcTan}[\delta\,(\text{d}\xi-\epsilon)]\right)\left(-\frac{\text{d}\theta\,\text{E1 r1}}{\text{l10}}+\frac{1}{\text{cp1 mw1}}\right.$$
$$\left.\text{Aw1 h0}\,(-\text{T}+\text{Ta})\left(\Theta+\frac{1}{2}\,\text{aA}\,\xi\text{M}\,\Omega\,\text{Sin}\left[\text{aA}\left(-\text{As}+\text{T}-\frac{\sigma}{\text{cM}}\right)\right]\right)\right)$$
$$\xi\text{T}^{(\{0,0,1\})}[\{\theta,\text{d}\theta,\sigma\}]\,\xi\text{T}^{(\{0,1,0\})}[\{\theta,\text{d}\theta,\sigma\}]-$$
$$\left(\Omega\left(\frac{\pi}{2}-\text{ArcTan}[\delta\,(\text{d}\xi+\epsilon)]\right)\left(-\frac{\text{d}\theta\,\text{E1 r1}}{\text{l10}}+\frac{1}{\text{cp1 mw1}}\text{Aw1 h0}\right.\right.$$
$$\left.(-\text{T}+\text{Ta})\left(\Theta+\frac{1}{2}\,\text{aM}\,(1-\xi\text{A})\,\Omega\,\text{Sin}\left[\text{aM}\left(-\text{Mf}+\text{T}-\frac{\sigma}{\text{cA}}\right)\right]\right)\right)$$
$$\left.\xi\text{T}^{(\{0,1,1\})}[\{\theta,\text{d}\theta,\sigma\}]\right)\Big/\left(\text{cA}\,\pi\left(1+\frac{\Omega\,\xi\text{T}[\{\theta,\text{d}\theta,\sigma\}]}{\text{cA}}\right)^2\right)-$$
$$\left(\Omega\left(\frac{\pi}{2}+\text{ArcTan}[\delta\,(\text{d}\xi-\epsilon)]\right)\left(-\frac{\text{d}\theta\,\text{E1 r1}}{\text{l10}}+\frac{1}{\text{cp1 mw1}}\right.\right.$$
$$\left.\text{Aw1 h0}\,(-\text{T}+\text{Ta})\left(\Theta+\frac{1}{2}\,\text{aA}\,\xi\text{M}\,\Omega\,\text{Sin}\left[\text{aA}\left(-\text{As}+\text{T}-\frac{\sigma}{\text{cM}}\right)\right]\right)\right)$$
$$\left.\left.\xi\text{T}^{(\{0,1,1\})}[\{\theta,\text{d}\theta,\sigma\}]\right)\Big/\left(\text{cM}\,\pi\left(1+\frac{\Omega\,\xi\text{T}[\{\theta,\text{d}\theta,\sigma\}]}{\text{cM}}\right)^2\right)\right)+$$
$$\frac{1}{\text{J}}(-(\text{b1}+\text{bs})\,\text{d}\theta-\text{ks}\,\theta+\text{A1 r1}\,\sigma-\text{g ml rl Cos}[\theta])$$
$$\left(\left(2\,\Omega^2\left(\frac{\pi}{2}-\text{ArcTan}[\delta\,(\text{d}\xi+\epsilon)]\right)\left(\Theta+\frac{1}{2}\,\text{aM}\,(1-\xi\text{A})\,\Omega\,\text{Sin}\left[\right.\right.\right.\right.$$
$$\left.\left.\left.\left.\text{aM}\left(-\text{Mf}+\text{T}-\frac{\sigma}{\text{cA}}\right)\right]\right)\xi\text{T}^{(\{0,1,0\})}[\{\theta,\text{d}\theta,\sigma\}]^2\right)\Big/$$
$$\left(\text{cA}^2\,\text{cp1 mw1}\,\pi\,\text{R1}\left(1+\frac{\Omega\,\xi\text{T}[\{\theta,\text{d}\theta,\sigma\}]}{\text{cA}}\right)^3\right)+$$

$$\left(2\,\Omega^2\,\left(\frac{\pi}{2}+\text{ArcTan}[\delta\,(d\xi-\epsilon)]\right)\,\left(\Theta+\frac{1}{2}\,aA\,\xi M\,\Omega\,\text{Sin}\Big[aA\,\left(-As+T-\frac{\sigma}{cM}\right)\Big]\right)\,\xi T^{(\{0,1,0\})}[\{\theta,\,d\theta,\,\sigma\}]^2\right)\Big/\left(cM^2\,cp1\,mw1\,\pi\,R1\,\left(1+\frac{\Omega\,\xi T[\{\theta,\,d\theta,\,\sigma\}]}{cM}\right)^3\right)-\left(\Omega\,\left(\frac{\pi}{2}-\text{ArcTan}[\delta\,(d\xi+\epsilon)]\right)\,\left(\Theta+\frac{1}{2}\,aM\,(1-\xi A)\,\Omega\,\text{Sin}\Big[aM\,\left(-Mf+T-\frac{\sigma}{cA}\right)\Big]\right)\,\xi T^{(\{0,2,0\})}[\{\theta,\,d\theta,\,\sigma\}]\right)\Big/\left(cA\,cp1\,mw1\,\pi\,R1\,\left(1+\frac{\Omega\,\xi T[\{\theta,\,d\theta,\,\sigma\}]}{cA}\right)^2\right)-\left(\Omega\,\left(\frac{\pi}{2}+\text{ArcTan}[\delta\,(d\xi-\epsilon)]\right)\,\left(\Theta+\frac{1}{2}\,aA\,\xi M\,\Omega\,\text{Sin}\Big[aA\,\left(-As+T-\frac{\sigma}{cM}\right)\Big]\right)\,\xi T^{(\{0,2,0\})}[\{\theta,\,d\theta,\,\sigma\}]\right)\Big/\left(cM\,cp1\,mw1\,\pi\,R1\,\left(1+\frac{\Omega\,\xi T[\{\theta,\,d\theta,\,\sigma\}]}{cM}\right)^2\right)\right)-\left(\Omega\,\left(\frac{\pi}{2}-\text{ArcTan}[\delta\,(d\xi+\epsilon)]\right)\,\left(\Theta+\frac{1}{2}\,aM\,(1-\xi A)\,\Omega\,\text{Sin}\Big[aM\,\left(-Mf+T-\frac{\sigma}{cA}\right)\Big]\right)\,\xi T^{(\{1,0,0\})}[\{\theta,\,d\theta,\,\sigma\}]\right)\Big/\left(cA\,cp1\,mw1\,\pi\,R1\,\left(1+\frac{\Omega\,\xi T[\{\theta,\,d\theta,\,\sigma\}]}{cA}\right)^2\right)-\left(\Omega\,\left(\frac{\pi}{2}+\text{ArcTan}[\delta\,(d\xi-\epsilon)]\right)\,\left(\Theta+\frac{1}{2}\,aA\,\xi M\,\Omega\,\text{Sin}\Big[aA\,\left(-As+T-\frac{\sigma}{cM}\right)\Big]\right)\,\xi T^{(\{1,0,0\})}[\{\theta,\,d\theta,\,\sigma\}]\right)\Big/\left(cM\,cp1\,mw1\,\pi\,R1\,\left(1+\frac{\Omega\,\xi T[\{\theta,\,d\theta,\,\sigma\}]}{cM}\right)^2\right)+d\theta\,\left(\left(2\,\Omega^2\,\left(\frac{\pi}{2}-\text{ArcTan}[\delta\,(d\xi+\epsilon)]\right)\,\left(\Theta+\frac{1}{2}\,aM\,(1-\xi A)\,\Omega\,\text{Sin}\Big[aM\,\left(-Mf+T-\frac{\sigma}{cA}\right)\Big]\right)\,\xi T^{(\{0,1,0\})}[\{\theta,\,d\theta,\,\sigma\}]\,\xi T^{(\{1,0,0\})}[\{\theta,\,d\theta,\,\sigma\}]\right)\Big/\left(cA^2\,cp1\,mw1\,\pi\,R1\,\left(1+\frac{\Omega\,\xi T[\{\theta,\,d\theta,\,\sigma\}]}{cA}\right)^3\right)+\left(2\,\Omega^2\,\left(\frac{\pi}{2}+\text{ArcTan}[\delta\,(d\xi-\epsilon)]\right)\,\left(\Theta+\frac{1}{2}\,aA\,\xi M\,\Omega\,\text{Sin}\Big[aA\,\left(-As+T-\frac{\sigma}{cM}\right)\Big]\right)\,\xi T^{(\{0,1,0\})}[\{\theta,\,d\theta,\,\sigma\}]\,\xi T^{(\{1,0,0\})}[\{\theta,\,d\theta,\,\sigma\}]\right)\Big/\left(cM^2\,cp1\,mw1\,\pi\,R1\,\left(1+\frac{\Omega\,\xi T[\{\theta,\,d\theta,\,\sigma\}]}{cM}\right)^3\right)-\left(\Omega\,\left(\frac{\pi}{2}-\text{ArcTan}[\delta\,(d\xi+\epsilon)]\right)\,\left(\Theta+\frac{1}{2}\,aM\,(1-\xi A)\,\Omega\,\text{Sin}\Big[aM\,\left(-Mf+T-\frac{\sigma}{cA}\right)\Big]\right)\,\xi T^{(\{1,1,0\})}[\{\theta,\,d\theta,\,\sigma\}]\right)\Big/\left(cA\,cp1\,mw1\,\pi\,R1\,\left(1+\frac{\Omega\,\xi T[\{\theta,\,d\theta,\,\sigma\}]}{cA}\right)^2\right)-\left(\Omega\,\left(\frac{\pi}{2}+\text{ArcTan}[\delta\,(d\xi-\epsilon)]\right)\,\left(\Theta+\frac{1}{2}\,aA\,\xi M\,\Omega\,\text{Sin}\Big[$$

```
aA (-As + T - σ/cM)]) ξT^({1,1,0})[{θ, dθ, σ}]) /
(cM cp1 mw1 π R1 (1 + (Ω ξT[{θ, dθ, σ}])/cM)^2))) +

dθ (1/J (-ks + g ml rl Sin[θ]) (-((Ω (π/2 - ArcTan[δ (dξ + ϵ)])
   (Θ + 1/2 aM (1 - ξA) Ω Sin[aM (-Mf + T - σ/cA)]) ξT^({0,1,0})[{θ,
      dθ, σ}]) / (cA cp1 mw1 π R1 (1 + (Ω ξT[{θ, dθ, σ}])/cA)^2)) -
  (Ω (π/2 + ArcTan[δ (dξ - ϵ)]) (Θ + 1/2 aA ξM Ω Sin[
      aA (-As + T - σ/cM)]) ξT^({0,1,0})[{θ, dθ, σ}]) /
   (cM cp1 mw1 π R1 (1 + (Ω ξT[{θ, dθ, σ}])/cM)^2)) -
 (-((aM^2 Aw1 h0 (-T + Ta) (1 - ξA) Ω (π/2 - ArcTan[δ (dξ + ϵ)])
      Cos[aM (-Mf + T - σ/cA)]) /
    (2 cA cp1 mw1 π (1 + (Ω ξT[{θ, dθ, σ}])/cA))) -
  (aA^2 Aw1 h0 (-T + Ta) ξM Ω (π/2 + ArcTan[δ (dξ - ϵ)])
     Cos[aA (-As + T - σ/cM)]) /
   (2 cM cp1 mw1 π (1 + (Ω ξT[{θ, dθ, σ}])/cM)) -
  (Ω (π/2 - ArcTan[δ (dξ + ϵ)]) (-(dθ E1 r1)/l10 + 1/(cp1 mw1) Aw1 h0
      (-T + Ta) (Θ + 1/2 aM (1 - ξA) Ω Sin[aM (-Mf + T - σ/cA)]))
     ξT^({0,0,1})[{θ, dθ, σ}]) / (cA π (1 + (Ω ξT[{θ, dθ, σ}])/cA)^2) -
  (Ω (π/2 + ArcTan[δ (dξ - ϵ)]) (-(dθ E1 r1)/l10 + 1/(cp1 mw1)
      Aw1 h0 (-T + Ta) (Θ + 1/2 aA ξM Ω Sin[aA (-As + T - σ/cM)]))
     ξT^({0,0,1})[{θ, dθ, σ}]) / (cM π (1 + (Ω ξT[{θ, dθ, σ}])/cM)^2))
 (-((Ω (π/2 - ArcTan[δ (dξ + ϵ)]) (Θ + 1/2 aM (1 - ξA) Ω
       Sin[aM (-Mf + T - σ/cA)]) ξT^({1,0,0})[{θ, dθ, σ}]) /
    (cA cp1 mw1 π R1 (1 + (Ω ξT[{θ, dθ, σ}])/cA)^2)) -
  (Ω (π/2 + ArcTan[δ (dξ - ϵ)]) (Θ + 1/2 aA ξM Ω Sin[
       aA (-As + T - σ/cM)]) ξT^({1,0,0})[{θ, dθ, σ}]) /
```

$$\left(\text{cM cp1 mw1 } \pi \text{ R1 } \left(1+\frac{\Omega\, \xi\text{T}[\{\theta,\, \text{d}\theta,\, \sigma\}]}{\text{cM}}\right)^2\right)\Bigg) +$$
$$\Bigg(-\Bigg(\Bigg(\text{aM}^2\ (1-\xi\text{A})\ \Omega\ \left(\frac{\pi}{2}-\text{ArcTan}[\delta\ (\text{d}\xi+\epsilon)]\right)\ \text{Cos}\Big[\text{aM}\ \left(-\text{Mf}+\text{T}-\frac{\sigma}{\text{cA}}\right)\Big]\Bigg)\Big/\ \left(2\ \text{cA cp1 mw1 }\pi\ \text{R1 }\left(1+\frac{\Omega\, \xi\text{T}[\{\theta,\, \text{d}\theta,\, \sigma\}]}{\text{cA}}\right)\right)\Bigg) -$$
$$\Bigg(\text{aA}^2\ \xi\text{M}\,\Omega\ \left(\frac{\pi}{2}+\text{ArcTan}[\delta\ (\text{d}\xi-\epsilon)]\right)\ \text{Cos}\Big[\text{aA}\ \left(-\text{As}+\text{T}-\frac{\sigma}{\text{cM}}\right)\Big]\Bigg)\Big/$$
$$\left(2\ \text{cM cp1 mw1 }\pi\ \text{R1 }\left(1+\frac{\Omega\, \xi\text{T}[\{\theta,\, \text{d}\theta,\, \sigma\}]}{\text{cM}}\right)\right) -$$
$$\Bigg(\Omega\ \left(\frac{\pi}{2}-\text{ArcTan}[\delta\ (\text{d}\xi+\epsilon)]\right)\ \Bigg(\Theta+\frac{1}{2}\ \text{aM}\ (1-\xi\text{A})\ \Omega\ \text{Sin}\Big[$$
$$\text{aM}\ \left(-\text{Mf}+\text{T}-\frac{\sigma}{\text{cA}}\right)\Big]\Bigg)\ \xi\text{T}^{(\{0,0,1\})}[\{\theta,\, \text{d}\theta,\, \sigma\}]\Bigg)\Big/$$
$$\left(\text{cA cp1 mw1 }\pi\ \text{R1 }\left(1+\frac{\Omega\, \xi\text{T}[\{\theta,\, \text{d}\theta,\, \sigma\}]}{\text{cA}}\right)^2\right) -$$
$$\Bigg(\Omega\ \left(\frac{\pi}{2}+\text{ArcTan}[\delta\ (\text{d}\xi-\epsilon)]\right)\ \Bigg(\Theta+\frac{1}{2}\ \text{aA}\ \xi\text{M}\,\Omega\ \text{Sin}\Big[$$
$$\text{aA}\ \left(-\text{As}+\text{T}-\frac{\sigma}{\text{cM}}\right)\Big]\Bigg)\ \xi\text{T}^{(\{0,0,1\})}[\{\theta,\, \text{d}\theta,\, \sigma\}]\Bigg)\Big/$$
$$\left(\text{cM cp1 mw1 }\pi\ \text{R1 }\left(1+\frac{\Omega\, \xi\text{T}[\{\theta,\, \text{d}\theta,\, \sigma\}]}{\text{cM}}\right)^2\right)\Bigg)$$
$$\Bigg(-\Bigg(\Bigg(\Omega\ \left(\frac{\pi}{2}-\text{ArcTan}[\delta\ (\text{d}\xi+\epsilon)]\right)\ \Bigg(-\frac{\text{d}\theta\ \text{E1 r1}}{\text{l10}}+\frac{1}{\text{cp1 mw1}}\text{Aw1 h0}$$
$$(-\text{T}+\text{Ta})\ \Bigg(\Theta+\frac{1}{2}\ \text{aM}\ (1-\xi\text{A})\ \Omega\ \text{Sin}\Big[\text{aM}\ \left(-\text{Mf}+\text{T}-\frac{\sigma}{\text{cA}}\right)\Big]\Bigg)\Bigg)$$
$$\xi\text{T}^{(\{1,0,0\})}[\{\theta,\, \text{d}\theta,\, \sigma\}]\Bigg)\Big/\ \Bigg(\text{cA}\,\pi$$
$$\left(1+\frac{\Omega\, \xi\text{T}[\{\theta,\, \text{d}\theta,\, \sigma\}]}{\text{cA}}\right)^2\Bigg)\Bigg) -$$
$$\Bigg(\Omega\ \left(\frac{\pi}{2}+\text{ArcTan}[\delta\ (\text{d}\xi-\epsilon)]\right)\ \Bigg(-\frac{\text{d}\theta\ \text{E1 r1}}{\text{l10}}+\frac{1}{\text{cp1 mw1}}$$
$$\text{Aw1 h0}\ (-\text{T}+\text{Ta})\ \Bigg(\Theta+\frac{1}{2}\ \text{aA}\ \xi\text{M}\,\Omega\ \text{Sin}\Big[\text{aA}\ \left(-\text{As}+\text{T}-\frac{\sigma}{\text{cM}}\right)\Big]\Bigg)\Bigg)$$
$$\xi\text{T}^{(\{1,0,0\})}[\{\theta,\, \text{d}\theta,\, \sigma\}]\Bigg)\Big/\ \left(\text{cM}\,\pi\ \left(1+\frac{\Omega\, \xi\text{T}[\{\theta,\, \text{d}\theta,\, \sigma\}]}{\text{cM}}\right)^2\right)\Bigg) +$$
$$\Bigg(\frac{1}{\pi}\Bigg(-\frac{\text{d}\theta\ \text{E1 r1}}{\text{l10}}+\frac{\text{Aw1 h0}\ (-\text{T}+\text{Ta})\ \Theta}{\text{cp1 mw1}}\Bigg)\ (-\text{ArcTan}[\delta\ (\text{d}\xi-\epsilon)]+$$
$$\text{ArcTan}[\delta\ (\text{d}\xi+\epsilon)])+$$
$$\Bigg(\left(\frac{\pi}{2}-\text{ArcTan}[\delta\ (\text{d}\xi+\epsilon)]\right)\ \Bigg(-\frac{\text{d}\theta\ \text{E1 r1}}{\text{l10}}+\frac{1}{\text{cp1 mw1}}\text{Aw1 h0}$$
$$(-\text{T}+\text{Ta})\ \Bigg(\Theta+\frac{1}{2}\ \text{aM}\ (1-\xi\text{A})\ \Omega\ \text{Sin}\Big[\text{aM}\ \left(-\text{Mf}+\text{T}-\frac{\sigma}{\text{cA}}\right)\Big]\Bigg)\Bigg)\Bigg)\Big/$$
$$\left(\pi\ \left(1+\frac{\Omega\, \xi\text{T}[\{\theta,\, \text{d}\theta,\, \sigma\}]}{\text{cA}}\right)\right)+\Bigg(\left(\frac{\pi}{2}+\text{ArcTan}[\delta\ (\text{d}\xi-\epsilon)]\right)$$
$$\Bigg(-\frac{\text{d}\theta\ \text{E1 r1}}{\text{l10}}+\frac{1}{\text{cp1 mw1}}\text{Aw1 h0}\ (-\text{T}+\text{Ta})\ \Bigg(\Theta+\frac{1}{2}\ \text{aA}\ \xi\text{M}\,\Omega\ \text{Sin}\Big[$$
$$\text{aA}\ \left(-\text{As}+\text{T}-\frac{\sigma}{\text{cM}}\right)\Big]\Bigg)\Bigg)\Bigg)\Big/\ \left(\pi\ \left(1+\frac{\Omega\, \xi\text{T}[\{\theta,\, \text{d}\theta,\, \sigma\}]}{\text{cM}}\right)\right)\Bigg)$$
$$\Bigg(\Bigg(\text{aM}^2\ (1-\xi\text{A})\ \Omega^2\ \left(\frac{\pi}{2}-\text{ArcTan}[\delta\ (\text{d}\xi+\epsilon)]\right)\ \text{Cos}\Big[\text{aM}\ \left(-\text{Mf}+\text{T}-\frac{\sigma}{\text{cA}}\right)\Big]$$
$$\xi\text{T}^{(\{1,0,0\})}[\{\theta,\, \text{d}\theta,\, \sigma\}]\Bigg)\Big/$$

$$\left(2\,cA^2\,cp1\,mw1\,\pi\,R1\,\left(1+\frac{\Omega\,\xi T[\{\theta,\,d\theta,\,\sigma\}]}{cA}\right)^2\right)+$$
$$\left(aA^2\,\xi M\,\Omega^2\,\left(\frac{\pi}{2}+\text{ArcTan}[\delta\,(d\xi-\epsilon)]\right)\right.$$
$$\left.\text{Cos}\left[aA\,\left(-As+T-\frac{\sigma}{cM}\right)\right]\,\xi T^{(\{1,0,0\})}[\{\theta,\,d\theta,\,\sigma\}]\right)\Big/$$
$$\left(2\,cM^2\,cp1\,mw1\,\pi\,R1\,\left(1+\frac{\Omega\,\xi T[\{\theta,\,d\theta,\,\sigma\}]}{cM}\right)^2\right)+$$
$$\left(2\,\Omega^2\,\left(\frac{\pi}{2}-\text{ArcTan}[\delta\,(d\xi+\epsilon)]\right)\right.$$
$$\left(\Theta+\frac{1}{2}\,aM\,(1-\xi A)\,\Omega\,\text{Sin}\left[aM\,\left(-Mf+T-\frac{\sigma}{cA}\right)\right]\right)$$
$$\left.\xi T^{(\{0,0,1\})}[\{\theta,\,d\theta,\,\sigma\}]\,\xi T^{(\{1,0,0\})}[\{\theta,\,d\theta,\,\sigma\}]\right)\Big/$$
$$\left(cA^2\,cp1\,mw1\,\pi\,R1\,\left(1+\frac{\Omega\,\xi T[\{\theta,\,d\theta,\,\sigma\}]}{cA}\right)^3\right)+$$
$$\left(2\,\Omega^2\,\left(\frac{\pi}{2}+\text{ArcTan}[\delta\,(d\xi-\epsilon)]\right)\right.$$
$$\left(\Theta+\frac{1}{2}\,aA\,\xi M\,\Omega\,\text{Sin}\left[aA\,\left(-As+T-\frac{\sigma}{cM}\right)\right]\right)$$
$$\left.\xi T^{(\{0,0,1\})}[\{\theta,\,d\theta,\,\sigma\}]\,\xi T^{(\{1,0,0\})}[\{\theta,\,d\theta,\,\sigma\}]\right)\Big/$$
$$\left(cM^2\,cp1\,mw1\,\pi\,R1\,\left(1+\frac{\Omega\,\xi T[\{\theta,\,d\theta,\,\sigma\}]}{cM}\right)^3\right)-$$
$$\left(\Omega\,\left(\frac{\pi}{2}-\text{ArcTan}[\delta\,(d\xi+\epsilon)]\right)\,\left(\Theta+\frac{1}{2}\,aM\,(1-\xi A)\,\Omega\,\text{Sin}\left[\right.\right.\right.$$
$$\left.\left.\left.aM\,\left(-Mf+T-\frac{\sigma}{cA}\right)\right]\right)\,\xi T^{(\{1,0,1\})}[\{\theta,\,d\theta,\,\sigma\}]\right)\Big/$$
$$\left(cA\,cp1\,mw1\,\pi\,R1\,\left(1+\frac{\Omega\,\xi T[\{\theta,\,d\theta,\,\sigma\}]}{cA}\right)^2\right)-$$
$$\left(\Omega\,\left(\frac{\pi}{2}+\text{ArcTan}[\delta\,(d\xi-\epsilon)]\right)\,\left(\Theta+\frac{1}{2}\,aA\,\xi M\,\Omega\,\text{Sin}\left[\right.\right.\right.$$
$$\left.\left.\left.aA\,\left(-As+T-\frac{\sigma}{cM}\right)\right]\right)\,\xi T^{(\{1,0,1\})}[\{\theta,\,d\theta,\,\sigma\}]\right)\Big/$$
$$\left.\left(cM\,cp1\,mw1\,\pi\,R1\,\left(1+\frac{\Omega\,\xi T[\{\theta,\,d\theta,\,\sigma\}]}{cM}\right)^2\right)\right)-$$
$$\left((\Theta\,(-\text{ArcTan}[\delta\,(d\xi-\epsilon)]+\text{ArcTan}[\delta\,(d\xi+\epsilon)]))\,/\,(cp1\,mw1\,\pi\,R1)+\right.$$
$$\left(\left(\frac{\pi}{2}-\text{ArcTan}[\delta\,(d\xi+\epsilon)]\right)\right.$$
$$\left.\left(\Theta+\frac{1}{2}\,aM\,(1-\xi A)\,\Omega\,\text{Sin}\left[aM\,\left(-Mf+T-\frac{\sigma}{cA}\right)\right]\right)\right)\Big/$$
$$\left(cp1\,mw1\,\pi\,R1\,\left(1+\frac{\Omega\,\xi T[\{\theta,\,d\theta,\,\sigma\}]}{cA}\right)\right)+$$
$$\left(\left(\frac{\pi}{2}+\text{ArcTan}[\delta\,(d\xi-\epsilon)]\right)\right.$$
$$\left.\left(\Theta+\frac{1}{2}\,aA\,\xi M\,\Omega\,\text{Sin}\left[aA\,\left(-As+T-\frac{\sigma}{cM}\right)\right]\right)\right)\Big/$$
$$\left.\left(cp1\,mw1\,\pi\,R1\,\left(1+\frac{\Omega\,\xi T[\{\theta,\,d\theta,\,\sigma\}]}{cM}\right)\right)\right)$$
$$\left(\left(aM^2\,Aw1\,h0\,(-T+Ta)\,(1-\xi A)\,\Omega^2\,\left(\frac{\pi}{2}-\text{ArcTan}[\delta\,(d\xi+\epsilon)]\right)\right.\right.$$

$$\text{Cos}\left[\text{aM}\left(-\text{Mf}+\text{T}-\frac{\sigma}{\text{cA}}\right)\right]\ \xi\text{T}^{(\{1,0,0\})}[\{\theta,\ \text{d}\theta,\ \sigma\}]\Big)\Big/$$

$$\left(2\ \text{cA}^2\ \text{cp1 mw1}\ \pi\left(1+\frac{\Omega\ \xi\text{T}[\{\theta,\ \text{d}\theta,\ \sigma\}]}{\text{cA}}\right)^2\right)+$$

$$\Big(\text{aA}^2\ \text{Aw1 h0}\ (-\text{T}+\text{Ta})\ \xi\text{M}\ \Omega^2\left(\frac{\pi}{2}+\text{ArcTan}[\delta\ (\text{d}\xi-\epsilon)]\right)$$

$$\text{Cos}\left[\text{aA}\left(-\text{As}+\text{T}-\frac{\sigma}{\text{cM}}\right)\right]\ \xi\text{T}^{(\{1,0,0\})}[\{\theta,\ \text{d}\theta,\ \sigma\}]\Big)\Big/$$

$$\left(2\ \text{cM}^2\ \text{cp1 mw1}\ \pi\left(1+\frac{\Omega\ \xi\text{T}[\{\theta,\ \text{d}\theta,\ \sigma\}]}{\text{cM}}\right)^2\right)+$$

$$\frac{1}{\text{cA}^2\ \pi\left(1+\frac{\Omega\ \xi\text{T}[\{\theta,\text{d}\theta,\sigma\}]}{\text{cA}}\right)^3}$$

$$2\ \Omega^2\left(\frac{\pi}{2}-\text{ArcTan}[\delta\ (\text{d}\xi+\epsilon)]\right)\Bigg(-\frac{\text{d}\theta\ \text{E1 r1}}{\text{l10}}+\frac{1}{\text{cp1 mw1}}$$

$$\text{Aw1 h0}\ (-\text{T}+\text{Ta})\left(\Theta+\frac{1}{2}\ \text{aM}\ (1-\xi\text{A})\ \Omega\ \text{Sin}\left[\text{aM}\left(-\text{Mf}+\text{T}-\frac{\sigma}{\text{cA}}\right)\right]\right)\Bigg)$$

$$\xi\text{T}^{(\{0,0,1\})}[\{\theta,\ \text{d}\theta,\ \sigma\}]\ \xi\text{T}^{(\{1,0,0\})}[\{\theta,\ \text{d}\theta,\ \sigma\}]+$$

$$\frac{1}{\text{cM}^2\ \pi\left(1+\frac{\Omega\ \xi\text{T}[\{\theta,\text{d}\theta,\sigma\}]}{\text{cM}}\right)^3}$$

$$2\ \Omega^2\left(\frac{\pi}{2}+\text{ArcTan}[\delta\ (\text{d}\xi-\epsilon)]\right)\Bigg(-\frac{\text{d}\theta\ \text{E1 r1}}{\text{l10}}+\frac{1}{\text{cp1 mw1}}$$

$$\text{Aw1 h0}\ (-\text{T}+\text{Ta})\left(\Theta+\frac{1}{2}\ \text{aA}\ \xi\text{M}\ \Omega\ \text{Sin}\left[\text{aA}\left(-\text{As}+\text{T}-\frac{\sigma}{\text{cM}}\right)\right]\right)\Bigg)$$

$$\xi\text{T}^{(\{0,0,1\})}[\{\theta,\ \text{d}\theta,\ \sigma\}]\ \xi\text{T}^{(\{1,0,0\})}[\{\theta,\ \text{d}\theta,\ \sigma\}]-$$

$$\Bigg(\Omega\left(\frac{\pi}{2}-\text{ArcTan}[\delta\ (\text{d}\xi+\epsilon)]\right)\Bigg(-\frac{\text{d}\theta\ \text{E1 r1}}{\text{l10}}+\frac{1}{\text{cp1 mw1}}\text{Aw1 h0}$$

$$(-\text{T}+\text{Ta})\left(\Theta+\frac{1}{2}\ \text{aM}\ (1-\xi\text{A})\ \Omega\ \text{Sin}\left[\text{aM}\left(-\text{Mf}+\text{T}-\frac{\sigma}{\text{cA}}\right)\right]\right)\Bigg)$$

$$\xi\text{T}^{(\{1,0,1\})}[\{\theta,\ \text{d}\theta,\ \sigma\}]\Bigg)\Bigg/\left(\text{cA}\ \pi\left(1+\frac{\Omega\ \xi\text{T}[\{\theta,\ \text{d}\theta,\ \sigma\}]}{\text{cA}}\right)^2\right)-$$

$$\Bigg(\Omega\left(\frac{\pi}{2}+\text{ArcTan}[\delta\ (\text{d}\xi-\epsilon)]\right)\Bigg(-\frac{\text{d}\theta\ \text{E1 r1}}{\text{l10}}+\frac{1}{\text{cp1 mw1}}$$

$$\text{Aw1 h0}\ (-\text{T}+\text{Ta})\left(\Theta+\frac{1}{2}\ \text{aA}\ \xi\text{M}\ \Omega\ \text{Sin}\left[\text{aA}\left(-\text{As}+\text{T}-\frac{\sigma}{\text{cM}}\right)\right]\right)\Bigg)$$

$$\xi\text{T}^{(\{1,0,1\})}[\{\theta,\ \text{d}\theta,\ \sigma\}]\Bigg)\Bigg/\left(\text{cM}\ \pi\left(1+\frac{\Omega\ \xi\text{T}[\{\theta,\ \text{d}\theta,\ \sigma\}]}{\text{cM}}\right)^2\right)\Bigg)+$$

$$\frac{1}{\text{J}}(-(\text{b1}+\text{bs})\ \text{d}\theta-\text{ks}\ \theta+\text{A1 r1}\ \sigma-\text{g ml rl Cos}[\theta])$$

$$\Bigg(\Bigg(2\ \Omega^2\left(\frac{\pi}{2}-\text{ArcTan}[\delta\ (\text{d}\xi+\epsilon)]\right)$$

$$\left(\Theta+\frac{1}{2}\ \text{aM}\ (1-\xi\text{A})\ \Omega\ \text{Sin}\left[\text{aM}\left(-\text{Mf}+\text{T}-\frac{\sigma}{\text{cA}}\right)\right]\right)$$

$$\xi\text{T}^{(\{0,1,0\})}[\{\theta,\ \text{d}\theta,\ \sigma\}]\ \xi\text{T}^{(\{1,0,0\})}[\{\theta,\ \text{d}\theta,\ \sigma\}]\Bigg)\Bigg/$$

$$\left(\text{cA}^2\ \text{cp1 mw1}\ \pi\ \text{R1}\left(1+\frac{\Omega\ \xi\text{T}[\{\theta,\ \text{d}\theta,\ \sigma\}]}{\text{cA}}\right)^3\right)+$$

$$\Bigg(2\ \Omega^2\left(\frac{\pi}{2}+\text{ArcTan}[\delta\ (\text{d}\xi-\epsilon)]\right)$$

$$\left(\Theta+\frac{1}{2}\ \text{aA}\ \xi\text{M}\ \Omega\ \text{Sin}\left[\text{aA}\left(-\text{As}+\text{T}-\frac{\sigma}{\text{cM}}\right)\right]\right)$$

$$\xi T^{(\{0,1,0\})}[\{\theta, d\theta, \sigma\}]\ \xi T^{(\{1,0,0\})}[\{\theta, d\theta, \sigma\}]\Bigg)\Bigg/\left(cM^2\ cp1\ mw1\ \pi\ R1\left(1+\frac{\Omega\,\xi T[\{\theta, d\theta, \sigma\}]}{cM}\right)^3\right)-\left(\Omega\left(\frac{\pi}{2}-\text{ArcTan}[\delta\ (d\xi+\epsilon)]\right)\left(\Theta+\frac{1}{2}\,aM\ (1-\xi A)\ \Omega\ \text{Sin}\Big[aM\left(-Mf+T-\frac{\sigma}{cA}\right)\Big]\right)\xi T^{(\{1,1,0\})}[\{\theta, d\theta, \sigma\}]\right)\Bigg/\left(cA\ cp1\ mw1\ \pi\ R1\left(1+\frac{\Omega\,\xi T[\{\theta, d\theta, \sigma\}]}{cA}\right)^2\right)-\left(\Omega\left(\frac{\pi}{2}+\text{ArcTan}[\delta\ (d\xi-\epsilon)]\right)\left(\Theta+\frac{1}{2}\,aA\,\xi M\,\Omega\ \text{Sin}\Big[aA\left(-As+T-\frac{\sigma}{cM}\right)\Big]\right)\xi T^{(\{1,1,0\})}[\{\theta, d\theta, \sigma\}]\right)\Bigg/\left(cM\ cp1\ mw1\ \pi\ R1\left(1+\frac{\Omega\,\xi T[\{\theta, d\theta, \sigma\}]}{cM}\right)^2\right)\Bigg)+d\theta\Bigg(\Bigg(2\,\Omega^2\left(\frac{\pi}{2}-\text{ArcTan}[\delta\ (d\xi+\epsilon)]\right)\left(\Theta+\frac{1}{2}\,aM\ (1-\xi A)\ \Omega\ \text{Sin}\Big[aM\left(-Mf+T-\frac{\sigma}{cA}\right)\Big]\right)\xi T^{(\{1,0,0\})}[\{\theta, d\theta, \sigma\}]^2\Bigg)\Bigg/\left(cA^2\ cp1\ mw1\ \pi\ R1\left(1+\frac{\Omega\,\xi T[\{\theta, d\theta, \sigma\}]}{cA}\right)^3\right)+\left(2\,\Omega^2\left(\frac{\pi}{2}+\text{ArcTan}[\delta\ (d\xi-\epsilon)]\right)\left(\Theta+\frac{1}{2}\,aA\,\xi M\,\Omega\ \text{Sin}\Big[aA\left(-As+T-\frac{\sigma}{cM}\right)\Big]\right)\xi T^{(\{1,0,0\})}[\{\theta, d\theta, \sigma\}]^2\right)\Bigg/\left(cM^2\ cp1\ mw1\ \pi\ R1\left(1+\frac{\Omega\,\xi T[\{\theta, d\theta, \sigma\}]}{cM}\right)^3\right)-\left(\Omega\left(\frac{\pi}{2}-\text{ArcTan}[\delta\ (d\xi+\epsilon)]\right)\left(\Theta+\frac{1}{2}\,aM\ (1-\xi A)\ \Omega\ \text{Sin}\Big[aM\left(-Mf+T-\frac{\sigma}{cA}\right)\Big]\right)\xi T^{(\{2,0,0\})}[\{\theta, d\theta, \sigma\}]\right)\Bigg/\left(cA\ cp1\ mw1\ \pi\ R1\left(1+\frac{\Omega\,\xi T[\{\theta, d\theta, \sigma\}]}{cA}\right)^2\right)-\left(\Omega\left(\frac{\pi}{2}+\text{ArcTan}[\delta\ (d\xi-\epsilon)]\right)\left(\Theta+\frac{1}{2}\,aA\,\xi M\,\Omega\ \text{Sin}\Big[aA\left(-As+T-\frac{\sigma}{cM}\right)\Big]\right)\xi T^{(\{2,0,0\})}[\{\theta, d\theta, \sigma\}]\right)\Bigg/\left(cM\ cp1\ mw1\ \pi\ R1\left(1+\frac{\Omega\,\xi T[\{\theta, d\theta, \sigma\}]}{cM}\right)^2\right)\Bigg)\Bigg\}\Bigg\}$$

```
Controllability Matrix Rank
```

Out[292]= 3

```
Due to the constraints over the control
  input, although the controllability matrix is full
  rank for all x, the system is proved to be reachable.
```

B.2.2 Discrete Nonlinear Controllability

The nonlinear controllability proof for the discrete-time system presented in Eq. (6.47) was computed using Wolfram Mathematica, and is provided in the following pages.

```
x = {θ, σ};
u = {V^2};
b = bs + b1;

ξT1[x_]:=(ξM/2)Sin[aA(T − As − (1/cM)x[[2]])]aA
ξσ1[x_]:= − (1/cM)ξT[x]
ξT2[x_]:=((1 − ξA)/2)Sin[aM(T − Mf − (1/cA)x[[2]])]aM
ξσ2[x_]:= − (1/cA)ξT[x]

hpk[x_]:=(A1r1(x[[2]]) − mlgrlSin[x[[1]]] − ksx[[1]])/b

f1[x_]:=((−E1r1/l10)hpk[x] + (Θ + ΩξT1[x])(−(T − Ta)h0Aw1/(mw1cp1)))/(1 − Ωξσ1[x])
g1[x_]:=(Θ + ΩξT1[x])(1/(R1mw1cp1))/(1 − Ωξσ1[x])
f2[x_]:=((−E1r1/l10)hpk[x] + (Θ + ΩξT2[x])(−(T − Ta)h0Aw1/(mw1cp1)))/(1 − Ωξσ2[x])
g2[x_]:=(Θ + ΩξT2[x])(1/(R1mw1cp1))/(1 − Ωξσ2[x])
f3[x_]:=(−E1r1/l10)hpk[x] + Θ(−(T − Ta)h0Aw1/(mw1cp1))
g3[x_]:=(Θ)(1/(R1mw1cp1))

Z1[ξk1_]:=(ArcTan[δ(ξk1 − ϵ)] + Pi/2)(1/Pi)
Z2[ξk1_]:=(ArcTan[−δ(ξk1 + ϵ)] + Pi/2)(1/Pi)
Z3[ξk1_]:=(ArcTan[δ(ξk1 + ϵ)] + ArcTan[−δ(ξk1 − ϵ)])(1/Pi)

fx4[ξk1_]:=f1[x]Z1[ξk1] + f2[x]Z2[ξk1] + f3[x]Z3[ξk1]
g4[ξk1_]:=g1[x]Z1[ξk1] + g2[x]Z2[ξk1] + g3[x]Z3[ξk1]

f[x_]:={{x[[1]] + hpk[x]Ts}, {x[[2]] + fx4[dξ]Ts}}
g[x_]:={{0}, {g4[ξk1]Ts}}
```

```
Print["Controllability Matrix"]
Print["Construction the Accesibility algebra C"]

C11 = D[g[x], {x}].f[x]; C11 = {C11[[1, 1]], C11[[2, 1]]};
C12 = D[f[x], {x}].g[x]; C12 = {C12[[1, 1]], C12[[2, 1]]};
C1 = C11 - C12;
C21 = D[C1, {x}].f[x]; C21 = {C21[[1, 1]], C21[[2, 1]]};
C22 = D[f[x], {x}].C1; C22 = {C22[[1, 1]], C22[[2, 1]]};
C2 = C21 - C22;

a = Transpose[f[x]]; a = a[[1]]
b = Transpose[g[x]]; b = b[[1]]
c = Transpose[C1];  c = c[[1]]
d = Transpose[C2];  d = d[[1]]
aC = {a, b}
Print["Controllability Matrix Rank"]
MatrixRank[aC]
Print[
"Due to the constraints over the control input, although the controllability matrix is
full rank for all x, the system is proved to be reachable."]
```

Controllability Matrix

Construction the Accesibility algebra C

```
Controllability Matrix

Construction the Accesibility algebra C
```

Out[246]=
$$\Bigg\{\Theta + \frac{\text{Ts}\ (-\text{ks}\,\Theta + \text{A1 r1}\,\sigma - \text{g ml rl Sin}[\theta])}{\text{b1} + \text{bs}},$$
$$\sigma + \text{Ts}\left(\frac{1}{\pi}(-\text{ArcTan}[\delta\ (\text{d}\xi - \epsilon)] + \text{ArcTan}[\delta\ (\text{d}\xi + \epsilon)])\right.$$
$$\left(\frac{\text{Aw1 h0}\ (-\text{T} + \text{Ta})\ \Theta}{\text{cp1 mw1}} - (\text{E1 r1}\ (-\text{ks}\,\Theta + \text{A1 r1}\,\sigma - \text{g ml rl Sin}[\theta]))\ /\right.$$
$$\left.((\text{b1} + \text{bs})\ \text{l10})\right) + \left(\left(\frac{\pi}{2} - \text{ArcTan}[\delta\ (\text{d}\xi + \epsilon)]\right)\right.$$
$$\left(-((\text{E1 r1}\ (-\text{ks}\,\Theta + \text{A1 r1}\,\sigma - \text{g ml rl Sin}[\theta]))\ /\ ((\text{b1} + \text{bs})\ \text{l10})) +\right.$$
$$\frac{1}{\text{cp1 mw1}}\text{Aw1 h0}\ (-\text{T} + \text{Ta})$$
$$\left.\left.\left.\left(\Theta + \frac{1}{2}\,\text{aM}\ (1 - \xi\text{A})\ \Omega\ \text{Sin}\left[\text{aM}\left(-\text{Mf} + \text{T} - \frac{\sigma}{\text{cA}}\right)\right]\right)\right)\right)\Big/$$
$$\left(\pi\left(1 + \frac{\Omega\ \xi\text{T}[\{\theta,\ \sigma\}]}{\text{cA}}\right)\right) + \left(\left(\frac{\pi}{2} + \text{ArcTan}[\delta\ (\text{d}\xi - \epsilon)]\right)\right.$$
$$\left(-((\text{E1 r1}\ (-\text{ks}\,\Theta + \text{A1 r1}\,\sigma - \text{g ml rl Sin}[\theta]))\ /\ ((\text{b1} + \text{bs})\ \text{l10})) +\right.$$
$$\frac{1}{\text{cp1 mw1}}\text{Aw1 h0}\ (-\text{T} + \text{Ta})\ \left(\Theta + \frac{1}{2}\,\text{aA}\ \xi\text{M}\ \Omega\right.$$
$$\left.\left.\left.\text{Sin}\left[\text{aA}\left(-\text{As} + \text{T} - \frac{\sigma}{\text{cM}}\right)\right]\right)\right)\right)\Big/\left(\pi\left(1 + \frac{\Omega\ \xi\text{T}[\{\theta,\ \sigma\}]}{\text{cM}}\right)\right)\Big)\Bigg\}$$

Out[247]=
$$\Bigg\{0,\ \text{Ts}\left(\frac{\Theta\ (-\text{ArcTan}[\delta\ (-\epsilon + \xi\text{k1})] + \text{ArcTan}[\delta\ (\epsilon + \xi\text{k1})])}{\text{cp1 mw1}\,\pi\,\text{R1}} +\right.$$
$$\frac{\left(\frac{\pi}{2} - \text{ArcTan}[\delta\ (\epsilon + \xi\text{k1})]\right)\ \left(\Theta + \frac{1}{2}\,\text{aM}\ (1 - \xi\text{A})\ \Omega\ \text{Sin}\left[\text{aM}\left(-\text{Mf} + \text{T} - \frac{\sigma}{\text{cA}}\right)\right]\right)}{\text{cp1 mw1}\,\pi\,\text{R1}\left(1 + \frac{\Omega\,\xi\text{T}[\{\theta,\sigma\}]}{\text{cA}}\right)} +$$
$$\left.\frac{\left(\frac{\pi}{2} + \text{ArcTan}[\delta\ (-\epsilon + \xi\text{k1})]\right)\ \left(\Theta + \frac{1}{2}\,\text{aA}\ \xi\text{M}\,\Omega\,\text{Sin}\left[\text{aA}\left(-\text{As} + \text{T} - \frac{\sigma}{\text{cM}}\right)\right]\right)}{\text{cp1 mw1}\,\pi\,\text{R1}\left(1 + \frac{\Omega\,\xi\text{T}[\{\theta,\sigma\}]}{\text{cM}}\right)}\right)\Bigg\}$$

Out[248]=
$$\Bigg\{-\frac{1}{\text{b1} + \text{bs}}\text{A1 r1 Ts}^2$$
$$\left((\Theta\ (-\text{ArcTan}[\delta\ (-\epsilon + \xi\text{k1})] + \text{ArcTan}[\delta\ (\epsilon + \xi\text{k1})]))\ /\ (\text{cp1 mw1}\,\pi\,\text{R1}) +\right.$$
$$\left(\left(\frac{\pi}{2} - \text{ArcTan}[\delta\ (\epsilon + \xi\text{k1})]\right)\right.$$
$$\left.\left.\left(\Theta + \frac{1}{2}\,\text{aM}\ (1 - \xi\text{A})\ \Omega\ \text{Sin}\left[\text{aM}\left(-\text{Mf} + \text{T} - \frac{\sigma}{\text{cA}}\right)\right]\right)\right)\Big/$$
$$\left(\text{cp1 mw1}\,\pi\,\text{R1}\left(1 + \frac{\Omega\,\xi\text{T}[\{\theta,\ \sigma\}]}{\text{cA}}\right)\right) +$$
$$\left(\left(\frac{\pi}{2} + \text{ArcTan}[\delta\ (-\epsilon + \xi\text{k1})]\right)\ \left(\Theta + \frac{1}{2}\,\text{aA}\ \xi\text{M}\,\Omega\,\text{Sin}\left[\text{aA}\left(-\text{As} + \text{T} - \frac{\sigma}{\text{cM}}\right)\right]\right)\right)\Big/$$
$$\left.\left(\text{cp1 mw1}\,\pi\,\text{R1}\left(1 + \frac{\Omega\,\xi\text{T}[\{\theta,\ \sigma\}]}{\text{cM}}\right)\right)\right),$$
$$\text{Ts}\left(\sigma + \text{Ts}\left(\frac{1}{\pi}(-\text{ArcTan}[\delta\ (\text{d}\xi - \epsilon)] + \text{ArcTan}[\delta\ (\text{d}\xi + \epsilon)])\right.\right.$$
$$\left(\frac{\text{Aw1 h0}\ (-\text{T} + \text{Ta})\ \Theta}{\text{cp1 mw1}} - (\text{E1 r1}\ (-\text{ks}\,\Theta + \text{A1 r1}\,\sigma - \text{g ml rl Sin}[\theta]))\ /\right.$$
$$\left.((\text{b1} + \text{bs})\ \text{l10})\right) + \left(\left(\frac{\pi}{2} - \text{ArcTan}[\delta\ (\text{d}\xi + \epsilon)]\right)\right.$$

$$\left(-\left((\text{E1 r1}\ (-\text{ks}\,\Theta+\text{A1 r1}\,\sigma-\text{g ml rl Sin}[\theta]))\ /\right.\right.$$
$$((\text{b1}+\text{bs})\ \text{l10}))+\frac{1}{\text{cp1 mw1}}\text{Aw1 h0}\ (-\text{T}+\text{Ta})$$
$$\left.\left.\left(\Theta+\frac{1}{2}\,\text{aM}\ (1-\xi\text{A})\ \Omega\,\text{Sin}\left[\text{aM}\left(-\text{Mf}+\text{T}-\frac{\sigma}{\text{cA}}\right)\right]\right)\right)\Bigg/$$
$$\left(\pi\left(1+\frac{\Omega\,\xi\text{T}[\{\theta,\sigma\}]}{\text{cA}}\right)\right)+\left(\left(\frac{\pi}{2}+\text{ArcTan}[\delta\ (\text{d}\xi-\epsilon)]\right)\right.$$
$$\left(-\left((\text{E1 r1}\ (-\text{ks}\,\Theta+\text{A1 r1}\,\sigma-\text{g ml rl Sin}[\theta]))\ /\ ((\text{b1}+\text{bs})\right.\right.$$
$$\text{l10}))+\frac{1}{\text{cp1 mw1}}\text{Aw1 h0}\ (-\text{T}+\text{Ta})\left(\Theta+\frac{1}{2}\,\text{aA}\,\xi\text{M}\,\Omega\right.$$
$$\left.\left.\text{Sin}\left[\text{aA}\left(-\text{As}+\text{T}-\frac{\sigma}{\text{cM}}\right)\right]\right)\right)\Bigg/\left(\pi\left(1+\frac{\Omega\,\xi\text{T}[\{\theta,\sigma\}]}{\text{cM}}\right)\right)\Bigg)\Bigg)$$
$$\left(-\left(\left(\text{aM}^2\ (1-\xi\text{A})\ \Omega\left(\frac{\pi}{2}-\text{ArcTan}[\delta\ (\epsilon+\xi\text{k1})]\right)\text{Cos}\left[\text{aM}\left(-\text{Mf}+\text{T}-\frac{\sigma}{\text{cA}}\right)\right]\right)\Bigg/\right.\right.$$
$$\left.\left(2\ \text{cA cp1 mw1}\,\pi\,\text{R1}\left(1+\frac{\Omega\,\xi\text{T}[\{\theta,\sigma\}]}{\text{cA}}\right)\right)\right)-$$
$$\left(\text{aA}^2\,\xi\text{M}\,\Omega\left(\frac{\pi}{2}+\text{ArcTan}[\delta\ (-\epsilon+\xi\text{k1})]\right)\text{Cos}\left[\text{aA}\left(-\text{As}+\text{T}-\frac{\sigma}{\text{cM}}\right)\right]\right)\Bigg/$$
$$\left(2\ \text{cM cp1 mw1}\,\pi\,\text{R1}\left(1+\frac{\Omega\,\xi\text{T}[\{\theta,\sigma\}]}{\text{cM}}\right)\right)-$$
$$\left(\Omega\left(\frac{\pi}{2}-\text{ArcTan}[\delta\ (\epsilon+\xi\text{k1})]\right)\right.$$
$$\left.\left(\Theta+\frac{1}{2}\,\text{aM}\ (1-\xi\text{A})\ \Omega\,\text{Sin}\left[\text{aM}\left(-\text{Mf}+\text{T}-\frac{\sigma}{\text{cA}}\right)\right]\right)\xi\text{T}^{(\{0,1\})}[\{\theta,\sigma\}]\right)\Bigg/$$
$$\left(\text{cA cp1 mw1}\,\pi\,\text{R1}\left(1+\frac{\Omega\,\xi\text{T}[\{\theta,\sigma\}]}{\text{cA}}\right)^2\right)-$$
$$\left(\Omega\left(\frac{\pi}{2}+\text{ArcTan}[\delta\ (-\epsilon+\xi\text{k1})]\right)\left(\Theta+\frac{1}{2}\,\text{aA}\,\xi\text{M}\,\Omega\,\text{Sin}\left[\text{aA}\left(-\text{As}+\text{T}-\frac{\sigma}{\text{cM}}\right)\right]\right)\right.$$
$$\left.\xi\text{T}^{(\{0,1\})}[\{\theta,\sigma\}]\right)\Bigg/\left(\text{cM cp1 mw1}\,\pi\,\text{R1}\left(1+\frac{\Omega\,\xi\text{T}[\{\theta,\sigma\}]}{\text{cM}}\right)^2\right)\Bigg)-$$
$$\text{Ts}\left((\Theta\ (-\text{ArcTan}[\delta\ (-\epsilon+\xi\text{k1})]+\text{ArcTan}[\delta\ (\epsilon+\xi\text{k1})]))\ /\right.$$
$$(\text{cp1 mw1}\,\pi\,\text{R1})+\left(\left(\frac{\pi}{2}-\text{ArcTan}[\delta\ (\epsilon+\xi\text{k1})]\right)\right.$$
$$\left.\left(\Theta+\frac{1}{2}\,\text{aM}\ (1-\xi\text{A})\ \Omega\,\text{Sin}\left[\text{aM}\left(-\text{Mf}+\text{T}-\frac{\sigma}{\text{cA}}\right)\right]\right)\right)\Bigg/$$
$$\left(\text{cp1 mw1}\,\pi\,\text{R1}\left(1+\frac{\Omega\,\xi\text{T}[\{\theta,\sigma\}]}{\text{cA}}\right)\right)+$$
$$\left(\left(\frac{\pi}{2}+\text{ArcTan}[\delta\ (-\epsilon+\xi\text{k1})]\right)\left(\Theta+\frac{1}{2}\,\text{aA}\,\xi\text{M}\,\Omega\,\text{Sin}\left[\text{aA}\left(-\text{As}+\text{T}-\frac{\sigma}{\text{cM}}\right)\right]\right)\right)\Bigg/$$
$$\left.\left(\text{cp1 mw1}\,\pi\,\text{R1}\left(1+\frac{\Omega\,\xi\text{T}[\{\theta,\sigma\}]}{\text{cM}}\right)\right)\right)$$
$$\left(1+\text{Ts}\left(-\left(\left(\text{A1 E1 r1}^2\ (-\text{ArcTan}[\delta\ (\text{d}\xi-\epsilon)]+\text{ArcTan}[\delta\ (\text{d}\xi+\epsilon)])\right)\Big/\right.\right.\right.$$
$$\left.\left.((\text{b1}+\text{bs})\ \text{l10}\,\pi)\right)+\right.$$
$$\left(\left(\frac{\pi}{2}-\text{ArcTan}[\delta\ (\text{d}\xi+\epsilon)]\right)\left(-\frac{\text{A1 E1 r1}^2}{(\text{b1}+\text{bs})\ \text{l10}}-\left(\text{aM}^2\ \text{Aw1 h0}\ (-\text{T}+\text{Ta})\right.\right.\right.$$
$$\left.\left.\left.(1-\xi\text{A})\ \Omega\,\text{Cos}\left[\text{aM}\left(-\text{Mf}+\text{T}-\frac{\sigma}{\text{cA}}\right)\right]\right)\Big/\ (2\ \text{cA cp1 mw1})\right)\Bigg)\Bigg/$$
$$\left(\pi\left(1+\frac{\Omega\,\xi\text{T}[\{\theta,\sigma\}]}{\text{cA}}\right)\right)+\left(\left(\frac{\pi}{2}+\text{ArcTan}[\delta\ (\text{d}\xi-\epsilon)]\right)\right.$$

$$\left(-\frac{\text{A1 E1 r1}^2}{(\text{b1}+\text{bs})\ \text{l10}}-\left(\text{aA}^2\ \text{Aw1 h0}\ (-\text{T}+\text{Ta})\ \xi\text{M}\,\Omega\right.\right.$$
$$\left.\left.\text{Cos}\left[\text{aA}\left(-\text{As}+\text{T}-\frac{\sigma}{\text{cM}}\right)\right]\right)\Big/\ (2\ \text{cM cp1 mw1})\right)\Big/$$
$$\left(\pi\left(1+\frac{\Omega\,\xi\text{T}[\{\theta,\sigma\}]}{\text{cM}}\right)\right)-\left(\Omega\left(\frac{\pi}{2}-\text{ArcTan}[\delta\ (\text{d}\xi+\epsilon)]\right)\right.$$
$$\left(-((\text{E1 r1}\ (-\text{ks}\,\theta+\text{A1 r1}\,\sigma-\text{g ml rl Sin}[\theta]))\ /\right.$$
$$((\text{b1}+\text{bs})\ \text{l10}))+\frac{1}{\text{cp1 mw1}}\text{Aw1 h0}\ (-\text{T}+\text{Ta})$$
$$\left.\left(\Theta+\frac{1}{2}\,\text{aM}\ (1-\xi\text{A})\ \Omega\,\text{Sin}\left[\text{aM}\left(-\text{Mf}+\text{T}-\frac{\sigma}{\text{cA}}\right)\right]\right)\right)$$
$$\xi\text{T}^{(\{0,1\})}[\{\theta,\sigma\}]\Big)\Big/\left(\text{cA}\,\pi\left(1+\frac{\Omega\,\xi\text{T}[\{\theta,\sigma\}]}{\text{cA}}\right)^2\right)-$$
$$\left(\Omega\left(\frac{\pi}{2}+\text{ArcTan}[\delta\ (\text{d}\xi-\epsilon)]\right)\left(-((\text{E1 r1}\ (-\text{ks}\,\theta+\text{A1 r1}\,\sigma-\right.\right.\right.$$
$$\left.\left.\left.\text{g ml rl Sin}[\theta]))\ /\ ((\text{b1}+\text{bs})\ \text{l10}))+\frac{1}{\text{cp1 mw1}}\right.\right.$$
$$\left.\left.\text{Aw1 h0}\ (-\text{T}+\text{Ta})\left(\Theta+\frac{1}{2}\,\text{aA}\,\xi\text{M}\,\Omega\,\text{Sin}\left[\text{aA}\left(-\text{As}+\text{T}-\frac{\sigma}{\text{cM}}\right)\right]\right)\right)$$
$$\left.\xi\text{T}^{(\{0,1\})}[\{\theta,\sigma\}]\right)\Big/\left(\text{cM}\,\pi\left(1+\frac{\Omega\,\xi\text{T}[\{\theta,\sigma\}]}{\text{cM}}\right)^2\right)\Big)\Big)+$$
$$\text{Ts}\left(\theta+\frac{\text{Ts}\ (-\text{ks}\,\theta+\text{A1 r1}\,\sigma-\text{g ml rl Sin}[\theta])}{\text{b1}+\text{bs}}\right)$$
$$\left(-\left(\left(\Omega\left(\frac{\pi}{2}-\text{ArcTan}[\delta\ (\epsilon+\xi\text{k1})]\right)\right.\right.\right.$$
$$\left.\left.\left.\left(\Theta+\frac{1}{2}\,\text{aM}\ (1-\xi\text{A})\ \Omega\,\text{Sin}\left[\text{aM}\left(-\text{Mf}+\text{T}-\frac{\sigma}{\text{cA}}\right)\right]\right)\xi\text{T}^{(\{1,0\})}[\{\theta,\sigma\}]\right)\Big/\right.\right.$$
$$\left.\left.\left(\text{cA cp1 mw1}\,\pi\,\text{R1}\left(1+\frac{\Omega\,\xi\text{T}[\{\theta,\sigma\}]}{\text{cA}}\right)^2\right)\right)-\right.$$
$$\left(\Omega\left(\frac{\pi}{2}+\text{ArcTan}[\delta\ (-\epsilon+\xi\text{k1})]\right)\left(\Theta+\frac{1}{2}\,\text{aA}\,\xi\text{M}\,\Omega\,\text{Sin}\left[\text{aA}\left(-\text{As}+\text{T}-\frac{\sigma}{\text{cM}}\right)\right]\right)\right.$$
$$\left.\xi\text{T}^{(\{1,0\})}[\{\theta,\sigma\}]\right)\Big/$$
$$\left.\left.\left(\text{cM cp1 mw1}\,\pi\,\text{R1}\left(1+\frac{\Omega\,\xi\text{T}[\{\theta,\sigma\}]}{\text{cM}}\right)^2\right)\right)\right\}$$
$$\left\{\frac{1}{\text{b1}+\text{bs}}\text{A1 r1 Ts}^2\left(1+\frac{\text{Ts}\ (-\text{ks}-\text{g ml rl Cos}[\theta])}{\text{b1}+\text{bs}}\right)\right.$$
$$\left(\left(\Theta\ (-\text{ArcTan}[\delta\ (-\epsilon+\xi\text{k1})]+\text{ArcTan}[\delta\ (\epsilon+\xi\text{k1})]))\ /\ (\text{cp1 mw1}\,\pi\,\text{R1})+\right.\right.$$
$$\left(\left(\frac{\pi}{2}-\text{ArcTan}[\delta\ (\epsilon+\xi\text{k1})]\right)\right.$$
$$\left.\left(\Theta+\frac{1}{2}\,\text{aM}\ (1-\xi\text{A})\ \Omega\,\text{Sin}\left[\text{aM}\left(-\text{Mf}+\text{T}-\frac{\sigma}{\text{cA}}\right)\right]\right)\right)\Big/$$
$$\left(\text{cp1 mw1}\,\pi\,\text{R1}\left(1+\frac{\Omega\,\xi\text{T}[\{\theta,\sigma\}]}{\text{cA}}\right)\right)+$$
$$\left(\left(\frac{\pi}{2}+\text{ArcTan}[\delta\ (-\epsilon+\xi\text{k1})]\right)\left(\Theta+\frac{1}{2}\,\text{aA}\,\xi\text{M}\,\Omega\,\text{Sin}\left[\text{aA}\left(-\text{As}+\text{T}-\frac{\sigma}{\text{cM}}\right)\right]\right)\right)\Big/$$
$$\left.\left.\left(\text{cp1 mw1}\,\pi\,\text{R1}\left(1+\frac{\Omega\,\xi\text{T}[\{\theta,\sigma\}]}{\text{cM}}\right)\right)\right)-\frac{1}{\text{b1}+\text{bs}}\right.$$
$$\text{A1 r1 Ts}^2\left(\sigma+\text{Ts}\left(\frac{1}{\pi}(-\text{ArcTan}[\delta\ (\text{d}\xi-\epsilon)]+\text{ArcTan}[\delta\ (\text{d}\xi+\epsilon)])\right.\right.$$
$$\left.\left(\frac{\text{Aw1 h0}\ (-\text{T}+\text{Ta})\ \Theta}{\text{cp1 mw1}}-(\text{E1 r1}\ (-\text{ks}\,\theta+\text{A1 r1}\,\sigma-\text{g ml rl Sin}[\theta]))\ /\right.\right.$$

$$((b1 + bs)\ l10)\Big) + \Big(\Big(\frac{\pi}{2} - \text{ArcTan}[\delta\ (d\xi + \epsilon)]\Big)$$
$$\Big(-((E1\ r1\ (-ks\ \Theta + A1\ r1\ \sigma - g\ ml\ rl\ \text{Sin}[\theta]))\ /$$
$$((b1 + bs)\ l10)) + \frac{1}{cp1\ mw1} Aw1\ h0\ (-T + Ta)$$
$$\Big(\Theta + \frac{1}{2}\ aM\ (1 - \xi A)\ \Omega\ \text{Sin}\Big[aM\ \Big(-Mf + T - \frac{\sigma}{cA}\Big)\Big]\Big)\Big)\Big)\Big/$$
$$\Big(\pi\ \Big(1 + \frac{\Omega\ \xi T[\{\theta, \sigma\}]}{cA}\Big)\Big) + \Big(\Big(\frac{\pi}{2} + \text{ArcTan}[\delta\ (d\xi - \epsilon)]\Big)$$
$$\Big(-((E1\ r1\ (-ks\ \Theta + A1\ r1\ \sigma - g\ ml\ rl\ \text{Sin}[\theta]))\ /\ ((b1 + bs)$$
$$l10)) + \frac{1}{cp1\ mw1} Aw1\ h0\ (-T + Ta)\ \Big(\Theta + \frac{1}{2}\ aA\ \xi M\ \Omega$$
$$\text{Sin}\Big[aA\ \Big(-As + T - \frac{\sigma}{cM}\Big)\Big]\Big)\Big)\Big)\Big/\ \Big(\pi\ \Big(1 + \frac{\Omega\ \xi T[\{\theta, \sigma\}]}{cM}\Big)\Big)\Big)\Big)$$
$$\Big(-\Big(\Big(aM^2\ (1 - \xi A)\ \Omega\ \Big(\frac{\pi}{2} - \text{ArcTan}[\delta\ (\epsilon + \xi k1)]\Big)\ \text{Cos}\Big[aM\ \Big(-Mf + T - \frac{\sigma}{cA}\Big)\Big]\Big)\Big/$$
$$\Big(2\ cA\ cp1\ mw1\ \pi\ R1\ \Big(1 + \frac{\Omega\ \xi T[\{\theta, \sigma\}]}{cA}\Big)\Big)\Big) -$$
$$\Big(aA^2\ \xi M\ \Omega\ \Big(\frac{\pi}{2} + \text{ArcTan}[\delta\ (-\epsilon + \xi k1)]\Big)\ \text{Cos}\Big[aA\ \Big(-As + T - \frac{\sigma}{cM}\Big)\Big]\Big)\Big/$$
$$\Big(2\ cM\ cp1\ mw1\ \pi\ R1\ \Big(1 + \frac{\Omega\ \xi T[\{\theta, \sigma\}]}{cM}\Big)\Big) -$$
$$\Big(\Omega\ \Big(\frac{\pi}{2} - \text{ArcTan}[\delta\ (\epsilon + \xi k1)]\Big)$$
$$\Big(\Theta + \frac{1}{2}\ aM\ (1 - \xi A)\ \Omega\ \text{Sin}\Big[aM\ \Big(-Mf + T - \frac{\sigma}{cA}\Big)\Big]\Big)\ \xi T^{(\{0,1\})}[\{\theta, \sigma\}]\Big)\Big/$$
$$\Big(cA\ cp1\ mw1\ \pi\ R1\ \Big(1 + \frac{\Omega\ \xi T[\{\theta, \sigma\}]}{cA}\Big)^2\Big) -$$
$$\Big(\Omega\ \Big(\frac{\pi}{2} + \text{ArcTan}[\delta\ (-\epsilon + \xi k1)]\Big)\ \Big(\Theta + \frac{1}{2}\ aA\ \xi M\ \Omega\ \text{Sin}\Big[aA\ \Big(-As + T - \frac{\sigma}{cM}\Big)\Big]\Big)$$
$$\xi T^{(\{0,1\})}[\{\theta, \sigma\}]\Big)\Big/\ \Big(cM\ cp1\ mw1\ \pi\ R1\ \Big(1 + \frac{\Omega\ \xi T[\{\theta, \sigma\}]}{cM}\Big)^2\Big)\Big) -$$
$$\frac{1}{b1 + bs} A1\ r1\ Ts^2\ \Big(\theta + \frac{Ts\ (-ks\ \Theta + A1\ r1\ \sigma - g\ ml\ rl\ \text{Sin}[\theta])}{b1 + bs}\Big)$$
$$\Big(-\Big(\Big(\Omega\ \Big(\frac{\pi}{2} - \text{ArcTan}[\delta\ (\epsilon + \xi k1)]\Big)$$
$$\Big(\Theta + \frac{1}{2}\ aM\ (1 - \xi A)\ \Omega\ \text{Sin}\Big[aM\ \Big(-Mf + T - \frac{\sigma}{cA}\Big)\Big]\Big)\ \xi T^{(\{1,0\})}[\{\theta, \sigma\}]\Big)\Big/$$
$$\Big(cA\ cp1\ mw1\ \pi\ R1\ \Big(1 + \frac{\Omega\ \xi T[\{\theta, \sigma\}]}{cA}\Big)^2\Big)\Big) -$$
$$\Big(\Omega\ \Big(\frac{\pi}{2} + \text{ArcTan}[\delta\ (-\epsilon + \xi k1)]\Big)\ \Big(\Theta + \frac{1}{2}\ aA\ \xi M\ \Omega\ \text{Sin}\Big[aA\ \Big(-As + T - \frac{\sigma}{cM}\Big)\Big]\Big)$$
$$\xi T^{(\{1,0\})}[\{\theta, \sigma\}]\Big)\Big/\ \Big(cM\ cp1\ mw1\ \pi\ R1\ \Big(1 + \frac{\Omega\ \xi T[\{\theta, \sigma\}]}{cM}\Big)^2\Big)\Big) -$$
$$\frac{1}{b1 + bs} A1\ r1\ Ts\ \Big(Ts\ \Big(\sigma + Ts\ \Big(\frac{1}{\pi}(-\text{ArcTan}[\delta\ (d\xi - \epsilon)] + \text{ArcTan}[\delta\ (d\xi + \epsilon)])$$
$$\Big(\frac{Aw1\ h0\ (-T + Ta)\ \Theta}{cp1\ mw1} - (E1\ r1$$
$$(-ks\ \Theta + A1\ r1\ \sigma - g\ ml\ rl\ \text{Sin}[\theta]))\ /\ ((b1 + bs)\ l10)\Big) +$$

$$\left(\left(\frac{\pi}{2}-\text{ArcTan}[\delta\ (\text{d}\xi+\epsilon)]\right)\ \left(-\left((\text{E1 r1}\ (-\text{ks}\,\theta+\text{A1 r1}\,\sigma-\text{g ml rl Sin}[\theta]))\ /\ ((\text{b1}+\text{bs})\ \text{l10})\right)+\left(\text{Aw1 h0}\ (-\text{T}+\text{Ta})\ \left(\Theta+\frac{1}{2}\,\text{aM}\ (1-\xi\text{A})\ \Omega\ \text{Sin}\left[\text{aM}\left(-\text{Mf}+\text{T}-\frac{\sigma}{\text{cA}}\right)\right]\right)\right)\Big/\ (\text{cp1 mw1})\right)\Big/\left(\pi\left(1+\frac{\Omega\,\xi\text{T}[\{\theta,\sigma\}]}{\text{cA}}\right)\right)+\left(\left(\frac{\pi}{2}+\text{ArcTan}[\delta\ (\text{d}\xi-\epsilon)]\right)\ \left(-\left((\text{E1 r1}\ (-\text{ks}\,\theta+\text{A1 r1}\,\sigma-\text{g ml rl Sin}[\theta]))\ /\ ((\text{b1}+\text{bs})\ \text{l10})\right)+\left(\text{Aw1 h0}\ (-\text{T}+\text{Ta})\ \left(\Theta+\frac{1}{2}\,\text{aA}\,\xi\text{M}\,\Omega\,\text{Sin}\left[\text{aA}\left(-\text{As}+\text{T}-\frac{\sigma}{\text{cM}}\right)\right]\right)\right)\Big/\ (\text{cp1 mw1})\right)\Big/\left(\pi\left(1+\frac{\Omega\,\xi\text{T}[\{\theta,\sigma\}]}{\text{cM}}\right)\right)\right)\right)$$

$$\left(-\left(\left(\text{aM}^2\ (1-\xi\text{A})\ \Omega\ \left(\frac{\pi}{2}-\text{ArcTan}[\delta\ (\epsilon+\xi\text{k1})]\right)\ \text{Cos}\left[\text{aM}\left(-\text{Mf}+\text{T}-\frac{\sigma}{\text{cA}}\right)\right]\right)\Big/\left(2\ \text{cA cp1 mw1}\,\pi\ \text{R1}\left(1+\frac{\Omega\,\xi\text{T}[\{\theta,\sigma\}]}{\text{cA}}\right)\right)\right)-\left(\text{aA}^2\,\xi\text{M}\,\Omega\left(\frac{\pi}{2}+\text{ArcTan}[\delta\ (-\epsilon+\xi\text{k1})]\right)\ \text{Cos}\left[\text{aA}\left(-\text{As}+\text{T}-\frac{\sigma}{\text{cM}}\right)\right]\right)\Big/\left(2\ \text{cM cp1 mw1}\,\pi\ \text{R1}\left(1+\frac{\Omega\,\xi\text{T}[\{\theta,\sigma\}]}{\text{cM}}\right)\right)-\left(\Omega\left(\frac{\pi}{2}-\text{ArcTan}[\delta\ (\epsilon+\xi\text{k1})]\right)\left(\Theta+\frac{1}{2}\,\text{aM}\ (1-\xi\text{A})\ \Omega\ \text{Sin}\left[\text{aM}\left(-\text{Mf}+\text{T}-\frac{\sigma}{\text{cA}}\right)\right]\right)\,\xi\text{T}^{(\{0,1\})}[\{\theta,\sigma\}]\right)\Big/\left(\text{cA cp1 mw1}\,\pi\ \text{R1}\left(1+\frac{\Omega\,\xi\text{T}[\{\theta,\sigma\}]}{\text{cA}}\right)^2\right)-\left(\Omega\left(\frac{\pi}{2}+\text{ArcTan}[\delta\ (-\epsilon+\xi\text{k1})]\right)\left(\Theta+\frac{1}{2}\,\text{aA}\,\xi\text{M}\,\Omega\,\text{Sin}\left[\text{aA}\left(-\text{As}+\text{T}-\frac{\sigma}{\text{cM}}\right)\right]\right)\,\xi\text{T}^{(\{0,1\})}[\{\theta,\sigma\}]\right)\Big/\left(\text{cM cp1 mw1}\,\pi\ \text{R1}\left(1+\frac{\Omega\,\xi\text{T}[\{\theta,\sigma\}]}{\text{cM}}\right)^2\right)\right)-\text{Ts}\left((\Theta\ (-\text{ArcTan}[\delta\ (-\epsilon+\xi\text{k1})]+\text{ArcTan}[\delta\ (\epsilon+\xi\text{k1})]))\ /\ (\text{cp1 mw1}\,\pi\ \text{R1})+\left(\left(\frac{\pi}{2}-\text{ArcTan}[\delta\ (\epsilon+\xi\text{k1})]\right)\left(\Theta+\frac{1}{2}\,\text{aM}\ (1-\xi\text{A})\ \Omega\ \text{Sin}\left[\text{aM}\left(-\text{Mf}+\text{T}-\frac{\sigma}{\text{cA}}\right)\right]\right)\right)\Big/\left(\text{cp1 mw1}\,\pi\ \text{R1}\left(1+\frac{\Omega\,\xi\text{T}[\{\theta,\sigma\}]}{\text{cA}}\right)\right)+\left(\left(\frac{\pi}{2}+\text{ArcTan}[\delta\ (-\epsilon+\xi\text{k1})]\right)\left(\Theta+\frac{1}{2}\,\text{aA}\,\xi\text{M}\,\Omega\,\text{Sin}\left[\text{aA}\left(-\text{As}+\text{T}-\frac{\sigma}{\text{cM}}\right)\right]\right)\right)\Big/\left(\text{cp1 mw1}\,\pi\ \text{R1}\left(1+\frac{\Omega\,\xi\text{T}[\{\theta,\sigma\}]}{\text{cM}}\right)\right)\right)\left(1+\text{Ts}\left(-\left(\left(\text{A1 E1 r1}^2\ (-\text{ArcTan}[\delta\ (\text{d}\xi-\epsilon)]+\text{ArcTan}[\delta\ (\text{d}\xi+\epsilon)])\right)\Big/\ ((\text{b1}+\text{bs})\ \text{l10}\,\pi)\right)+\left(\left(\frac{\pi}{2}-\text{ArcTan}[\delta\ (\text{d}\xi+\epsilon)]\right)\left(-\frac{\text{A1 E1 r1}^2}{(\text{b1}+\text{bs})\ \text{l10}}-\left(\text{aM}^2\ \text{Aw1 h0}\ (-\text{T}+\text{Ta})\ (1-\xi\text{A})\ \Omega\ \text{Cos}\left[\text{aM}\left(-\text{Mf}+\text{T}-\frac{\sigma}{\text{cA}}\right)\right]\right)\Big/\right.\right.\right.$$

$$
\begin{aligned}
&(2\ \mathrm{cA}\ \mathrm{cp1}\ \mathrm{mw1})\Big)\Big)\Big/\left(\pi\left(1+\frac{\Omega\,\xi\mathrm{T}[\{\theta,\ \sigma\}]}{\mathrm{cA}}\right)\right)+\\
&\left(\left(\frac{\pi}{2}+\mathrm{ArcTan}[\delta\ (\mathrm{d}\xi-\epsilon)]\right)\left(-\frac{\mathrm{A1}\ \mathrm{E1}\ \mathrm{r1}^2}{(\mathrm{b1}+\mathrm{bs})\ \mathrm{l10}}-\right.\right.\\
&\left.\left(\mathrm{aA}^2\ \mathrm{Aw1}\ \mathrm{h0}\ (-\mathrm{T}+\mathrm{Ta})\ \xi\mathrm{M}\,\Omega\,\mathrm{Cos}\left[\mathrm{aA}\left(-\mathrm{As}+\mathrm{T}-\frac{\sigma}{\mathrm{cM}}\right)\right]\right)\Big/\right.\\
&\left.(2\ \mathrm{cM}\ \mathrm{cp1}\ \mathrm{mw1})\right)\Big)\Big/\left(\pi\left(1+\frac{\Omega\,\xi\mathrm{T}[\{\theta,\ \sigma\}]}{\mathrm{cM}}\right)\right)-\\
&\frac{1}{\mathrm{cA}\,\pi\left(1+\frac{\Omega\,\xi\mathrm{T}[\{\theta,\sigma\}]}{\mathrm{cA}}\right)^2}\Omega\left(\frac{\pi}{2}-\mathrm{ArcTan}[\delta\ (\mathrm{d}\xi+\epsilon)]\right)\\
&\left(-\left((\mathrm{E1}\ \mathrm{r1}\ (-\mathrm{ks}\,\theta+\mathrm{A1}\ \mathrm{r1}\,\sigma-\mathrm{g}\ \mathrm{ml}\ \mathrm{rl}\ \mathrm{Sin}[\theta]))\Big/\right.\right.\\
&\left.((\mathrm{b1}+\mathrm{bs})\ \mathrm{l10})\right)+\left(\mathrm{Aw1}\ \mathrm{h0}\ (-\mathrm{T}+\mathrm{Ta})\ \left(\theta+\frac{1}{2}\,\mathrm{aM}\right.\right.\\
&\left.\left.(1-\xi\mathrm{A})\,\Omega\,\mathrm{Sin}\left[\mathrm{aM}\left(-\mathrm{Mf}+\mathrm{T}-\frac{\sigma}{\mathrm{cA}}\right)\right]\right)\Big)\Big/(\mathrm{cp1}\ \mathrm{mw1})\right)\\
&\xi\mathrm{T}^{(\{0,1\})}[\{\theta,\ \sigma\}]-\left(\Omega\left(\frac{\pi}{2}+\mathrm{ArcTan}[\delta\ (\mathrm{d}\xi-\epsilon)]\right)\right.\\
&\left(-\left((\mathrm{E1}\ \mathrm{r1}\ (-\mathrm{ks}\,\theta+\mathrm{A1}\ \mathrm{r1}\,\sigma-\mathrm{g}\ \mathrm{ml}\ \mathrm{rl}\ \mathrm{Sin}[\theta]))\Big/\right.\right.\\
&\left.((\mathrm{b1}+\mathrm{bs})\ \mathrm{l10})\right)+\left(\mathrm{Aw1}\ \mathrm{h0}\ (-\mathrm{T}+\mathrm{Ta})\right.\\
&\left.\left.\left(\theta+\frac{1}{2}\,\mathrm{aA}\,\xi\mathrm{M}\,\Omega\,\mathrm{Sin}\left[\mathrm{aA}\left(-\mathrm{As}+\mathrm{T}-\frac{\sigma}{\mathrm{cM}}\right)\right]\right)\Big)\Big/(\mathrm{cp1}\ \mathrm{mw1})\right)\\
&\left.\left.\xi\mathrm{T}^{(\{0,1\})}[\{\theta,\ \sigma\}]\right)\Big/\left(\mathrm{cM}\,\pi\left(1+\frac{\Omega\,\xi\mathrm{T}[\{\theta,\ \sigma\}]}{\mathrm{cM}}\right)^2\right)\right)\Big)+\\
&\mathrm{Ts}\left(\theta+\frac{\mathrm{Ts}\ (-\mathrm{ks}\,\theta+\mathrm{A1}\ \mathrm{r1}\,\sigma-\mathrm{g}\ \mathrm{ml}\ \mathrm{rl}\ \mathrm{Sin}[\theta])}{\mathrm{b1}+\mathrm{bs}}\right)\\
&\left(-\left(\left(\Omega\left(\frac{\pi}{2}-\mathrm{ArcTan}[\delta\ (\epsilon+\xi\mathrm{k1})]\right)\left(\theta+\frac{1}{2}\,\mathrm{aM}\ (1-\xi\mathrm{A})\ \Omega\right.\right.\right.\right.\\
&\left.\left.\left.\left.\mathrm{Sin}\left[\mathrm{aM}\left(-\mathrm{Mf}+\mathrm{T}-\frac{\sigma}{\mathrm{cA}}\right)\right]\right)\xi\mathrm{T}^{(\{1,0\})}[\{\theta,\ \sigma\}]\right)\Big/\right.\\
&\left.\left(\mathrm{cA}\ \mathrm{cp1}\ \mathrm{mw1}\,\pi\,\mathrm{R1}\left(1+\frac{\Omega\,\xi\mathrm{T}[\{\theta,\ \sigma\}]}{\mathrm{cA}}\right)^2\right)\right)-\\
&\left(\Omega\left(\frac{\pi}{2}+\mathrm{ArcTan}[\delta\ (-\epsilon+\xi\mathrm{k1})]\right)\right.\\
&\left.\left(\theta+\frac{1}{2}\,\mathrm{aA}\,\xi\mathrm{M}\,\Omega\,\mathrm{Sin}\left[\mathrm{aA}\left(-\mathrm{As}+\mathrm{T}-\frac{\sigma}{\mathrm{cM}}\right)\right]\right)\xi\mathrm{T}^{(\{1,0\})}[\{\theta,\ \sigma\}]\right)\Big/\\
&\left.\left(\mathrm{cM}\ \mathrm{cp1}\ \mathrm{mw1}\,\pi\,\mathrm{R1}\left(1+\frac{\Omega\,\xi\mathrm{T}[\{\theta,\ \sigma\}]}{\mathrm{cM}}\right)^2\right)\right)\Big),\\
&\frac{1}{\mathrm{b1}+\mathrm{bs}}\mathrm{A1}\ \mathrm{r1}\ \mathrm{Ts}^3\left((\theta\ (-\mathrm{ArcTan}[\delta\ (-\epsilon+\xi\mathrm{k1})]+\mathrm{ArcTan}[\delta\ (\epsilon+\xi\mathrm{k1})]))\Big/\right.\\
&(\mathrm{cp1}\ \mathrm{mw1}\,\pi\,\mathrm{R1})+\\
&\left(\left(\frac{\pi}{2}-\mathrm{ArcTan}[\delta\ (\epsilon+\xi\mathrm{k1})]\right)\right.\\
&\left.\left(\theta+\frac{1}{2}\,\mathrm{aM}\ (1-\xi\mathrm{A})\ \Omega\,\mathrm{Sin}\left[\mathrm{aM}\left(-\mathrm{Mf}+\mathrm{T}-\frac{\sigma}{\mathrm{cA}}\right)\right]\right)\Big)\Big/\right.\\
&\left.\left(\mathrm{cp1}\ \mathrm{mw1}\,\pi\,\mathrm{R1}\left(1+\frac{\Omega\,\xi\mathrm{T}[\{\theta,\ \sigma\}]}{\mathrm{cA}}\right)\right)+\right.\\
&\left.\left(\left(\frac{\pi}{2}+\mathrm{ArcTan}[\delta\ (-\epsilon+\xi\mathrm{k1})]\right)\left(\theta+\frac{1}{2}\,\mathrm{aA}\,\xi\mathrm{M}\,\Omega\,\mathrm{Sin}\left[\mathrm{aA}\left(-\mathrm{As}+\mathrm{T}-\frac{\sigma}{\mathrm{cM}}\right)\right]\right)\right)\Big)\Big/\right.
\end{aligned}
$$

$$\left(\text{cp1 mw1 } \pi \text{ R1 } \left(1+\frac{\Omega\, \xi\text{T}[\{\theta,\ \sigma\}]}{\text{cM}}\right)\right)\Bigg)\Bigg(-\left(\left(\text{E1 r1 } \left(-\text{ArcTan}[\delta\ (\text{d}\xi-\epsilon)]+\text{ArcTan}[\delta\ (\text{d}\xi+\epsilon)]\right)\right.\right.$$
$$\left.\left.(-\text{ks}-\text{g ml rl Cos}[\theta])\right)/\left((\text{b1}+\text{bs})\ \text{l10}\ \pi\right)\right)-$$
$$\left(\text{E1 r1 } \left(\frac{\pi}{2}-\text{ArcTan}[\delta\ (\text{d}\xi+\epsilon)]\right)\ (-\text{ks}-\text{g ml rl Cos}[\theta])\right)\Big/$$
$$\left((\text{b1}+\text{bs})\ \text{l10}\ \pi\ \left(1+\frac{\Omega\, \xi\text{T}[\{\theta,\ \sigma\}]}{\text{cA}}\right)\right)-$$
$$\left(\text{E1 r1 } \left(\frac{\pi}{2}+\text{ArcTan}[\delta\ (\text{d}\xi-\epsilon)]\right)\ (-\text{ks}-\text{g ml rl Cos}[\theta])\right)\Big/$$
$$\left((\text{b1}+\text{bs})\ \text{l10}\ \pi\ \left(1+\frac{\Omega\, \xi\text{T}[\{\theta,\ \sigma\}]}{\text{cM}}\right)\right)-$$
$$\left(\Omega\ \left(\frac{\pi}{2}-\text{ArcTan}[\delta\ (\text{d}\xi+\epsilon)]\right)\right.$$
$$\left(-\left((\text{E1 r1 } (-\text{ks}\,\theta+\text{A1 r1}\,\sigma-\text{g ml rl Sin}[\theta]))/((\text{b1}+\text{bs})\ \text{l10})\right)+\right.$$
$$\frac{1}{\text{cp1 mw1}}\text{Aw1 h0 } (-\text{T}+\text{Ta})$$
$$\left.\left.\left(\Theta+\frac{1}{2}\ \text{aM}\ (1-\xi\text{A})\ \Omega\ \text{Sin}\left[\text{aM}\ \left(-\text{Mf}+\text{T}-\frac{\sigma}{\text{cA}}\right)\right]\right)\right)$$
$$\left.\xi\text{T}^{(\{1,0\})}[\{\theta,\ \sigma\}]\right)\Big/\left(\text{cA}\,\pi\ \left(1+\frac{\Omega\, \xi\text{T}[\{\theta,\ \sigma\}]}{\text{cA}}\right)^2\right)-$$
$$\left(\Omega\ \left(\frac{\pi}{2}+\text{ArcTan}[\delta\ (\text{d}\xi-\epsilon)]\right)\right.$$
$$\left(-\left((\text{E1 r1 } (-\text{ks}\,\theta+\text{A1 r1}\,\sigma-\text{g ml rl Sin}[\theta]))/((\text{b1}+\text{bs})\ \text{l10})\right)+\right.$$
$$\frac{1}{\text{cp1 mw1}}\text{Aw1 h0 } (-\text{T}+\text{Ta})\ \left(\Theta+\frac{1}{2}\ \text{aA}\ \xi\text{M}\ \Omega\ \text{Sin}\left[\text{aA}\ \left(-\text{As}+\text{T}-\frac{\sigma}{\text{cM}}\right)\right]\right)\Bigg)$$
$$\left.\xi\text{T}^{(\{1,0\})}[\{\theta,\ \sigma\}]\right)\Big/\left(\text{cM}\,\pi\ \left(1+\frac{\Omega\, \xi\text{T}[\{\theta,\ \sigma\}]}{\text{cM}}\right)^2\right)\Bigg)-$$
$$\left(1+\text{Ts}\ \left(-\left(\left(\text{A1 E1 r1}^2\ (-\text{ArcTan}[\delta\ (\text{d}\xi-\epsilon)]+\text{ArcTan}[\delta\ (\text{d}\xi+\epsilon)])\right)\Big/\right.\right.\right.$$
$$\left.\left.\left.((\text{b1}+\text{bs})\ \text{l10}\ \pi)\right)+\right.$$
$$\left(\left(\frac{\pi}{2}-\text{ArcTan}[\delta\ (\text{d}\xi+\epsilon)]\right)\ \left(-\frac{\text{A1 E1 r1}^2}{(\text{b1}+\text{bs})\ \text{l10}}-\left(\text{aM}^2\ \text{Aw1 h0 } (-\text{T}+\text{Ta})\right.\right.\right.$$
$$\left.\left.\left.(1-\xi\text{A})\ \Omega\ \text{Cos}\left[\text{aM}\ \left(-\text{Mf}+\text{T}-\frac{\sigma}{\text{cA}}\right)\right]\right)\Big/\ (2\ \text{cA cp1 mw1})\right)\Bigg)\Big/$$
$$\left(\pi\ \left(1+\frac{\Omega\, \xi\text{T}[\{\theta,\ \sigma\}]}{\text{cA}}\right)\right)+\left(\left(\frac{\pi}{2}+\text{ArcTan}[\delta\ (\text{d}\xi-\epsilon)]\right)\right.$$
$$\left(-\frac{\text{A1 E1 r1}^2}{(\text{b1}+\text{bs})\ \text{l10}}-\left(\text{aA}^2\ \text{Aw1 h0 } (-\text{T}+\text{Ta})\ \xi\text{M}\,\Omega\right.\right.$$
$$\left.\left.\text{Cos}\left[\text{aA}\ \left(-\text{As}+\text{T}-\frac{\sigma}{\text{cM}}\right)\right]\right)\Big/\ (2\ \text{cM cp1 mw1})\Bigg)\Big/$$
$$\left(\pi\ \left(1+\frac{\Omega\, \xi\text{T}[\{\theta,\ \sigma\}]}{\text{cM}}\right)\right)-\left(\Omega\ \left(\frac{\pi}{2}-\text{ArcTan}[\delta\ (\text{d}\xi+\epsilon)]\right)\right.$$
$$\left(-\left((\text{E1 r1 } (-\text{ks}\,\theta+\text{A1 r1}\,\sigma-\text{g ml rl Sin}[\theta]))/\right.\right.$$
$$\left.\left.((\text{b1}+\text{bs})\ \text{l10})\right)+\frac{1}{\text{cp1 mw1}}\text{Aw1 h0 } (-\text{T}+\text{Ta})\right.$$
$$\left.\left.\left(\Theta+\frac{1}{2}\ \text{aM}\ (1-\xi\text{A})\ \Omega\ \text{Sin}\left[\text{aM}\ \left(-\text{Mf}+\text{T}-\frac{\sigma}{\text{cA}}\right)\right]\right)\right)$$

$$\xi T^{(\{0,1\})}[\{\theta,\ \sigma\}]\Big)\Big/\left(cA\,\pi\left(1+\frac{\Omega\,\xi T[\{\theta,\ \sigma\}]}{cA}\right)^2\right)-$$
$$\left(\Omega\left(\frac{\pi}{2}+\text{ArcTan}[\delta\ (d\xi-\epsilon)]\right)\left(-((E1\ r1\ (-ks\,\theta+A1\ r1\ \sigma-\right.\right.$$
$$g\ ml\ rl\ \text{Sin}[\theta]))\ /\ ((b1+bs)\ l10))+\frac{1}{cp1\ mw1}$$
$$\left.Aw1\ h0\ (-T+Ta)\left(\Theta+\frac{1}{2}\,aA\,\xi M\,\Omega\,\text{Sin}\left[aA\left(-As+T-\frac{\sigma}{cM}\right)\right]\right)\right)$$
$$\left.\xi T^{(\{0,1\})}[\{\theta,\ \sigma\}]\Big)\Big/\left(cM\,\pi\left(1+\frac{\Omega\,\xi T[\{\theta,\ \sigma\}]}{cM}\right)^2\right)\right)\Bigg)$$

$$\Bigg(Ts\left(\sigma+Ts\left(\frac{1}{\pi}(-\text{ArcTan}[\delta\ (d\xi-\epsilon)]+\text{ArcTan}[\delta\ (d\xi+\epsilon)]\right)\right.$$
$$\left(\frac{Aw1\ h0\ (-T+Ta)\ \Theta}{cp1\ mw1}-(E1\ r1\right.$$
$$\left.(-ks\,\theta+A1\ r1\ \sigma-g\ ml\ rl\ \text{Sin}[\theta]))\ /\ ((b1+bs)\ l10)\right)+$$
$$\left(\left(\frac{\pi}{2}-\text{ArcTan}[\delta\ (d\xi+\epsilon)]\right)\left(-((E1\ r1\ (-ks\,\theta+A1\ r1\ \sigma-g\ ml\right.\right.$$
$$rl\ \text{Sin}[\theta]))\ /\ ((b1+bs)\ l10))+\left(Aw1\ h0\ (-T+\right.$$
$$\left.\left.Ta)\left(\Theta+\frac{1}{2}\,aM\,(1-\xi A)\,\Omega\,\text{Sin}\left[aM\left(-Mf+T-\frac{\sigma}{cA}\right)\right]\right)\right)\Big/$$
$$\left.(cp1\ mw1)\right)\Big)\Big/\left(\pi\left(1+\frac{\Omega\,\xi T[\{\theta,\ \sigma\}]}{cA}\right)\right)+$$
$$\left(\left(\frac{\pi}{2}+\text{ArcTan}[\delta\ (d\xi-\epsilon)]\right)\left(-((E1\ r1\ (-ks\,\theta+A1\ r1\ \sigma-\right.\right.$$
$$g\ ml\ rl\ \text{Sin}[\theta]))\ /\ ((b1+bs)\ l10))+\left(Aw1\ h0\right.$$
$$\left.\left.(-T+Ta)\left(\Theta+\frac{1}{2}\,aA\,\xi M\,\Omega\,\text{Sin}\left[aA\left(-As+T-\frac{\sigma}{cM}\right)\right]\right)\right)\Big/\right.$$
$$\left.\left.(cp1\ mw1)\right)\Big)\Big/\left(\pi\left(1+\frac{\Omega\,\xi T[\{\theta,\ \sigma\}]}{cM}\right)\right)\right)\right)$$
$$\left(-\left(\left(aM^2\ (1-\xi A)\,\Omega\left(\frac{\pi}{2}-\text{ArcTan}[\delta\ (\epsilon+\xi k1)]\right)\text{Cos}\left[aM\left(-Mf+\right.\right.\right.\right.\right.$$
$$\left.\left.\left.\left.\left.T-\frac{\sigma}{cA}\right)\right]\right)\Big/\left(2\ cA\ cp1\ mw1\ \pi\ R1\left(1+\frac{\Omega\,\xi T[\{\theta,\ \sigma\}]}{cA}\right)\right)\right)-$$
$$\left(aA^2\,\xi M\,\Omega\left(\frac{\pi}{2}+\text{ArcTan}[\delta\ (-\epsilon+\xi k1)]\right)\text{Cos}\left[aA\left(-As+T-\frac{\sigma}{cM}\right)\right]\right)\Big/$$
$$\left(2\ cM\ cp1\ mw1\ \pi\ R1\left(1+\frac{\Omega\,\xi T[\{\theta,\ \sigma\}]}{cM}\right)\right)-$$
$$\left(\Omega\left(\frac{\pi}{2}-\text{ArcTan}[\delta\ (\epsilon+\xi k1)]\right)\right.$$
$$\left(\Theta+\frac{1}{2}\,aM\,(1-\xi A)\,\Omega\,\text{Sin}\left[aM\left(-Mf+T-\frac{\sigma}{cA}\right)\right]\right)$$
$$\left.\xi T^{(\{0,1\})}[\{\theta,\ \sigma\}]\right)\Big/\left(cA\ cp1\ mw1\ \pi\ R1\left(1+\frac{\Omega\,\xi T[\{\theta,\ \sigma\}]}{cA}\right)^2\right)-$$
$$\left(\Omega\left(\frac{\pi}{2}+\text{ArcTan}[\delta\ (-\epsilon+\xi k1)]\right)\right.$$
$$\left.\left(\Theta+\frac{1}{2}\,aA\,\xi M\,\Omega\,\text{Sin}\left[aA\left(-As+T-\frac{\sigma}{cM}\right)\right]\right)\xi T^{(\{0,1\})}[\{\theta,\ \sigma\}]\right)\Big/$$
$$\left.\left(cM\ cp1\ mw1\ \pi\ R1\left(1+\frac{\Omega\,\xi T[\{\theta,\ \sigma\}]}{cM}\right)^2\right)\right)-$$

$$
\begin{aligned}
&\mathrm{Ts}\left(\left(\Theta\left(-\mathrm{ArcTan}[\delta\,(-\epsilon+\xi\mathrm{k1})]+\mathrm{ArcTan}[\delta\,(\epsilon+\xi\mathrm{k1})]\right)\right)\Big/\right.\\
&\quad(\mathrm{cp1\,mw1}\,\pi\,\mathrm{R1})+\left(\left(\frac{\pi}{2}-\mathrm{ArcTan}[\delta\,(\epsilon+\xi\mathrm{k1})]\right)\right.\\
&\qquad\left.\left(\Theta+\frac{1}{2}\,\mathrm{aM}\,(1-\xi\mathrm{A})\,\Omega\,\mathrm{Sin}\left[\mathrm{aM}\left(-\mathrm{Mf}+\mathrm{T}-\frac{\sigma}{\mathrm{cA}}\right)\right]\right)\right)\Big/\\
&\quad\left(\mathrm{cp1\,mw1}\,\pi\,\mathrm{R1}\left(1+\frac{\Omega\,\xi\mathrm{T}[\{\theta,\sigma\}]}{\mathrm{cA}}\right)\right)+\left(\left(\frac{\pi}{2}+\mathrm{ArcTan}[\delta\,(-\epsilon+\xi\mathrm{k1})]\right)\right.\\
&\qquad\left.\left(\Theta+\frac{1}{2}\,\mathrm{aA}\,\xi\mathrm{M}\,\Omega\,\mathrm{Sin}\left[\mathrm{aA}\left(-\mathrm{As}+\mathrm{T}-\frac{\sigma}{\mathrm{cM}}\right)\right]\right)\right)\Big/\\
&\quad\left.\left(\mathrm{cp1\,mw1}\,\pi\,\mathrm{R1}\left(1+\frac{\Omega\,\xi\mathrm{T}[\{\theta,\sigma\}]}{\mathrm{cM}}\right)\right)\right)\\
&\left(1+\mathrm{Ts}\left[-\left(\left(\mathrm{A1\,E1\,r1}^2\,(-\mathrm{ArcTan}[\delta\,(\mathrm{d}\xi-\epsilon)]+\mathrm{ArcTan}[\delta\,(\mathrm{d}\xi+\epsilon)])\right)\Big/\right.\right.\right.\\
&\qquad\left.\left.\left.((\mathrm{b1}+\mathrm{bs})\,\mathrm{l10}\,\pi)\right)+\right.\\
&\qquad\left(\left(\frac{\pi}{2}-\mathrm{ArcTan}[\delta\,(\mathrm{d}\xi+\epsilon)]\right)\left(-\frac{\mathrm{A1\,E1\,r1}^2}{(\mathrm{b1}+\mathrm{bs})\,\mathrm{l10}}-\left(\mathrm{aM}^2\,\mathrm{Aw1}\right.\right.\right.\\
&\qquad\qquad\left.\left.\left.\mathrm{h0}\,(-\mathrm{T}+\mathrm{Ta})\,(1-\xi\mathrm{A})\,\Omega\,\mathrm{Cos}\left[\mathrm{aM}\left(-\mathrm{Mf}+\mathrm{T}-\frac{\sigma}{\mathrm{cA}}\right)\right]\right)\Big/\right.\\
&\qquad\left.\left.\left.(2\,\mathrm{cA\,cp1\,mw1})\right)\right)\Big/\left(\pi\left(1+\frac{\Omega\,\xi\mathrm{T}[\{\theta,\sigma\}]}{\mathrm{cA}}\right)\right)+\right.\\
&\qquad\left(\left(\frac{\pi}{2}+\mathrm{ArcTan}[\delta\,(\mathrm{d}\xi-\epsilon)]\right)\left(-\frac{\mathrm{A1\,E1\,r1}^2}{(\mathrm{b1}+\mathrm{bs})\,\mathrm{l10}}-\right.\right.\\
&\qquad\qquad\left.\left.\left(\mathrm{aA}^2\,\mathrm{Aw1\,h0}\,(-\mathrm{T}+\mathrm{Ta})\,\xi\mathrm{M}\,\Omega\,\mathrm{Cos}\left[\mathrm{aA}\left(-\mathrm{As}+\mathrm{T}-\frac{\sigma}{\mathrm{cM}}\right)\right]\right)\Big/\right.\\
&\qquad\left.\left.(2\,\mathrm{cM\,cp1\,mw1})\right)\right)\Big/\left(\pi\left(1+\frac{\Omega\,\xi\mathrm{T}[\{\theta,\sigma\}]}{\mathrm{cM}}\right)\right)-\\
&\qquad\frac{1}{\mathrm{cA}\,\pi\left(1+\frac{\Omega\,\xi\mathrm{T}[\{\theta,\sigma\}]}{\mathrm{cA}}\right)^2}\Omega\left(\frac{\pi}{2}-\mathrm{ArcTan}[\delta\,(\mathrm{d}\xi+\epsilon)]\right)\\
&\qquad\left(-\left((\mathrm{E1\,r1}\,(-\mathrm{ks}\,\theta+\mathrm{A1\,r1}\,\sigma-\mathrm{g\,ml\,rl\,Sin}[\theta]))\Big/\right.\right.\\
&\qquad\qquad\left.\left.((\mathrm{b1}+\mathrm{bs})\,\mathrm{l10})\right)+\left(\mathrm{Aw1\,h0}\,(-\mathrm{T}+\mathrm{Ta})\left(\Theta+\frac{1}{2}\,\mathrm{aM}\right.\right.\right.\\
&\qquad\qquad\left.\left.\left.(1-\xi\mathrm{A})\,\Omega\,\mathrm{Sin}\left[\mathrm{aM}\left(-\mathrm{Mf}+\mathrm{T}-\frac{\sigma}{\mathrm{cA}}\right)\right]\right)\right)\Big/(\mathrm{cp1\,mw1})\Big)\\
&\qquad\xi\mathrm{T}^{(\{0,1\})}[\{\theta,\sigma\}]-\left(\Omega\left(\frac{\pi}{2}+\mathrm{ArcTan}[\delta\,(\mathrm{d}\xi-\epsilon)]\right)\right.\\
&\qquad\qquad\left(-\left((\mathrm{E1\,r1}\,(-\mathrm{ks}\,\theta+\mathrm{A1\,r1}\,\sigma-\mathrm{g\,ml\,rl\,Sin}[\theta]))\Big/\right.\right.\\
&\qquad\qquad\qquad\left.\left.((\mathrm{b1}+\mathrm{bs})\,\mathrm{l10})\right)+\left(\mathrm{Aw1\,h0}\,(-\mathrm{T}+\mathrm{Ta})\right.\right.\\
&\qquad\qquad\qquad\left.\left.\left(\Theta+\frac{1}{2}\,\mathrm{aA}\,\xi\mathrm{M}\,\Omega\,\mathrm{Sin}\left[\mathrm{aA}\left(-\mathrm{As}+\mathrm{T}-\frac{\sigma}{\mathrm{cM}}\right)\right]\right)\right)\Big/(\mathrm{cp1\,mw1})\Big)\\
&\qquad\left.\left.\xi\mathrm{T}^{(\{0,1\})}[\{\theta,\sigma\}]\right)\Big/\left(\mathrm{cM}\,\pi\left(1+\frac{\Omega\,\xi\mathrm{T}[\{\theta,\sigma\}]}{\mathrm{cM}}\right)^2\right)\right)\Bigg]+\\
&\mathrm{Ts}\left(\Theta+\frac{\mathrm{Ts}\,(-\mathrm{ks}\,\theta+\mathrm{A1\,r1}\,\sigma-\mathrm{g\,ml\,rl\,Sin}[\theta])}{\mathrm{b1}+\mathrm{bs}}\right)\\
&\left(-\left(\left(\Omega\left(\frac{\pi}{2}-\mathrm{ArcTan}[\delta\,(\epsilon+\xi\mathrm{k1})]\right)\right)\left(\Theta+\frac{1}{2}\,\mathrm{aM}\,(1-\xi\mathrm{A})\,\Omega\right.\right.\right.\\
&\qquad\left.\left.\left.\mathrm{Sin}\left[\mathrm{aM}\left(-\mathrm{Mf}+\mathrm{T}-\frac{\sigma}{\mathrm{cA}}\right)\right]\right)\xi\mathrm{T}^{(\{1,0\})}[\{\theta,\sigma\}]\right)\Big/
\end{aligned}
$$

$$\left(\text{cA cp1 mw1 }\pi\text{ R1 }\left(1+\frac{\Omega\,\xi\text{T}[\{\theta,\,\sigma\}]}{\text{cA}}\right)^2\right)\Bigg)-$$
$$\left(\Omega\left(\frac{\pi}{2}+\text{ArcTan}[\delta\,(-\epsilon+\xi\text{k1})]\right)\right.$$
$$\left.\left(\Theta+\frac{1}{2}\,\text{aA}\,\xi\text{M}\,\Omega\,\text{Sin}\left[\text{aA}\left(-\text{As}+\text{T}-\frac{\sigma}{\text{cM}}\right)\right]\right)\xi\text{T}^{(\{1,0\})}[\{\theta,\,\sigma\}]\right)\Big/$$
$$\left.\left(\text{cM cp1 mw1 }\pi\text{ R1 }\left(1+\frac{\Omega\,\xi\text{T}[\{\theta,\,\sigma\}]}{\text{cM}}\right)^2\right)\right)\Bigg)+$$
$$\left(\sigma+\text{Ts}\left(\frac{1}{\pi}(-\text{ArcTan}[\delta\,(\text{d}\xi-\epsilon)]+\text{ArcTan}[\delta\,(\text{d}\xi+\epsilon)])\right.\right.$$
$$\left(\frac{\text{Aw1 h0 }(-\text{T}+\text{Ta})\,\Theta}{\text{cp1 mw1}}-\right.$$
$$\left.(\text{E1 r1 }(-\text{ks}\,\Theta+\text{A1 r1}\,\sigma-\text{g ml rl Sin}[\theta]))\,/\,((\text{b1}+\text{bs})\,\text{l10})\right)+$$
$$\left(\left(\frac{\pi}{2}-\text{ArcTan}[\delta\,(\text{d}\xi+\epsilon)]\right)\left(-((\text{E1 r1 }(-\text{ks}\,\Theta+\text{A1 r1}\,\sigma-\text{g ml}\right.\right.\right.$$
$$\text{rl Sin}[\theta]))\,/\,((\text{b1}+\text{bs})\,\text{l10}))+\frac{1}{\text{cp1 mw1}}\text{Aw1 h0}$$
$$\left.\left.\left.(-\text{T}+\text{Ta})\left(\Theta+\frac{1}{2}\,\text{aM}\,(1-\xi\text{A})\,\Omega\,\text{Sin}\left[\text{aM}\left(-\text{Mf}+\text{T}-\frac{\sigma}{\text{cA}}\right)\right]\right)\right)\right)\Big/$$
$$\left(\pi\left(1+\frac{\Omega\,\xi\text{T}[\{\theta,\,\sigma\}]}{\text{cA}}\right)\right)+\left(\left(\frac{\pi}{2}+\text{ArcTan}[\delta\,(\text{d}\xi-\epsilon)]\right)\right.$$
$$\left(-((\text{E1 r1 }(-\text{ks}\,\Theta+\text{A1 r1}\,\sigma-\text{g ml rl Sin}[\theta]))\,/\,((\text{b1}+\text{bs})\right.$$
$$\text{l10}))+\frac{1}{\text{cp1 mw1}}\text{Aw1 h0 }(-\text{T}+\text{Ta})\left(\Theta+\frac{1}{2}\,\text{aA}\,\xi\text{M}\,\Omega\right.$$
$$\left.\left.\left.\text{Sin}\left[\text{aA}\left(-\text{As}+\text{T}-\frac{\sigma}{\text{cM}}\right)\right]\right)\right)\right)\Big/\left(\pi\left(1+\frac{\Omega\,\xi\text{T}[\{\theta,\,\sigma\}]}{\text{cM}}\right)\right)\Bigg)\Bigg)$$
$$\left(\text{Ts}\left(\sigma+\text{Ts}\left(\frac{1}{\pi}(-\text{ArcTan}[\delta\,(\text{d}\xi-\epsilon)]+\text{ArcTan}[\delta\,(\text{d}\xi+\epsilon)])\right.\right.\right.$$
$$\left(\frac{\text{Aw1 h0 }(-\text{T}+\text{Ta})\,\Theta}{\text{cp1 mw1}}-(\text{E1 r1}\right.$$
$$\left.(-\text{ks}\,\Theta+\text{A1 r1}\,\sigma-\text{g ml rl Sin}[\theta]))\,/\,((\text{b1}+\text{bs})\,\text{l10})\right)+$$
$$\left(\left(\frac{\pi}{2}-\text{ArcTan}[\delta\,(\text{d}\xi+\epsilon)]\right)\left(-((\text{E1 r1 }(-\text{ks}\,\Theta+\text{A1 r1}\,\sigma-\text{g ml}\right.\right.\right.$$
$$\text{rl Sin}[\theta]))\,/\,((\text{b1}+\text{bs})\,\text{l10}))+\left(\text{Aw1 h0 }(-\text{T}+\right.$$
$$\left.\left.\text{Ta})\left(\Theta+\frac{1}{2}\,\text{aM}\,(1-\xi\text{A})\,\Omega\,\text{Sin}\left[\text{aM}\left(-\text{Mf}+\text{T}-\frac{\sigma}{\text{cA}}\right)\right]\right)\right)\Big/$$
$$\left.\left.(\text{cp1 mw1})\right)\right)\Big/\left(\pi\left(1+\frac{\Omega\,\xi\text{T}[\{\theta,\,\sigma\}]}{\text{cA}}\right)\right)+$$
$$\left(\left(\frac{\pi}{2}+\text{ArcTan}[\delta\,(\text{d}\xi-\epsilon)]\right)\left(-((\text{E1 r1 }(-\text{ks}\,\Theta+\text{A1 r1}\,\sigma-\right.\right.\right.$$
$$\text{g ml rl Sin}[\theta]))\,/\,((\text{b1}+\text{bs})\,\text{l10}))+\left(\text{Aw1 h0}\right.$$
$$\left.\left.(-\text{T}+\text{Ta})\left(\Theta+\frac{1}{2}\,\text{aA}\,\xi\text{M}\,\Omega\,\text{Sin}\left[\text{aA}\left(-\text{As}+\text{T}-\frac{\sigma}{\text{cM}}\right)\right]\right)\right)\Big/$$
$$\left.\left.(\text{cp1 mw1})\right)\right)\Big/\left(\pi\left(1+\frac{\Omega\,\xi\text{T}[\{\theta,\,\sigma\}]}{\text{cM}}\right)\right)\Bigg)\Bigg)$$
$$\left(-\left(\left(\text{aM}^3\,(1-\xi\text{A})\,\Omega\left(\frac{\pi}{2}-\text{ArcTan}[\delta\,(\epsilon+\xi\text{k1})]\right)\text{Sin}\left[\text{aM}\left(-\text{Mf}+\right.\right.\right.\right.\right.$$

$$
\left(\mathrm{T}-\frac{\sigma}{\mathrm{cA}}\right)\right]\Big)\Big/\left(2\,\mathrm{cA}^2\,\mathrm{cp1}\,\mathrm{mw1}\,\pi\,\mathrm{R1}\left(1+\frac{\Omega\,\xi\mathrm{T}[\{\theta,\,\sigma\}]}{\mathrm{cA}}\right)\right)\Big)-
$$

$$
\left(\mathrm{aA}^3\,\xi\mathrm{M}\,\Omega\left(\frac{\pi}{2}+\mathrm{ArcTan}[\delta\,(-\epsilon+\xi\mathrm{k1})]\right)\mathrm{Sin}\left[\mathrm{aA}\left(-\mathrm{As}+\mathrm{T}-\frac{\sigma}{\mathrm{cM}}\right)\right]\right)\Big/
$$

$$
\left(2\,\mathrm{cM}^2\,\mathrm{cp1}\,\mathrm{mw1}\,\pi\,\mathrm{R1}\left(1+\frac{\Omega\,\xi\mathrm{T}[\{\theta,\,\sigma\}]}{\mathrm{cM}}\right)\right)+
$$

$$
\left(\mathrm{aM}^2\,(1-\xi\mathrm{A})\,\Omega^2\left(\frac{\pi}{2}-\mathrm{ArcTan}[\delta\,(\epsilon+\xi\mathrm{k1})]\right)\right.
$$

$$
\left.\mathrm{Cos}\left[\mathrm{aM}\left(-\mathrm{Mf}+\mathrm{T}-\frac{\sigma}{\mathrm{cA}}\right)\right]\,\xi\mathrm{T}^{(\{0,1\})}[\{\theta,\,\sigma\}]\right)\Big/
$$

$$
\left(\mathrm{cA}^2\,\mathrm{cp1}\,\mathrm{mw1}\,\pi\,\mathrm{R1}\left(1+\frac{\Omega\,\xi\mathrm{T}[\{\theta,\,\sigma\}]}{\mathrm{cA}}\right)^2\right)+
$$

$$
\left(\mathrm{aA}^2\,\xi\mathrm{M}\,\Omega^2\left(\frac{\pi}{2}+\mathrm{ArcTan}[\delta\,(-\epsilon+\xi\mathrm{k1})]\right)\right.
$$

$$
\left.\mathrm{Cos}\left[\mathrm{aA}\left(-\mathrm{As}+\mathrm{T}-\frac{\sigma}{\mathrm{cM}}\right)\right]\,\xi\mathrm{T}^{(\{0,1\})}[\{\theta,\,\sigma\}]\right)\Big/
$$

$$
\left(\mathrm{cM}^2\,\mathrm{cp1}\,\mathrm{mw1}\,\pi\,\mathrm{R1}\left(1+\frac{\Omega\,\xi\mathrm{T}[\{\theta,\,\sigma\}]}{\mathrm{cM}}\right)^2\right)+
$$

$$
\left(2\,\Omega^2\left(\frac{\pi}{2}-\mathrm{ArcTan}[\delta\,(\epsilon+\xi\mathrm{k1})]\right)\right.
$$

$$
\left(\Theta+\frac{1}{2}\,\mathrm{aM}\,(1-\xi\mathrm{A})\,\Omega\,\mathrm{Sin}\left[\mathrm{aM}\left(-\mathrm{Mf}+\mathrm{T}-\frac{\sigma}{\mathrm{cA}}\right)\right]\right)
$$

$$
\left.\xi\mathrm{T}^{(\{0,1\})}[\{\theta,\,\sigma\}]^2\right)\Big/\left(\mathrm{cA}^2\,\mathrm{cp1}\,\mathrm{mw1}\,\pi\,\mathrm{R1}\left(1+\frac{\Omega\,\xi\mathrm{T}[\{\theta,\,\sigma\}]}{\mathrm{cA}}\right)^3\right)+
$$

$$
\left(2\,\Omega^2\left(\frac{\pi}{2}+\mathrm{ArcTan}[\delta\,(-\epsilon+\xi\mathrm{k1})]\right)\right.
$$

$$
\left.\left(\Theta+\frac{1}{2}\,\mathrm{aA}\,\xi\mathrm{M}\,\Omega\,\mathrm{Sin}\left[\mathrm{aA}\left(-\mathrm{As}+\mathrm{T}-\frac{\sigma}{\mathrm{cM}}\right)\right]\right)\xi\mathrm{T}^{(\{0,1\})}[\{\theta,\,\sigma\}]^2\right)\Big/
$$

$$
\left(\mathrm{cM}^2\,\mathrm{cp1}\,\mathrm{mw1}\,\pi\,\mathrm{R1}\left(1+\frac{\Omega\,\xi\mathrm{T}[\{\theta,\,\sigma\}]}{\mathrm{cM}}\right)^3\right)-
$$

$$
\left(\Omega\left(\frac{\pi}{2}-\mathrm{ArcTan}[\delta\,(\epsilon+\xi\mathrm{k1})]\right)\right.
$$

$$
\left(\Theta+\frac{1}{2}\,\mathrm{aM}\,(1-\xi\mathrm{A})\,\Omega\,\mathrm{Sin}\left[\mathrm{aM}\left(-\mathrm{Mf}+\mathrm{T}-\frac{\sigma}{\mathrm{cA}}\right)\right]\right)
$$

$$
\left.\xi\mathrm{T}^{(\{0,2\})}[\{\theta,\,\sigma\}]\right)\Big/\left(\mathrm{cA}\,\mathrm{cp1}\,\mathrm{mw1}\,\pi\,\mathrm{R1}\left(1+\frac{\Omega\,\xi\mathrm{T}[\{\theta,\,\sigma\}]}{\mathrm{cA}}\right)^2\right)-
$$

$$
\left(\Omega\left(\frac{\pi}{2}+\mathrm{ArcTan}[\delta\,(-\epsilon+\xi\mathrm{k1})]\right)\right.
$$

$$
\left.\left(\Theta+\frac{1}{2}\,\mathrm{aA}\,\xi\mathrm{M}\,\Omega\,\mathrm{Sin}\left[\mathrm{aA}\left(-\mathrm{As}+\mathrm{T}-\frac{\sigma}{\mathrm{cM}}\right)\right]\right)\xi\mathrm{T}^{(\{0,2\})}[\{\theta,\,\sigma\}]\right)\Big/
$$

$$
\left.\left(\mathrm{cM}\,\mathrm{cp1}\,\mathrm{mw1}\,\pi\,\mathrm{R1}\left(1+\frac{\Omega\,\xi\mathrm{T}[\{\theta,\,\sigma\}]}{\mathrm{cM}}\right)^2\right)\right)-
$$

$$
\mathrm{Ts}^2\left(\left(\Theta\,(-\mathrm{ArcTan}[\delta\,(-\epsilon+\xi\mathrm{k1})]+\mathrm{ArcTan}[\delta\,(\epsilon+\xi\mathrm{k1})])\right)/\right.
$$

$$
(\mathrm{cp1}\,\mathrm{mw1}\,\pi\,\mathrm{R1})+\left(\left(\frac{\pi}{2}-\mathrm{ArcTan}[\delta\,(\epsilon+\xi\mathrm{k1})]\right)\right.
$$

$$
\left.\left.\left(\Theta+\frac{1}{2}\,\mathrm{aM}\,(1-\xi\mathrm{A})\,\Omega\,\mathrm{Sin}\left[\mathrm{aM}\left(-\mathrm{Mf}+\mathrm{T}-\frac{\sigma}{\mathrm{cA}}\right)\right]\right)\right)\Big/\right.
$$

$$
\left(\mathrm{cp1}\,\mathrm{mw1}\,\pi\,\mathrm{R1}\left(1+\frac{\Omega\,\xi\mathrm{T}[\{\theta,\,\sigma\}]}{\mathrm{cA}}\right)\right)+
$$

$$
\left(\left(\frac{\pi}{2}+\mathrm{ArcTan}[\delta\,(-\epsilon+\xi\mathrm{k1})]\right)\right.
$$

$$
\left.\left.\left(\Theta+\frac{1}{2}\,\mathrm{aA}\,\xi\mathrm{M}\,\Omega\,\mathrm{Sin}\left[\mathrm{aA}\left(-\mathrm{As}+\mathrm{T}-\frac{\sigma}{\mathrm{cM}}\right)\right]\right)\right)\Big/\right.
$$

$$\left(\text{cp1 mw1 } \pi \text{ R1 } \left(1+\frac{\Omega\, \xi T[\{\theta,\ \sigma\}]}{\text{cM}}\right)\right)\Bigg)$$

$$\Bigg(-\Bigg(\Big(\text{aM}^3 \text{ Aw1 h0 } (-\text{T}+\text{Ta}) \ (1-\xi\text{A})\ \Omega \left(\frac{\pi}{2}-\text{ArcTan}[\delta\ (\text{d}\xi+\epsilon)]\right) \text{Sin}\Big[\text{aM}$$

$$\left(-\text{Mf}+\text{T}-\frac{\sigma}{\text{cA}}\right)\Big]\Big)\Big/\left(2\ \text{cA}^2\ \text{cp1 mw1}\ \pi\left(1+\frac{\Omega\, \xi T[\{\theta,\ \sigma\}]}{\text{cA}}\right)\right)\Bigg)-$$

$$\Bigg(\text{aA}^3 \text{ Aw1 h0 } (-\text{T}+\text{Ta}) \ \xi\text{M}\,\Omega \left(\frac{\pi}{2}+\text{ArcTan}[\delta\ (\text{d}\xi-\epsilon)]\right)$$

$$\text{Sin}\Big[\text{aA}\left(-\text{As}+\text{T}-\frac{\sigma}{\text{cM}}\right)\Big]\Bigg)\Big/$$

$$\left(2\ \text{cM}^2\ \text{cp1 mw1}\ \pi\left(1+\frac{\Omega\, \xi T[\{\theta,\ \sigma\}]}{\text{cM}}\right)\right)-$$

$$\Bigg(2\,\Omega\left(\frac{\pi}{2}-\text{ArcTan}[\delta\ (\text{d}\xi+\epsilon)]\right)$$

$$\left(-\frac{\text{A1 E1 r1}^2}{(\text{b1}+\text{bs})\ \text{l10}}-\Big(\text{aM}^2 \text{ Aw1 h0 } (-\text{T}+\text{Ta}) \ (1-\xi\text{A})\ \Omega\right.$$

$$\left.\text{Cos}\Big[\text{aM}\left(-\text{Mf}+\text{T}-\frac{\sigma}{\text{cA}}\right)\Big]\Big)\Big/\ (2\ \text{cA cp1 mw1})\right)$$

$$\xi T^{(\{0,1\})}[\{\theta,\ \sigma\}]\Bigg)\Big/\left(\text{cA}\,\pi\left(1+\frac{\Omega\, \xi T[\{\theta,\ \sigma\}]}{\text{cA}}\right)^2\right)-$$

$$\Bigg(2\,\Omega\left(\frac{\pi}{2}+\text{ArcTan}[\delta\ (\text{d}\xi-\epsilon)]\right)\left(-\frac{\text{A1 E1 r1}^2}{(\text{b1}+\text{bs})\ \text{l10}}-\Big(\text{aA}^2 \text{ Aw1 h0}\right.$$

$$\left.(-\text{T}+\text{Ta}) \ \xi\text{M}\,\Omega\,\text{Cos}\Big[\text{aA}\left(-\text{As}+\text{T}-\frac{\sigma}{\text{cM}}\right)\Big]\Big)\Big/\ (2\ \text{cM cp1 mw1})\right)$$

$$\xi T^{(\{0,1\})}[\{\theta,\ \sigma\}]\Bigg)\Big/\left(\text{cM}\,\pi\left(1+\frac{\Omega\, \xi T[\{\theta,\ \sigma\}]}{\text{cM}}\right)^2\right)+$$

$$\frac{1}{\text{cA}^2\,\pi\left(1+\frac{\Omega\, \xi T[\{\theta,\sigma\}]}{\text{cA}}\right)^3}2\,\Omega^2\left(\frac{\pi}{2}-\text{ArcTan}[\delta\ (\text{d}\xi+\epsilon)]\right)$$

$$\Bigg(-((\text{E1 r1}\ (-\text{ks}\,\theta+\text{A1 r1}\,\sigma-\text{g ml rl Sin}[\theta]))\ /\ ((\text{b1}+\text{bs})\ \text{l10}))+$$

$$\frac{1}{\text{cp1 mw1}}\text{Aw1 h0 } (-\text{T}+\text{Ta})$$

$$\left(\Theta+\frac{1}{2}\ \text{aM}\ (1-\xi\text{A})\ \Omega\ \text{Sin}\Big[\text{aM}\left(-\text{Mf}+\text{T}-\frac{\sigma}{\text{cA}}\right)\Big]\right)\Bigg)$$

$$\xi T^{(\{0,1\})}[\{\theta,\ \sigma\}]^2+\Bigg(2\,\Omega^2\left(\frac{\pi}{2}+\text{ArcTan}[\delta\ (\text{d}\xi-\epsilon)]\right)$$

$$\Bigg(-((\text{E1 r1}\ (-\text{ks}\,\theta+\text{A1 r1}\,\sigma-\text{g ml rl Sin}[\theta]))\ /$$

$$((\text{b1}+\text{bs})\ \text{l10}))+\frac{1}{\text{cp1 mw1}}\text{Aw1 h0 } (-\text{T}+\text{Ta})\ \Bigg(\Theta+$$

$$\frac{1}{2}\ \text{aA}\ \xi\text{M}\,\Omega\ \text{Sin}\Big[\text{aA}\left(-\text{As}+\text{T}-\frac{\sigma}{\text{cM}}\right)\Big]\Bigg)\Bigg)\ \xi T^{(\{0,1\})}[\{\theta,\ \sigma\}]^2\Bigg)\Big/$$

$$\left(\text{cM}^2\,\pi\left(1+\frac{\Omega\, \xi T[\{\theta,\ \sigma\}]}{\text{cM}}\right)^3\right)-\Bigg(\Omega\left(\frac{\pi}{2}-\text{ArcTan}[\delta\ (\text{d}\xi+\epsilon)]\right)$$

$$\Bigg(-((\text{E1 r1}\ (-\text{ks}\,\theta+\text{A1 r1}\,\sigma-\text{g ml rl Sin}[\theta]))\ /$$

$$((\text{b1}+\text{bs})\ \text{l10}))+\frac{1}{\text{cp1 mw1}}\text{Aw1 h0 } (-\text{T}+\text{Ta})$$

$$\left(\Theta+\frac{1}{2}\ \text{aM}\ (1-\xi\text{A})\ \Omega\ \text{Sin}\Big[\text{aM}\left(-\text{Mf}+\text{T}-\frac{\sigma}{\text{cA}}\right)\Big]\right)\Bigg)$$

$$\left.\xi T^{(\{0,2\})}[\{\theta,\sigma\}]\right)\Big/\left(cA\,\pi\left(1+\frac{\Omega\,\xi T[\{\theta,\sigma\}]}{cA}\right)^2\right)-$$
$$\left(\Omega\left(\frac{\pi}{2}+\text{ArcTan}[\delta\,(d\xi-\epsilon)]\right)\left(-((E1\;r1\;(-ks\,\theta+A1\;r1\,\sigma-\right.\right.$$
$$\left.g\,ml\,rl\,\text{Sin}[\theta]))/((b1+bs)\;l10))+\frac{1}{cp1\;mw1}\right.$$
$$\left.Aw1\;h0\;(-T+Ta)\left(\Theta+\frac{1}{2}\,aA\,\xi M\,\Omega\,\text{Sin}\left[aA\left(-As+T-\frac{\sigma}{cM}\right)\right]\right)\right)$$
$$\left.\xi T^{(\{0,2\})}[\{\theta,\sigma\}]\right)\Big/\left(cM\,\pi\left(1+\frac{\Omega\,\xi T[\{\theta,\sigma\}]}{cM}\right)^2\right)\Bigg)+$$

$$\frac{1}{b1+bs}A1\;r1\;Ts^2\left(-\left(\left(\Omega\left(\frac{\pi}{2}-\text{ArcTan}[\delta\,(\epsilon+\xi k1)]\right)\right.\right.\right.$$
$$\left.\left.\left(\Theta+\frac{1}{2}\,aM\,(1-\xi A)\,\Omega\,\text{Sin}\left[aM\left(-Mf+T-\frac{\sigma}{cA}\right)\right]\right)\right.\right.$$
$$\left.\left.\xi T^{(\{1,0\})}[\{\theta,\sigma\}]\right)\Big/\left(cA\;cp1\;mw1\;\pi\;R1\left(1+\frac{\Omega\,\xi T[\{\theta,\sigma\}]}{cA}\right)^2\right)\right)-$$
$$\left(\Omega\left(\frac{\pi}{2}+\text{ArcTan}[\delta\,(-\epsilon+\xi k1)]\right)\left(\Theta+\frac{1}{2}\,aA\,\xi M\,\Omega\right.\right.$$
$$\left.\left.\text{Sin}\left[aA\left(-As+T-\frac{\sigma}{cM}\right)\right]\right)\xi T^{(\{1,0\})}[\{\theta,\sigma\}]\right)\Big/$$
$$\left.\left(cM\;cp1\;mw1\;\pi\;R1\left(1+\frac{\Omega\,\xi T[\{\theta,\sigma\}]}{cM}\right)^2\right)\right)+$$
$$Ts\left(\Theta+\frac{Ts\;(-ks\,\theta+A1\;r1\,\sigma-g\,ml\;rl\,\text{Sin}[\theta])}{b1+bs}\right)$$
$$\left(\left(aM^2\;(1-\xi A)\;\Omega^2\left(\frac{\pi}{2}-\text{ArcTan}[\delta\,(\epsilon+\xi k1)]\right)\right.\right.$$
$$\left.\left.\text{Cos}\left[aM\left(-Mf+T-\frac{\sigma}{cA}\right)\right]\xi T^{(\{1,0\})}[\{\theta,\sigma\}]\right)\Big/$$
$$\left.\left(2\;cA^2\;cp1\;mw1\;\pi\;R1\left(1+\frac{\Omega\,\xi T[\{\theta,\sigma\}]}{cA}\right)^2\right)+\right.$$
$$\left(aA^2\;\xi M\,\Omega^2\left(\frac{\pi}{2}+\text{ArcTan}[\delta\,(-\epsilon+\xi k1)]\right)\right.$$
$$\left.\text{Cos}\left[aA\left(-As+T-\frac{\sigma}{cM}\right)\right]\xi T^{(\{1,0\})}[\{\theta,\sigma\}]\right)\Big/$$
$$\left.\left(2\;cM^2\;cp1\;mw1\;\pi\;R1\left(1+\frac{\Omega\,\xi T[\{\theta,\sigma\}]}{cM}\right)^2\right)+\right.$$
$$\left(2\,\Omega^2\left(\frac{\pi}{2}-\text{ArcTan}[\delta\,(\epsilon+\xi k1)]\right)\right.$$
$$\left.\left(\Theta+\frac{1}{2}\,aM\,(1-\xi A)\,\Omega\,\text{Sin}\left[aM\left(-Mf+T-\frac{\sigma}{cA}\right)\right]\right)\right.$$
$$\left.\xi T^{(\{0,1\})}[\{\theta,\sigma\}]\;\xi T^{(\{1,0\})}[\{\theta,\sigma\}]\right)\Big/$$
$$\left.\left(cA^2\;cp1\;mw1\;\pi\;R1\left(1+\frac{\Omega\,\xi T[\{\theta,\sigma\}]}{cA}\right)^3\right)+\right.$$
$$\left(2\,\Omega^2\left(\frac{\pi}{2}+\text{ArcTan}[\delta\,(-\epsilon+\xi k1)]\right)\right.$$
$$\left.\left(\Theta+\frac{1}{2}\,aA\,\xi M\,\Omega\,\text{Sin}\left[aA\left(-As+T-\frac{\sigma}{cM}\right)\right]\right)\right.$$
$$\left.\xi T^{(\{0,1\})}[\{\theta,\sigma\}]\;\xi T^{(\{1,0\})}[\{\theta,\sigma\}]\right)\Big/$$
$$\left.\left(cM^2\;cp1\;mw1\;\pi\;R1\left(1+\frac{\Omega\,\xi T[\{\theta,\sigma\}]}{cM}\right)^3\right)-\right.$$

$$\left(\Omega\left(\frac{\pi}{2}-\text{ArcTan}[\delta\ (\epsilon+\xi\text{k1})]\right)\right.$$
$$\left(\Theta+\frac{1}{2}\,\text{aM}\ (1-\xi\text{A})\ \Omega\ \text{Sin}\left[\text{aM}\left(-\text{Mf}+\text{T}-\frac{\sigma}{\text{cA}}\right)\right]\right)$$
$$\left.\xi\text{T}^{(\{1,1\})}[\{\theta,\ \sigma\}]\right)\Big/\left(\text{cA}\ \text{cp1}\ \text{mw1}\ \pi\ \text{R1}\left(1+\frac{\Omega\,\xi\text{T}[\{\theta,\ \sigma\}]}{\text{cA}}\right)^2\right)-$$
$$\left(\Omega\left(\frac{\pi}{2}+\text{ArcTan}[\delta\ (-\epsilon+\xi\text{k1})]\right)\right.$$
$$\left.\left(\Theta+\frac{1}{2}\,\text{aA}\,\xi\text{M}\,\Omega\,\text{Sin}\left[\text{aA}\left(-\text{As}+\text{T}-\frac{\sigma}{\text{cM}}\right)\right]\right)\xi\text{T}^{(\{1,1\})}[\{\theta,\ \sigma\}]\right)\Big/$$
$$\left.\left(\text{cM}\ \text{cp1}\ \text{mw1}\ \pi\ \text{R1}\left(1+\frac{\Omega\,\xi\text{T}[\{\theta,\ \sigma\}]}{\text{cM}}\right)^2\right)\right)\Bigg)+$$
$$\left(\theta+\frac{\text{Ts}\ (-\text{ks}\,\theta+\text{A1}\ \text{r1}\,\sigma-\text{g ml rl Sin}[\theta])}{\text{b1}+\text{bs}}\right)$$
$$\Bigg(\text{Ts}$$
$$\left(1+\frac{\text{Ts}\ (-\text{ks}-\text{g ml rl Cos}[\theta])}{\text{b1}+\text{bs}}\right)$$
$$\left(-\left(\left(\Omega\left(\frac{\pi}{2}-\text{ArcTan}[\delta\ (\epsilon+\xi\text{k1})]\right)\left(\Theta+\frac{1}{2}\,\text{aM}\ (1-\xi\text{A})\ \Omega\right.\right.\right.\right.$$
$$\left.\left.\left.\left.\text{Sin}\left[\text{aM}\left(-\text{Mf}+\text{T}-\frac{\sigma}{\text{cA}}\right)\right]\right)\xi\text{T}^{(\{1,0\})}[\{\theta,\ \sigma\}]\right)\Big/\right.\right.$$
$$\left.\left.\left(\text{cA}\ \text{cp1}\ \text{mw1}\ \pi\ \text{R1}\left(1+\frac{\Omega\,\xi\text{T}[\{\theta,\ \sigma\}]}{\text{cA}}\right)^2\right)\right)-$$
$$\left(\Omega\left(\frac{\pi}{2}+\text{ArcTan}[\delta\ (-\epsilon+\xi\text{k1})]\right)\right.$$
$$\left.\left(\Theta+\frac{1}{2}\,\text{aA}\,\xi\text{M}\,\Omega\,\text{Sin}\left[\text{aA}\left(-\text{As}+\text{T}-\frac{\sigma}{\text{cM}}\right)\right]\right)\xi\text{T}^{(\{1,0\})}[\{\theta,\ \sigma\}]\right)\Big/$$
$$\left.\left(\text{cM}\ \text{cp1}\ \text{mw1}\ \pi\ \text{R1}\left(1+\frac{\Omega\,\xi\text{T}[\{\theta,\ \sigma\}]}{\text{cM}}\right)^2\right)\right)-$$
$$\text{Ts}\left(1+\text{Ts}\left(-\left(\left(\text{A1 E1 r1}^2\ (-\text{ArcTan}[\delta\ (\text{d}\xi-\epsilon)]+\text{ArcTan}[\delta\ (\text{d}\xi+\epsilon)])\right)\Big/\right.\right.\right.$$
$$\left.\left.\left.((\text{b1}+\text{bs})\ \text{l10}\ \pi)\right)+\right.$$
$$\left(\left(\frac{\pi}{2}-\text{ArcTan}[\delta\ (\text{d}\xi+\epsilon)]\right)\left(-\frac{\text{A1 E1 r1}^2}{(\text{b1}+\text{bs})\ \text{l10}}-\left(\text{aM}^2\ \text{Aw1}\right.\right.\right.$$
$$\left.\left.\left.\text{h0}\ (-\text{T}+\text{Ta})\ (1-\xi\text{A})\ \Omega\ \text{Cos}\left[\text{aM}\left(-\text{Mf}+\text{T}-\frac{\sigma}{\text{cA}}\right)\right]\right)\Big/\right.\right.$$
$$\left.\left.(2\ \text{cA cp1 mw1})\right)\right)\Big/\left(\pi\left(1+\frac{\Omega\,\xi\text{T}[\{\theta,\ \sigma\}]}{\text{cA}}\right)\right)+$$
$$\left(\left(\frac{\pi}{2}+\text{ArcTan}[\delta\ (\text{d}\xi-\epsilon)]\right)\left(-\frac{\text{A1 E1 r1}^2}{(\text{b1}+\text{bs})\ \text{l10}}-\right.\right.$$
$$\left.\left.\left(\text{aA}^2\ \text{Aw1 h0}\ (-\text{T}+\text{Ta})\ \xi\text{M}\,\Omega\ \text{Cos}\left[\text{aA}\left(-\text{As}+\text{T}-\frac{\sigma}{\text{cM}}\right)\right]\right)\Big/\right.\right.$$
$$\left.\left.(2\ \text{cM cp1 mw1})\right)\right)\Big/\left(\pi\left(1+\frac{\Omega\,\xi\text{T}[\{\theta,\ \sigma\}]}{\text{cM}}\right)\right)-$$
$$\frac{1}{\text{cA}\,\pi\left(1+\frac{\Omega\,\xi\text{T}[\{\theta,\ \sigma\}]}{\text{cA}}\right)^2}\Omega\left(\frac{\pi}{2}-\text{ArcTan}[\delta\ (\text{d}\xi+\epsilon)]\right)$$

$$\left(-\left(\left(\text{E1 r1}\left(-\text{ks}\,\Theta+\text{A1 r1}\,\sigma-\text{g ml rl Sin}[\theta]\right)\right)/\left(\left(\text{b1}+\text{bs}\right)\text{l10}\right)\right)+\left(\text{Aw1 h0}\left(-\text{T}+\text{Ta}\right)\left(\Theta+\frac{1}{2}\,\text{aM}\left(1-\xi\text{A}\right)\Omega\,\text{Sin}\left[\text{aM}\left(-\text{Mf}+\text{T}-\frac{\sigma}{\text{cA}}\right)\right]\right)\right)\Big/\left(\text{cp1 mw1}\right)\right)\xi\text{T}^{(\{0,1\})}[\{\theta,\,\sigma\}]-\left(\Omega\left(\frac{\pi}{2}+\text{ArcTan}[\delta\,(\text{d}\xi-\epsilon)]\right)\left(-\left(\left(\text{E1 r1}\left(-\text{ks}\,\Theta+\text{A1 r1}\,\sigma-\text{g ml rl Sin}[\theta]\right)\right)/\left(\left(\text{b1}+\text{bs}\right)\text{l10}\right)\right)+\left(\text{Aw1 h0}\left(-\text{T}+\text{Ta}\right)\left(\Theta+\frac{1}{2}\,\text{aA}\,\xi\text{M}\,\Omega\,\text{Sin}\left[\text{aA}\left(-\text{As}+\text{T}-\frac{\sigma}{\text{cM}}\right)\right]\right)\right)\Big/\left(\text{cp1 mw1}\right)\right)\xi\text{T}^{(\{0,1\})}[\{\theta,\,\sigma\}]\right)\Big/\left(\text{cM}\,\pi\left(1+\frac{\Omega\,\xi\text{T}[\{\theta,\,\sigma\}]}{\text{cM}}\right)^2\right)\right)\Bigg)$$

$$\left(-\left(\left(\Omega\left(\frac{\pi}{2}-\text{ArcTan}[\delta\,(\epsilon+\xi\text{k1})]\right)\left(\Theta+\frac{1}{2}\,\text{aM}\left(1-\xi\text{A}\right)\Omega\,\text{Sin}\left[\text{aM}\left(-\text{Mf}+\text{T}-\frac{\sigma}{\text{cA}}\right)\right]\right)\xi\text{T}^{(\{1,0\})}[\{\theta,\,\sigma\}]\right)\Big/\left(\text{cA cp1 mw1}\,\pi\,\text{R1}\left(1+\frac{\Omega\,\xi\text{T}[\{\theta,\,\sigma\}]}{\text{cA}}\right)^2\right)\right)-\left(\Omega\left(\frac{\pi}{2}+\text{ArcTan}[\delta\,(-\epsilon+\xi\text{k1})]\right)\left(\Theta+\frac{1}{2}\,\text{aA}\,\xi\text{M}\,\Omega\,\text{Sin}\left[\text{aA}\left(-\text{As}+\text{T}-\frac{\sigma}{\text{cM}}\right)\right]\right)\xi\text{T}^{(\{1,0\})}[\{\theta,\,\sigma\}]\right)\Big/\left(\text{cM cp1 mw1}\,\pi\,\text{R1}\left(1+\frac{\Omega\,\xi\text{T}[\{\theta,\,\sigma\}]}{\text{cM}}\right)^2\right)\right)+\text{Ts}^2\left(-\left(\left(\text{aM}^2\left(1-\xi\text{A}\right)\Omega\left(\frac{\pi}{2}-\text{ArcTan}[\delta\,(\epsilon+\xi\text{k1})]\right)\text{Cos}\left[\text{aM}\left(-\text{Mf}+\text{T}-\frac{\sigma}{\text{cA}}\right)\right]\right)\Big/\left(2\,\text{cA cp1 mw1}\,\pi\,\text{R1}\left(1+\frac{\Omega\,\xi\text{T}[\{\theta,\,\sigma\}]}{\text{cA}}\right)\right)\right)-\left(\text{aA}^2\,\xi\text{M}\,\Omega\left(\frac{\pi}{2}+\text{ArcTan}[\delta\,(-\epsilon+\xi\text{k1})]\right)\text{Cos}\left[\text{aA}\left(-\text{As}+\text{T}-\frac{\sigma}{\text{cM}}\right)\right]\right)\Big/\left(2\,\text{cM cp1 mw1}\,\pi\,\text{R1}\left(1+\frac{\Omega\,\xi\text{T}[\{\theta,\,\sigma\}]}{\text{cM}}\right)\right)-\left(\Omega\left(\frac{\pi}{2}-\text{ArcTan}[\delta\,(\epsilon+\xi\text{k1})]\right)\left(\Theta+\frac{1}{2}\,\text{aM}\left(1-\xi\text{A}\right)\Omega\,\text{Sin}\left[\text{aM}\left(-\text{Mf}+\text{T}-\frac{\sigma}{\text{cA}}\right)\right]\right)\xi\text{T}^{(\{0,1\})}[\{\theta,\,\sigma\}]\right)\Big/\left(\text{cA cp1 mw1}\,\pi\,\text{R1}\left(1+\frac{\Omega\,\xi\text{T}[\{\theta,\,\sigma\}]}{\text{cA}}\right)^2\right)-\left(\Omega\left(\frac{\pi}{2}+\text{ArcTan}[\delta\,(-\epsilon+\xi\text{k1})]\right)\left(\Theta+\frac{1}{2}\,\text{aA}\,\xi\text{M}\,\Omega\,\text{Sin}\left[\text{aA}\left(-\text{As}+\text{T}-\frac{\sigma}{\text{cM}}\right)\right]\right)\xi\text{T}^{(\{0,1\})}[\{\theta,\,\sigma\}]\right)\Big/\left(\text{cM cp1 mw1}\,\pi\,\text{R1}\left(1+\frac{\Omega\,\xi\text{T}[\{\theta,\,\sigma\}]}{\text{cM}}\right)^2\right)\Bigg)$$

$$\left(-\left(\left(\text{E1 r1}\left(-\text{ArcTan}[\delta\,(\text{d}\xi-\epsilon)]+\text{ArcTan}[\delta\,(\text{d}\xi+\epsilon)]\right)\left(-\text{ks}-\text{g ml rl Cos}[\theta]\right)\right)/\left(\left(\text{b1}+\text{bs}\right)\text{l10}\,\pi\right)\right)-\left(\text{E1 r1}\left(\frac{\pi}{2}-\text{ArcTan}[\delta\,(\text{d}\xi+\epsilon)]\right)\left(-\text{ks}-\text{g ml rl Cos}[\theta]\right)\right)\Big/$$

$$\left((b1+bs)\ l10\,\pi\left(1+\frac{\Omega\,\xi T[\{\theta,\sigma\}]}{cA}\right)\right)-\left(E1\ r1\left(\frac{\pi}{2}+\text{ArcTan}[\delta\ (d\xi-\epsilon)]\right)\ (-ks-g\ ml\ rl\ \text{Cos}[\theta])\right)\Big/\left((b1+bs)\ l10\,\pi\left(1+\frac{\Omega\,\xi T[\{\theta,\sigma\}]}{cM}\right)\right)-\left(\Omega\left(\frac{\pi}{2}-\text{ArcTan}[\delta\ (d\xi+\epsilon)]\right)\left(-((E1\ r1\ (-ks\,\theta+A1\ r1\,\sigma-g\ ml\ rl\ \text{Sin}[\theta]))/((b1+bs)\ l10))+\frac{1}{cp1\ mw1}Aw1\ h0\ (-T+Ta)\left(\Theta+\frac{1}{2}\,aM\ (1-\xi A)\ \Omega\ \text{Sin}\left[aM\left(-Mf+T-\frac{\sigma}{cA}\right)\right]\right)\right)\xi T^{(\{1,0\})}[\{\theta,\sigma\}]\right)\Big/\left(cA\,\pi\left(1+\frac{\Omega\,\xi T[\{\theta,\sigma\}]}{cA}\right)^2\right)-\left(\Omega\left(\frac{\pi}{2}+\text{ArcTan}[\delta\ (d\xi-\epsilon)]\right)\left(-((E1\ r1\ (-ks\,\theta+A1\ r1\,\sigma-g\ ml\ rl\ \text{Sin}[\theta]))/((b1+bs)\ l10))+\frac{1}{cp1\ mw1}Aw1\ h0\ (-T+Ta)\left(\Theta+\frac{1}{2}\,aA\,\xi M\,\Omega\,\text{Sin}\left[aA\left(-As+T-\frac{\sigma}{cM}\right)\right]\right)\right)\xi T^{(\{1,0\})}[\{\theta,\sigma\}]\right)\Big/\left(cM\,\pi\left(1+\frac{\Omega\,\xi T[\{\theta,\sigma\}]}{cM}\right)^2\right)\right)+Ts\left(\sigma+Ts\left(\frac{1}{\pi}(-\text{ArcTan}[\delta\ (d\xi-\epsilon)]+\text{ArcTan}[\delta\ (d\xi+\epsilon)])\left(\frac{Aw1\ h0\ (-T+Ta)\ \Theta}{cp1\ mw1}-(E1\ r1\ (-ks\,\theta+A1\ r1\,\sigma-g\ ml\ rl\ \text{Sin}[\theta]))/((b1+bs)\ l10)\right)+\left(\left(\frac{\pi}{2}-\text{ArcTan}[\delta\ (d\xi+\epsilon)]\right)\left(-((E1\ r1\ (-ks\,\theta+A1\ r1\,\sigma-g\ ml\ rl\ \text{Sin}[\theta]))/((b1+bs)\ l10))+\left(Aw1\ h0\ (-T+Ta)\left(\Theta+\frac{1}{2}\,aM\ (1-\xi A)\ \Omega\ \text{Sin}\left[aM\left(-Mf+T-\frac{\sigma}{cA}\right)\right]\right)\right)\Big/(cp1\ mw1)\right)\right)\Big/\left(\pi\left(1+\frac{\Omega\,\xi T[\{\theta,\sigma\}]}{cA}\right)\right)+\left(\left(\frac{\pi}{2}+\text{ArcTan}[\delta\ (d\xi-\epsilon)]\right)\left(-((E1\ r1\ (-ks\,\theta+A1\ r1\,\sigma-g\ ml\ rl\ \text{Sin}[\theta]))/((b1+bs)\ l10))+\left(Aw1\ h0\ (-T+Ta)\left(\Theta+\frac{1}{2}\,aA\,\xi M\,\Omega\,\text{Sin}\left[aA\left(-As+T-\frac{\sigma}{cM}\right)\right]\right)\right)\Big/(cp1\ mw1)\right)\right)\Big/\left(\pi\left(1+\frac{\Omega\,\xi T[\{\theta,\sigma\}]}{cM}\right)\right)\right)\right)+\left(\left(aM^2\ (1-\xi A)\ \Omega^2\left(\frac{\pi}{2}-\text{ArcTan}[\delta\ (\epsilon+\xi k1)]\right)\text{Cos}\left[aM\left(-Mf+T-\frac{\sigma}{cA}\right)\right]\xi T^{(\{1,0\})}[\{\theta,\sigma\}]\right)\Big/\left(2\ cA^2\ cp1\ mw1\,\pi\,R1\left(1+\frac{\Omega\,\xi T[\{\theta,\sigma\}]}{cA}\right)^2\right)+\left(aA^2\,\xi M\,\Omega^2\left(\frac{\pi}{2}+\text{ArcTan}[\delta\ (-\epsilon+\xi k1)]\right)\text{Cos}\left[aA\left(-As+T-\frac{\sigma}{cM}\right)\right]\xi T^{(\{1,0\})}[\{\theta,\sigma\}]\right)\Big/\left(2\ cM^2\ cp1\ mw1\,\pi\,R1\left(1+\frac{\Omega\,\xi T[\{\theta,\sigma\}]}{cM}\right)^2\right)+$$

$$\left(2\,\Omega^2\left(\frac{\pi}{2}-\text{ArcTan}[\delta\,(\epsilon+\xi\text{k1})]\right)\right.$$
$$\left(\Theta+\frac{1}{2}\,\text{aM}\,(1-\xi\text{A})\,\Omega\,\text{Sin}\left[\text{aM}\left(-\text{Mf}+\text{T}-\frac{\sigma}{\text{cA}}\right)\right]\right)$$
$$\left.\xi\text{T}^{(\{0,1\})}[\{\theta,\,\sigma\}]\;\xi\text{T}^{(\{1,0\})}[\{\theta,\,\sigma\}]\right)\Big/$$
$$\left(\text{cA}^2\,\text{cp1}\,\text{mw1}\,\pi\,\text{R1}\left(1+\frac{\Omega\,\xi\text{T}[\{\theta,\,\sigma\}]}{\text{cA}}\right)^3\right)+$$
$$\left(2\,\Omega^2\left(\frac{\pi}{2}+\text{ArcTan}[\delta\,(-\epsilon+\xi\text{k1})]\right)\right.$$
$$\left(\Theta+\frac{1}{2}\,\text{aA}\,\xi\text{M}\,\Omega\,\text{Sin}\left[\text{aA}\left(-\text{As}+\text{T}-\frac{\sigma}{\text{cM}}\right)\right]\right)$$
$$\left.\xi\text{T}^{(\{0,1\})}[\{\theta,\,\sigma\}]\;\xi\text{T}^{(\{1,0\})}[\{\theta,\,\sigma\}]\right)\Big/$$
$$\left(\text{cM}^2\,\text{cp1}\,\text{mw1}\,\pi\,\text{R1}\left(1+\frac{\Omega\,\xi\text{T}[\{\theta,\,\sigma\}]}{\text{cM}}\right)^3\right)-$$
$$\left(\Omega\left(\frac{\pi}{2}-\text{ArcTan}[\delta\,(\epsilon+\xi\text{k1})]\right)\right.$$
$$\left(\Theta+\frac{1}{2}\,\text{aM}\,(1-\xi\text{A})\,\Omega\,\text{Sin}\left[\text{aM}\left(-\text{Mf}+\text{T}-\frac{\sigma}{\text{cA}}\right)\right]\right)$$
$$\left.\xi\text{T}^{(\{1,1\})}[\{\theta,\,\sigma\}]\right)\Big/\left(\text{cA}\,\text{cp1}\,\text{mw1}\,\pi\,\text{R1}\left(1+\frac{\Omega\,\xi\text{T}[\{\theta,\,\sigma\}]}{\text{cA}}\right)^2\right)-$$
$$\left(\Omega\left(\frac{\pi}{2}+\text{ArcTan}[\delta\,(-\epsilon+\xi\text{k1})]\right)\right.$$
$$\left.\left(\Theta+\frac{1}{2}\,\text{aA}\,\xi\text{M}\,\Omega\,\text{Sin}\left[\text{aA}\left(-\text{As}+\text{T}-\frac{\sigma}{\text{cM}}\right)\right]\right)\xi\text{T}^{(\{1,1\})}[\{\theta,\,\sigma\}]\right)\Big/$$
$$\left.\left(\text{cM}\,\text{cp1}\,\text{mw1}\,\pi\,\text{R1}\left(1+\frac{\Omega\,\xi\text{T}[\{\theta,\,\sigma\}]}{\text{cM}}\right)^2\right)\right)-$$
$$\text{Ts}^2\left((\Theta\,(-\text{ArcTan}[\delta\,(-\epsilon+\xi\text{k1})]+\text{ArcTan}[\delta\,(\epsilon+\xi\text{k1})]))\,/\right.$$
$$(\text{cp1}\,\text{mw1}\,\pi\,\text{R1})+\left(\left(\frac{\pi}{2}-\text{ArcTan}[\delta\,(\epsilon+\xi\text{k1})]\right)\right.$$
$$\left.\left(\Theta+\frac{1}{2}\,\text{aM}\,(1-\xi\text{A})\,\Omega\,\text{Sin}\left[\text{aM}\left(-\text{Mf}+\text{T}-\frac{\sigma}{\text{cA}}\right)\right]\right)\right)\Big/$$
$$\left(\text{cp1}\,\text{mw1}\,\pi\,\text{R1}\left(1+\frac{\Omega\,\xi\text{T}[\{\theta,\,\sigma\}]}{\text{cA}}\right)\right)+$$
$$\left(\left(\frac{\pi}{2}+\text{ArcTan}[\delta\,(-\epsilon+\xi\text{k1})]\right)\right.$$
$$\left.\left(\Theta+\frac{1}{2}\,\text{aA}\,\xi\text{M}\,\Omega\,\text{Sin}\left[\text{aA}\left(-\text{As}+\text{T}-\frac{\sigma}{\text{cM}}\right)\right]\right)\right)\Big/$$
$$\left.\left(\text{cp1}\,\text{mw1}\,\pi\,\text{R1}\left(1+\frac{\Omega\,\xi\text{T}[\{\theta,\,\sigma\}]}{\text{cM}}\right)\right)\right)$$
$$\left(\left(\text{E1}\,\text{r1}\,\Omega\left(\frac{\pi}{2}-\text{ArcTan}[\delta\,(\text{d}\xi+\epsilon)]\right)\,(-\text{ks}-\text{g}\,\text{ml}\,\text{rl}\,\text{Cos}[\theta])\right.\right.$$
$$\left.\xi\text{T}^{(\{0,1\})}[\{\theta,\,\sigma\}]\right)\Big/\left((\text{b1}+\text{bs})\,\text{cA}\,\text{l10}\,\pi\left(1+\frac{\Omega\,\xi\text{T}[\{\theta,\,\sigma\}]}{\text{cA}}\right)^2\right)+$$
$$\left(\text{E1}\,\text{r1}\,\Omega\left(\frac{\pi}{2}+\text{ArcTan}[\delta\,(\text{d}\xi-\epsilon)]\right)\,(-\text{ks}-\text{g}\,\text{ml}\,\text{rl}\,\text{Cos}[\theta])\right.$$
$$\left.\xi\text{T}^{(\{0,1\})}[\{\theta,\,\sigma\}]\right)\Big/\left((\text{b1}+\text{bs})\,\text{cM}\,\text{l10}\,\pi\left(1+\frac{\Omega\,\xi\text{T}[\{\theta,\,\sigma\}]}{\text{cM}}\right)^2\right)-$$
$$\left(\Omega\left(\frac{\pi}{2}-\text{ArcTan}[\delta\,(\text{d}\xi+\epsilon)]\right)\left(-\frac{\text{A1}\,\text{E1}\,\text{r1}^2}{(\text{b1}+\text{bs})\,\text{l10}}-\right.\right.$$

$$\Big(\text{aM}^2\,\text{Aw1 h0}\,(-\text{T}+\text{Ta})\,(1-\xi\text{A})\,\Omega\,\text{Cos}\Big[\text{aM}\Big(-\text{Mf}+\text{T}-\frac{\sigma}{\text{cA}}\Big)\Big]\Big)\Big/(2\,\text{cA cp1 mw1})\Big)$$

$$\xi\text{T}^{(\{1,0\})}[\{\theta,\sigma\}]\Big)\Big/\Big(\text{cA}\,\pi\Big(1+\frac{\Omega\,\xi\text{T}[\{\theta,\sigma\}]}{\text{cA}}\Big)^2\Big)-$$

$$\Big(\Omega\Big(\frac{\pi}{2}+\text{ArcTan}[\delta\,(\text{d}\xi-\epsilon)]\Big)\Big(-\frac{\text{A1 E1 r1}^2}{(\text{b1}+\text{bs})\,\text{l10}}-\Big(\text{aA}^2\,\text{Aw1 h0}$$

$$(-\text{T}+\text{Ta})\,\xi\text{M}\,\Omega\,\text{Cos}\Big[\text{aA}\Big(-\text{As}+\text{T}-\frac{\sigma}{\text{cM}}\Big)\Big]\Big)\Big/(2\,\text{cM cp1 mw1})\Big)$$

$$\xi\text{T}^{(\{1,0\})}[\{\theta,\sigma\}]\Big)\Big/\Big(\text{cM}\,\pi\Big(1+\frac{\Omega\,\xi\text{T}[\{\theta,\sigma\}]}{\text{cM}}\Big)^2\Big)+$$

$$\frac{1}{\text{cA}^2\,\pi\Big(1+\frac{\Omega\,\xi\text{T}[\{\theta,\sigma\}]}{\text{cA}}\Big)^3}2\,\Omega^2\Big(\frac{\pi}{2}-\text{ArcTan}[\delta\,(\text{d}\xi+\epsilon)]\Big)$$

$$\Big(-((\text{E1 r1}\,(-\text{ks}\,\theta+\text{A1 r1}\,\sigma-\text{g ml rl Sin}[\theta]))/((\text{b1}+\text{bs})\,\text{l10}))+$$

$$\frac{1}{\text{cp1 mw1}}\text{Aw1 h0}\,(-\text{T}+\text{Ta})$$

$$\Big(\Theta+\frac{1}{2}\text{aM}\,(1-\xi\text{A})\,\Omega\,\text{Sin}\Big[\text{aM}\Big(-\text{Mf}+\text{T}-\frac{\sigma}{\text{cA}}\Big)\Big]\Big)\Big)$$

$$\xi\text{T}^{(\{0,1\})}[\{\theta,\sigma\}]\;\xi\text{T}^{(\{1,0\})}[\{\theta,\sigma\}]+\frac{1}{\text{cM}^2\,\pi\Big(1+\frac{\Omega\,\xi\text{T}[\{\theta,\sigma\}]}{\text{cM}}\Big)^3}$$

$$2\,\Omega^2\Big(\frac{\pi}{2}+\text{ArcTan}[\delta\,(\text{d}\xi-\epsilon)]\Big)$$

$$\Big(-((\text{E1 r1}\,(-\text{ks}\,\theta+\text{A1 r1}\,\sigma-\text{g ml rl Sin}[\theta]))/((\text{b1}+\text{bs})\,\text{l10}))+$$

$$\frac{1}{\text{cp1 mw1}}\text{Aw1 h0}\,(-\text{T}+\text{Ta})$$

$$\Big(\Theta+\frac{1}{2}\text{aA}\,\xi\text{M}\,\Omega\,\text{Sin}\Big[\text{aA}\Big(-\text{As}+\text{T}-\frac{\sigma}{\text{cM}}\Big)\Big]\Big)\Big)\;\xi\text{T}^{(\{0,1\})}[\{\theta,\sigma\}]$$

$$\xi\text{T}^{(\{1,0\})}[\{\theta,\sigma\}]-\Big(\Omega\Big(\frac{\pi}{2}-\text{ArcTan}[\delta\,(\text{d}\xi+\epsilon)]\Big)$$

$$\Big(-((\text{E1 r1}\,(-\text{ks}\,\theta+\text{A1 r1}\,\sigma-\text{g ml rl Sin}[\theta]))/$$

$$((\text{b1}+\text{bs})\,\text{l10}))+\frac{1}{\text{cp1 mw1}}\text{Aw1 h0}\,(-\text{T}+\text{Ta})$$

$$\Big(\Theta+\frac{1}{2}\text{aM}\,(1-\xi\text{A})\,\Omega\,\text{Sin}\Big[\text{aM}\Big(-\text{Mf}+\text{T}-\frac{\sigma}{\text{cA}}\Big)\Big]\Big)\Big)$$

$$\xi\text{T}^{(\{1,1\})}[\{\theta,\sigma\}]\Big)\Big/\Big(\text{cA}\,\pi\Big(1+\frac{\Omega\,\xi\text{T}[\{\theta,\sigma\}]}{\text{cA}}\Big)^2\Big)-$$

$$\Big(\Omega\Big(\frac{\pi}{2}+\text{ArcTan}[\delta\,(\text{d}\xi-\epsilon)]\Big)\Big(-((\text{E1 r1}\,(-\text{ks}\,\theta+\text{A1 r1}\,\sigma-$$

$$\text{g ml rl Sin}[\theta]))/((\text{b1}+\text{bs})\,\text{l10}))+\frac{1}{\text{cp1 mw1}}$$

$$\text{Aw1 h0}\,(-\text{T}+\text{Ta})\,\Big(\Theta+\frac{1}{2}\text{aA}\,\xi\text{M}\,\Omega\,\text{Sin}\Big[\text{aA}\Big(-\text{As}+\text{T}-\frac{\sigma}{\text{cM}}\Big)\Big]\Big)\Big)$$

$$\xi\text{T}^{(\{1,1\})}[\{\theta,\sigma\}]\Big)\Big/\Big(\text{cM}\,\pi\Big(1+\frac{\Omega\,\xi\text{T}[\{\theta,\sigma\}]}{\text{cM}}\Big)^2\Big)\Big)+$$

$$\text{Ts}\Big(\theta+\frac{\text{Ts}\,(-\text{ks}\,\theta+\text{A1 r1}\,\sigma-\text{g ml rl Sin}[\theta])}{\text{b1}+\text{bs}}\Big)$$

$$\left(\left(2\,\Omega^2\,\left(\frac{\pi}{2}-\text{ArcTan}[\delta\,(\epsilon+\xi\text{k1})]\right)\right.\right.$$
$$\left(\Theta+\frac{1}{2}\,\text{aM}\,(1-\xi\text{A})\,\Omega\,\text{Sin}\left[\text{aM}\,\left(-\text{Mf}+\text{T}-\frac{\sigma}{\text{cA}}\right)\right]\right)$$
$$\left.\xi\text{T}^{(\{1,0\})}[\{\theta,\,\sigma\}]^2\right)\Big/\left(\text{cA}^2\,\text{cp1}\,\text{mw1}\,\pi\,\text{R1}\,\left(1+\frac{\Omega\,\xi\text{T}[\{\theta,\,\sigma\}]}{\text{cA}}\right)^3\right)+$$
$$\left(2\,\Omega^2\,\left(\frac{\pi}{2}+\text{ArcTan}[\delta\,(-\epsilon+\xi\text{k1})]\right)\right.$$
$$\left.\left(\Theta+\frac{1}{2}\,\text{aA}\,\xi\text{M}\,\Omega\,\text{Sin}\left[\text{aA}\,\left(-\text{As}+\text{T}-\frac{\sigma}{\text{cM}}\right)\right]\right)\,\xi\text{T}^{(\{1,0\})}[\{\theta,\,\sigma\}]^2\right)\Big/$$
$$\left(\text{cM}^2\,\text{cp1}\,\text{mw1}\,\pi\,\text{R1}\,\left(1+\frac{\Omega\,\xi\text{T}[\{\theta,\,\sigma\}]}{\text{cM}}\right)^3\right)-$$
$$\left(\Omega\,\left(\frac{\pi}{2}-\text{ArcTan}[\delta\,(\epsilon+\xi\text{k1})]\right)\right.$$
$$\left(\Theta+\frac{1}{2}\,\text{aM}\,(1-\xi\text{A})\,\Omega\,\text{Sin}\left[\text{aM}\,\left(-\text{Mf}+\text{T}-\frac{\sigma}{\text{cA}}\right)\right]\right)$$
$$\left.\xi\text{T}^{(\{2,0\})}[\{\theta,\,\sigma\}]\right)\Big/\left(\text{cA}\,\text{cp1}\,\text{mw1}\,\pi\,\text{R1}\,\left(1+\frac{\Omega\,\xi\text{T}[\{\theta,\,\sigma\}]}{\text{cA}}\right)^2\right)-$$
$$\left(\Omega\,\left(\frac{\pi}{2}+\text{ArcTan}[\delta\,(-\epsilon+\xi\text{k1})]\right)\right.$$
$$\left.\left(\Theta+\frac{1}{2}\,\text{aA}\,\xi\text{M}\,\Omega\,\text{Sin}\left[\text{aA}\,\left(-\text{As}+\text{T}-\frac{\sigma}{\text{cM}}\right)\right]\right)\,\xi\text{T}^{(\{2,0\})}[\{\theta,\,\sigma\}]\right)\Big/$$
$$\left.\left.\left(\text{cM}\,\text{cp1}\,\text{mw1}\,\pi\,\text{R1}\,\left(1+\frac{\Omega\,\xi\text{T}[\{\theta,\,\sigma\}]}{\text{cM}}\right)^2\right)\right)\right)\Bigg\}$$

Out[250]=
$$\left\{\left\{\Theta + \frac{\text{Ts}\ (-\text{ks}\,\Theta + \text{A1}\ \text{r1}\ \sigma - \text{g}\ \text{ml}\ \text{rl}\ \text{Sin}[\Theta])}{\text{b1} + \text{bs}},\right.\right.$$
$$\sigma + \text{Ts}\left(\frac{1}{\pi}(-\text{ArcTan}[\delta\ (\text{d}\xi - \epsilon)] + \text{ArcTan}[\delta\ (\text{d}\xi + \epsilon)])\left(\frac{\text{Aw1}\ \text{h0}\ (-\text{T} + \text{Ta})\ \Theta}{\text{cp1}\ \text{mw1}} - \right.\right.$$
$$(\text{E1}\ \text{r1}\ (-\text{ks}\,\Theta + \text{A1}\ \text{r1}\ \sigma - \text{g}\ \text{ml}\ \text{rl}\ \text{Sin}[\Theta]))\ /\ ((\text{b1} + \text{bs})\ \text{l10})\Big) +$$
$$\frac{1}{\pi\left(1 + \frac{\Omega\,\xi\text{T}[\{\Theta,\sigma\}]}{\text{cA}}\right)}\left(\frac{\pi}{2} - \text{ArcTan}[\delta\ (\text{d}\xi + \epsilon)]\right)$$
$$\left(-((\text{E1}\ \text{r1}\ (-\text{ks}\,\Theta + \text{A1}\ \text{r1}\ \sigma - \text{g}\ \text{ml}\ \text{rl}\ \text{Sin}[\Theta]))\ /\ ((\text{b1} + \text{bs})\ \text{l10})) + \right.$$
$$\frac{1}{\text{cp1}\ \text{mw1}}\text{Aw1}\ \text{h0}\ (-\text{T} + \text{Ta})$$
$$\left.\left(\Theta + \frac{1}{2}\ \text{aM}\ (1 - \xi\text{A})\ \Omega\ \text{Sin}\left[\text{aM}\left(-\text{Mf} + \text{T} - \frac{\sigma}{\text{cA}}\right)\right]\right)\right) +$$
$$\frac{1}{\pi\left(1 + \frac{\Omega\,\xi\text{T}[\{\Theta,\sigma\}]}{\text{cM}}\right)}\left(\frac{\pi}{2} + \text{ArcTan}[\delta\ (\text{d}\xi - \epsilon)]\right)$$
$$\left(-((\text{E1}\ \text{r1}\ (-\text{ks}\,\Theta + \text{A1}\ \text{r1}\ \sigma - \text{g}\ \text{ml}\ \text{rl}\ \text{Sin}[\Theta]))\ /\ ((\text{b1} + \text{bs})\ \text{l10})) + \right.$$
$$\frac{1}{\text{cp1}\ \text{mw1}}\text{Aw1}\ \text{h0}\ (-\text{T} + \text{Ta})$$
$$\left.\left.\left.\left(\Theta + \frac{1}{2}\ \text{aA}\ \xi\text{M}\ \Omega\ \text{Sin}\left[\text{aA}\left(-\text{As} + \text{T} - \frac{\sigma}{\text{cM}}\right)\right]\right)\right)\right)\right\},$$
$$\left\{0,\ \text{Ts}\left((\Theta\ (-\text{ArcTan}[\delta\ (-\epsilon + \xi\text{k1})] + \text{ArcTan}[\delta\ (\epsilon + \xi\text{k1})]))\ /\right.\right.$$
$$(\text{cp1}\ \text{mw1}\ \pi\ \text{R1}) + \left(\left(\frac{\pi}{2} - \text{ArcTan}[\delta\ (\epsilon + \xi\text{k1})]\right)\right.$$
$$\left.\left.\left(\Theta + \frac{1}{2}\ \text{aM}\ (1 - \xi\text{A})\ \Omega\ \text{Sin}\left[\text{aM}\left(-\text{Mf} + \text{T} - \frac{\sigma}{\text{cA}}\right)\right]\right)\right)\Big/$$
$$\left(\text{cp1}\ \text{mw1}\ \pi\ \text{R1}\left(1 + \frac{\Omega\,\xi\text{T}[\{\Theta,\ \sigma\}]}{\text{cA}}\right)\right) +$$
$$\left(\left(\frac{\pi}{2} + \text{ArcTan}[\delta\ (-\epsilon + \xi\text{k1})]\right)\left(\Theta + \frac{1}{2}\ \text{aA}\ \xi\text{M}\ \Omega\ \text{Sin}\left[\text{aA}\left(-\text{As} + \text{T} - \frac{\sigma}{\text{cM}}\right)\right]\right)\right)\Big/$$
$$\left.\left.\left(\text{cp1}\ \text{mw1}\ \pi\ \text{R1}\left(1 + \frac{\Omega\,\xi\text{T}[\{\Theta,\ \sigma\}]}{\text{cM}}\right)\right)\right)\right\}\}$$

```
Controllability Matrix Rank
```

Out[252]= 2

```
Due to the constraints over the control
  input, although the controllability matrix is full
  rank for all x, the system is proved to be reachable.
```

Bibliography

[1] F. Ruggiero, M. A. Trujillo, R. Cano, H. Ascorbe, A. Viguria, C. Peréz, V. Lippiello, A. Ollero, and B. Siciliano, "A multilayer control for multirotor UAVs equipped with a servo robot arm," *IEEE International Conference on Robotics and Automation (ICRA)*, pp. 4014–4020, 2015.

[2] C. M. Korpela, T. W. Danko, and P. Y. Oh, "Designing a system for mobile manipulation from an Unmanned Aerial Vehicle," *Technologies for Practical Robot Applications (TePRA), 2011 IEEE Conference on*, pp. 109–114, 2011.

[3] T. W. Danko and P. Y. Oh, "A hyper-redundant manipulator for mobile manipulating unmanned aerial vehicles," in *2013 International Conference on Unmanned Aircraft Systems (ICUAS)*, pp. 974–981, IEEE, 2013.

[4] A. Albers, S. Trautmann, T. Howard, T. A. Nguyen, M. Frietsch, and C. Sauter, "Semi-autonomous flying robot for physical interaction with environment," *2010 IEEE Conference on Robotics, Automation and Mechatronics, RAM 2010*, pp. 441–446, 2010.

[5] M. Fumagalli, R. Naldi, A. Macchelli, F. Forte, A. Q. L. Keemink, S. Stramigioli, R. Carloni, and L. Marconi, "Developing an aerial manipulator prototype: Physical interaction with the environment," *IEEE Robotics and Automation Magazine*, vol. 21, no. 3, pp. 41–50, 2014.

[6] H. Tsukagoshi, T. Hamada, M. Watanabe, R. Iizuka, and A. Dameitry, "Aerial manipulator aimed for door opening mission," *12th IEEE International Symposium on Safety, Security and Rescue Robotics, SSRR 2014 - Symposium Proceedings*, pp. 3–4, 2014.

[7] C. D. Bellicoso, L. R. Buonocore, V. Lippiello, and B. Siciliano, "Design, modeling and control of a 5-DoF light-weight robot arm for aerial manipulation," *2015 23rd Mediterranean Conference on Control and Automation, MED 2015 - Conference Proceedings*, pp. 853–858, 2015.

[8] A. E. Jimenez-Cano, J. Martin, G. Heredia, A. Ollero, and R. Cano, "Control of an aerial robot with multi-link arm for assembly tasks," *Proceedings - IEEE International Conference on Robotics and Automation*, pp. 4916–4921, 2013.

[9] C. Mavroidis, "Development of advanced actuators using shape memory alloys and electrorheological fluids," *Research in Nondestructive Evaluation*, vol. 14, no. 1, pp. 1–32, 2002.

[10] D. C. Lagoudas, *Shape memory alloys: modeling and engineering applications*. Springer Science & Business Media, 2008.

[11] Z. Guo, Y. Pan, L. B. Wee, and H. Yu, "Design and control of a novel compliant differential shape memory alloy actuator," *Sensors and Actuators A: Physical*, vol. 225, pp. 71–80, April 2015.

[12] K. Paul, "Development of a robotic manipulator based on Shape Memory Alloy wires," Master's thesis, University of Luxembourg, Luxembourg, 2018.

[13] M. Elahinia, J. Koo, M. Ahmadian, and C. Woolsey, "Backstepping control of a shape memory alloy actuated robotic arm," *Modal Analysis*, vol. 11, no. 3, pp. 407–429, 2005.

[14] B. K. Nguyen and K. K. Ahn, "Feedforward control of shape memory alloy actuators using fuzzy-based inverse preisach model," *IEEE Transactions on control systems technology*, vol. 17, no. 2, pp. 434–441, 2009.

[15] I. D. Landau and G. Zito, "Digital control systems: Design," *Identification and Implementation*, 2006.

[16] T. Ikeda, S. Yasui, M. Fujihara, K. Ohara, S. Ashizawa, A. Ichikawa, A. Okino, T. Oomichi, and T. Fukuda, "Wall contact by octo-rotor UAV with one DoF manipulator for bridge inspection," in *2017 IEEE/RSJ International Conference on Intelligent Robots and Systems (IROS)*, pp. 5122–5127, Sep. 2017.

[17] A. Suarez, P. R. Soria, G. Heredia, B. C. Arrue, and A. Ollero, "Anthropomorphic, compliant and lightweight dual arm system for aerial manipulation," in *2017 IEEE/RSJ International Conference on Intelligent Robots and Systems (IROS)*, pp. 992–997, Sep. 2017.

[18] F. Janzen, A. Tusset, V. Piccirillo, J. Balthazar, and R. Brasil, "Motion and vibration control of a slewing flexible structure by SMA actuators and parameter sensitivity analysis," *The European Physical Journal Special Topics*, vol. 224, pp. 3041–3054, Nov 2015.

[19] J. José De Lima, A. Tusset, F. Conrad Janzen, V. Piccirillo, C. Nascimento, J. Manoel Balthazar, and R. Da Fonseca Brasil, "SDRE applied to position and vibration control of a robot manipulator with a flexible link," *Journal of Theoretical and Applied Mechanics*, vol. 54, pp. 1067–1078, 12 2016.

[20] B. Siciliano, "Ijars video series: Aerial manipulation." https://youtu.be/Jp0jvMExAKc, 2015. DOI: 10.5772/60874, consulted on: 2019-03-08.

[21] A. Suarez, G. Heredia, and A. Ollero, "Lightweight compliant arm for aerial manipulation," in *Intelligent Robots and Systems (IROS), 2015 IEEE/RSJ International Conference on*, pp. 1627–1632, Sept 2015.

[22] A. Rao, A. R. Srinivasa, and J. N. Reddy, *Design of shape memory alloy (SMA) actuators*. Springer, 2015.

[23] A. R. Shahin, P. H. Meckl, J. D. Jones, and M. A. Thrasher, "Enhanced cooling of shape memory alloy wires using semiconductor "heat pump" modules," *Journal of Intelligent Material Systems and Structures*, vol. 5, no. 1, pp. 95–104, 1994.

[24] V. A. Tabrizi and M. Moallem, "Nonlinear position control of antagonistic shape memory alloy actuators," in *2007 American Control Conference*, pp. 88–93, July 2007.

[25] C. Liang and C. A. Rogers, "One-dimensional thermomechanical constitutive relations for shape memory materials," *Journal of intelligent material systems and structures*, vol. 1, no. 2, pp. 207–234, 1990.

[26] M. H. Elahinia and H. Ashrafiuon, "Nonlinear control of a shape memory alloy actuated manipulator," *Journal of Vibration and Acoustics*, vol. 124, no. 4, pp. 566–575, 2002.

[27] J. Liu and X. Wang, *Advanced Sliding Mode Control for Mechanical Systems: Design, Analysis and MATLAB Simulation*. Springer-Verlag Berlin Heidelberg, 2011.

[28] I. D. Landau, R. Lozano, M. M'Saad, and A. Karimi, *Adaptive control: algorithms, analysis and applications*. Springer Science & Business Media, 2011.

[29] S. Kannan, S. Bezzaoucha, S. Quintanar-Guzmán, M. A. Olivares-Mendez, and H. Voos, "Adaptive control of robotic arm with hysteretic joint," in *Proceedings of the 4th International Conference on Control, Mechatronics and Automation*, ICCMA '16, (New York, NY, USA), pp. 46–50, ACM, 2016.

[30] A. Martinelli, "Nonlinear Unknown Input Observability: The General Analytic Solution," *ArXiv e-prints*, Apr. 2017.

[31] T. Çimen, "Systematic and effective design of nonlinear feedback controllers via the state-dependent riccati equation (SDRE) method," *Annual Reviews in Control*, vol. 34, no. 1, pp. 32 – 51, 2010.

[32] PwC, "Clarity from above." https://www.pwc.pl/pl/pdf/clarity-from-above-pwc.pdf, 2016. Consulted on: 2019-03-08.

[33] M. Orsag, C. Korpela, S. Bogdan, and P. Oh, "Valve turning using a dual-arm aerial manipulator," in *2014 International Conference on Unmanned Aircraft Systems (ICUAS)*, pp. 836–841, May 2014.

[34] J. R. Kutia, K. A. Stol, and W. Xu, "Canopy sampling using an aerial manipulator: A preliminary study," in *2015 International Conference on Unmanned Aircraft Systems (ICUAS)*, pp. 477–484, June 2015.

[35] H. B. Khamseh, F. Janabi-Sharifi, and A. Abdessameud, "Aerial manipulation — a literature survey," *Robotics and Autonomous Systems*, vol. 107, pp. 221 – 235, 2018.

[36] S. Quintanar-Guzmán, S. Kannan, H. Voos, M. Darouach, and M. Alma, "Adaptive control for a lightweight robotic arm actuated by a shape memory alloy wire," in *ACTUATOR 2018 16th International Conference on New Actuators*, 2018.

[37] S. Quintanar-Guzmán, S. Kannan, H. Voos, M. Darouach, and M. Alma, "Experimental validation of adaptive control for a shape memory alloy actuated lightweight robotic arm," in *ASME. Smart Materials, Adaptive Structures and Intelligent Systems, Volume 1: Development and Characterization of Multifunctional Materials; Modeling, Simulation, and Control of Adaptive Systems; Integrated System Design and Implementation*, no. 51944, p. V001T03A032, 2018.

[38] S. Quintanar-Guzmán, S. Kannan, H. Voos, M. Darouach, and M. Alma, "Observer design for lightweight robotic arm actuated by shape memory alloy (SMA) wire," in *14th International Workshop on Advanced Control and Diagnosis (ACD)*, 2017.

[39] S. Quintanar-Guzmán, S. Kannan, A. Aguilera-González, M. A. Olivares-Mendez, and H. Voos, "Operational space control of a lightweight robotic arm actuated by shape memory alloy wires: A comparative study," *Journal of Intelligent Material Systems and Structures*, vol. 30, no. 9, pp. 1368–1384, 2019.

[40] S. Quintanar-Guzmán, S. Kannan, M. A. Olivares-Mendez, and H. Voos, "Lightweight robotic arm actuated by shape memory alloy (SMA) wires," in *2016 8th International Conference on Electronics, Computers and Artificial Intelligence (ECAI)*, pp. 1–6, June 2016.

[41] S. Quintanar-Guzmán, S. Kannan, M. A. Olivares-Mendez, and H. Voos, "Operational space control of a lightweight robotic arm actuated by shape memory alloy (SMA) wires," in *ASME. Smart Materials, Adaptive Structures and Intelligent Systems, Volume 2: Modeling, Simulation and Control; Bio-Inspired Smart Materials and Systems; Energy Harvesting*, no. 50497, p. V002T03A012, 2016.

[42] S. Kannan, S. Bezzaoucha, S. Quintanar-Guzmán, J. Dentler, M. A. Olivares-Mendez, and H. Voos, "Hierarchical control of aerial manipulation vehicle," in *International Conference on Mathematical Problems in Engineering, Aerospace and Sciences*, vol. 1798 of *American Institute of Physics Conference Series*, p. 020069, Jan. 2017.

[43] L. A. van der Elst, S. Quintanar-Guzmán, and J.-R. Hadji-Minaglou, "Design of an electromechanical prosthetic finger using shape memory alloy wires," in *2017 IEEE International Symposium on Robotics and Intelligent Sensors (IRIS)*, pp. 56–61, October 2017.

[44] S. Kannan, S. Quintanar-Guzmán, S. Bezzaoucha, M. A. Olivares-Mendez, and H. Voos, "Adaptive control of hysteretic robotic arm in operational space," in *Proceedings of the 5th International Conference on Mechatronics and Control Engineering*, ICMCE '16, (New York, NY, USA), pp. 92–96, ACM, 2016.

[45] S. Kannan, S. Quintanar-Guzmán, J. Dentler, M. A. Olivares-Mendez, and H. Voos, "Control of aerial manipulation vehicle in operational space," in *2016 8th International Conference on Electronics, Computers and Artificial Intelligence (ECAI)*, pp. 1–4, June 2016.

[46] L. A. van der Elst, "Design of an electromechanical prosthetic finger using shape memory alloy wires," Master's thesis, University of Luxembourg, Luxembourg, 2017.

[47] P. J. Sanchez-Cuevas, G. Heredia, and A. Ollero, "Multirotor uas for bridge inspection by contact using the ceiling effect," in *2017 International Conference on Unmanned Aircraft Systems (ICUAS)*, pp. 767–774, June 2017.

[48] F. Augugliaro, S. Lupashin, M. Hamer, C. Male, M. Hehn, M. W. Mueller, J. S. Willmann, F. Gramazio, M. Kohler, and R. D'Andrea, "The flight assembled architecture installation: Cooperative construction with flying machines," *IEEE Control Systems Magazine*, vol. 34, pp. 46–64, Aug 2014.

[49] T. W. Danko and P. Y. Oh, "Design and control of a hyper-redundant manipulator for mobile manipulating unmanned aerial vehicles," *Journal of Intelligent & Robotic Systems*, vol. 73, no. 1, pp. 709–723, 2014.

[50] R. Cano, C. Perez, F. Pruano, A. Ollero, and G. Heredia, "Mechanical design of a 6-DoF aerial manipulator for assembling bar structures using UAVs," in *2nd IFAC Workshop on Research, Education and Development of Unmanned Aerial Systems*, pp. –, IFAC, 2013.

[51] T. Zheng, Y. Yang, D. T. Branson, R. Kang, E. Guglielmino, M. Cianchetti, D. G. Caldwell, and G. Yang, "Control design of shape memory alloy based multi-arm continuum robot inspired by octopus," in *2014 IEEE 9th Conference on Industrial Electronics and Applications (ICIEA)*, pp. 1108–1113, August 2014.

[52] Y. H. Teh, *Fast , Accurate Force and Position Control of Shape Memory Alloy Actuators*. PhD thesis, ANU College of Engineering and Computer Science, 2008.

[53] J. Ortín and L. Delaey, "Hysteresis in shape-memory alloys," *International Journal of Non-Linear Mechanics*, vol. 37, no. 8, pp. 1275–1281, 2002.

[54] H. Luo, Y. Liao, E. Abel, Z. Wang, and X. Liu, "Hysteresis behaviour and modeling of SMA actuators," in *Shape Memory Alloys*, InTech, 2010.

[55] K. Ikuta, M. Tsukamoto, and S. Hirose, "Mathematical model and experimental verification of shape memory alloy for designing micro actuator," in *[1991] Proceedings. IEEE Micro Electro Mechanical Systems*, pp. 103–108, Jan 1991.

[56] C. Lexcellent, *Shape-memory alloys handbook*. John Wiley & Sons, 2013.

[57] J. Qiu, J. Tani, D. Osanai, Y. Urushiyama, and D. Lewinnek, "High-speed response of SMA actuators," *International Journal of Applied Electromagnetics and Mechanics*, vol. 12, no. 1, 2, pp. 87–100, 2000.

[58] M. Sreekumar, M. Singaperumal, T. Nagarajan, M. Zoppi, and R. Molfino, "Recent advances in nonlinear control technologies for shape memory alloy actuators," *Journal of Zhejiang University-Science A*, vol. 8, no. 5, pp. 818–829, 2007.

[59] S. Zaidi, F. Lamarque, J. Favergeon, O. Carton, and C. Prelle, "Nitinol thin foil irradiated by continuous mode laser diode for wireless chromatic micro-actuation," in *Mechatronics, 2009. ICM 2009. IEEE International Conference on*, pp. 1–6, IEEE, 2009.

[60] R. Romano and E. A. Tannuri, "Modeling, control and experimental validation of a novel actuator based on shape memory alloys," *Mechatronics*, vol. 19, no. 7, pp. 1169–1177, 2009.

[61] C. W. Müller, R. Pfeifer, T. El-Kashef, C. Hurschler, D. Herzog, M. Oszwald, C. Haasper, C. Krettek, and T. Gösling, "Electromagnetic induction heating of

an orthopaedic nickel–titanium shape memory device," *Journal of Orthopaedic Research*, vol. 28, no. 12, pp. 1671–1676, 2010.

[62] D. Reynaerts and H. Van Brussel, "Design aspects of shape memory actuators," *Mechatronics*, vol. 8, no. 6, pp. 635–656, 1998.

[63] K. O'Toole, *A Methodology Towards Comprehensive Evaluation of Shape Memory Alloy Actuators for Prosthetic Finger Design. Doctoral Thesis.* PhD thesis, Dublin Institute of Technology, 2011.

[64] J. J. Craig, *Introduction to robotics: mechanics and control*, vol. 3. Pearson Prentice Hall Upper Saddle River, 2005.

[65] A. Khodayari, M. Talari, and M. M. Kheirikhah, "Fuzzy PID controller design for artificial finger based SMA actuators," in *2011 IEEE International Conference on Fuzzy Systems (FUZZ-IEEE 2011)*, pp. 727–732, June 2011.

[66] J. Colorado, A. Barrientos, and C. Rossi, "Músculos inteligentes en robots biológicamente inspirados: Modelado, control y actuación," *Revista Iberoamericana de Automática e Informática Industrial RIAI*, vol. 8, no. 4, pp. 385 – 396, 2011.

[67] F. Gao, Z. Wang, Y. Wang, Y. Wang, and J. Li, "A prototype of a biomimetic mantle jet propeller inspired by cuttlefish actuated by SMA wires and a theoretical model for its jet thrust," *Journal of Bionic Engineering*, vol. 11, no. 3, pp. 412–422, 2014.

[68] B. H. Shin, K.-M. Lee, and S.-Y. Lee, "A miniaturized tadpole robot using an electromagnetic oscillatory actuator," *Journal of Bionic Engineering*, vol. 12, no. 1, pp. 29–36, 2015.

[69] F. Nematzadeh and S. Sadrnezhaad, "Effects of material properties on mechanical performance of nitinol stent designed for femoral artery: Finite element analysis," *Scientia Iranica*, vol. 19, no. 6, pp. 1564 – 1571, 2012.

[70] A. Nespoli, V. Dallolio, E. Villa, and F. Passaretti, "A new design of a nitinol ring-like wire for suturing in deep surgical field," *Materials Science and Engineering C*, vol. 56, pp. 30–36, 2015.

[71] M. T. Andani, W. Anderson, and M. Elahinia, "Design, modeling and experimental evaluation of a minimally invasive cage for spinal fusion surgery utilizing superelastic nitinol hinges," *Journal of intelligent material systems and structures*, vol. 26, no. 6, pp. 631–638, 2015.

[72] M. G. Mataee, M. T. Andani, and M. Elahinia, "Adaptive ankle–foot orthoses based on superelasticity of shape memory alloys," *Journal of intelligent material systems and structures*, vol. 26, no. 6, pp. 639–651, 2015.

[73] N. S. Moghaddam, R. Skoracki, M. Miller, M. Elahinia, and D. Dean, "Three dimensional printing of stiffness-tuned, nitinol skeletal fixation hardware with an example of mandibular segmental defect repair," *Procedia CIRP*, vol. 49, pp. 45–50, August 2016.

[74] J. Jafari, S. Zebarjad, and S. Sajjadi, "Effect of pre-strain on microstructure of Ni–Ti orthodontic archwires," *Materials Science and Engineering A*, vol. 473, no. 1–2, pp. 42–48, 2008.

[75] N. Pandis and C. P. Bourauel, "Nickel-Titanium (NiTi) arch wires: the clinical significance of super elasticity," *Seminars in Orthodontics*, vol. 16, no. 4, pp. 249–257, 2010. Latest Controversies in Orthodontics: From in Vitro Data to in Vivo Evidence.

[76] H. Rodrigue, S. Cho, M.-W. Han, B. Bhandari, J.-E. Shim, and S.-H. Ahn, "Effect of twist morphing wing segment on aerodynamic performance of UAV," *Journal of Mechanical Science and Technology*, vol. 30, no. 1, pp. 229–236, 2016.

[77] S. Barbarino, S. Ameduri, L. Lecce, and A. Concilio, "Wing shape control through an SMA-Based device," *Journal of intelligent material systems and structures*, vol. 20, no. 3, pp. 283–296, 2009.

[78] D. K. Kennedy, F. K. Straub, L. M. Schetky, Z. Chaudhry, and R. Roznoy, "Development of a SMA actuator for in-flight rotor blade tracking," *Journal of intelligent material systems and structures*, vol. 15, no. 4, pp. 235–248, 2004.

[79] M. Sreekumar, T. Nagarajan, and M. Singaperumal, "Application of trained NiTi SMA actuators in a spatial compliant mechanism: Experimental investigations," *Materials & Design*, vol. 30, no. 8, pp. 3020–3029, 2009.

[80] H.-M. Son, M. Y. Kim, and Y.-J. Lee, "Tunable-focus liquid lens system controlled by antagonistic winding-type SMA actuator," *Optics Express*, vol. 17, pp. 14339–14350, July 2009.

[81] E. A. Williams, G. Shaw, and M. Elahinia, "Control of an automotive shape memory alloy mirror actuator," *Mechatronics*, vol. 20, no. 5, pp. 527–534, 2010.

[82] S. Quintanar-Guzmán, J. Reyes-Reyes, and M. d. c. Arellano-Sánchez, "Modelado y control de un sistema electrotérmico-mecánico móvil basado en alambres musculares," in *XVI Congreso Latinoamericano de Control Automático, CLCA 2014*, pp. 834–839, Asociación de México de Control Automático, 2014.

[83] M. Hulea and C. F. Caruntu, "Spiking neural network for controlling the artificial muscles of a humanoid robotic arm," in *2014 18th International Conference on System Theory, Control and Computing (ICSTCC)*, pp. 163–168, IEEE, oct 2014.

[84] J. Ko, M. B. Jun, G. Gilardi, E. Haslam, and E. J. Park, "Fuzzy PWM-PID control of cocontracting antagonistic shape memory alloy muscle pairs in an artificial finger," *Mechatronics*, vol. 21, no. 7, pp. 1190–1202, 2011.

[85] M. C. Carrozza, A. Arena, D. Accoto, A. Menciassi, and P. Dario, "A SMA actuated miniature pressure regulator for a miniature robot for colonoscopy," *Sensors and Actuators A: Physical*, vol. 105, no. 2, pp. 119–131, 2003.

[86] W. Makishi, T. Matunaga, Y. Haga, and M. Esashi, "Active bending electric endoscope using shape memory alloy coil actuators," in *Biomedical Robotics and Biomechatronics, 2006. BioRob 2006. The First IEEE/RAS-EMBS International Conference on*, pp. 217–219, IEEE, 2006.

[87] J. C. Hannen, J. H. Crews, and G. D. Buckner, "Indirect intelligent sliding mode control of a shape memory alloy actuated flexible beam using hysteretic recurrent neural networks," *Smart Materials and Structures*, vol. 21, no. 8, p. 085015, 2012.

[88] S. Choi, Y. Han, J. Kim, and C. Cheong, "Force tracking control of a flexible gripper featuring shape memory alloy actuators," *Mechatronics*, vol. 11, no. 6, pp. 677–690, 2001.

[89] S. K. Chaitanya and K. Dhanalakshmi, "Control of shape memory alloy actuated gripper using sliding mode control," in *Control Applications (CCA), 2013 IEEE International Conference on*, pp. 1247–1252, IEEE, 2013.

[90] C.-M. Lin, C.-H. Fan, and C.-C. Lan, "A shape memory alloy actuated microgripper with wide handling ranges," in *Advanced Intelligent Mechatronics, 2009. AIM 2009. IEEE/ASME International Conference on*, pp. 12–17, IEEE, 2009.

[91] S. Kannan, C. Giraud-Audine, and E. Patoor, "Laguerre model based adaptive control of antagonistic shape memory alloy (SMA) actuator," in *Proc. SPIE 7643, Active and Passive Smart Structures and Integrated Systems 2010*, vol. 7643, pp. 764307–764307–12, 2010.

[92] S. Kannan, C. Giraud-Audine, and E. Patoor, "Application of Laguerre based adaptive predictive control to shape memory alloy (SMA) actuator," *ISA Transactions*, vol. 52, no. 4, pp. 469 – 479, 2013.

[93] S. Kannan, *Modélisation et Commande d'Actionneurs à Alliage à Mémoire de Forme*. PhD thesis, l'École Nationale Supérieure d'Arts et Métiers, 2011.

[94] A. Khandelwal and V. Buravalla, "Models for shape memory alloy behavior: an overview of modeling approaches," *The International Journal of Structural Changes in Solids*, vol. 1, no. 1, pp. 111–148, 2009.

[95] D. Hughes and J. T. Wen, "Preisach modeling of piezoceramic and shape memory alloy hysteresis," *Smart materials and structures*, vol. 6, no. 3, p. 287, 1997.

[96] B.-J. Choi and Y.-J. Lee, "Preisach model of SMA actuators using proportional relationship of major loop of hysteresis," in *Intelligent Robots and Systems, 2002. IEEE/RSJ International Conference on*, vol. 2, pp. 1986–1991, IEEE, 2002.

[97] X. Tan and J. S. Baras, "Adaptive identification and control of hysteresis in smart materials," *IEEE Transactions on automatic control*, vol. 50, no. 6, pp. 827–839, 2005.

[98] K. K. Ahn and N. B. Kha, "Internal model control for shape memory alloy actuators using fuzzy based preisach model," *Sensors and Actuators A: Physical*, vol. 136, no. 2, pp. 730–741, 2007.

[99] S. M. Dutta and F. H. Ghorbel, "Differential hysteresis modeling of a shape memory alloy wire actuator," *IEEE/ASME Transactions on Mechatronics*, vol. 10, no. 2, pp. 189–197, 2005.

[100] A. Visintin, *Differential models of hysteresis*, vol. 111. Springer Science & Business Media, 2013.

[101] M. Sjöström and C. Visone, ""Moving" Prandtl-Ishilinskii operators with compensator in a closed form," *Physica B: Condensed Matter*, vol. 372, no. 1, pp. 97–100, 2006.

[102] P.-A. Gédouin, C. Join, E. Delaleau, J.-M. Bourgeot, S. A. Chirani, and S. Calloch, "A new control strategy for shape memory alloys actuators," in *European Symposium on Martensitic Transformations*, p. 07007, EDP Sciences, 2009.

[103] Y. H. Teh and R. Featherstone, "Accurate force control and motion disturbance rejection for shape memory alloy actuators," in *Robotics and Automation, 2007 IEEE International Conference on*, pp. 4454–4459, IEEE, 2007.

[104] F. Falk, "Model free energy, mechanics, and thermodynamics of shape memory alloys," *Acta Metallurgica*, vol. 28, no. 12, pp. 1773–1780, 1980.

[105] C. Cisse, W. Zaki, and T. B. Zineb, "A review of constitutive models and modeling techniques for shape memory alloys," *International Journal of Plasticity*, vol. 76, pp. 244 – 284, 2016.

[106] F. Fischer and K. Tanaka, "A micromechanical model for the kinetics of martensitic transformation," *International Journal of Solids and Structures*, vol. 29, no. 14, pp. 1723 – 1728, 1992.

[107] M. Brocca, L. Brinson, and Z. Bažant, "Three-dimensional constitutive model for shape memory alloys based on microplane model," *Journal of the Mechanics and Physics of Solids*, vol. 50, no. 5, pp. 1051 – 1077, 2002.

[108] A. C. Souza, E. N. Mamiya, and N. Zouain, "Three-dimensional model for solids undergoing stress-induced phase transformations," *European Journal of Mechanics - A/Solids*, vol. 17, no. 5, pp. 789 – 806, 1998.

[109] J. Boyd and D. Lagoudas, "A thermodynamical constitutive model for shape memory materials. part I. the monolithic shape memory alloy," *International Journal of Plasticity*, vol. 12, no. 6, pp. 805 – 842, 1996.

[110] W. Zaki and Z. Moumni, "A three-dimensional model of the thermomechanical behavior of shape memory alloys," *Journal of the Mechanics and Physics of Solids*, vol. 55, no. 11, pp. 2455 – 2490, 2007.

[111] B. Peultier, T. B. Zineb, and E. Patoor, "Macroscopic constitutive law of shape memory alloy thermomechanical behaviour. application to structure computation by fem," *Mechanics of Materials*, vol. 38, no. 5, pp. 510 – 524, 2006. Shape Memory Alloys.

[112] S. Leclercq and C. Lexcellent, "A general macroscopic description of the thermomechanical behavior of shape memory alloys," *Journal of the Mechanics and Physics of Solids*, vol. 44, no. 6, pp. 953 – 980, 1996.

[113] J. Lubliner and F. Auricchio, "Generalized plasticity and shape-memory alloys," *International Journal of Solids and Structures*, vol. 33, no. 7, pp. 991 – 1003, 1996.

[114] A. Masud, M. Panahandeh, and F. Aurrichio, "A finite-strain finite element model for the pseudoelastic behavior of shape memory alloys," *Computer Methods in Applied Mechanics and Engineering*, vol. 148, no. 1, pp. 23 – 37, 1997.

[115] A. Bhattacharyya and D. Lagoudas, "A stochastic thermodynamic model for the gradual thermal transformation of SMA polycrystals," *Smart materials and structures*, vol. 6, no. 3, p. 235, 1997.

[116] K. Ikuta, "Micro/miniature shape memory alloy actuator," in *Robotics and Automation, 1990. Proceedings., 1990 IEEE International Conference on*, pp. 2156–2161, IEEE, 1990.

[117] D. R. Madill and D. Wang, "The modelling and L_2-stability of a shape memory alloy position control system," in *Robotics and Automation, 1994. Proceedings., 1994 IEEE International Conference on*, pp. 293–299, IEEE, 1994.

[118] K. Tanaka, "A thermomechanical sketch of shape memory effect: one-dimensional tensile behavior," *Res. Mechanica*, vol. 18, pp. 251–263, 1986.

[119] L. C. Brinson, "One-dimensional constitutive behavior of shape memory alloys: thermomechanical derivation with non-constant material functions and redefined martensite internal variable," *Journal of intelligent material systems and structures*, vol. 4, no. 2, pp. 229–242, 1993.

[120] K. Ikuta, M. Tsukamoto, and S. Hirose, "Shape memory alloy servo actuator system with electric resistance feedback and application for active endoscope," in *Proceedings. 1988 IEEE International Conference on Robotics and Automation*, pp. 427–430 vol.1, April 1988.

[121] V. Novák, P. Šittner, G. Dayananda, F. Braz-Fernandes, and K. Mahesh, "Electric resistance variation of NiTi shape memory alloy wires in thermomechanical tests: Experiments and simulation," *Materials Science and Engineering: A*, vol. 481-482, pp. 127 – 133, 2008. Proceedings of the 7th European Symposium on Martensitic Transformations, ESOMAT 2006.

[122] M. S. De Queiroz, D. M. Dawson, S. P. Nagarkatti, and F. Zhang, *Lyapunov-based control of mechanical systems*. Springer Science & Business Media, 2012.

[123] L. Ljung, "System identification toolbox for use with MATLAB," *The Mathworks Inc.*, 01 2006.

[124] O. K. Rediniotis, L. N. Wilson, D. C. Lagoudas, and M. M. Khan, "Development of a shape-memory-alloy actuated biomimetic hydrofoil," *Journal of Intelligent Material Systems and Structures*, vol. 13, no. 1, pp. 35–49, 2002.

[125] N. Troisfontaine, P. Bidaud, and P. Dario, "Control experiments on two SMA based micro-actuators," *Experimental Robotics V*, pp. 490–499, 1998.

[126] N. Ma and G. Song, "Control of shape memory alloy actuator using pulse width modulation," *Smart materials and structures*, vol. 12, no. 5, p. 712, 2003.

[127] M. Ho and J. P. Desai, "Towards a MRI-compatible meso-scale SMA-actuated robot using PWM control," in *Biomedical Robotics and Biomechatronics (BioRob), 2010 3rd IEEE RAS and EMBS International Conference on*, pp. 361–366, IEEE, 2010.

[128] A. Khodayari, M. M. Kheirikhah, and S. Rabiee, "Fuzzy PID controller design for snake robot based SMA actuators," in *Control System, Computing and Engineering (ICCSCE), 2011 IEEE International Conference on*, pp. 274–278, IEEE, 2011.

[129] J.-H. Wang, C.-H. Fan, and C.-C. Lan, "A compact rotational manipulator using shape memory alloy wire actuated flexures," in *Robotics and Automation, 2009. ICRA'09. IEEE International Conference on*, pp. 550–555, IEEE, 2009.

[130] Z. Shi, T. Wang, D. Liu, C. Ma, and X. Yuan, "A fuzzy PID-controlled SMA actuator for a two-DoF joint," *Chinese Journal of Aeronautics*, vol. 27, no. 2, pp. 453–460, 2014.

[131] M. H. Elahinia and M. Ahmadian, "Application of the extended Kalman filter to control of a shape memory alloy arm," *Smart materials and structures*, vol. 15, no. 5, p. 1370, 2006.

[132] D. Grant and V. Hayward, "Variable structure control of shape memory alloy actuators," *IEEE Control Systems Magazine*, vol. 17, no. 3, pp. 80–88, 1997.

[133] J. H. Wiest and G. D. Buckner, "Indirect intelligent sliding mode control of antagonistic shape memory alloy actuators using hysteretic recurrent neural networks," *IEEE Transactions on Control Systems Technology*, vol. 22, no. 3, pp. 921–929, 2014.

[134] J. Lee, M. Jin, and K. K. Ahn, "Precise tracking control of shape memory alloy actuator systems using hyperbolic tangential sliding mode control with time delay estimation," *Mechatronics*, vol. 23, no. 3, pp. 310–317, 2013.

[135] K. Arai, S. Aramaki, and K. Yanagisawa, "Feedback linearization for SMA (shape memory alloy)," in *SICE'95. Proceedings of the 34th SICE Annual Conference. International Session Papers*, pp. 1383–1386, IEEE, 1995.

[136] Y. Pan, Z. Guo, X. Li, and H. Yu, "Output-feedback adaptive neural control of a compliant differential SMA actuator," *IEEE Transactions on Control Systems Technology*, vol. PP, no. 99, pp. 1–9, 2017.

[137] L. Riccardi, D. Naso, B. Turchiano, and H. Janocha, "Adaptive control of positioning systems with hysteresis based on magnetic shape memory alloys," *IEEE Transactions on Control Systems Technology*, vol. 21, no. 6, pp. 2011–2023, 2013.

[138] Y. Wang, C.-Y. Su, and H. Hong, "Model reference control including adaptive inverse hysteresis for systems with unknown input hysteresis," in *Networking, Sensing and Control, 2007 IEEE International Conference on*, pp. 70–75, IEEE, 2007.

[139] Y. Feng, C. A. Rabbath, H. Hong, C.-Y. Su, and W. Lin, "Inverse hysteresis control for shape memory alloy micro-actuators based flap positioning system," in *Decision and Control (CDC), 2010 49th IEEE*, pp. 3662–3667, IEEE, 2010.

[140] G. Song, V. Chaudhry, and C. Batur, "A neural network inverse model for a shape memory alloy wire actuator," *Journal of intelligent material systems and structures*, vol. 14, no. 6, pp. 371–377, 2003.

[141] V. Hassani, T. Tjahjowidodo, and T. N. Do, "A survey on hysteresis modeling, identification and control," *Mechanical Systems and Signal Processing*, vol. 49, no. 1–2, pp. 209 – 233, 2014.

[142] K. D. Young, V. I. Utkin, and U. Ozguner, "A control engineer's guide to sliding mode control," *IEEE Transactions on Control Systems Technology*, vol. 7, no. 3, pp. 328–342, 1999.

[143] H. Mai, G. Song, and X. Liao, "Adaptive online inverse control of a shape memory alloy wire actuator using a dynamic neural network," *Smart Materials and Structures*, vol. 22, no. 1, p. 015001, 2013.

[144] N. T. Tai and K. K. Ahn, "Output feedback direct adaptive controller for a SMA actuator with a Kalman filter," *IEEE Transactions on Control Systems Technology*, vol. 20, pp. 1081–1091, July 2012.

[145] M. S. Queiroz, D. M. Dawson, S. P. Nagarkatti, and F. Zhang, *Lyapunov-Based Control of Mechanical Systems*. Springer, 2000.

[146] M. H. Elahinia, M. Ahmadian, and H. Ashrafiuon, "Design of a Kalman filter for rotary shape memory alloy actuators," *Smart Materials and Structures*, vol. 13, no. 4, p. 691, 2004.

[147] I. Hassanzadeh, N. Nikdel, and N. Motlagh, "Design of Augmented EKF for Shape Memory Alloy Actuated Manipulator," *International Journal of Engineering Science and Technology*, vol. 2, no. 7, pp. 3188–3198, 2010.

[148] M. L. Guckert, M. D. Naish, and R. V. Patel, "Position control of a spherical joint using feedback linearization for SMA wire actuators," in *Advanced Intelligent Mechatronics (AIM), 2010 IEEE/ASME International Conference on*, pp. 1350–1355, IEEE, 2010.

[149] A. Ianagui and E. A. Tannuri, "A sliding mode torque and position controller for an antagonistic SMA actuator," *Mechatronics*, vol. 30, pp. 126–139, 2015.

[150] H. Gurung and A. Banerjee, "Self-sensing SMA Actuator Using Extended Kalman Filter and Artificial Neural Network," *Procedia Engineering*, vol. 144, pp. 629–634, 2016.

[151] S. Jabeen, A. V. Yeganeh, G. M. Simsek, G. G. Yapici, K. Abidi, and O. Bebek, "Discrete-Time Integral Sliding Mode Control of a Smart Joint for Minimally Invasive Surgeries," *6th IEEE RAS/EMBS International Conference on Biomedical Robotics and Biomechatronics (BioRob)*, 2016.

[152] K. Kubik, A. Gurley, D. Beale, and A. Skalitzky, "Linear parameter varying modeling and estimation of a SMA wire actuator," in *ASME 2018 Conference on Smart Materials, Adaptive Structures and Intelligent Systems*, pp. V001T03A023–V001T03A023, American Society of Mechanical Engineers, 2018.

[153] H. K. Khalil and J. Grizzle, *Nonlinear systems*, vol. 3. Prentice hall Upper Saddle River, NJ, 2002.

[154] K. C. Veluvolu and S. Y. Chai, "High gain observers with multiple sliding mode for state and unknown input estimations," *2009 4th IEEE Conference on Industrial Electronics and Applications, ICIEA 2009*, vol. 56, no. 9, pp. 1179–1186, 2009.

[155] A. Aguilera-González, H. Voos, and M. Darouach, "States and unknown input estimation via non-linear sliding mode high-gain observers for a glucose-insulin system," in *2016 IEEE EMBS Conference on Biomedical Engineering and Sciences (IECBES)*, pp. 388–393, Dec 2016.

[156] M. Witczak, "Fault diagnosis and fault-tolerant control strategies for non-linear systems," *Lecture Notes in Electrical Engineering*, vol. 266, pp. 375–392, 2014.

[157] M. M. Barzegari, M. Dardel, and A. Fathi, "Control of aeroelastic characteristics of cantilever wing with smart materials using state-dependent riccati equation method," *Journal of Intelligent Material Systems and Structures*, vol. 26, no. 8, pp. 988–1005, 2015.

[158] A. S. Dutka, A. W. Ordys, and M. J. Grimble, "Optimized discrete-time state dependent riccati equation regulator," in *Proceedings of the 2005, American Control Conference, 2005.*, pp. 2293–2298 vol. 4, June 2005.

[159] T. Çimen, "State-dependent riccati equation (SDRE) control: A survey," *IFAC Proceedings Volumes*, vol. 41, no. 2, pp. 3761 – 3775, 2008. 17th IFAC World Congress.

[160] J. R. Cloutier and J. C. Cockburn, "The state-dependent nonlinear regulator with state constraints," in *Proceedings of the 2001 American Control Conference. (Cat. No.01CH37148)*, vol. 1, pp. 390–395 vol.1, June 2001.

Abstract

Nonlinear Observation and Control of a Lightweight Robotic Manipulator Actuated by Shape Memory Alloy (SMA) Wires

In the last decade, the industry of Unmanned Aerial Vehicles (UAV) has gone through immense growth and diversification. Nowadays, we find drone based applications in a wide range of industries, such as infrastructure, agriculture, transport, among others. This phenomenon has generated an increasing interest in the field of aerial manipulation. The implementation of aerial manipulators in the UAV industry could generate a significant increase in possible applications. However, the restriction on the available payload is one of the main setbacks of this approach. The impossibility to equip UAVs with heavy dexterous industrial robotic arms has driven the interest in the development of lightweight manipulators suitable for these applications. In the pursuit of providing an alternative lightweight solution for the aerial manipulators, this thesis proposes a lightweight robotic arm actuated by Shape Memory Alloy (SMA) wires.

Although SMA wires represent a great alternative to conventional actuators for lightweight applications, they also imply highly nonlinear dynamics, which makes them difficult to control. Seeking to present a solution for the challenging task of controlling SMA wires, this work investigates the implications and advantages of the implementation of state feedback control techniques. The final aim of this study is the experimental implementation of a state feedback control for position regulation of the proposed lightweight robotic arm.

Firstly, a mathematical model based on a constitutive model of the SMA wire is developed and experimentally validated. This model describes the dynamics of the proposed lightweight robotic arm from a mechatronics perspective. The proposed robotic arm is tested with three output feedback controllers for angular position control, namely a PID, a Sliding Mode and an Adaptive Controller. The controllers are tested in a MATLAB simulation and finally implemented and experimentally tested in various different scenarios.

Following, in order to perform the experimental implementation of a state feedback control technique, a state and unknown input observer is developed. First, a non-switching observable model with unknown input of the proposed robotic arm is derived from the model previously presented. This model takes the martensite fraction rate of the original model as an unknown input, making it possible to eliminate the switching terms in the model. Then, a state and unknown input observer is proposed. This observer is

based on the Extended Kalman Filter (EKF) for state estimation and sliding mode approach for unknown input estimation. Sufficient conditions for stability and convergence are established. The observer is tested in a MATLAB simulation and experimentally validated in various different scenarios.

Finally, a state feedback control technique is tested in simulation and experimentally implemented for angular position control of the proposed lightweight robotic arm. Specifically, continuous and discrete-time State-Dependent Riccati Equation (SDRE) control laws are derived and implemented. To conclude, a quantitative and qualitative comparative analysis between an output feedback control approach and the implemented state feedback control is carried out under multiple scenarios, including position regulation, position tracking and tracking with changing payloads.

Résumé

Observation et Commande non Linéaire d'un Manipulateur Robotique Léger Actionné Par Des Fils En Alliage À Mémoire De Forme (SMA)

Au cours de la dernière décennie, l'industrie des véhicules aériens sans pilote (UAV) a connu une croissance et une diversification immenses. De nos jours, nous trouvons des applications basées sur les drones dans un large éventail d'industries, telles que les infrastructures, l'agriculture, les transports, etc. Ce phénomène a suscité un intérêt croissant dans le domaine de la manipulation aérienne. La mise en œuvre de manipulateurs aériens dans l'industrie des UAV pourrait générer une augmentation significative du nombre d'applications possibles. Cependant, la restriction de la charge utile disponible est l'un des principaux inconvénients de cette approche. L'impossibilité d'équiper les drones de bras robotiques industriels puissants et habiles a suscité l'intérêt pour le développement de manipulateurs légers adaptés à ces applications. Dans le but de fournir une solution légère alternative aux manipulateurs aériens, cette thèse propose un bras robotique léger actionné par des fils en alliage à mémoire de forme (SMA).

Bien que les fils SMA représentent une excellente alternative aux actionneurs conventionnels pour les applications légères, ils impliquent également une dynamique hautement non linéaire, ce qui les rend difficiles à contrôler. Cherchant à présenter une solution pour la tâche difficile de contrôler les fils SMA, ce travail étudie les conséquences et les avantages de la mise en œuvre des techniques de commande par retour d'état. L'objectif final de cette étude est la mise en œuvre expérimentale d'un contrôle à rétroaction d'état pour la régulation de la position du bras robotique léger proposé.

Tout d'abord, un modèle mathématique basé sur un modèle physique du comportement des câbles SMA est développé et validé expérimentalement. Ce modèle décrit la dynamique du bras robotique léger proposé du point de vue de la mécatronique. Le bras robotique proposé est testé avec trois contrôleurs de retour de sortie pour le contrôle de position angulaire, à savoir un PID, un mode coulissant et une commande adaptative. Les contrôleurs sont testés dans une simulation MATLAB, puis mis en œuvre et testés expérimentalement selon différents scénarios.

Ensuite, afin de réaliser la mise en œuvre expérimentale d'une technique de commande par retour d'état, un observateur d'état, à entrée inconnue, est développé. Premièrement, un modèle observable sans commutation avec une entrée inconnue est dérivé du modèle présenté précédemment. Ce modèle prend comme entrée inconnue le taux de fraction de martensite du modèle d'origine, ce qui permet d'éliminer les termes de commutation dans le modèle. Ensuite, un observateur, à entrées inconnues, basé sur le filtre de Kalman

étendu et sur l'observateur à mode glissant est développé. Cet observateur permet l'estimation simultanée de l'état et des entrées inconnues. Les conditions suffisantes de convergence et de stabilité sont établies. L'observateur est testé dans une simulation MATLAB et validé expérimentalement dans différents scénarios.

Enfin, une technique de commande par retour d'état est testée en simulation et implémentée de manière expérimentale pour le contrôle de position angulaire du bras robotique léger proposé. Elle est basée sur la résolution d'une équation de Riccati (SDRE). En conclusion, une analyse comparative quantitative et qualitative entre une approche de commande par retour de sortie et la une de commande par retour d'état mis en œuvre est effectuée selon plusieurs scénarios, y compris la régulation de position, le suivi de position et le suivi de charges utiles changeantes.